Minimising vibration in a flexible golf club during robotic simulations of a golf swing

By

Kirsty Ellis

A Doctoral thesis submitted in partial fulfilment of the requirements for the award of the degree Doctor of Philosophy (PhD), at Loughborough University

December 2013

Acknowledgements

The author would like to express her thanks and appreciation to all the people who have helped provide inspiration and encouragement for this project.

Special thanks go to my academic supervisors Dr Jonathan Roberts and Professor Steve Rothberg for their continuous help, guidance, and support throughout this research.

Also I would like to thank my friends, particularly Dr Andrea Vinet and Dr David Rogers for their emotional support and for generally being awesome.

Thank you to my brother David for being such an inspiration and to my sister Charlotte for always bringing the cake.

I would like to give a special mention to Nikhil Datta. He has provided unconditional support and encouragement for me to complete this thesis; words cannot express how grateful I am to him for this, he truly has been amazing.

Finally and most importantly I would like to thank my parents. Without the support and love from my mum through my most troubled times I would not have been able to complete this project. I would like to thank my dad for being an inspiration; I hope I have made him proud.

Abstract

Robots are widely used as substitutes for humans in situations involving repetitive tasks where a precise and repeatable motion is required. Sports technology is an area which has seen an increase in the implementation of robots which simulate specific human motions required for a sport. One purpose is to test sports equipment, where the requirement is for a motion to be performed with consistent variables. One issue which has arisen frequently in the robot simulation of humans is the inherent presence of vibration excited in a flexible object being manipulated by a robot, and this issue is not unfounded in the situation presented in this research, of a golf robot manipulating a flexible golf club during the simulation of a golf swing. It had been found that during robotic simulations of golf swings performed with the Miyamae Robo V at the Sports Technology Institute at Loughborough University, swing variables such as shaft deformation and clubhead orientation were dissimilar to those measured for human golf swings. Vibrations present in the golf club were identified as the key cause of the disparity between human and robot swing variables. This research sought to address this issue and find a method which could be applied to reduce clubhead vibrations present in robot simulations of a golf swing to improve their similarity to human swings. This would facilitate the use of the golf robot for equipment testing and club fitting.

Golf swing variables were studied and measured for 14 human subjects with the aim being to understand the motion that the robot is required to simulate. A vibration damping gripper was then fitted to the robot to test the effect that changing the interface between the robot-excited vibrations and the club would have, this was achieved with a selection of silicone sleeves with differing material properties which could be attached to the club. Preliminary results showed a noticeable reduction in clubhead vibrations and this solution was investigated further. Mathematically modelling the robot was seen as the most suitable method for this as it meant the robot remained functional and allowed a number of solutions to be tested. Several iterations of a mathematical model were developed with the final model being structurally similar to the robot with the addition of a compliant grip and wrist. The method by which the robot is driven was also recognised as having a large effect on the level of vibration excited in the clubhead and the methodology behind generating smooth robot swing profiles is presented. The mathematical model was used to perform 6 swings and the resulting shaft deformation and clubhead vibration were compared with data from human swings. It was found that the model was capable of producing swing variables comparable to human swings, however in the downswing portion of the swing the magnitude of these variables were larger for the simulations. Simulations were made which sought to demonstrate the difference between the model replicating the rigid robot and a compliant system. Reductions in vibration were achieved in all swings, including those driven with robot feedback data which contains oscillations excited by the method with which the robot is driven.

List of figures

List of tables

Publications

Ellis KL, Roberts JR, Sanghera J. Development of a method for monitoring clubhead path and orientation through impact. 8th Conference of the International Sports Engineering Association (ISEA). Procedia Engineering 2010 6;2(2):2955-2960.

Chapter 1

Introduction

1.1 Thesis Context

Historically, robots were created to take the place of a human in scenarios which were undesirable or unsafe for a human being. More recently as technology has progressed, they have been implemented as a means to simulate humans and human motions. One avenue where the use of robots has become more prominent is in the testing of sports equipment, where a defined motion is required to be repeated to enable variables that can be attributed to a change in the equipment to be measured. Robots are viewed as preferable in this instance as a human subject can tire and is unable to repeatedly produce precisely the same motion; this makes it difficult to differentiate between variable changes due to the equipment and those due to a change in the subject's motion. However, developing a robot which can simulate a human motion is problematic, particularly for fast movements such as many racket and bat sports, and in the area in which this research is concerned, golf. There is usually a trade-off between the speed and accuracy of the motion and its similarity to the motion of which it is simulating. Robots are frequently actuated by a motor, and the drive transmitted to the end effector being via a system of gears. The robot would most likely be controlled by a PID controller which monitors the robot's positional error and attempts to correct this with near instant accelerations, with the goal being to match the input position regardless of how severe the acceleration changes may be. A system which lacks compliance and is driven with a turbulent acceleration profile will be susceptible to vibration problems.

A human motion which has been simulated by a robot is the golf swing. Clubhead path and orientation contribute significantly to the outcome of a shot and these clubhead parameters are determined by swing biomechanics and shaft deformation. Repeatability of individual swing parameters with a robot would allow a scenario where golf clubs could be custom fitted to a particular individual's style of swing as well as allow the testing of golf equipment under a more realistic loading. The research laboratory in the Sports Technology Institute at Loughborough University

houses two of only 4 golf robots in Europe. One of these, the Miyamae Robo V, has the potential to be the most advanced golf robot in the world. However, the usability of this robot, as with other robots of this type, is dramatically decreased due to the vibrations it excites in a golf club during a swing simulation. This issue needs to be addressed as the vibrations excited in the clubhead cause an unrealistic shaft loading during a swing and it is hypothesised that this subsequently results in a clubhead orientation very different to its expected position for the swing being simulated. With the progression of technology and the increase in competition seen in golf, a robot which is able to accurately simulate different golfers' swings rather than performing a standard unrealistic swing profile is now quite fundamental.

Harper (2002) made a substantial progression towards this goal during research that modified the method by which the Miyamae Robo V robot is programmed. Harper developed a methodology which involved collecting kinematic data from golfers' swings and generating individual swing profiles as a method to drive the robot to replicate each golfer's swing. The success of this method was varied. While the robot was capable of repeating the angular positions of each swing profile, the swing variables were not analogous to the variables measured for the corresponding golfer's swing. It was hypothesised that initial erratic accelerations of the robot were creating unwanted oscillation of the clubhead that intensified throughout the simulation, culminating in a violent finale.

Schmidt (2007) studied the grip force applied by a golfer to the golf club grip during a golf swing and found that each golfer possesses a very unique and dynamic grip force profile. Based on this it was hypothesised that the method by which the golf club was rigidly clamped into the robot lacked the compliance and damping of a human hand which was contributing to excessive club vibrations. Schmidt's findings led to the rationale that adaptions of the robot may be required, with the method of attaching the club to the robot being of greatest interest.

In the more general case of robot induced vibration into flexible objects a successful solution that has been reported is to actively damp the vibrations through altering the trajectory of the robot's end effector to essentially cancel out the vibration (Henrich (2000), Schutter (1996), Ragunathan (2008)). An active solution with regards to altering the robot's simulated motion is not possible for this situation where the

simulation of a precise motion is being attempted. An alternative solution could be found in the application of a passive solution, such as in the study by Lin (1999) where a compliant material is used to reduce the level of vibration in a system. A passive approach was taken in this thesis, through the consideration of how the structure of the robot could be adapted to increase its similarity to a human.

1.2 Aim & Objectives

The aim of this thesis is to reduce clubhead vibrations during swing simulations with the Miyamae Robo V with a view to better replicating club dynamics during a golfer's swing. This aim will be achieved by meeting the following objectives:

- To measure the current level of clubhead vibration present in robot simulations to provide a level to which improvements can be quantified against
- To develop measurement methods to enable club dynamics such as shaft deflection, club vibration, clubhead path and orientation at impact to be quantified.
- To collect kinematic data from a range of golfers which can be used as inputs for swing simulations.
- To collect corresponding club dynamic data against which swing simulations can be evaluated.
- To investigate the effect on clubhead vibrations of adding a visco-elastic gripper to the robot
- To develop a mathematical model of the golf robot to enable virtual golf swings to be simulated.
- To measure material properties of the aforementioned visco-elastic gripper to enable validation of the mathematical model
- To use the mathematical model to investigate the effect of design changes without the need to dismantle the robot or develop a multitude of physical prototypes.
- To evaluate the success of the simulations generated by the mathematical model and to make recommendations for future design changes to the robot.

1.3 Thesis Structure

Following a thorough review of the literature relevant to this work, an in depth study was conducted of the relevant variables that constitute a golf swing. A sample of 14 golfers each performed 20 full drives with an instrumented golf club. During each swing, a CODA motion analysis system was implemented to capture the biomechanics of the swing to provide data to program the robot as well as provide a

time of impact for the mathematical models. Other measured variables included shaft deflection, clubhead acceleration, clubhead trajectory and clubhead orientation. A new methodology was generated to measure and process clubhead trajectory and orientation through an analysis of its six degrees of freedom. A subsidiary study was made of the robot's swing in order to demonstrate its deficiency in simulating a golfer's swing with regards to shaft deflection and clubhead acceleration, the two factors of concern in this study.

A passive gripping mechanism was developed to provide an early indication of the results, in terms of effectiveness at damping clubhead vibrations, which might be achieved through implementing different materials as a vibration absorbing layer between the robot and the golf club. Initially a pneumatic grip was developed, which could be inflated to a range of pressures, resulting in a simple method of adjusting the grip's spring properties. A satisfactory level of damping could not be achieved as the damping element of the mechanism was provided solely by the rubber, and this value was a constant. A materials selection process was undertaken to find a material that would most suit this application. A silicone was selected as its properties could be tailored to mimic those of skin while provided flexibility in production, as a range of silicones could be cured with differing properties. Silicones grips containing 0%, 25% and 50% deadener were cured, with the most compliant (50% deadened) silicone providing the highest levels of damping and lowest stiffness. Clubhead vibration was dramatically decreased and the decision was made to mathematically model the system to provide a method of selecting optimal material properties that a grip should possess and an insight into further changes that could be made to the robot to decrease further the level of clubhead oscillation.

A mathematical model was derived to simulate the club and the motion of the robot's collet clamp during a swing and the effect of adding springs and dashpots between the robot collet and the club were quantified. Initial modelling involved a fixed collet where the clubhead was set into motion and the response observed. This was then compared to measured clubhead responses from a robot grasped club and good agreement found. Material tests were carried out on silicone samples produced in the preceding chapter and spring and damping constants were derived so that they could be entered into the model simulations to provide model validation. A further iteration was made to allow the collet to be driven with a torque profile (later adapted

to a position driven model to increase similarity to the method of robot control) and again these responses were found to have good agreement with measured data. Tests conducted to determine the level of clubhead vibration in a human grasped club during a simple swing revealed the flexibility of the human wrist and led to the premise that the addition of a flexible wrist joint could provide a much higher level of damping than a simple visco-elastic gripper.

A second model was developed to include a flexible wrist joint after was found that a compliant grip could not provide enough damping to provide a clubhead motion comparable to that of a golfer. It was predicted that the model required an additional element comparable to the flexibility of the human wrist. The final model featured an arm link and flexible wrist joint. Positional data could be used to drive both the wrist and arm link and the clubhead response was monitored. The flexibility exists between the robot grip and the drive at the wrist.

The robot control method was considered as an additional means of tackling the issues with vibration to work alongside the addition of compliance. A complimentary investigation was made by a student at Loughborough University (Cockram, 2010) into developing a new method of producing swing profiles to provide swings with a smooth acceleration profile throughout resulting in a reduction of clubhead vibration from the initial takeaway. The resulting swing profiles were found to reduce the acceleration induced vibrations in the robot/club system and were implemented as a drive for all further simulations.

Validation of the success of the model's ability to simulate a golfer's swing was completed. Variables such as shaft deflection and clubhead acceleration measured from a selection of golfer's swing are compared to those from a simulation of that swing.

Finally recommendations are made for future design changes to the robot. Implementation of these changes is outside the scope of this research. This thesis is closed with a summary of its contents and a recommendation for future work.

Chapter 2

Literature Review

2.1 Golf

The game of golf has come a long way since the days when the ball was a pebble and the club just a simple stick in the 1500's, when it was first invented on the East coast of Scotland. As with most modern day sports, the huge increase in competition has led to levels of research and development in sports equipment escalating to the point where every aspect of a product down to the size of the dimples in a golf ball is under scrutiny. Every human is unique and no golfer has exactly the same style of swing, it is logical therefore that one golf club does not fit all.

2.1.1 Custom fitting golf equipment

Many different aspects of a Golf club can be customised to the individual golfer, but of most interest to this study is the shaft due to the difficulties found previously in reproducing a player's shaft deflection profile with the Miyamae V. The long term aim of this research is to develop a robot based on the Miyamae V that is accurate enough in simulating golfer's swings that it can be used in the process of producing custom fit equipment.

At present the most common form of club fitting is shaft fitting, even though the shaft still remains the most mysterious component of a golf club (Wishon, 1992) in terms of its role in the swing. Many theories have been made of how it contributes but so far there has been limited scientific proof to back up these claims and they remain just that. Early shaft fitting consisted of matching a strong player to a stiff shaft and a weaker player to a flexible shaft. Once club manufacturers started to release more information about their shaft's properties, club fitting advanced a stage to matching clubhead speed and ball carry to shaft flexibility (Wishon, 1992). More recent methods of shaft fitting consider the flexibility of the shaft, the material it is made from and the bending distribution of the shaft (Wishon, 1992).

2.1.2 Shaftlab

The Shaftlab system is a shaft fitting tool which bases its recommendation on the deflection of the shaft during the swing. The system uses clubs instrumented with 2 strain gauges mounted just below the grip, one in the direction of the shot measuring lead/lag deflection and one perpendicular to measure toe up/toe down deflection. The gauges measure the deflection in each of these directions throughout the swing and their outputs give a deflection profile for that particular golfer in the form of a plot of inches of deflection at the clubhead versus time. The loading profile that a golfer produces fits one of 3 standard types, ramp, peak and double peak and illustrates the way that the golfer utilizes the flex of the shaft i.e. the timing of the wrist uncocking (Butler and Winfield, 1994). Based on the level of deflection, a type of flex is advised; the higher the deflection of the shaft, the stiffer the recommendation.

2.1.3 Modelling the golf swing

To aid analysis of the golf swing so that recommendations can be made to improve technique and performance, many authors have developed golf swing models. The first, developed by Cochran (1968) models the swing as a double pendulum as shown in Figure 1. The fixed pivot represents the hub position; this is defined as a point midway between the shoulders of the golfer and is the point about which the two levers rotate. The upper lever represents an imaginary line from the hub to the golfer's hands and the lower lever represents the golf club. A golfer’s left arm will remain straight throughout a swing; this enables the assumption that the upper lever remains at a constant length. There is a hinge between the levers which defines the wrist and restricts it from cocking more than 90˚, around the maximum range of a wrist. An interesting finding of this model was that when set in free fall from the top of backswing, driven by gravity alone, this model completes a motion that is a good simulation of a golf swing.

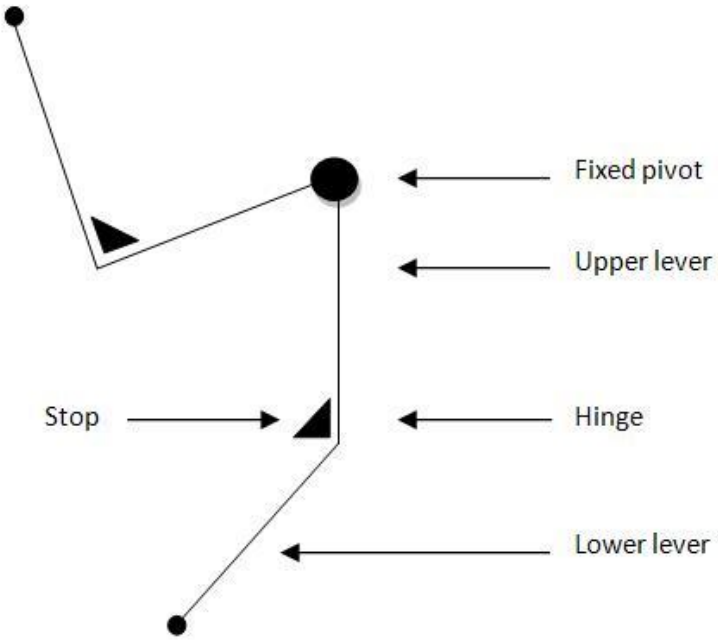

Figure 1 - Double pendulum model of a golf swing (adapted from Cochran (1968))

When a golfer swings a club, the motion of the golfer's arms and the club can be approximated to a single plane, dubbed the swing plane. Therefore, to complete the golf swing model, it needs to be rotated to the angle of that golfer's swing plane. Cochran (1968) recognised that between players the angle and position of the swing plane changed slightly whereas other authors have defined the plane as a line from the neck down to the clubhead (Snead,1961) or even a plane based purely on the path that the club follows (Blakemore, 2013).

Many versions of this model have been produced, some more complex such as the triple pendulum proposed by Campbell and Reid (1983), where an extra lever was added above the first to represent the rotation of the shoulders. Cochran (1968) also adapted the double pendulum into a triple pendulum with the second hinge representing the 'whip' of the shaft.

The Miyamae V's architecture is based on the double pendulum model which simplifies the motion while maintaining a good simulation of a swing as well as repeatability. The robot's grip however is a simple collet mechanism which is proving an unrealistic method of replicating the golfer's grip; allowing vibrations from the

robot to be transferred to the club whilst not providing a sufficient level of damping of any induced clubhead vibration.

2.1.4 The golf grip

Many authors have differing views of the importance of a golfer's grip to a good swing as well as the level of pressure and where this pressure should be applied. It is the view of Snead (1961) that playing golf is not possible without a good grip whereas Luxton (1985) places less importance on the grip and has the opinion that as long as there is the realisation that the way a club is held can affect the angle of the clubface to the ball, then this is enough. There are three basic grips in golf as illustrated in Figure 2; the overlap, interlock and the baseball grip, the overlap being the most popular (Irwin, 1980). The type of grip selected is based on player preference and recommendations from professionals such as the view that a baseball grip will best suit a player with small hands (Irwin, 1980).

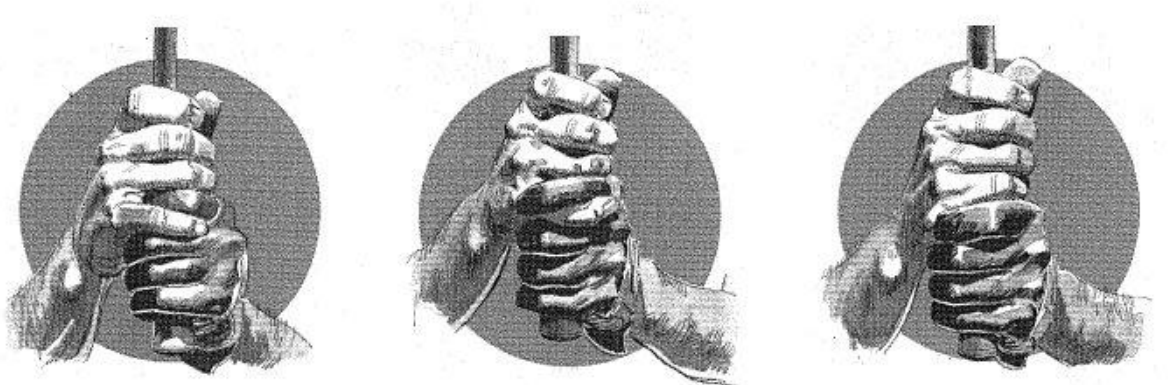

Figure 2 - The 3 basic grips (Irwin, 1980)

During a golf lesson, an instructor can instruct the pupil on how to hold and apply force to the golf club grip, but it can be difficult for the instructor to assess whether the pupil has successfully implemented the instructions. Budney (1979) presented the idea of using an instrumented golf club so that an instructor may compare the

grip pressure applied with the instructions given. The instrumented club contained electrical resistance strain gauges in the grip of the club to measure grip force applied in key areas said by authors to be the most crucial to the grip. Schmidt (2007) used thin film force sensors to measure total grip forces applied to a golf club grip and reported the phenomenon of grip force 'signatures' where a golfer's total grip force was consistent from swing to swing but varied between golfers. Schmidt (2007) also found that the grip force applied was linked to the amount of vibration transferred to the player's hands. The outcomes from these studies, particularly the discovery of grip force 'signatures' has led to the belief that the problematic oscillations present in the Miyamae's swing could be due to the rigid grip and that a new method of attaching the club to the robot will need to be developed.

2.2 Robots

New technology in the field of robotics is forever advancing especially in industries where there are large sums of money available to spend on research and development. There has always been a fascination with the creation of new technology in robotics perhaps because of the desire to be able to build a machine as complex as a human.

Japan is at the forefront of robot technology, now with 295 robots per 10,000 workers (Jones, 2009). The low birth-rate in Japan means that in just 3 years' time, 25% of the population of Tokyo will be over the age of 65 resulting in a dramatic increase in demand for carers, the plan is that they will come in the form of humanoids (Jones, 2009).

Using robots to test sports equipment has been a very logical step. Human subjects often have limited availability, are unable to exactly reproduce the same action more than once (even elite sports people have slight variations in each swing), and will suffer from fatigue. When testing a sports product, it is desirable to be able to repeatedly produce a motion so that the only variables are in the equipment.

2.2.1 Golf robots

As mentioned previously in this report, golf swings are most frequently modelled by the double pendulum model and this is also the model which most golf robots are based upon.

It has been shown that when developing a robot to simulate fast sports actions, there is usually a trade-off between level of accuracy & repeatability and similarity to real life. When trying to model every aspect in as much detail as possible, more potential for errors is introduced and the robot motions are far too complicated to be achieved at the highest speeds. The simple double pendulum model used for golf swings has been found to be a good compromise in terms of these two extremes.

Loughborough University has two golf robots, the Miyamae III and V golf shot robots shown in Figure 3 and Figure 4 and respectively. Of the two, version V is the more advanced and allows the user to have a higher level of control over the type of swing the robot executes. Both robots have the same three axis of rotation but the Miyamae III's are linked together through a series of gears and belt drives reducing its capabilities to one standard golf swing with only the speed of the swing being user defined. The Miyamae V allows the input of a user defined swing profile where the profile for three axis of rotation can be defined. Therefore, it is The Miyamae V robot that is to be developed further in this research to achieve the most accurate simulation of a golfer's swing.

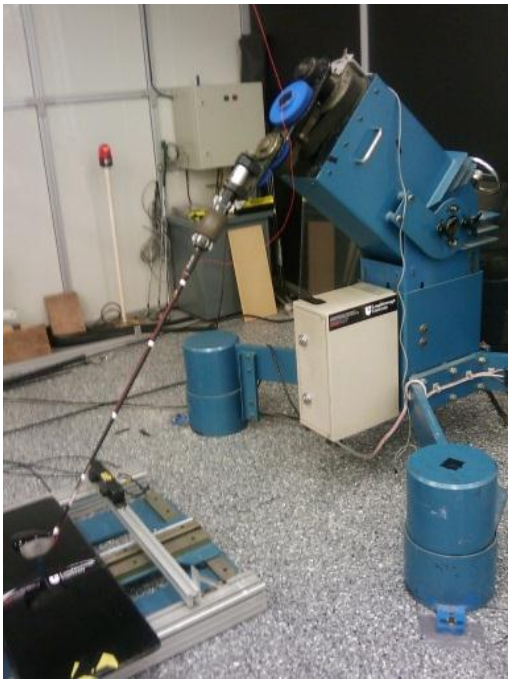

Figure 3 - The Miyamae III

Figure 4 - The Miyamae V

Previous work conducted by Harper (2006) involved collecting kinematic data of golfers' swings and programming them into the Miyamae V. The Miyamae V has a similar architecture to the double pendulum model, with its 3 axes representing the arm's rotation around the hub (first link), the wrist cocking angle (second link) and the grip rotation. A robot swing profile can be created by defining these angles at 1000 points throughout the swing; an example profile is given in Figure 5.

In Harper's study, the robot was capable of following the pre-defined swing profile angles to within ±5 degrees and appeared to be accurately simulating the whole swing. However, when measuring shaft deflection using the Shaftlab system, the robot was found to load the shaft with a completely different strain profile compared to the golfer. When the robot's shaft deflection profile was measured, it was found to be unlike any of the standard 3 deformation patterns.

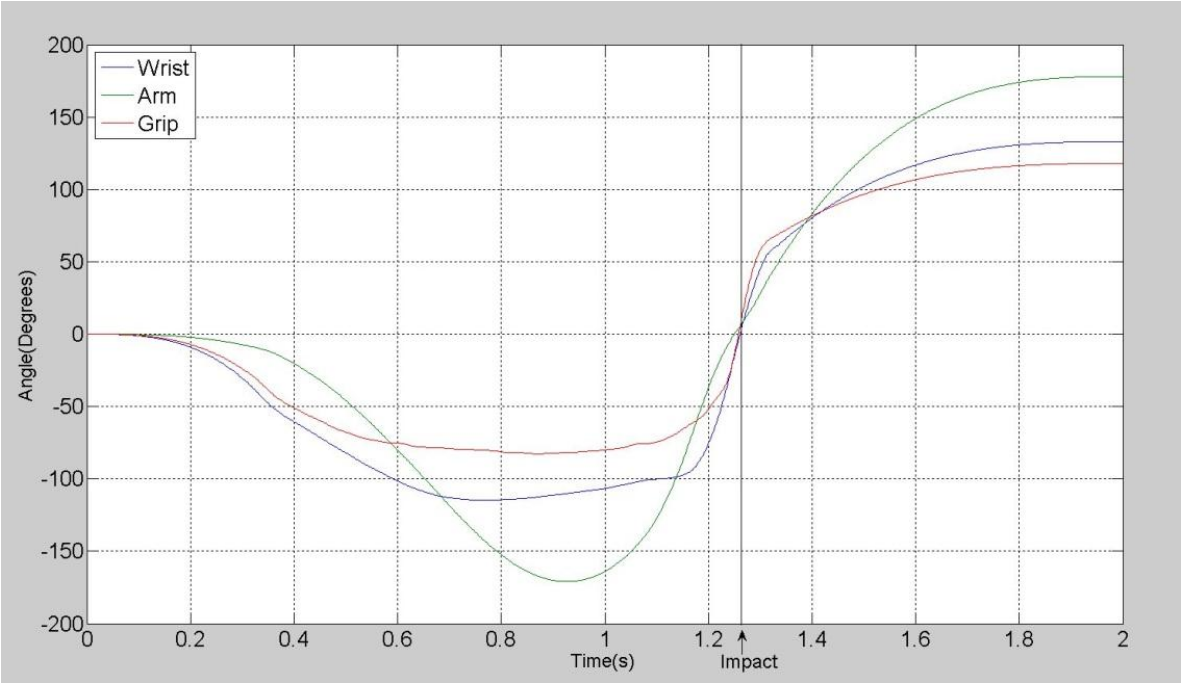

Figure 5 - Swing profile plot

Figure 6 is an example of a golfer's ramp shaft deformation profile as measured by Shaftlab; the graph shows the deflection of the clubhead in inches in the toe up/down direction (blue line) and deflection in the lead/lag direction (pink line) up until impact. The second part of Figure 6 shows a shaft deflection profile of a club swung by the robot programmed to simulate the same golfer's swing. Oscillatory motions are clearly visible in the club response during every swing performed by the robot. It was concluded that these oscillations were amplified by the rigid grip of the robot which meant that characteristics such as dynamic loft angle, attack angle, clubhead speed and consequently ball launch conditions, would all be different when comparing the robot's swing to the golfer's, limiting the validity of any equipment tests carried out by the robot.

a) Golfer's swing

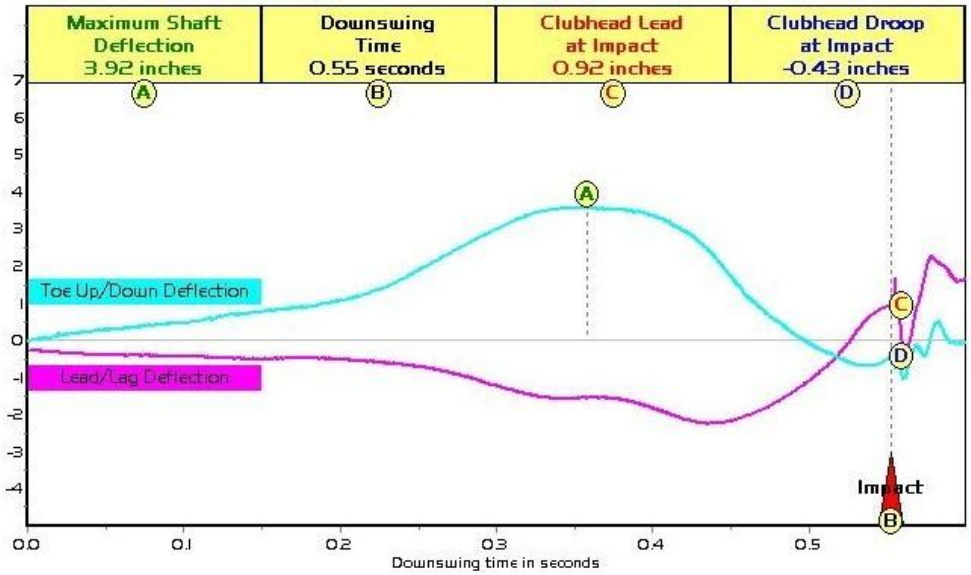

b) Robot swing

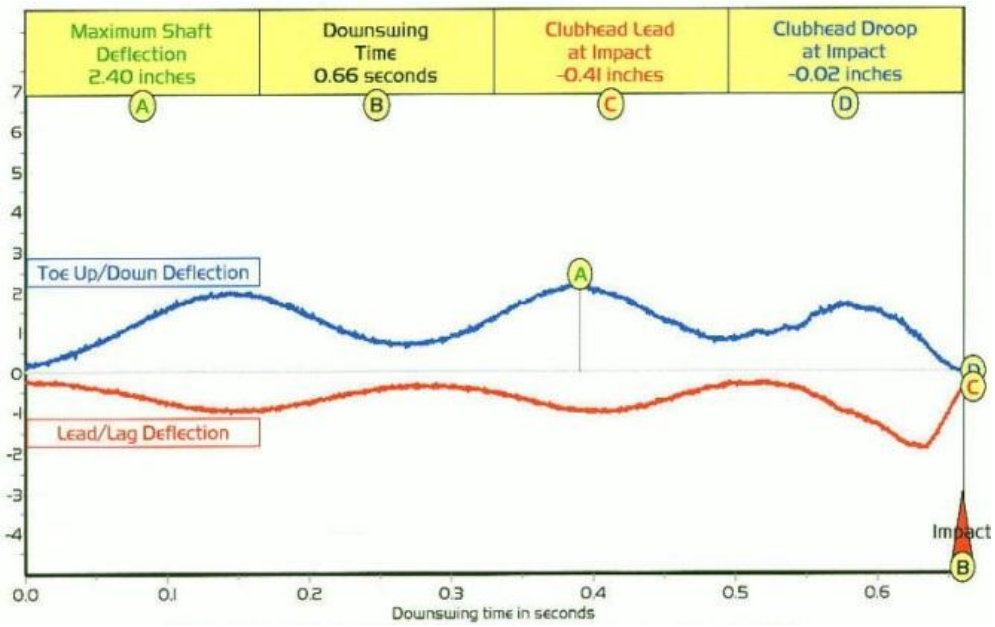

Figure 6 - Shaft deformation when a) swung by a golfer b) swung by the Miyamae V golf robot (Harper, 2006).

2.2.2 Other racket sport robots

The research carried out by Lin (1999) on the development of a tennis robot is probably the most relevant to this research. This study by Lin describes the development of a robot quite similar to the Miyamae V but rotated to move in the horizontal plane. The robot models the tennis swing with two links, the first being the lightweight Carbon Fibre Reinforced Plastic (CFRP) and aluminium robot arm and the second, the tennis racket. There are two motor driven joints, one either end of the robot arm representing the shoulder and wrist. In order to accurately represent the human tennis player's grip, damping characteristics of the human hand were considered and recreated through both experimental means and simulations. During the experiments, a tennis racket embedded with strain gauges was used to determine the vibration characteristics of the swing. Results were achieved on a trial and error basis where different thicknesses and types of visco-elastic materials were attached inside the grip until one was found to provide the same strains in the racket as a human tennis player. A more precise method of material selection was also implemented through the derivation of a mathematical model. The whole tennis robot system was modelled, robot, racket and ball. The racket was modelled as a 1D flexible beam and solved by the Gauss Runge Kutta method and the ball and strings as lumped masses. Through simulation the following parameter values were selected for the viscoelastic material, an elastic constant of 1.2*10^4N/m and a viscosity co-efficient of 6.0Ns/m. The results of both methods are illustrated in Figure 7, which shows the strain variations in the tennis racket in 3 scenarios, grasped by the human, the robot with attached visco-elastic material and as calculated mathematically. Both approaches were found to work well with strains being created in the racket similar to when held by a human. The limitation of the information presented in this report is that the tests were carried out with the robot's arm stationary instead of completing a full tennis swing. As both the golfer's and (one would assume) the tennis player's grip forces are dynamic throughout the swing, this is an unrealistic test and does not fully model the damping characteristics or forces applied by a human hand. The experiment conducted was also an inaccurate test of the racket as it was not undergoing the correct forces that it would experience in a swing, this method was more of a quick fix to something which could be a problem with the destruction of tennis rackets when tested at full speeds in a rigid clamp.

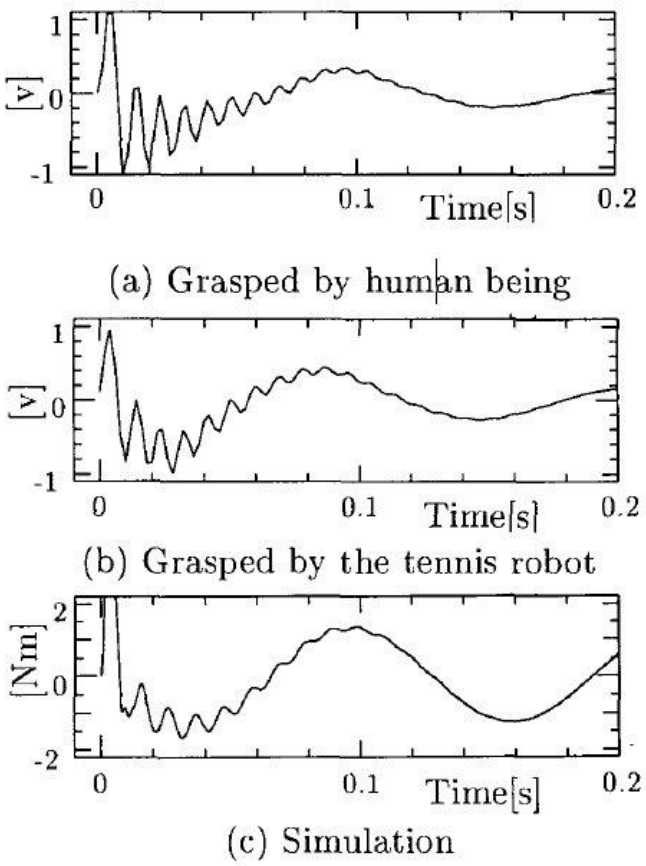

Figure 7 - Strain variations in tennis racket (Lin, 1999)

A non-robotic device has also been used for the testing of rackets. The Manusimulator (see Figure 8) was developed and used by Hatze (1976, 1992) in many of his studies on the properties of tennis rackets. The Manusimulator is a passive arm mechanism with the same architecture as the human arm, capable of moving with the same ranges of motion and embodying all of its important properties such as tissue and muscle simulators (Hatze, 1992). The motion of the arm can be described by three co-ordinates representing the shoulder motion, two for the elbow and two for the wrist (Hatze, 1992). Characteristics such as the sizes and masses of major sections of the arm were based on the averages of four typical male tennis players. Muscle contraction in skilled players was measured and recreated by the arm's muscle simulators in order to produce the same joint torques. An experiment which considered an alternative direction to Lin's was conducted with this simulator

where grip bands on rackets were tested for their damping properties, but instead of determining their effect on vibration in the racket, the tests were aimed at finding their effect on level of vibration transferred to the players arm.

The Manusimulator produced reliable and accurate results but has remained mostly disused since the 90's due to its lengthy set-up time. Generally in the case of human mimetic robots, complex systems are abandoned in favour of something that gives a good repeatable and solid approximation, rather than something which simulates every component and results in a level of complexity which is not required.

Figure 8 - The Manusimulator (Hatze, 1992)

Due to a competition proposed by John Billingsley, who in 1983 defined a set of rules for the game of robot ping pong, there have been many robotic ping pong players developed (Modi, 2006; Andersson, 1989; Fassler, 1990). This was followed up by the formation of the European ROBAT championships in 1985. One of the most successful designs to evolve from this competition was Fässler et al's 1988 entry which won against three other entries from universities in England, Finland and Sweden (Fassler et al, 1990). The reason behind development of these robots was not for testing sports equipment or to produce any new information which could advance the game or player ability, it was merely to produce a challenge to new young engineers and to advance technology in robotics, robot control and vision

(Modi, 2006). Because of the rules imposed by Billingsley, the robot game of ping pong was quite unlike that of the actual game and meant that the only requirements placed on the motion of the robot were for it to move in a single plane. The robot 'arm' used in Fässler's research composed of the ping-pong racket actuated by a lightweight pulley system giving translational motion in two directions, the 'hand' also has rotational motion about both two axis' actuated by Bowden cables.

Perhaps the most interesting outcome from these studies is the development of robots that are capable of working in changing environments one of the main reasons why humans are unable to enter a robots workspace (Fassler, 1990). The vision systems developed in these studies are sensor driven and are continuously changing their path depending on the obstacles met.

2.3 The human hand-arm

2.3.1 Anatomy

The human hand-arm is essentially the mechanism that this study is aiming to mimic with the possible addition of an interface which can be attached to the Miyamae V to provide a similar level of damping as the human hand-arm does to a golf club. Through the understanding of how a human hand works and the theory behind its control, key elements can be drawn out which are necessary to create a gripping mechanism that behaves in a similar manner. It has been found that often, the best solutions to problems arising when designing a dexterous robot hand can be found from the way nature has evolved the human hand (Saliba, 1997).

The human hand and wrist contain 27 bones in total (Jones, 2006). Each finger consists of a proximal, medial and a distal phalanx illustrated in Figure 9. The proximal and medial are connected by the PIP joint and the medial and distal by the DIP. A third joint is located at the knuckle and is called the MCP joint. The thumb however, lacks the third phalanx but has an extra rotational degree of freedom (DOF) which allows it to oppose the fingers. Angle of abduction of the thumb is about 70˚ and when the hand is placed palm down on a flat surface, the thumbs natural resting angle is at 20˚ to the surface (Saliba, 1997).

The PIP and DIP joints allow flexion and extension of the digit, whereas the MCP also allows abduction and adduction motion. The metacarpal bones are an unseen extension of the finger, extending from its base at the MCP joint down to the wrist; the palm region of the hand is therefore not a flat plate but is dominated by these bones which allow it to produce a cupping form.

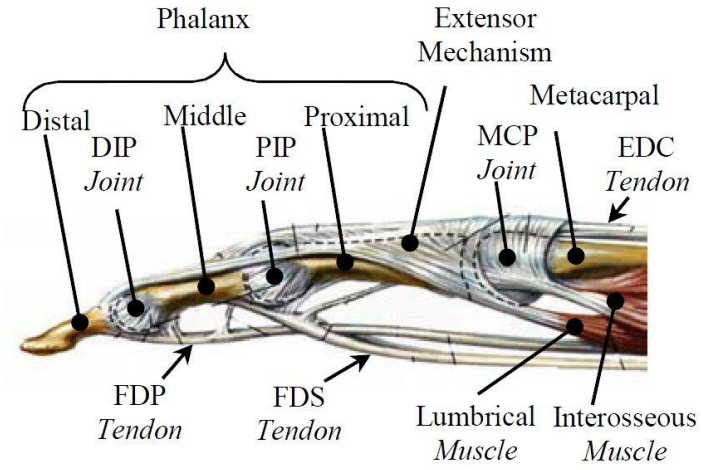

Figure 9 - Anatomy of the finger (Wilkinson, 2003)

The metacarpals connect to the more distal row of 4 carpel bones in the wrist and the remaining 4 in the proximal row are connected to the radius and ulna bones in the forearm (Jones, 2006).

The human hand has 27 DOF, 4 for each finger, 5 for the thumb and 6 for the rotational and translational movements of the palm. In many studies on the operation of the human hand, the DOF of the palm are often ignored as they are only required for the gross movement of the hand. This movement can be adopted by the robot's arm (Saliba, 1997). It was discussed by Wilkinson (2003) how the DOF of a finger are reduced to 3 without an external force due to the link between the DIP and PIP which disables them from moving independently from each other. It seems, based on assumptions made and the level of complexity a study wants to achieve, the DOF of the human hand can be considered variable; Price (2007) considers there to be over 25, whereas the Shadow company list 24 (Shadow, 2012).

The total range of motion of a finger is 260 ˚, 85˚ at the MCP, 110˚ at the PIP and 65˚ at the DIP joint.

2.3.2 The muscular system

The human hand is actuated by 29 muscles (Jones, 2006), both intrinsic and extrinsic, via tendons. It is the extrinsic muscles however which contribute the majority of the actuation force.

Muscles work in antagonistic pairs one each for extension and flexion although the force produced at the biological hand is flexion dominant (Wilkinson, 2003). Actuation of each finger is achieved through 6 muscles, 3 extrinsic and 3 intrinsic apart from the index finger which has an extra extrinsic extensor muscle to allow an independent degree of freedom (Wilkinson, 2003).

Actuation is achieved from the muscle to the hand via a tendon. Tendon is a composite material, largely consisting of collagen and elastic tissue (Crows, 1980). Tendons are attached to the finger via a web-like collection of tendon-like material on the dorsal side of the finger called the extensor. The extensor is connected to the proximal section of the distal phalanx and the proximal section of the middle phalanx at a small distance from the joints to create a torque. Another function of this mechanism is to keep the tendon close to the skeleton to prevent bowstringing (Price, 2007). Wilkinson (2003), developed an artificial extensor for an anatomical robotic hand based on an in depth study of the biological equivalent, this had not been done before due to the complexity of its structure.

The biological muscle also plays the part of a dashpot in the human body, providing damping of vibrations. Its combination of properties has so far been difficult to reproduce with an artificial equivalent. Muscle fibres aren't themselves very elastic; a muscles change in length is mainly due to Actin and Myosin protein filaments shown in Figure 10 sliding past each other. The actuation forces are generated in the cross-bridges between these filaments (Alexander, 1988; Crowe 1980). Whilst small elastic length changes can occur without detachment of these fibres, larger displacements require the cross-bridges to detach and reattach further along. Huxley and Simmons (1971) (cited by Alexander, 1988) found that the majority of the compliance present in a muscle is from the cross bridges.

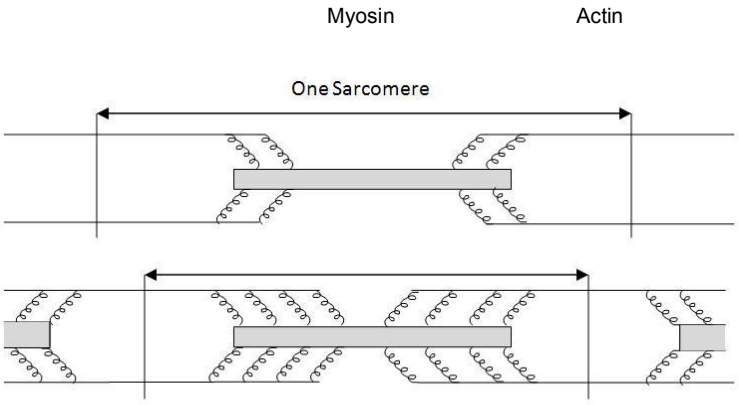

Figure 10 - Diagram of striated muscle adapted from Alexander (1988)

Power density of muscle is 200 mW/g and the force per cross sectional area it produces is in the region of 20-40N/cm^2 (Caldwell, 1990).

The maximum grip force at the fingers is in the region of 80-110N, whilst at the muscle the force generated is around 3.3 times this value (Biddiss, 2006). Muscles contract between 0-100% with stresses of 0.007-0.8MPa, joint angular velocities of 3-8rad/s are general for grasping movements. Mid humorous to hand weighs 3kg (500g hand only) although the drive towards finding lightweight actuators to drive prosthetics is due to the prosthetic wearer finding a prosthetic hand of similar weight to its biological equivalent uncomfortable (Biddiss, 2006).

2.4 Robot end-effectors

In order for a robot to interact with its surroundings, it requires an end-effector, the human equivalent is the hand. A robot end effector can be as simple as a brush or at the more complex end of the spectrum, an anthropomorphic robotic hand, capable of moving with the same DOF's as a human hand. The end-effector is the last element in the chain from the programming of the robot to the completion of the programmed manipulation of its environment. The Miyamae V's existing end-effector (shown in Figure 11) is a simple collet grip in which the golf club is rigidly clamped. Due to the robots problematic oscillations it is apparent that this grip does not correctly simulate the human golfer's.

Figure 11 - The current grip on the Miyamae V golf robot

The ensuing section of the literature review examines existing robot end-effectors in order to assess the current technology in this area and discover whether or not the challenges faced in this project have been considered previously and identify any existing designs which have attempted to overcome these issues.

2.4.1 Complex gripping mechanisms

The idea of dexterous robots isn't new; the first were being developed as early as the 1980's, but most work in the field of robotics has tended to focus on a more obvious human characteristic, walking. It has been commented that after decades of research into robot gaits and navigation, we now have robots that can walk down the hall without bumping into the walls but it seems we have forgotten why we wanted to get there in the first place (Huang, 2006).

Current levels of research involved in developing dexterous robotic hands are high,

mostly in the interest of developing a prosthetic hand which is as life-like as possible; this is due to the large number of rejected prostheses (due to weight, lack of degrees of freedom and general awkwardness in use). Another incentive for the large amount of research in this area is to produce a robot capable of mimicking a human in every way (moving, interacting with things, generally able to take the place of a human). This would be particularly useful for space exploration. When a mission is unsuitable or too dangerous for a human, a robot could take their place or even tackle more everyday tasks like automated care for the elderly (Huang, 2006).

For these two applications, particularly in the case of the prosthetics, one of the most important specifications is a low mass. For this reason a large emphasis is placed on simple lightweight mechanisms and finding a new actuator technology that is small enough to be housed inside the hand. Another important consideration is number of DOF's; to make a robotic hand as life-like as possible, it needs to have the same range of movement as a human hand, and this has been achieved by many research groups (Wilkinson, 2003; Nishino, 2007; Schulz, 2001).

The maximum number of DOF of a human hand is 27 but as the small finger is said to add little to dexterity of a hand, it is seldom included in robotic hand designs (Saliba, 1997). It is this opinion and the level of complexity required by the robotic hand that results in a wide variety of hands with differing degrees of freedom. Of the anthropomorphic hands which have been developed, there are three, four and five fingered hands. The three fingered hands reviewed all have 9 DOF (Fischer, 1998; Price, 2006; Cura, 2003; Doll, 1989), with four fingers the DOF implemented have been either 10 (Saliba, 1997) or 12 (Cura, 2003) depending on the number of couplings between joints. Five fingered hands tend to have a lot higher DOF (4 DOF (Wilkinson, 2003) 13 DOF (Schulz, 2001) 16 DOF (Nishino, 2007) and 24 DOF (Shadow, 2012)) as the inclusion of the fifth digit implies the developer is trying to achieve a high level of anthropomorphism. As well as a range of freedom of movement, anthropomorphic hands have been constrained to have the same range of movement as the human hand as well as allowing abduction/adduction at the MCP joints (Price, 2007; Nishino, 2007) to increase realism when implemented as a prosthetic. The linkage between the PIP and DIP joint which causes the rotation of the middle and distal phalanges to be co-dependent on one another can be replicated by a gearing mechanism coupling the two joints (Saliba, 1997).

It seems that every mechanism in the human hand can be replicated in terms of motion but it is the actuation that provides the real challenge, as compromises have to be made. If a robotic hand is designed as a prosthetic then the major concerns are space and safety in contact with humans. The limited space requires actuators to be miniaturised as ideally they should be small enough to fit inside the fingers, therefore only small forces and small strains are achievable. Nishino (2007) installed small pneumatic actuators inside a robotic hand which provided enough force to hold a pen and perform other daily tasks in life. Space is also an issue when implementing shape memory alloy (SMA) actuators as the strain is proportional to the length of wire (Price, 2006). At the other extreme, the Shadow hand (declared by the Shadow Company as the most advanced dexterous hand in the world) requires a bank of 40 air muscles for actuation, located remotely from the hand. It is capable of producing forces that are comparable to the biological hand but as the Shadow company states, it is 'not as strong as a human and due to the lack of palmer DOF, its grip is nowhere near as stable' (Shadow, 2012). The speed of this hand, although variable at different parts of the hand, is always below half that of the biological equivalent. Generally, the full force production of a human hand has not been replicated; when considering the case of a prosthetic hand, it is generally unobtainable due to limited actuator size, whereas when considering a robot hand, the force output is restricted to ensure a safe machine human interaction.

Following biological inspiration, many researchers have adopted a tendon based system to deliver actuation forces to the hand. Flexion of the fingers is always the controlled variable whereas extension can be either driven by an antagonist muscle or through use of a simple return spring. For a fully anatomically similar hand design, an intricate mechanism such as the extensor mechanism has been replicated to study its relevance to the design of the hand (Wilkinson, 2003).

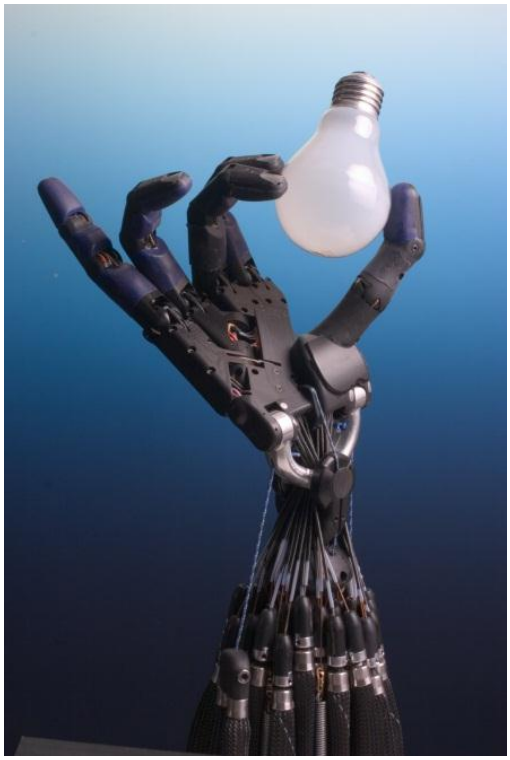

Figure 12 - The Shadow robot hand (Shadow, 2012)

Tactile sensing has been implemented in many robotic hand designs to enable control of the applied force and a step further has been taken by introducing grasp control. Grasp control enables a robot to detect slipping of an object and readjust its grasp. In a human hand, just before macroscopic slip occurs, tiny vibrations occur on the surface of the skin; detection of these vibrations is required to ensure a stable grasp (Ascari, 2009). Previous to the study by Ascari (2009), this had not been achieved due to the difficulties in processing large amounts of data in real-time but was overcome through the use of Cellular nonlinear network (CNN) architecture for the sensory processing.

One area which seems grossly neglected is the development of a prosthetic hand for playing sports, where larger gripping forces are required than for everyday tasks such as picking up a pen. Connecting prosthetics directly to a human's point of amputation has already been made possible by exploiting electrical signals produced by the muscle to cause actuation, where movements are made by 'imagining' them (DW-World, 2011).

So far, technology has been exploited to create a robotic hand that looks and moves like a human hand but not necessarily behave like one. Of all the hands reviewed in

this report, most have actuating mechanisms only capable of producing forces at a fraction of the human hand; this is of course mainly due to safety issues with human-machine interaction, but not a true representation. Another limitation that particularly affects their use in the testing of sports equipment is the way they model the hand in terms of damping and level of compliance. If a robot's 'hand' does not respond to the forces it is subjected to in the same way as the human hand, then even if the robot's range of motion is the same, the stresses applied to the manipulated object will not be and the test will not be representative. An example of this can be seen when using the Miyamae V. Due to the unrealistic loading placed on a golf club shaft by the rigid collet grip, very fast swings speeds cannot be completed without destruction of the golf club shaft.

2.4.2 Industrial robot grippers

As both process speed and demand on time are increased, robots are increasingly being used on production lines to carry out tasks such as welding and painting but their use for assembly has been somewhat limited. In the case of assembly, manipulation of flexible objects could be involved. Where there is a robot manipulating a flexible object, problems are often experienced with vibration whilst at the same time, for an assembly robot on a production line, there is less likely to be funding available for research. This low level of automation in the assembly process causes assembly costs to be one of the most dominating factors in a products final price (Henrich, 2000). It is interesting, therefore, to consider the types of grips used in industry and how these problems are overcome in a world where time is money.

Industrial robotic solutions to problems of this kind, usually take the form of an added vibration damping mechanism between the end-effector and the robot arm coupled with a high level of control, rather than adapting the end-effector which would be specifically designed for a task. This is how Schutter (1996) solved a problem of 'hard contact' when dealing with a rigid robot in a rigid environment.

Another industry where robot manipulation of flexible materials is hindering progress in levels of automation is the textile industry. Of the issues, the main problems are involved with singling out sheets of material, transportation of the material and achieving a balanced grasp (Ragunathan, 2008). Solutions adopted for manipulating

flexible objects in other industries by means of electrostatics, air jets, vacuum adhesives or freezing, have been found unsuitable for material handling, mainly based on the level of damage that could be caused (Ragunathan, 2008). A study by Ragunathan (2008) found a solution to robot manipulation of fabrics in the form of suction cups which could be driven along rectangular arms by a stepper motor.

A non-anthropomorphic robot hand can be referred to as a gripper and is often designed for industrial use. The advantage of using a gripper with multiple fingers is the capability of grasping objects of differing shapes and orientations without changing the end effector. The University of Karlsruhe developed 2 grippers for this application in the early 90's; the Karlsruhe I and II hands (Doll, 1989, Fischer, 1998). The Karlsruhe II saw an addition of a fourth finger to allow more stable grasps and a change in the grip orientation without dropping or losing contact with the object. Forces were measured at the fingertips by force sensors and state sensors provide feedback of joint positions allowing control of fine motions (Fischer, 1998).

2.5 Vibration

2.5.1 Robot manipulation of flexible objects

Vibration becomes a problem where a robot is required to manipulate a flexible object due to the spiky accelerations of the robot. This is all too clear when observing the Miyamae V swing a golf club. A human hand, however, is capable of absorbing these vibrations (Shigang, 2005).

Not only can there be vibration present in the manipulated object but also in a robot's links if they are not suitably damped. Many studies have considered robot manipulation of flexible objects but were concerned with selection and transportation rather than vibration induced problems, however the dynamic behaviour of a deformable linear object (DLO) cannot be ignored when manipulated by a robot (Shigang, 2005).

A few studies have concentrated on reducing vibration in deformable linear objects (DLO's) when moved at fast speeds by robots as these vibrations delay any further operation of the robot (Schlechter, 2002). Both Schlecter (2002) and Yue (2005) considered a situation where a robot is moving a flexible beam and trying to insert it

into a hole. Without any type of vibration control, after the initial fast movement of the object, an amount of time would be required to wait until the vibrations had died down until the next motion could be made. The problems arise from the unknown shape of the object which is influenced by gravity, inertia and contact forces (Schlechter, 2002). Yue (2005) based a solution on the method that a human would use to damp vibrations in an oscillating beam by producing a cancelling motion. The argument is that a robot could not produce the same delicate accelerations as a human, but whether they are required is still unknown (Yue, 2005).

2.5.2 Methods of damping

If a form of vibration is undesirable, then the main means of reducing it are by adding a damping element into the system to dissipate the unwanted energy. In a theoretical spring mass system, when given an initial displacement, the mass will oscillate with a harmonic motion infinitely about its equilibrium position (Thomson, 1996). Vibration can be particularly troublesome when a forced vibration has the same frequency as one of the natural frequencies of the system and resonance occurs which can cause dangerously large oscillations (Thomson, 1996).

There are two methods of damping vibration, either actively or passively. Active damping involves adding a force or additional motion to a system to cancel out unwanted oscillations. Active damping has been implemented for reducing vibrations in flexible structures (Bandopadhya, 2006; Anderson, 2008)) as well as in objects grasped by robots (Yue, 2005; Schlechter, 2002; Chen, 1995).

Two studies which were reviewed (Yue, 2005; Schlechter, 2002) have used a force/torque sensor based approach to actively damp vibrations. The implementation of sensors allows the on-line status of the DLO to be monitored and a sinusoidal corrective motion applied before and after a move is made. The corrective motion applied in (Yue, 2005) is shown in Figure 13 . An 85% reduction in vibration amplitude was achieved by adopting this method (Yue, 2005).

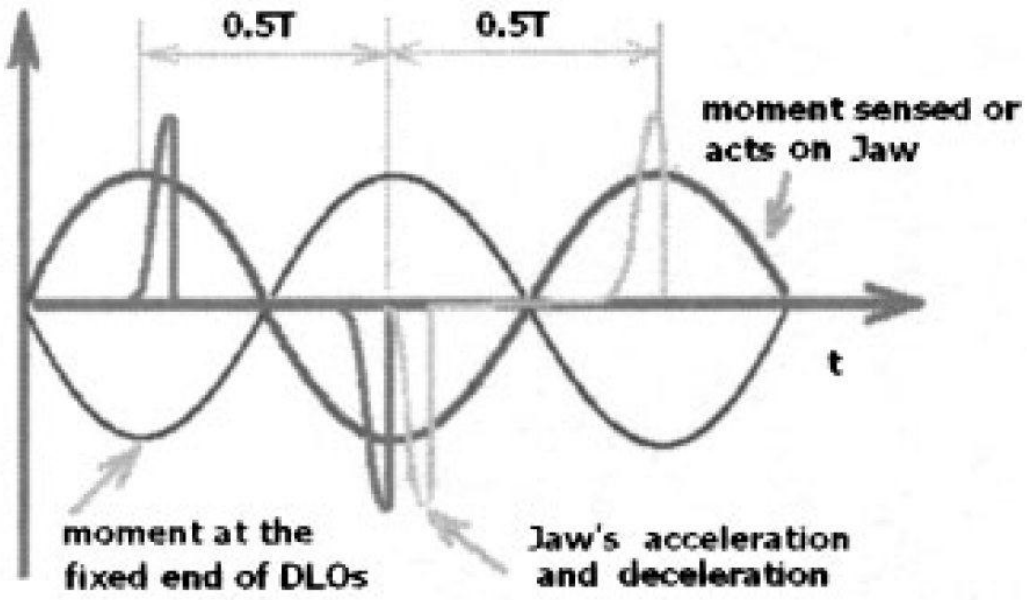

Figure 13 - An active sinusoidal motion correction (Yue, 2005).

A passive approach is achieved by adding an energy absorbing material between the excitation force and the mass which was an additional requirement in the study by Chen (1995) even after the end effector's trajectory had been altered. An example of where a passive approach has been implemented for controlling vibration of a robot is Lin's (1999) development of a tennis robot described earlier, where the passive element consisted of a viscoelastic material inserted into the robot's end effector.

A new approach to passive and active damping of vibrations has been found using smart materials. The most widely used materials for this application are piezoelectric laminates. Based on the theory of piezoelectricity, energy can be harvested from an oscillating system and converted to electrical charge, which is dissipated by connecting a resistor across the piezoelectric element. This creates a viscoelastic damper. If an inductor is also added in series, a damped electrical resonance is created; this is referred to as passive shunt damping (Behrens, 2000; Wilhelm, 2009). These circuits are capable of reducing vibration by 15-20dB (Wilhelm, 2009). For each mode of vibration, a separate piezoelectric laminate and shunting circuit will be required (Behrens, 2000). This can be overcome by connecting a parallel capacitor-inductor circuit in series with each resistance-inductor shunt (Wu, 1998

cited by Behrens, 2000).

This simple approach to vibration suppression is very stable and does not require an external power source (Wilhelm, 2009). An improvement on this system has been found by replacing the large inductor required with multiple pre-charged capacitors so that energy harvested from the vibrations can be used to power the circuit (Wilhelm, 2009). By introducing a sensor and controller, the piezoelectric shunt circuit can exploit feedback to damp multiple modes and converts the system to an active one (Anderson, 2008).

Other smart materials that have been implemented are SMAs (Smith, 1995) and EAPs (Bandopadhya, 2006). The difficulty with using SMAs stems from their complex stress-strain-temperature behaviour (Smith, 1995).

Combinations of both active and passive methods have been found to be most effective. Bhattacharya et al (2000) used a layer of magnetostrictive material as an active damper laminated with a ferro-magnetic passive damper and achieved good results whilst Chen (1995) combined a vibration-free motion trajectory with a passive rubber pad and spring to control robot induced vibrations of a beam. Very large reductions in vibrations were found when changing the motion of the end effector from accelerate-constant velocity-decelerate to two separate accelerations and decelerations.

In this study, the only viable method of damping would be passively. Active damping requires changing the motion of the robot and so is unsuitable, this is due to the importance placed on the trajectory of the end effector as it is one if the main outputs required from the simulation. Active damping could be implemented if it were constrained to the gripping mechanism although a human hand damps vibrations passively and this is the response we are interested in recreating.

2.5.3 Damping characteristics of the human hand

There are three types of boundary conditions that can be considered when trying to determine how an object or in this case, the golf club, is being supported. They are rigidly clamped, free and hand held. A golfer supports the club in his hands, applying a hand-held boundary condition (BC) whereas the rigid collet grip on the Miyamae V

applies the rigidly clamped condition. Although the hand-held condition is closer to a free BC than a clamped one, as both Brody (1989) and Hennig (1992) found, there are still large differences between the two. For example, Brody (1989) compared tennis racket vibrations when the racket was freely suspended and hand-held finding that the hand-held condition led to damping times an order of magnitude smaller than when free. Most previous studies have used the free BC as an approximation to the hand-held although while developing the Manusimulator, Hatze (1992) tried to achieve a balance between rigidly supported and free.

The passive damping methods discussed in the previous section have been applied to the technology of tennis rackets by Head in the development of their Intellifibre range (Head, 2009) and more recently in their skis. These rackets essentially have piezoelectric elements embedded into the racket to damp out vibrations so that less is transferred to the hand. These rackets are capable of damping 20% of racket vibrations in 1ms whereas a traditional racket damps the amplitude of oscillations to half value in 180-750ms (Brody, 1989). This is a large reduction in vibration, but 80% remains and will require damping from the hand which takes place in a rapid time of 20-30ms (Brody, 1989).

This study will involve trying to recreate the hand-held condition on the golf club.

2.5.4 Modal analysis

One method of vibration analysis of a golf club was described earlier in the report involving the use of the Shaftlab system. In order to gain a more comprehensive image of the vibration characteristics of an object, a modal analysis can be carried out this is the method used by Varoto (1995) and Thomas (1995) to evaluate the performance of golf clubs. By mounting an accelerometer onto the club and providing an excitation, the mode shapes and natural frequencies of an object can be found (Rao, 2004). The frequency of the excitation is increased and the amplitude of the response is then viewed in the frequency domain, this produces a plot displaying several large peaks, each peak corresponding to a natural frequency or mode of the object. The mode shapes can then be determined by exciting the object at each natural frequency and measuring the amplitude of response at different locations along its surface (Hocknell, 1998).

Hocknell (1998) used modal analysis to validate a FE model against a real club head although replaced the accelerometer with a non-contacting laser Doppler vibrometer to reduce interference of the modes of the low mass club head. In this study by Hocknell, a harmonic excitation between 0-20kHz was applied to the clubhead whilst its hosel was rigidly clamped and the ratio of target surface velocity to the input voltage could be used to determine the frequency response function at several positions on the club.

The modes of a golf club or any object depend on a number of variables but the one of most interest to this study is the effect of boundary conditions. It is not deemed necessary to conduct a modal analysis for this research and is not the most suitable method as it is the level of clubhead acceleration during the swing which is of most interest. Accelerometers could be used to monitor the clubhead acceleration throughout the swing and then processed with a Fast Fourier Transform to view the most dominant frequencies.

The literature studied in this review has shown that vibration of flexible objects when manipulated by a robot is not a new phenomenon and that the solutions can be categorised as either passive or active. The most relevant solutions are given where a passive method is considered as in this research the concern is to accurately simulate a motion. Where passive solutions have been applied, particularly in the case of Lin (1999) and for other sport simulations, a full speed complete motion has not been simulated and no results are presented for a full motion where variables have been measured and been found to be comparable to the human counterpart.

Chapter 3

Development of a New Clubhead Monitoring System

3.1 Introduction

A human golf swing is a complex motion which can be described by many different parameters. It is the overall aim of this research to mimic this motion with a mathematical model to assist in its simulation with a robot.

As mentioned previously, Harper (2005) has shown that when simulating a golfer's swing, the Miyamae V golf shot robot is not able to replicate the same shaft deflection profiles or ball launch conditions achieved by the golfer. It has also been determined through shaft deflection measurements that the clubhead's motion is heavily influenced by vibrations. As a result, it is highly unlikely that the clubhead will replicate the correct trajectory or orientation of the corresponding golfer and consequently, the ball launch conditions will be dissimilar. Clubhead dynamics through impact are therefore of considerable importance in providing valid simulations. The ability to measure parameters associated with clubhead path and orientation will enable target values to be obtained from golfers' swings and in future, enable the quality of robot simulations to be evaluated. However due to limitations in available clubhead trajectory monitors, it was deemed necessary to develop a new system in order to fully understand the mechanisms of a golf swing.

This chapter considers key variables which define a golf swing. The documentation of the development of a new clubhead trajectory monitoring system used in this study is included. This system utilises PONTOS, a 3D motion analysis package from GOM (a developer of optical measurement systems) coupled with high speed video (HSV) cameras to achieve frame rates of 5000Hz. This system can be used to monitor club dynamic loft, lie angle, attack angle, face angle, speed and impact location simultaneously. The high frame rate allows these variables to not only be measured at impact, but consider how they change throughout impact. The aim of developing this system is to generate a more thorough understanding of the mechanics of the human golf swing, through the measurement of several variables

simultaneously, so that these variables may be used to validate the ability of the mathematical model derived to simulate this swing. As a secondary focus, outside of the scope of this thesis, the new system which has been developed can be used as a golf swing monitoring system.

During a golf swing, clubhead path and orientation prior to and throughout impact can vary due to player characteristics and equipment parameters. Monitoring this variance is important as it has a significant influence on ball launch conditions and, therefore, the overall performance of a shot; a change of 2° in the angle of the clubface can result in a shot either hooked or sliced into the rough at a distance of 200yds from the tee (Cochran 1986). Another, less explored use for golf swing monitoring systems would be to assist in understanding the role of the shaft in a swing. According to Butler and Winfield, ideally the shaft should be straight at impact so that kinetic energy is maximized and strain energy minimised (Butler, J.H.; Winfield, D.C. (1994)). This can be difficult to time, as a clubhead will typically lead and droop at impact as the centre of mass of the clubhead attempts to align itself with the shaft.

The method developed in this chapter allows many parameters of the clubhead to be monitored, providing information about the clubhead's location in relation to shaft deflection. The knowledge of the shaft deflection gives an indication to the twist of the club head as found in an experiment by Butler and Winfield, for each 1 inch deflection of the shaft, the clubhead rotated 0.33° (Butler, J.H.; Winfield, D.C. (1994)). This ratio was measured in a static test whereas the system proposed in this chapter allows these variables to be measured during an actual swing.

Considering a robot simulation of a golf swing, this information is very important as it allows the user to assess the quality of the robot's simulation in terms of positioning the clubhead in the right orientation at impact. If the robot's clubhead orientation and trajectory did not match that of the drive which is being simulated, then as mentioned earlier, due to the sensitivity of a swing to the slightest of changes, the ball launch characteristics of that swing would not be replicated. The primary reason to develop the robot further, is so that it could be used for testing equipment such as clubs and balls. For the robotic testing of golf balls to be more informative than current methods, it is crucial that the robot achieves very similar, if not the same clubhead

trajectories and orientations to the golfer's swing.

A review of current clubhead trajectory monitors has found their results to be limited particularly in terms of measurement accuracy and flexibility. Therefore a new system which is capable of high measurement accuracy coupled with a high level of user control and flexibility is required for successfully capturing the variables that compose the complex motion of the golf swing. This system would also have a commercial use acting as a training tool and assisting with testing equipment performance.

The data captured with this system will provide an invaluable method of validation for any proposed alterations made to the robot in order to increase its functionality. Once the required shaft deformation has been achieved from the suppression of clubhead oscillations, it should follow that the clubhead's orientation would then be correct.

3.2 Development of an accurate method of measuring clubhead orientation.

Currently there is a variety of commercially available clubhead orientation monitors, however the accuracy of the results that they provide is debateable. Loughborough University's Sports Technology Institute has recently purchased a golf radar system, Trackman, which is capable of tracking both clubhead and ball path during a golf swing. This system exploits the Doppler shift effect, the shift in frequency of a laser light wave when reflected from a moving body, to measure a moving object's velocity while multiple receivers allow the object's 3D position to be calculated. By instrumenting a golf ball with a small reflective dot, variables such as spin rates and overall ball flight can be calculated. The radar box (see Figure 14) is positioned 3m behind the tee facing the direction of shot and provides a visual of the predicted ball flight and club path immediately after data capture as shown in Figure 15. This system is a very convenient plug and play type system but due to its many assumptions and calculations, its target use would be as a coaching aid as it gives a good overall prediction of the outcome of a shot, it is also used as a tool for research and development of golf equipment. Variables such as spin rate and clubhead and ball speed are measured, increasing the confidence in their reported values, whereas clubhead orientation variables, which the outcome of a shot is very

sensitive to, are calculated from a model, and therefore cannot be expected to be as accurate as a method which involves image processing.

Figure 14 - Trackman radar box

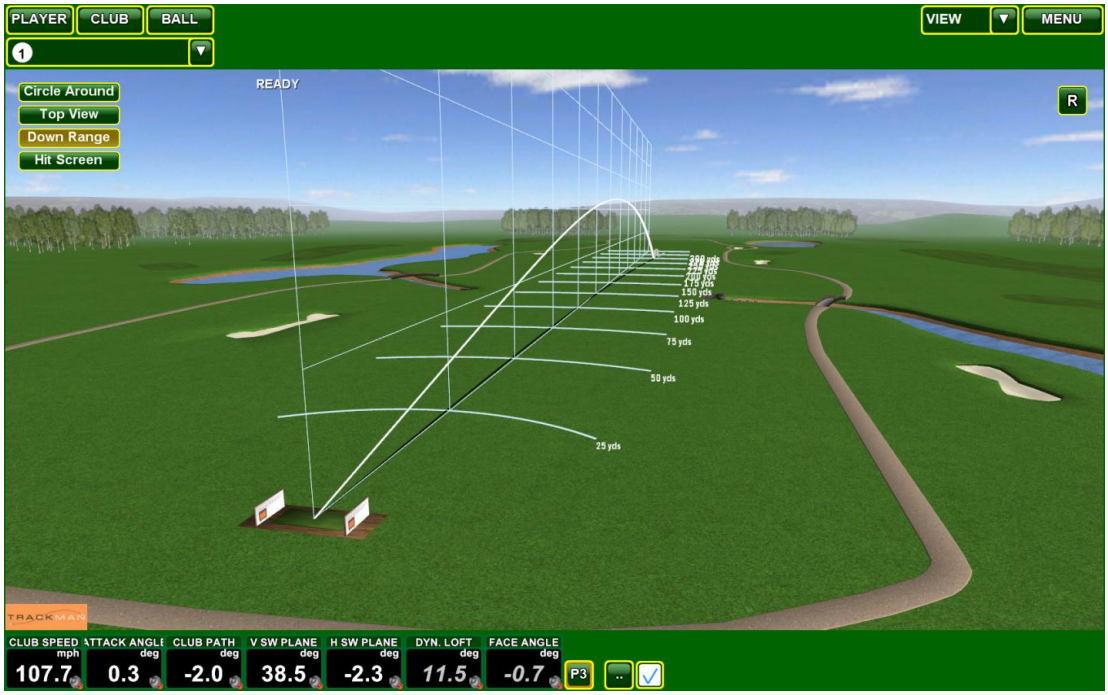

Figure 15 - Trackman system

Image based systems typically have limited frame rates providing a single measurement at impact but do not consider the change in variables during impact, such as the change in face angle during an off-centre shot or the decrease in dynamic loft as the clubhead is slowed and rotated as the shaft straightens.

Callaway Golf have developed an image based Performance Analysis System (Connolly, 2007) which uses two cameras arranged either side of the tee, angled towards the ball and four strobe units mounted on the ceiling, two either side of each camera. The strobe lights can flash up to nine times per capture, allowing multiple exposures per image. Clubhead orientation and trajectory data is calculated from passive reflective markers placed on the clubhead and the ball is instrumented with three lines, one on each axis to calculate ball launch data. The system has concentrated on capturing clubhead speeds (vertical and horizontal) and their relationship to ball launch data, the system could, however, easily be adapted to provide face angle and attack angle measurements. The cameras are able to capture 20 exposures during and after impact resulting in a system with a similar frame rate to the one presented in this chapter, however, the areas of the clubhead which can be tracked are limited to only those in view of the cameras. This system could be a possible solution to the requirements of this research if it were commercially available.

It is apparent that a more comprehensive method of measuring clubhead trajectory is required, particularly to enable an accurate comparison between robotic and human swings. One that is more accurate than current systems and more transparent in terms of providing the user access to the calculations which provide the results. A sample rate of approximately 5000 frames per second is required to enable a fast moving clubhead to be tracked through a very short duration impact (typically around 0.5ms), this frame rate would provide around 30 images during the 0.3m of clubhead travel through impact. To enable a comprehensive analysis of the clubhead's motion, it would be desirable to have the ability to complete an analysis of the six degrees of freedom of the club, whilst providing the user with a calculated point of impact to enable the correlation between impact position and the effect of this on the response of the clubhead. The method presented in this chapter aims to address this need.

3.2.1 Review of motion analysis systems

A summary of some of the available motion analysis systems which could provide the means by which clubhead orientation data could be captured as part of the new clubhead orientation monitoring system is presented in the following section.

3.2.1.1 CODA motion

CODA motion (Cartesian Optoelectronic Dynamic Anthropometer) is a 3D real time motion capture system using active markers and at least one large scanning unit. Infra-red control signals emmitted by the CODA scanning units cause the active markers to emit flashes of infra-red light.

Each marker requires a drive box, which can potentially be hard to attach, adds mass to the subject/equipment and can impede motion. Another disadvantage of the CODA system is that the markers can become 'lost' if they are not visible to the scanning units. The available sampling rates are inversely proportional to the number of markers used. For example, if 12 markers are required, the maximum sampling rate reduces to 400Hz.

3.2.1.2 Vicon

Vicon is an image based system used to track motion through either 2D video analysis or 3D digital optic systems. It consists of a number of cameras with strobe lights set around the lenses. The strobe lights emit an infra-red light, which strikes a passive marker system and is reflected back to the camera (Ehara et al. 1995). The captured images are then fed directly to the computer. The information contained in these images allows the position of the markers to be accurately determined and helps to build up a continuous 3D picture of the subject's motion (Sutherland, D 2002).

The advantages of Vicon include being able to use it in a range of environments from laboratories (Riley et al. 2007) to rehabilitation centres (Churchill, 2007). The system can also be used in conjunction with other capture devices (force plates, EMG and

audio). The images produced can be of very high resolution, up to 4 million pixels, depending on the quality of the camera used and can be recorded at up to 2000Hz.

One of the main disadvantages of Vicon is the requirement of at least six cameras to create accurate 3D results; in the study by Riley (2007) 10 cameras were implemented to obtain accurate results. Another issue with the Vicon system includes the possibility of marker identities getting switched as the markers are passive and do not have an individual identity. Markers can also be 'lost', by being blocked or falling out of the field of view.

3.2.1.3 PONTOS

PONTOS is a highly accurate (0.01 to 0.05mm, GOM, mbH), passive marker system consisting of two cameras which can track a point in 3D space based on the triangulation method. The passivity and size of its markers (see Figure 16) allows large numbers of markers to be used without affecting the item of interest's properties. This is desirable in this circumstance as increased weight on the clubhead can affect variables such as swingweight (Maltby, 1990) and mass distribution.

Crucially, the feature which sets this system apart is the ability to replace the standard PONTOS cameras with high speed video (HSV) cameras. This substitution results in a longer data processing time, however very high sampling rates are possible, which are vital for monitoring a clubhead moving in excess of 100mph (Winfield, 1994) and enables markers to be tracked during impact.

Figure 16 - PONTOS instrumented clubhead

Another advantage of PONTOS is that through the use of a sister programme to PONTOS, TRITOP, a wide range of additional benefits can be achieved. TRITOP is an optical co-ordinate measurement system which through the creation of a point cloud and the known positional relationship between each point, allows markers to be tracked by the PONTOS system, even when not in view of the cameras. Objects can be defined relative to a point cloud and their positions, velocities and angles etc. can also be tracked.

3.2.2 System selection table

The systems listed previously were all readily available for use during this study and were individually considered for this application.

Table 1 lists a summary of the advantages and disadvantages of each system and compares them against current launch monitor technology. It was decided that the system which would best meet the requirements set in the introduction to this chapter and be most suited to this application was the PONTOS system coupled with HSV cameras and a TRITOP generated point cloud.

	Method for measuring clubhead trajectory and orientation of a golf club head				
	PONTOS with TRITOP		VICON	CODA	Radar technology
	500Hz	High speed <10,000 Hz			
Summary of advantages	*High Accuracy *fast feedback time *Unlimited markers *Out of view markers can be tracked *Adapters representative of elements of the object can be created and tracked *Lightweight markers *Could be used outdoors	*Same as 500 Hz but has improved time resolution	*Quick feedback *Can be used in conjunction with other devices *Lightweight markers *Good accuracy	*Range of environments *Relatively fast feedback after initial configuration *Quick set-up time *Unique marker IDs *Good accuracy	*Resolution *Instant feedback *3D analysis *Large capture volume *Operating temperatures *Minimal instrumentation *Fast set up time *Can be used outdoors *Compact, portable system
	*High level of control over measurements/metrics				
Summary of disadvantages	*Markers required *Marker IDs can become mixed *Lengthy calibration	* Same as 500Hz but has an increased set up and processing time	*Markers required *Marker visibility can be lost *Markers can become mixed *calibration *At least 6 cameras are needed for accurate 3D analysis *Relatively low frequency of measurement *Difficult to use outdoors	* Large active markers required *Markers need a drive box. *Markers and wiring can impede movement *Marker visibility can be lost *set up time *Low frequency of measurements with high number of markers *Difficult to use outdoors	*Questionable accuracy *Does not measure axis rotation *Limited range of measurements/metrics
	*Provide extensive data processing but require a longer setup time. *Bulky heavy to transport *High cost				

Table 1 - Summary of several 3D motion analysis systems compared with current radar launch monitor technology

3.3 Definition of metrics

This section details the metrics of the golf swing that the new system will be required to measure.

The three rotations of a clubhead, its roll pitch and yaw can be linked to three of the swing variables that are often measured during a swing. These variables are the lie angle, dynamic loft and the face angle. The measurement of all three of these variables is required from the new system, as part of a 6 degree of freedom analysis of the clubhead, as the aim is to gain a comprehensive understanding of its motion during impact.

The three motions are defined as the following.

3.3.1 Lie angle

Informally, the lie angle of a club could be described as the angle that the shaft makes with the floor. This angle is dependent on the type of club used as a club with a short shaft will result in the player swinging the club with a steeper angle. In this study the lie angle is defined as the roll of the clubhead (the rotation around the x axis). A negative rotation would be considered as one where the toe lifts.

3.3.2 Dynamic loft

Every club has a static loft and this is defined as the angle of the clubface relative to a vertical plane. During a swing however, the shaft is bent, this leads to a change in the loft, referred to as dynamic loft. For this paper, dynamic loft is defined as the pitch rotation of a 6DOF analysis of the clubhead, where an increase in loft results in a negative rotation.

3.3.3 Face angle

The club face angle is usually discussed as being ‘closed’ or ‘open’ and is seen particularly at impact as the golfer twists his grip, closing the face into the ball. In the context of this study, face angle of a club during a swing has been defined as the ‘yaw’ component of a 6DOF calculation of the clubhead’s motion. An open face is defined as a negative rotation. For polarity of directions and rotations, refer to Figure 17.

Figure 17 - 6DOF of the clubhead

3.3.4 Impact location

Impact location can be used as an indication as to the quality of a golf shot, with the aim being to strike the ball out of the centre of the face with the centre of mass located somewhere on the perpendicular line from this plane. The impact location affects the ball launch conditions, therefore, if these conditions were to be replicated by the robot, the knowledge of where on the clubface the ball impacted is required.

3.3.5 Attack angle

Depending on the length of club used, a golfer's attack angle will change. To account for this a golfer could change his or her swing style which could be detrimental to performance. Monitoring this change will demonstrate the motion of the clubhead during impact and illustrate any clubhead vibrations, if any. Providing the feedback of this path during a golf swing could also be useful as a coaching tool. Attack angle is determined in this instance as the path of travel between two images and the angle this path makes with the floor.

3.3.6 Clubhead speed

Clubhead speed is directly related to ball launch speed, therefore, if the simulated clubhead speed is incorrect, the ball launch speed will be wrong, if the robot was required to simulate a swing where the ball launch conditions and outcome of shot were of highest importance, the calculated clubhead speed would need to be matched before any ball launch data should be captured. Most systems measure clubhead speed as a single variable for the clubhead as a whole. The new system developed in this chapter should enable a large number of possibilities in terms of areas of the clubhead that can be tracked, restricted only by the number and location of the markers in the TRITOP point cloud.

3.4 Method

The following section describes the stages that were required to capture data with the PONTOS system and the calculations which were made to provide the metrics defined in the previous section.

3.4.1 TRITOP point cloud

Prior to capturing data, a TRITOP point cloud of the clubhead was generated to determine the geometric relationship between each marker. The more markers used, the more accurate the fit would be between the TRITOP point cloud and the points captured during data collection using PONTOS. Forty passive reflective markers

were positioned randomly onto the clubhead and hosel to define its geometry along with some markers at key locations, on the clubhead. Seven markers were positioned on the clubface so that multiple smaller planes could be defined to account for the curvature of the face, two at the base of the shaft to help orientate the model and a single marker the on the centre of the face so that impact location could be found relative to this point. The clubhead was clamped in an upright position and surrounded by four GOM calibration crosses and two scale bars (as seen in Figure 18); these were required to enable the software to determine the scale of the object and the position of the markers.

Figure 18 - TRITOP set-up

The two calibration crosses positioned vertically were required to guarantee each image would contain uncoded markers on the clubhead as well as some coded markers on the crosses. Still images were then captured of this arrangement at a distance of 1m from multiple viewpoints with a digital SLR camera. There is no limit to the maximum number of images that can be taken but each marker must appear in several images for the software to correctly determine its 3D position. Four images

were first taken from directly above the clubhead at 0, 90, 180, 270 degree orientations to orientate the images.

Images were captured circumferentially at 3 different heights. This process was then repeated for the underside of the clubhead and the two sets of images were then imported into the TRITOP software.

The images are virtually combined to relate the image points to the calculated marker positions, this is based on the coded marker positions. Two separate point clouds were then generated for the top and bottom image groups. One point cloud was then set as the reference cloud and markers identified in both the upper and lower captures of the clubhead were used to stitch the two models together to form a single point cloud of the whole clubhead. The digitisation of the markers is shown in Figure 19

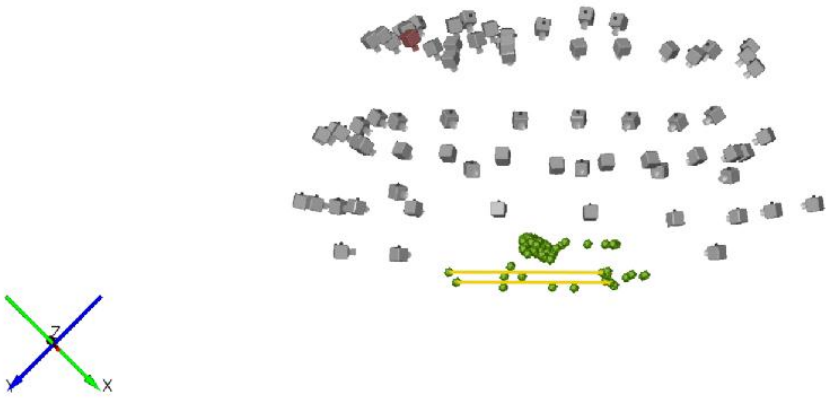

Figure 19 - TRITOP output showing camera angles and digitised markers

Elements, such as virtual points and planes were defined relative to the positions of the points in the cloud so that when imported into PONTOS, they could also be tracked. For any element to be tracked in PONTOS, the definition of an adapter is required, this involves selecting the object of interest and choosing an option in the menu. The most effective way of visually monitoring the orientation of the clubface at

impact was to define a plane to represent it. Three points are required to define a plane so the three markers which had been positioned centrally on the clubface were used for this purpose. Another main area of interest, which therefore required an adapter, was the centre of the clubface marker. Four random points positioned around the clubhead were selected from the point cloud and adapters created for them, these were required to calculate the clubhead rotations. The clubhead's local coordinate system in TRITOP was rotated to align it with the centre of the clubface, square to its face. The positions of these points in the local coordinate system were exported. The point cloud and some elements are shown in Figure 20.

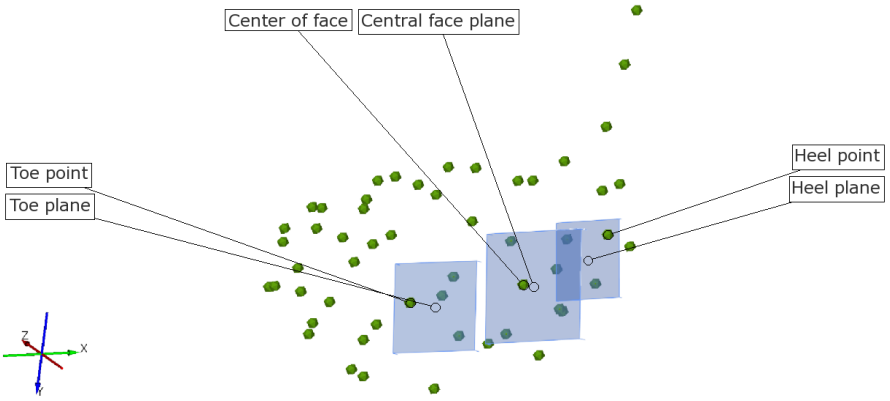

Figure 20 - TRITOP point cloud

The majority of the markers used to define the point cloud would not be in view of the cameras during an actual capture and therefore could be removed from the clubhead. Key areas of marker visibility during a golf swing were identified to be on the toe section on the crown of the clubhead and at the base of the shaft, as shown in Figure 16, so the markers in these areas were kept.

3.4.2 PONTOS data collection

To capture marker positions using PONTOS, two Photron Fastcam Ultima APX HSV cameras were used and configured to capture at a frame rate of 5,000 frames per second and a shutter speed of 1/30,000s. The cameras were mounted on a tripod

and positioned to enable captures of the clubhead for approximately 300mm before and after impact. This was achieved by tilting the cameras 30° to the horizontal and angling them in towards the tee at a distance of 0.36m as illustrated in Figure 21. The high shutter speed was required to prevent motion blur; a consequence of this was underexposed images and this was corrected for by using two ARRI Sun 1200W lights. Arrangement of the lighting was key to successful marker recognition, so before each test, the lights were positioned to give an even coverage of light in the capture area.

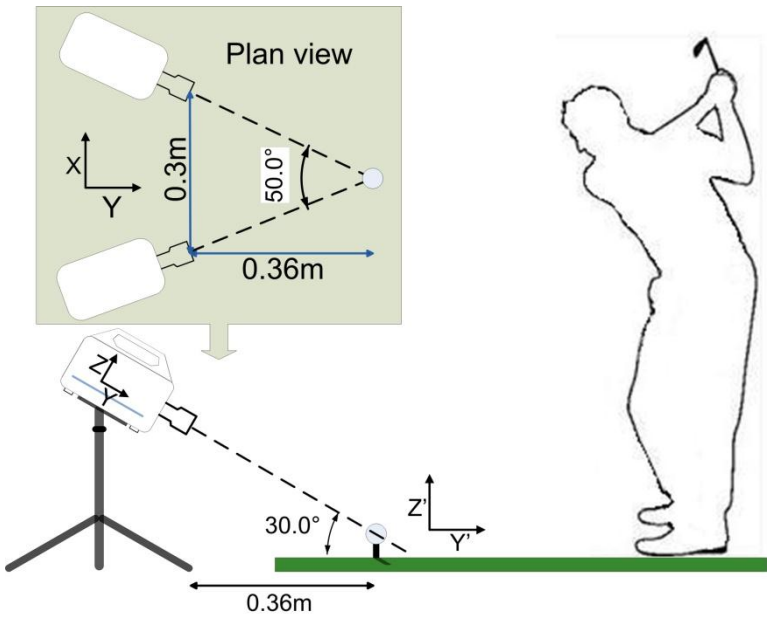

Figure 21 - Plan view of camera set-up

A calibration of the PONTOS system was performed before each day of testing using an uncoded (a pattern of basic white dots) calibration board provided with the GOM system. The selection of a calibration device is based on the desired capture volume; for this study 0.7m^3 was deemed suitable. The cameras were manually focussed onto a ball positioned on the tee. The tripod was carefully angled back up to the horizontal and remained in this position during the calibration to allow calibration of the full capture volume. The calibration involved taking thirteen images of the board in a number of orientations following a standard procedure as outlined in the GOM user manual. By replacing the GOM cameras with the HSV cameras, the

method of importing images was less automated. When importing any images, a selection had to be made in the software to allow the images to be imported as an image series. This substitution of cameras therefore, affected the calibration process as well as general motion capture, resulting in a slightly extended calibration procedure as the thirteen images had to be pre-organised into the correct sequence and imported through a function in the software. A satisfactory calibration quality value is given as being between 0.02 and 0.04 pixels and is a calculation of the deviation in pixels to be expected of a measured position. This guideline quality value was achieved for every calibration. After a successful calibration was computed, the cameras were carefully tilted back down towards the ball positioning it central to both cameras fields of view. A transformation tool as seen in Figure 22 was then placed next to the tee with the plane containing two markers facing the cameras and a ball instrumented with PONTOS markers was placed on the tee. One image (per camera) was then captured. This image was required for two reasons. When

Figure 22 - PONTOS axis transformation tool

images are first imported into the PONTOS software, their position and trajectory is calculated relative to the cameras, for the purpose of this study, angles are most relevant when relative to the floor, therefore, the transformation tool shown in Figure 22, had to be present in at least one image so that a transformation could be computed during processing. The instrumented ball enabled a sphere to be ‘best fit’ to the markers on its surface and could be used later to calculate impact position.

3.4.3 PONTOS data processing

Once testing had completed and all of the marker data captured, each set of images from each swing was loaded into the PONTOS software along with an image of the transformation tool and a new project was created. The software then computed each image, or stage as they are referred to by the software, recognizing the reflective markers as points. Once each stage had been found to contain a suitable number of points, an axis transformation was then completed, using an image of the transformation tool shown in Figure 22. At this stage in the analysis, the markers do not have an identity and no relationship exists between each other or each image. A relationship was created by importing the TRITOP model produced previously along with its defined elements. Figure 23 shows a typical screen from the PONTOS analysis; the still images from the HSV camera captures accompany the digitized clubhead markers and adapters.

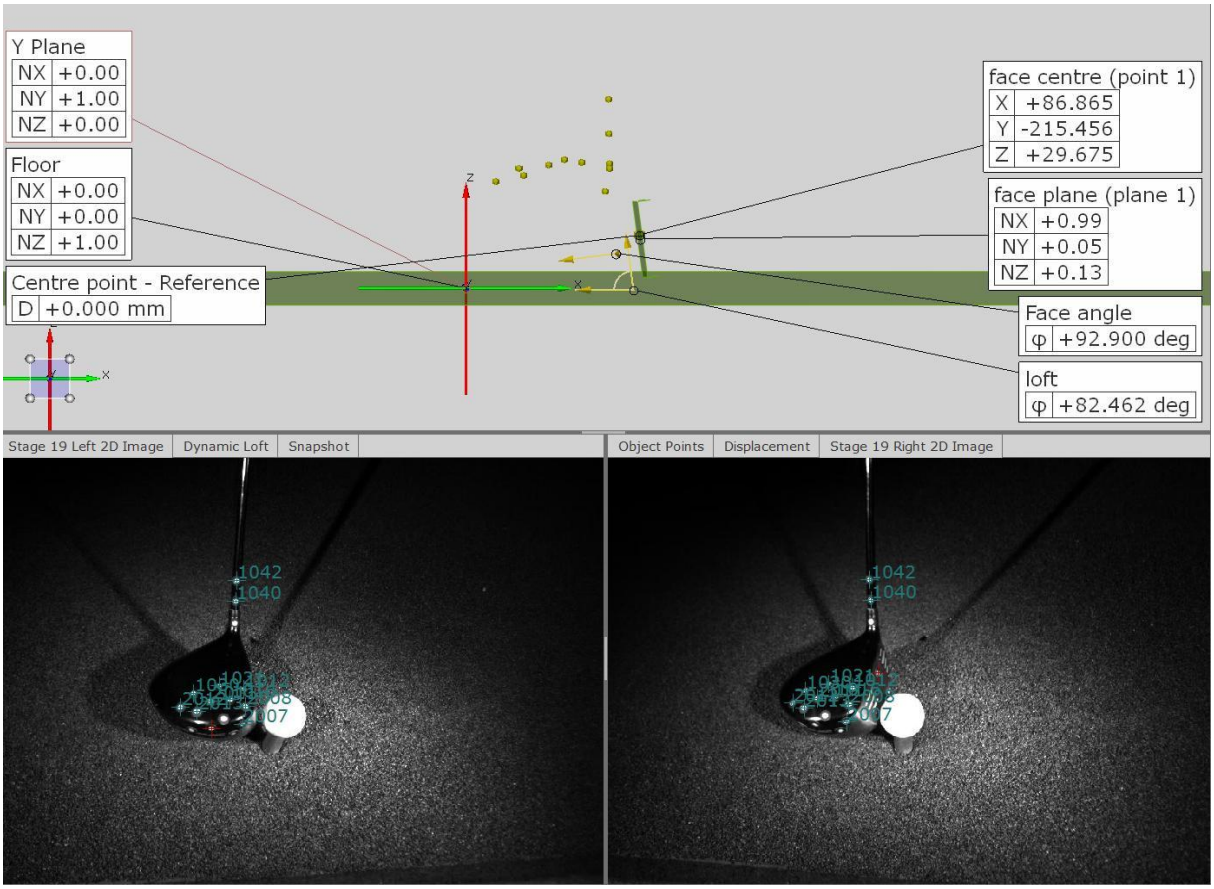

Figure 23 - PONTOS software, analysis screen

When considering the variables of a clubhead's motion during a swing, the three which are most commonly discussed are the face angle, dynamic loft and lie angle. The definition of these angles can be a bit ambiguous, but for the purposes of this study are defined in section 3.3. To calculate these variables from the PONTOS data, it was decided to map them to the roll, pitch and yaw of the club. This method of analysis would involve the computation of the rotation of the local co-ordinate system of the clubhead relative to the global coordinate system, defined by the transformation tool. Currently the GOM system does not have the functionality to calculate these rotations so an alternative solution was sought; the data was exported and processed via a Matlab script.

To enable a large number of swings to be processed, a macro was created with an inbuilt function in PONTOS. Each swing (or project) was imported and the image which contained the beginning of the impact between ball and clubface was flagged as the reference stage. All positions were measured relative to this stage. The image of the transformation was imported alongside each image series and a transformation was computed. A function in the software requires an input of the markers on the transformation tool which define each axis and based on this, positions of all markers would now be relative to the axis and origin defined by the transformation tool. The remaining stages could be automated by the macro. This involved importing the TRITOP model, computing its position in each image and exporting the positions for the 5 point adapters.

3.4.4 Calculation of clubhead path and orientation

To calculate the rotation of the local co-ordinate system (CoS) relative to the global co-ordinate system, the scenario presented in Figure 24 was considered. When the position of point P is of interest, one must first find the position of the local system in the global system and then the position of p in the local system. The local system's position can be related to the global CoS by the following equation;

$$[\hat{x}_{loc} \quad \hat{y}_{loc} \quad \hat{z}_{loc}] = [\hat{x}_g \quad \hat{y}_g \quad \hat{z}_g][x, \alpha][y, \beta][z, \gamma]I \tag{1}$$

Where the matrix on the LHS contains three unit vectors describing the direction of the local CoS. This equates to a matrix containing three unit vectors in the direction

of the global CoS, multiplied by three rotation matrices for the rotations about x, y and z (Equations 3a, 3b & 3c). The final element in this equation is I, a 3*3 identity matrix.

The position of points P_n can be described as follows;

$$\overrightarrow{O_g P}_n = \overrightarrow{o_g o}_{loc} + \begin{bmatrix} \hat{x}_{loc} & \hat{y}_{loc} & \hat{z}_{loc} \end{bmatrix} \begin{bmatrix} a_n \\ b_n \\ c_n \end{bmatrix} \quad (2)$$

n is the number of points which are used to calculate the rotation of the local CoS. Vector $\overrightarrow{o_g o}_{loc}$ describes the mapping of the global origin to the local origin and a_n, b_n and c_n are the x, y and z co-ordinates of the n points. Substituting equation 1 into equation 2 provides the relationship between the co-ordinates in the global system and the rotations about the x, y and z axis to map these points to the local CoS. The three resulting equations for rotations of the axis' can be solved to find α, β and γ, the roll, pitch and yaw rotations. The order in which the three rotational matrices were multiplied defined the order in which the clubhead would be rotated to its transformed state.

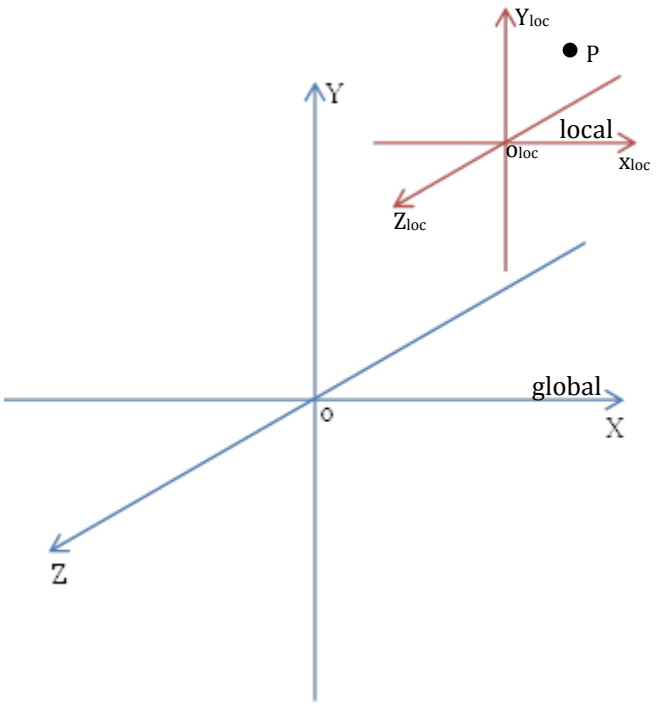

Figure 24 - Global and local co-ordinate systems

The order of rotation was selected as ZYX, yaw, pitch and roll, as applied in this order to the global system would be the same as applying the standard order of rotations, roll, pitch then yaw to the local system.

$$[x,\propto]=\begin{bmatrix}1 & 0 & 0\\ 0 & cos\propto & -sin\propto\\ 0 & sin\propto & cos\propto\end{bmatrix}\quad [y,\beta]=\begin{bmatrix}cos\beta & 0 & sin\beta\\ 0 & 1 & 0\\ -sin\beta & 0 & cos\beta\end{bmatrix}\quad [z,\gamma]=\begin{bmatrix}cos\gamma & -sin\gamma & 0\\ sin\gamma & cos\gamma & 0\\ 0 & 0 & 1\end{bmatrix}$$

(3a,3b,3c)

To process the data a Matlab script was written. This script requires two inputs, a file containing the local positions of the five club points exported from TRITOP, and the output file from PONTOS containing stage by stage the positions for each of the points relative to the global CoS. A user input is required to define the number of points for which positions are being provided. Equations 1-3 are implemented to produce the 3 rotations, roll, pitch and yaw, or as referred to here, dynamic loft, lie

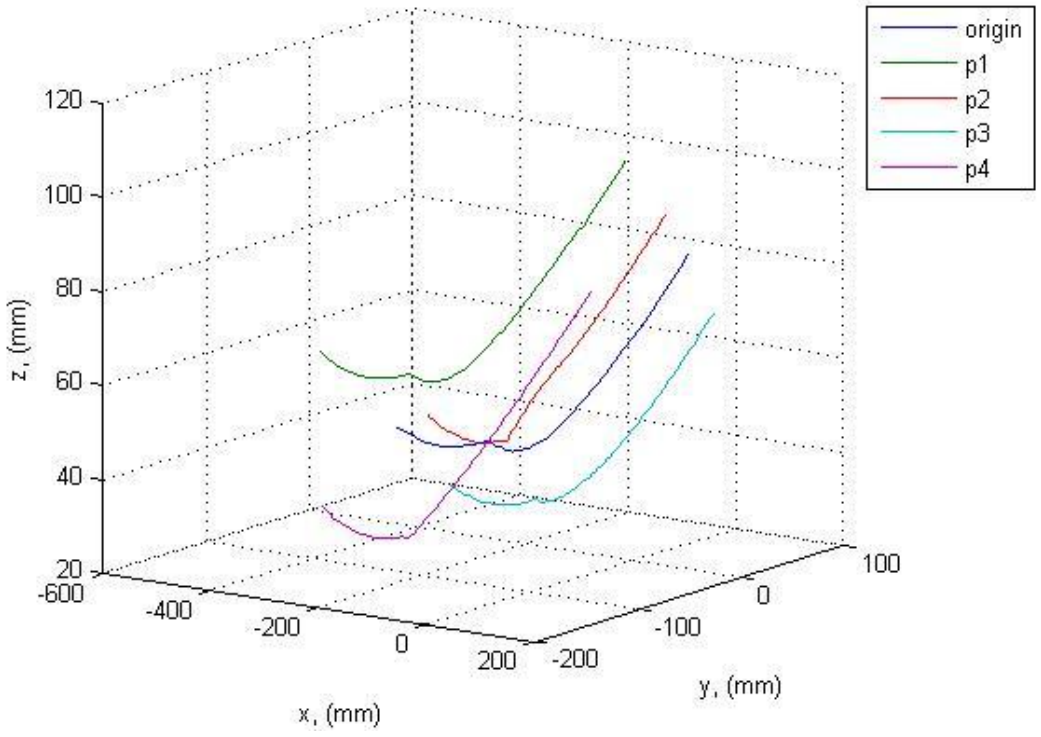

Figure 25 - Club point positions through impact

angle and face angle. An output is then produced in the form of a file containing the three rotations per stage and three plots to illustrate the point positions, as a sanity check, alongside the calculated rotations. The script processes just one swing per run.

Figure 25 gives an example of the first plot produced by the script. It shows the 3D position of the five points on the clubhead with the origin being the centre of the clubface. It is interesting to see that the impact position is clearly distinguishable by the 'notch' in the data, where the club path abruptly changes. Figure 26 shows the same data but for the centre of clubface alone with a clearer graphical representation of the motion through which the point travels. The calculated lie angle, dynamic loft and face angle plotted against impact time are displayed in Figure 27, with the impact line indicating the start of impact. A positive lie angle represents a toe-down position, a positive dynamic loft indicates less loft and a positive change in face angle represents the closing of the face.

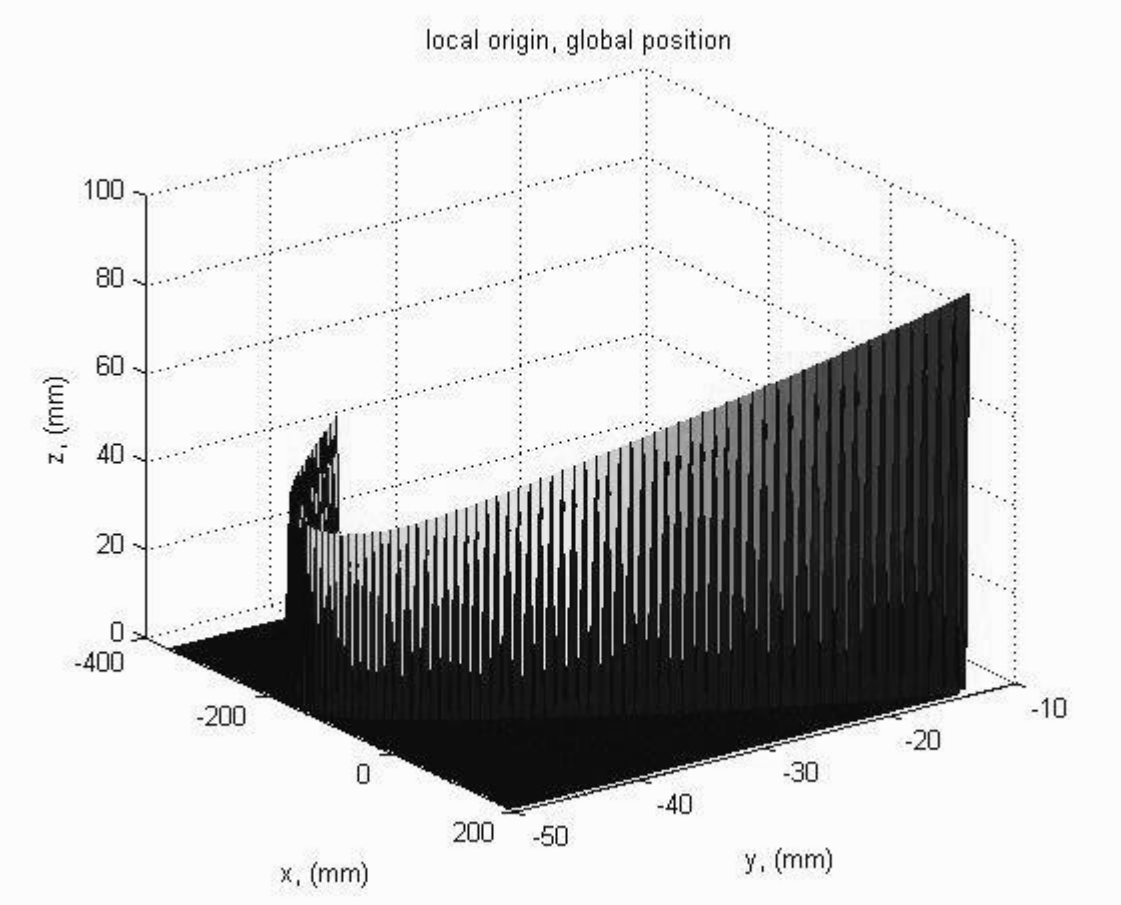

Figure 26 - Centre of clubhead position through impact

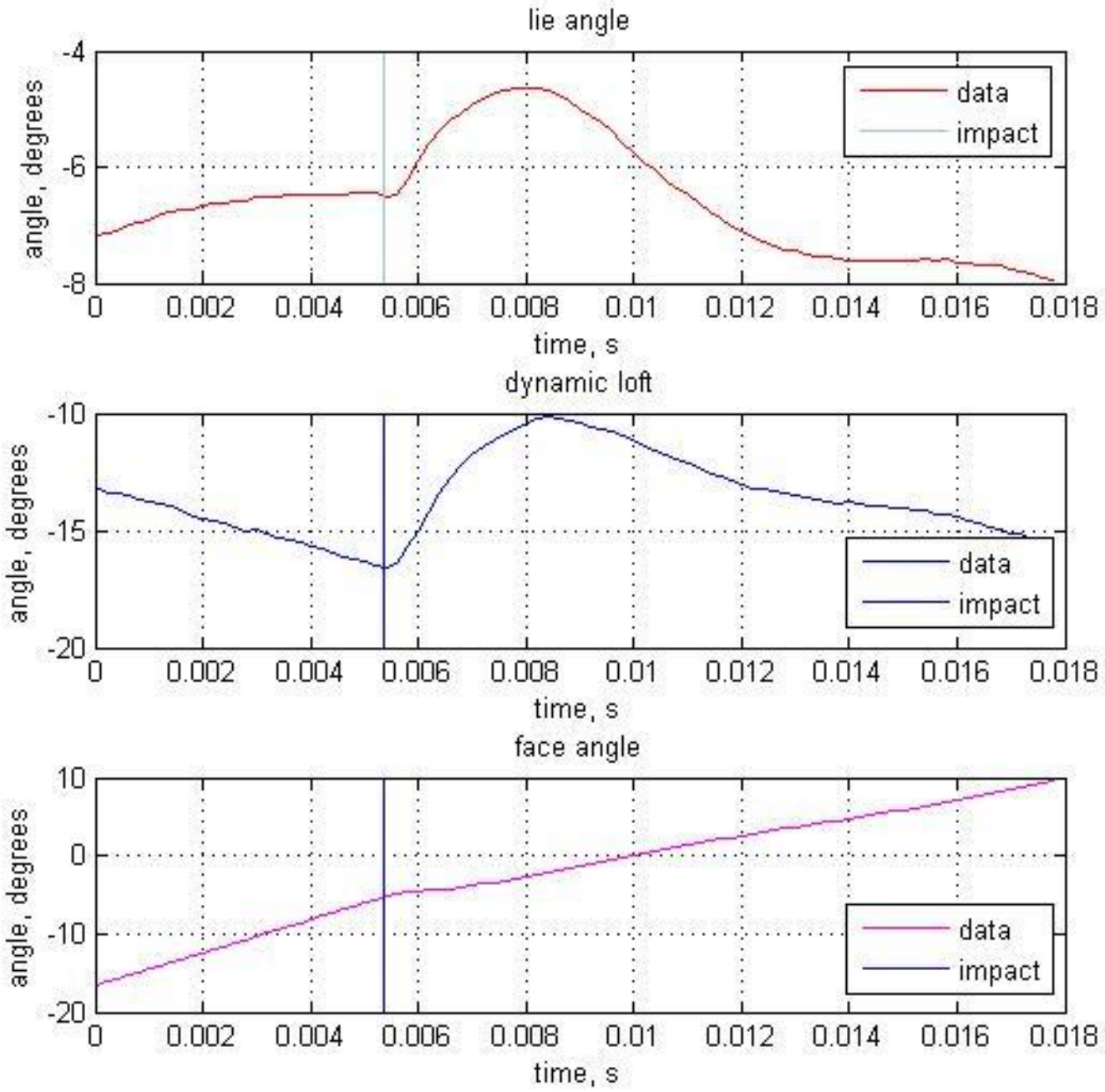

Figure 27 - Matlab output of clubhead rotations

3.4.5 Impact location

Impact stickers were employed during testing to measure impact location and to provide a visual aid to determine the success of the shot. The results shown in the previous sections all present data where the result of the impact location on the

clubface has a dramatic effect on the continued path of the clubhead. Therefore, to analyse these results correctly, they should be mapped to the impact location. Relying on the measurements given by an impact sticker does not provide us with a very accurate value as the error in positioning the sticker on the clubface was considered to be ±0.5mm, however they will give an indication to the accuracy of any calculated impact positions. The PONTOS system provides data which should allow an accurate and precise calculation of the impact location.

The images of the transformation tool, as mentioned previously, contained the instrumented ball. Once each of these images was imported into the PONTOS software, a 'best-fit' sphere was fitted to the markers on the ball. This was computed with an inbuilt function of the software which allows basic shapes to be fitted to the digitised markers. To generate a sphere, a minimum of 3 markers should be selected and the radius of the desired sphere entered. Once the sphere had been generated, the 3D position of its centre is given. This value for each transformation image was exported and the remaining calculations were completed via a Matlab script.

A Matlab script was also generated to calculate impact location, to begin with, a plane was created on the face of the club through the three central face points. Four additional points were added to the face, each one 10mm along the x or y axis (-ve and +ve). The new points were used to create two vectors along the face and a finely meshed plane was generated along these vectors. The position of this plane was plotted for the three preceding stages leading to impact to enable the calculation of the direction in which the plane was travelling. A second line running in parallel to this was generated from the centre of the ball. At the stage where impact starts, the intersection of this line and the club face plane was calculated, and this position was deemed the impact location.

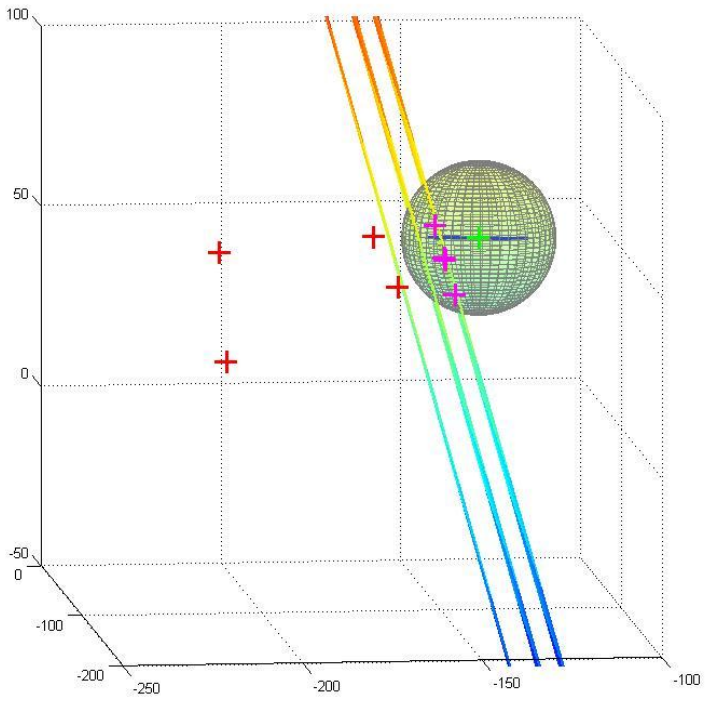

Figure 28 - Visual from Impact position calculation

Figure 28 illustrates one of the output plots provided by the Matlab script. The three clubface planes can be seen for the three stages at the start of impact. The magenta markers are the generated clubface markers, required to create the plane. The blue line seen through the centre of the ball shows the direction of the face plane during impact and the four red markers are the four points selected from the clubhead point cloud in section 3.4.1 to calculate the clubhead rotations. The surface plot of the ball is for visualisation purposes only.

3.4.6 Clubhead speed and attack angle calculation

The speed of any point in the point cloud can be measured, once an adapter has been created for the point of interest. These point positions were imported into Matlab via a script and the distance travelled in the x,y and z directions were found between each stage. The global distance travelled between each stage was calculated using the 3D Pythagorean Theorem as illustrated by Figure 29. Where the length of S can be found using the following equation,

$$S = \sqrt{x^2 + y^2 + z^2} \quad (4)$$

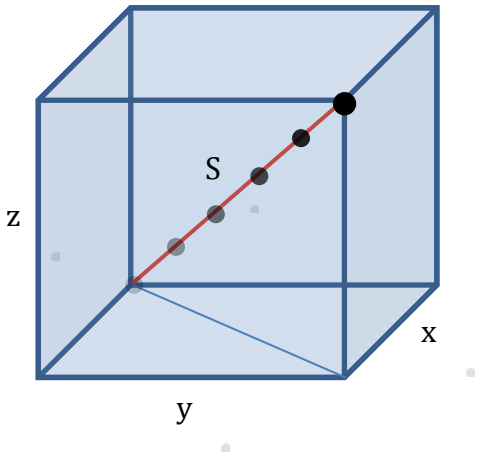

Figure 29 - 3D Pythagorean Theorem

Once the distance travelled per stage is known, the attack angle could be found by calculating the angle between the line of motion and the ground, dividing the distance by the sampling rate provided the calculated clubhead speed.

3.5 Conclusion

To gain a comprehensive understanding of the motion which the robot is required to simulate it was considered necessary to conduct a study to measuring and analyse the motion of a clubhead during a golf swing. Current golf swing monitor technologies were reviewed with the conclusion that a new image based system was required which provided the user with a greater control over the variables which were measured and which did so at a high frame rate and with greater accuracy. Therefore the aim of this chapter was to develop a new system which could monitor the clubhead path and orientation throughout the impact phase of a golf swing and meet these criteria.

A new methodology was developed to track and measure the trajectory and orientation of a clubhead leading up to and during the impact phase of a swing. This system implemented two systems from GOM, TRITOP and PONTOS. A point cloud of the clubhead was created in TRITOP and adapters were generated for key areas

of interest. Clubhead positional data which had been captured during golf swings via HS video were imported into PONTOS and then transformed to make all point locations relative to the ground. The TRITOP point cloud was then imported into PONTOS and matched to data captured with HS video cameras. Marker positions were exported and the remaining processing took place via a Matlab script. This chapter documented the method implemented to calculate the clubhead dynamic loft, lie angle, face angle, speed, attack angle and the impact location of the ball.

Chapter 4

A study of human golf swing parameters

4.1 Introduction

The new system developed in chapter 3 for monitoring clubhead trajectory and orientation was implemented to provide a comprehensive analysis of the motion of a clubhead during a swing by measuring dynamic loft, face angle, attack angle and clubhead speed during impact. The system was employed alongside additional systems for measuring shaft deformation, clubhead vibration and ball launch data in a study which sought to provide an exhaustive insight into the human golf swing. Key human kinematic data was captured to create corresponding robot swing profiles and also to be used as the driving mechanism for a mathematical model. Modelling the robot in the following chapters will allow an infinite number of simulations of a golf swing to be carried out to enable refinement of its structure to achieve the best possible match to the human data collected in this chapter. The measurement of shaft bending and clubhead vibration produced variables that can be compared to the output from the mathematical model and should be replicated by a successful model simulation. A comparison between the model and human swing data would also provide validation of the model's accuracy.

As part of the suggested future work from this research, if the robot were to be adapted, the golfer data captured in this study could also be used to validate the ability of the robot to simulate a variety of golf swing styles.

4.2 Participant golfers

Fourteen right-handed golfers between the ages 21-44 consisting of one female and thirteen males participated in the study. In order to test the system, a wide selection of swing styles and impact locations were required so golfers with handicaps across the whole range were selected for this study (handicaps of between 3-36). Ethical clearance was applied for and subsequently given for the study by the Loughborough university Ethical Advisory Committee. Participants were provided

with an information sheet prior to their session and were required to sign a consent form after the details of the study had been fully explained to them. Each golfer was required to complete one session of tests which lasted for around 60 minutes.

4.3 Instrumentation

In addition to the system developed to measure clubhead path and orientation, a number of other measurement systems were employed to measure golfer kinematics, shaft bending and clubhead vibration.

4.3.1 Club vibration

One of the main criteria which will enable validation of the mathematical model and one of the key variables considered in this study will be the level of clubhead oscillation, if any, present in the clubhead during the simulation of a golf swing. To enable a direct comparison between the level of oscillations present in a clubhead when swung by a golfer and the subsequent oscillations in a simulation of that swing, accelerometers were mounted to the hosel of the driver via a small aluminium clamp. The clamp was attached by joining its two halves around the hosel and a compliant material was attached to the mounting surface to isolate the accelerometers from high frequency vibrations in the shaft and to increase the friction between the clamp and the hosel. One accelerometer was orientated parallel to the direction of shot and one perpendicular. This was to enable the resultant oscillation in the swing plan to be calculated. Data was recorded from these accelerometers using a National Instruments 9234 Data acquisition (DAQ) module driven by Smart Office software. Data capture was triggered from a positive slope of 0.001V (equivalent to about 1.9m/s^2) and recorded for 4s at 2048Hz with a pre-trigger of 0.5s

4.3.2 Shaft bending

The inability to replicate shaft deformation during a robot simulation was one of the main drives towards recognising the need for further development of the golf robot. It is therefore a variable which should be measured and one which needs to be

replicated in model simulations of the swings. The STI own a commercially available shaft deformation system, however, raw strain data is not available for the user to view and data capture can be hard to trigger. To enable more flexibility in the way shaft strain data can be captured, two strain gauges were bonded below the grip on the driver used in this study in the same orientation as the accelerometers to enable strain in both the toe up/down and lead/lag directions to be measured. The strain gauges were connected to a second M+P module and their outputs measured simultaneously to acceleration in the same Smart Office project. The measured strains were calibrated by flexing the shaft to a known deformation and recording the strain seen in the gauge mounted in the direction of the displacement.

4.3.3 Golfer kinematics

CODA motion, (mentioned previously in section 3.2.1.1) is a motion capture system developed primarily for analysing human motion and was used in this study to collect kinematic data from each golfer's swing. CODA employs active markers as illustrated in Figure 30, which are powered by the blue battery box shown in the image. A single battery box can drive up to two markers. The method used in this study was adapted from a study by Harper (2005) which details the process of programming the Miyamae Golf Shot Robo V to emulate a golf swing from kinematic data.

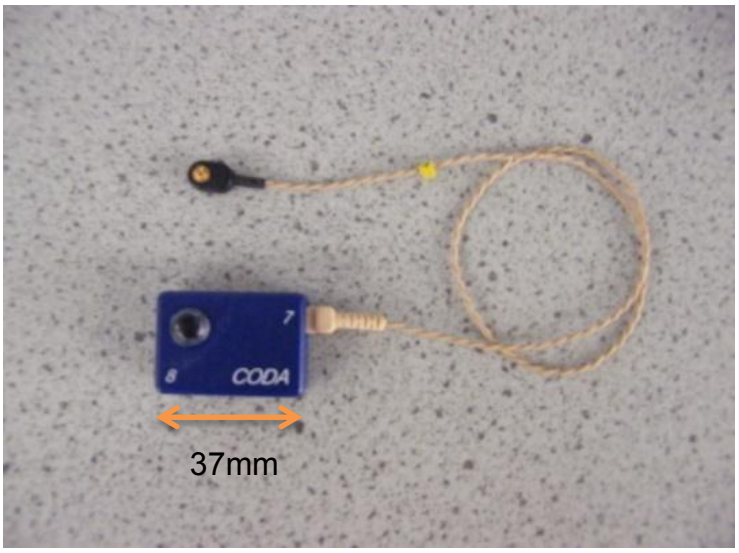

Figure 30 - CODA marker and battery box

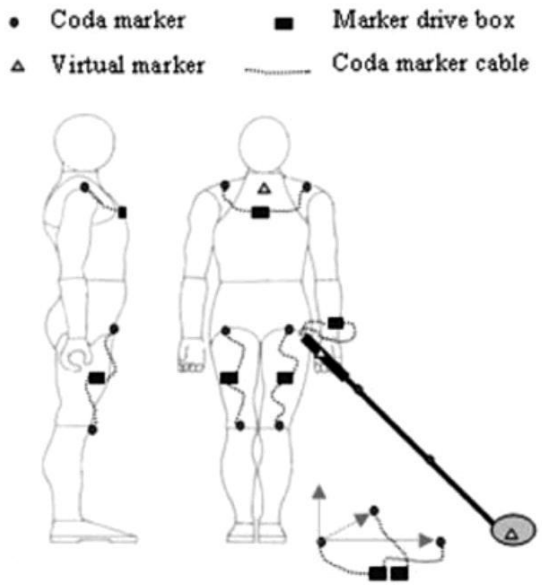

Figure 31 - Marker locations (Harper, 2005)

Data representing the golfer's motion during the swing is required to programme both the robot and the mathematical model. CODA was used to capture kinematic data of the golfer through the use of a few key marker positions from which virtual markers could be defined. Marker locations are shown in Figure 31, the two shoulder markers were used to define a virtual marker at the hub position (the base of the neck). Two markers were placed on the shaft at 265mm and 550mm from the top of the grip labelled top club marker and bottom club marker respectively, to define the line of the shaft. The two markers were used to define the shaft as a rigid body and, therefore, require the shaft to remain straight, to achieve this, the bottom club marker was positioned high enough so as to keep it outside of the area of high shaft deflection. A third marker was required to define a line perpendicular to the shaft in order to define the third rigid body axis and to enable the rotation of the club about the shaft axis to be calculated. For this purpose a tee piece was attached perpendicularly to the shaft, as shown in Figure 32b, and a marker mounted onto its tip. The rotation of this marker about the line of the shaft determined the parameter deemed 'grip' rotation. A further virtual marker was defined relative to the top and bottom shaft markers to represent the position of the hand at 55mm from the top of the grip. A link was defined between the hand marker and the hub position and the

angle calculated between this link and the y axis was defined as the ‘arm’ rotation, with the y axis being that which is perpendicular to the ground. A second link was defined from the hand marker to the bottom club marker, and allowed the ‘wrist’ rotation to be calculated relative to the ‘arm’ rotation. A virtual clubhead marker was defined at the base of the shaft so that clubhead position could be plotted.

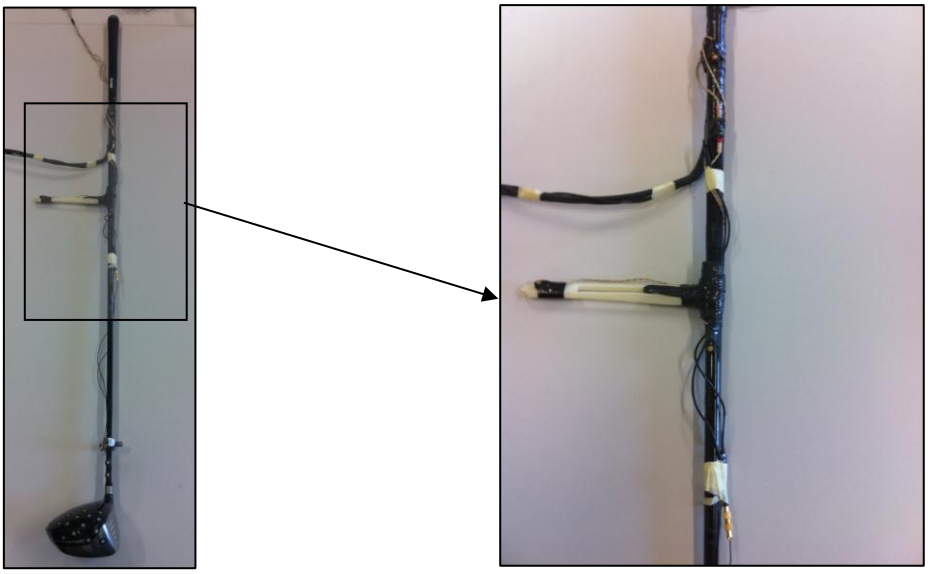

Figure 32 - (a) Instrumented club, (b) T-piece

Two CODA cameras were positioned in the locations shown in Figure 34, which were found to provide the best marker visibility throughout the swing. Three markers were required to define the global X and Y axis; two separated by a minimum distance of 0.5m for the X axis and a third placed at a distance of 0.5m to the X axis. CODA creates the Y axis as a perpendicular line connecting the 3rd marker to the X axis. The Z axis is defined relative to the X and Y axes. The axis markers were kept in view of the cameras throughout the swing as their positions would be required for an axis transformation during post processing, for the calculation of rotations when projected onto the swing plane. The markers were mounted onto an axis tool shown in Figure 33 to enable the direction of the axis to be easily aligned with the edge of the golf mat and ensured the marker positions were planar. This tool was aligned so that the tee was lying on the X axis which was aligned with the target line, it was then secured to the floor with tape.

Figure 33 - CODA axis tool

4.3.4 Ball launch data

A commercially available golf radar system, Trackman, was used to capture ball launch data and additionally, calculate clubhead orientation which could be compared to results obtained with the new PONTOS based system. Although there is little evidence available to support the published Trackman system accuracy data, it remains the industry standard, is widely used and well regarded. A requirement of the radar system is that the ball must complete two full revolutions before it contacts the net to be able to calculate ball spin data. A guideline minimum distance between tee position and the net is given as 3m, for this study the distance was set to 5m as trials suggested shots hit by ‘hard hitters’ were not completing the two required revolutions over the 3m distance. The radar box was positioned 3m behind the tee as per the guidelines and upon initialisation of the software, was aligned with the tee and target line using an on-screen visual aid. The software was then switched into launch mode and player names and ball and club details were selected from a menu. The radar system is then active and automatically triggers when it senses the moving club. A 40inch monitor was connected to the system’s laptop to provide participants with immediate feedback of the success of their shot. The monitor, however, had to be switched off during each capture as the frequency of the light emitted interfered with the CODA cameras.

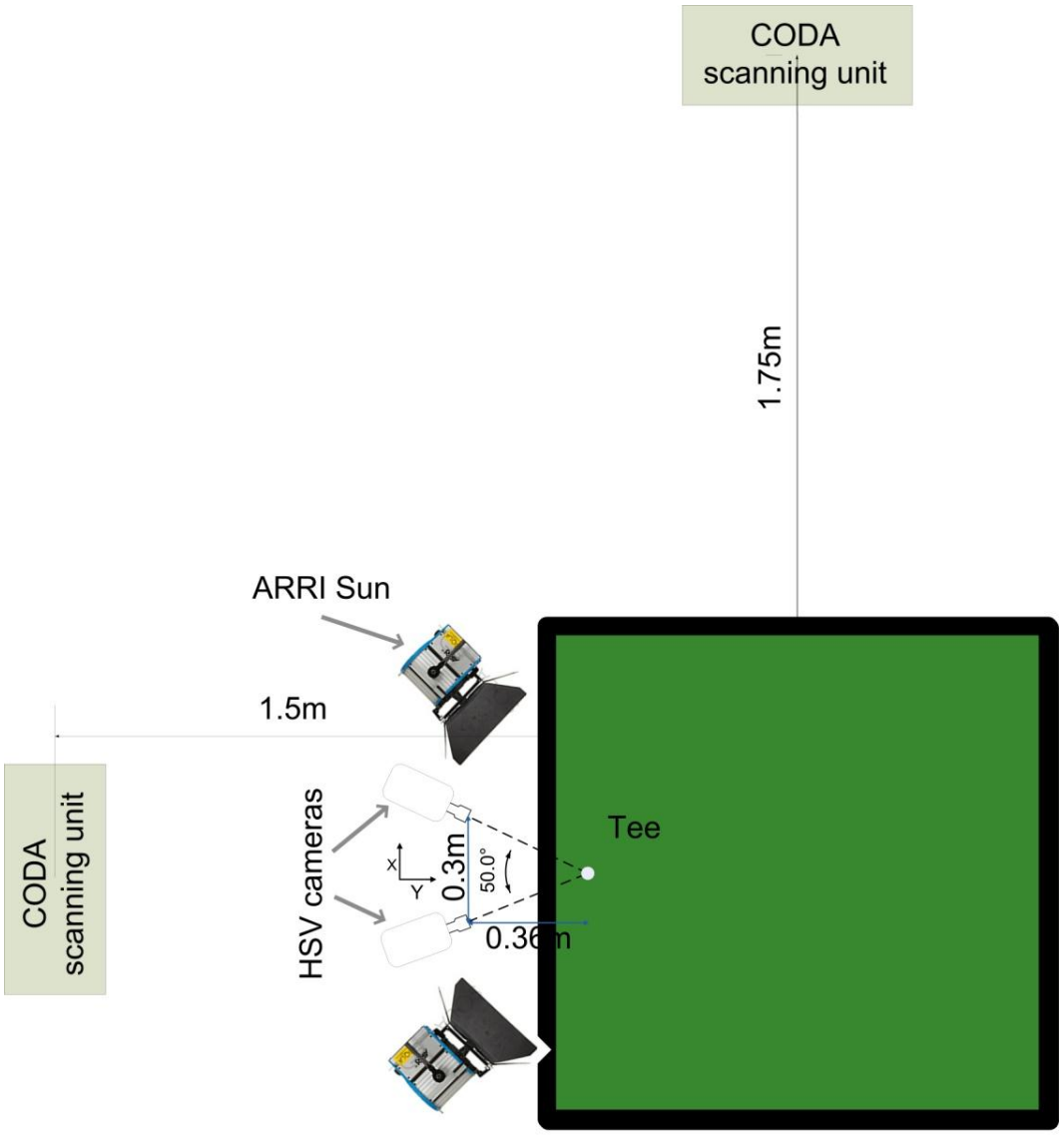

Figure 34 - Laboratory setup

4.4 Procedure

Prior to each testing session or in the event of relocation of the axis tool, the CODA cameras required an alignment calibration with the axis markers. This could be completed through a simple procedure in the software which calculated the axes' positions relative to the two cameras. A single image was also captured of a CODA marker positioned on the tee, this would enable clubhead position to be calculated relative to the tee and the time of impact found.

Preliminary trials indicated that during the top of the backswing phase of the swing, the participants' shirts were inclined to fold and cover the shoulder markers, limiting their visibility. This was prevented by specifying that the participants either complete the tests wearing a close-fitting top or shirtless. Participants were also required to wear golf shoes and a golf glove.

Participants were allocated time to warm up before testing commenced, this also provided an opportunity to check that the radar system was capturing both the club and ball data. Once the participant was happy to continue, the instrumented club was attached to the subject. The subject was asked to hold the club with their normal grip style whilst two CODA marker boxes were attached to their wrist with insulation tape onto a sweat band. These marker boxes provided power to the club markers. The long cable bundle providing connections to the accelerometers and strain gauges was strapped onto the back of the subject's forearm with an elasticated velcro strap and run along the arm to the base of the neck. The bundle was secured here in several locations with Micropore tape. A further marker box was secured to the subject's chest with Micropore tape and two markers powered by this box were attached to the shoulders. The subject was then asked to move through the full motion of a swing to check for any restrictions to their motion. Testing then commenced.

For each swing an impact location sticker was positioned onto the clubface to provide a record of impact location as a measure of swing quality and also to validate the new system's ability to measure impact location. Before each swing a trigger was set in Smart Office from the lead/lag accelerometer (channel 1).

Participants were asked to perform 20 full swings with the instrumented driver to allow the selection of 10 good swings where all systems had performed well and which the golfers felt were good representations of their style of swing. The conductor of the testing signalled the participant to start a swing and manual triggers were activated for both the HSV cameras and CODA, while Smart Office and Trackman triggered automatically. Shots were hit into a net in the STI laboratory from an artificial turf matt with a rubber tee. Once a shot had been completed, sufficient time was provided for data to be downloaded and for the participant to prepare for the next shot. The radar system automatically stored each swing into an archive for

that golfer. HSV data was captured for 1.9s; this was later cropped down to the frames in which the clubhead was present. CODA data for all markers was plotted in terms of Z position (height from ground) with respect to time. This enabled a good visual of each stage of the swing and marker visibility could be checked throughout the main section of the swing (the beginning and end would be cropped during processing). Accelerometer data and strain gauge data were checked for any obvious errors such as a loose cable/bad connection and automatically saved into a folder for that subject.

The participant was asked to rate each swing out of 10 in terms of how representative it was of their swing style. This would allow a selection of shots to be selected during processing, which could be converted into a swing profile which was representative of a good shot for that golfer. For each swing, the ball was tee'd up by the investigator to check the reflective dot was always facing the target line; the impact sticker was also changed.

At the end of testing the participant was unstrapped and all of the data from that session was saved to file.

4.5 Results

The methodology presented in section 3.3 was implemented to analyse the data captured during the golfer trials. The results are now presented alongside the captured strain gauge and accelerometer data.

4.5.1 Impact location

A comparison between the measured impact locations from the impact stickers and the calculated positions are shown in Figure 36. All of the swings that both measured and calculated data were obtained for are plotted for all 14 subjects. The positions are shown in mm with the centre of each plot being the geometric centre of the face. The measurements show good agreement for most of the data points. The two obvious outliers with the greatest discrepancy are seen in one of the measurements for Subject 2 and one for Subject 7. This was identified as the second swing for Subject 2 and the sixth for Subject 7. After further investigation it was found that both subjects performed an abnormal swing as can be seen in the plot of lie angle for that Subject 2, in Figure 35.

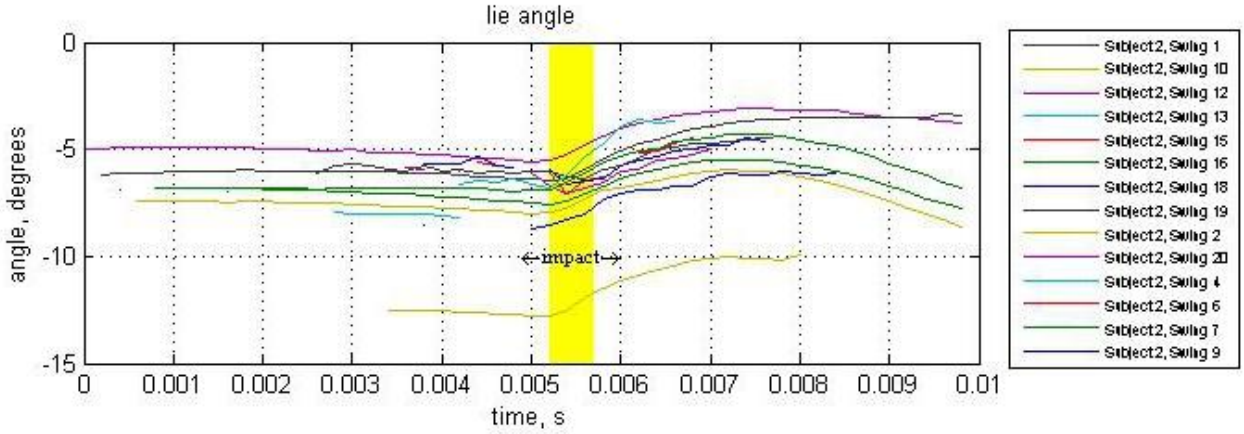

Figure 35 - Lie angle for Subject 2

The majority of the data points in the comparative plots are within 5mm of each other which is to be expected given the inaccuracy of placing the impact stickers onto the club face by eye. Average impact location discrepancies are shows in

Table 2 for each subject. Subject 13's impact locations stand out as the only set with high disparity between all data points. Interestingly, all of the calculated points are positioned lower on the z axis. This could be due to a systematic error in the positioning of the stickers for that set of tests, however, PONTOS project files for Subject 13 were reviewed and it was found that fewer markers were recognised by the software in many of the images and this could have caused a poor fit between the point cloud and the markers recognised as point locations. Consequently the results will contain an error in the predictions of clubhead positions and rotations.

The results from the impact position calculations are encouraging; a measured shot out of the toe has been calculated as a toe shot, and the same for the heel. When provided with an accurate set of point locations during impact, the script can calculate the impact location to an acceptable level. These measurements are believed accurate enough to be used as an implication of the effect impact location has on the path of the club during impact.

Subject 1	Subject 2	Subject 3	Subject 4	Subject 5	Subject 6	Subject 7
4.8mm	4.4mm	5.5mm	5.1mm	4.6mm	5.6mm	7.8mm
Subject 8	Subject 9	Subject 10	Subject 11	Subject 12	Subject 13	Subject 14
3.6mm	3.7mm	5.0mm	6.0mm	4.2mm	15.5mm	6.8mm

Table 2 - Average discrepancy between measured and calculated impacts for each golfer

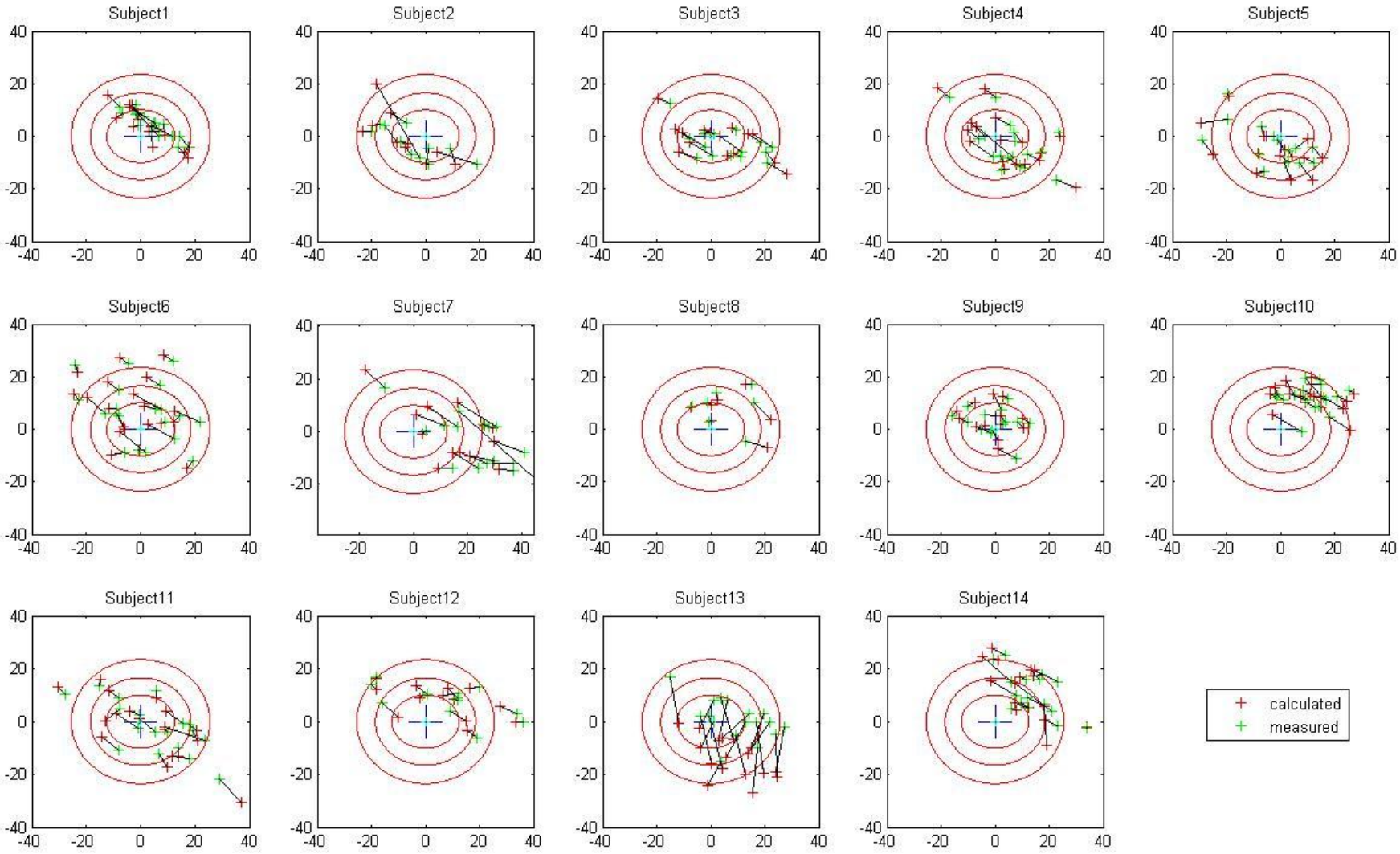

Figure 36 - Comparison between measured and calculated impact positions in mm from geometrical centre of clubface

4.5.2 Clubhead motion

4.5.2.1 Clubhead orientation

The 3 rotations, lie angle, dynamic loft and face angle were calculated for each golfer's swing using the method described in section 3.6.

Figure 38 shows all clubhead rotations for Subject 9's swings, a subject with a consistent central impact location, whereas Figure 37 displays the clubhead rotations for all of Subject 6's swings, a subject with a wide range of impact locations. The axes have been scaled to aid the comparison between the two golfer's swings. Comparing the three rotations between the subjects, it can be seen that for all three, the low spread of impact locations results in less variance in clubhead rotation between swings.

For all subjects, the dynamic loft angle gradually decreases before impact whereas the face angle increases. This relates to an increase in loft and a closing of the face. The lie angle shows more variance but generally stays at a constant angle leading to impact. There are some instances where a negative angle has been measured, such as in Figure 37 where in swing 1 and 2 the lie angle decreases noticeably leading up to impact. A review of the impact locations and the high speed video revealed that during these swings, the clubhead was travelling very close to the ground and it is suspected that the toe impacted the golf mat, causing the toe to rise. The impact for both of these swings was very high on the clubface.

Impact location can have a large effect on the change in clubhead orientation during the impact phase. An impact which isn't directed through the centre of gravity of the club will cause a rotation of the clubhead, with an impact in the toe region causing the face to open and an impact below the point of projection of the centre of gravity on the face will result in a decrease in dynamic loft.

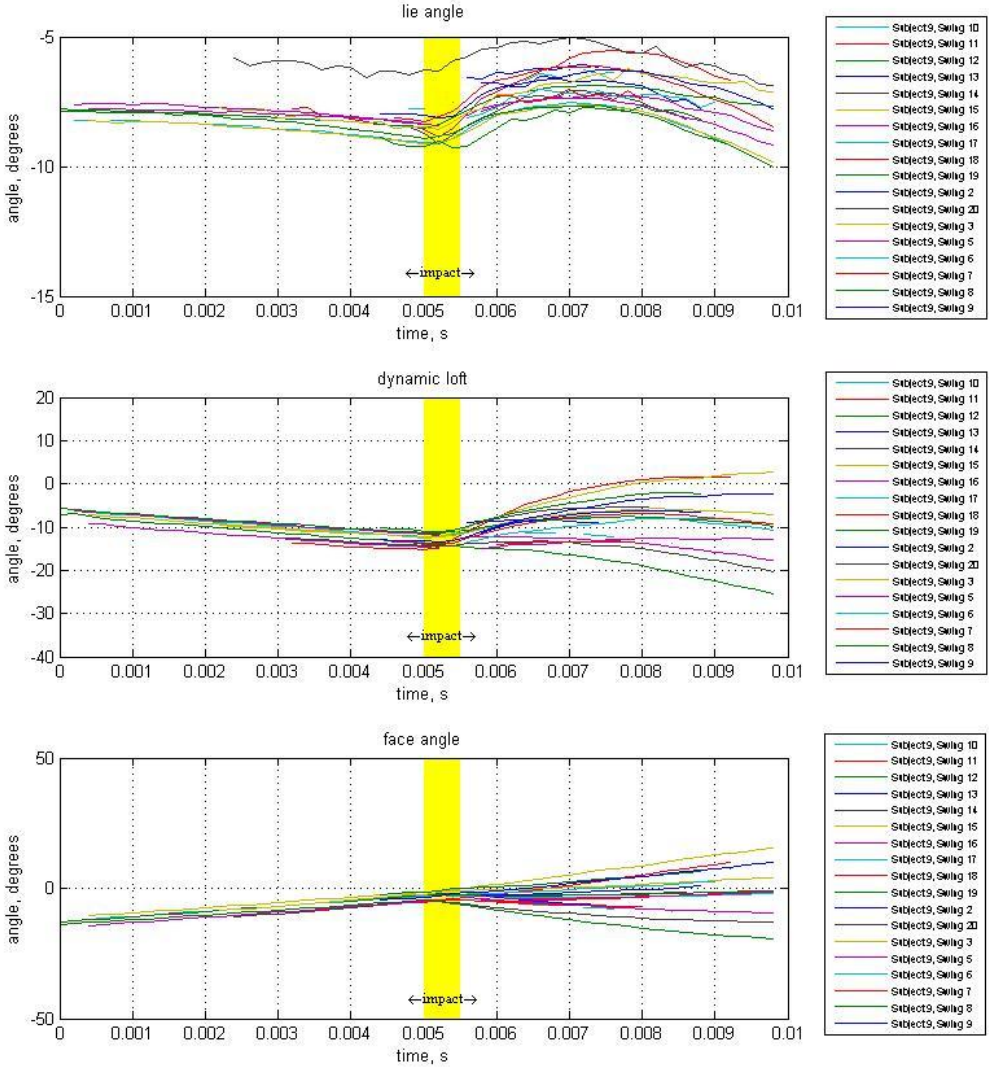

Figure 38 - Subject 9: Clubhead rotations

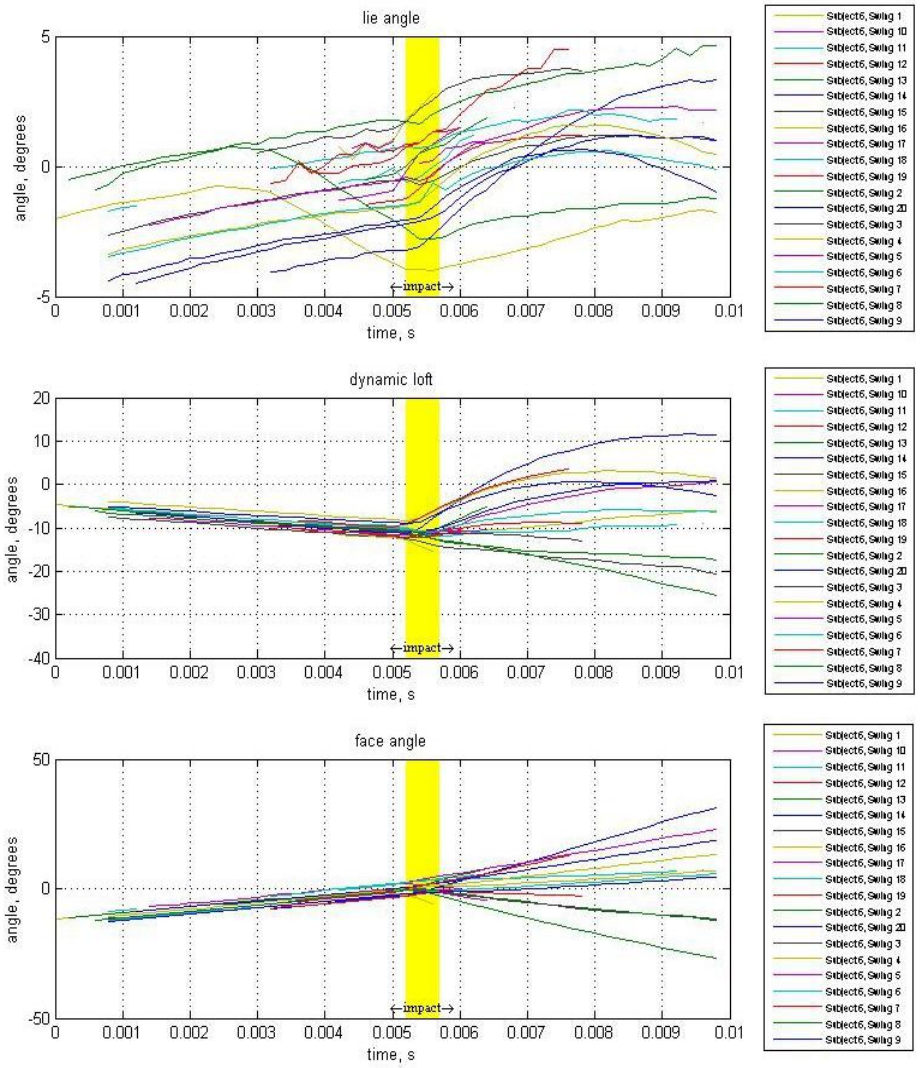

Figure 37 - Subject 6: Clubhead rotations

The average lie angle, dynamic loft and face angles were calculated for each subject and are presented in Figure 39 along with a shaded region showing the range for that subject. The purpose of this figure is to demonstrate the range across all of the swings for which data was collected. The ranges of the averages are as follows; 13 degrees for the lie angle, 11 degrees for dynamic loft and 9 degrees for the face angle at impact. All averages of clubhead rotations leading up to and during impact tend to follow the same path and the variance in the values is quite small. It is only after impact that the effect of impact position takes place and the spread of data wider. In terms of replicating these measurements with a simulation, this could prove problematic as there are no clear differences between golfer and their swing type. However, the combination of this data and the knowledge of shaft strain and clubhead acceleration provides a more comprehensive image of the golf swing and allow a greater range of variables to match via a mathematical model simulation.

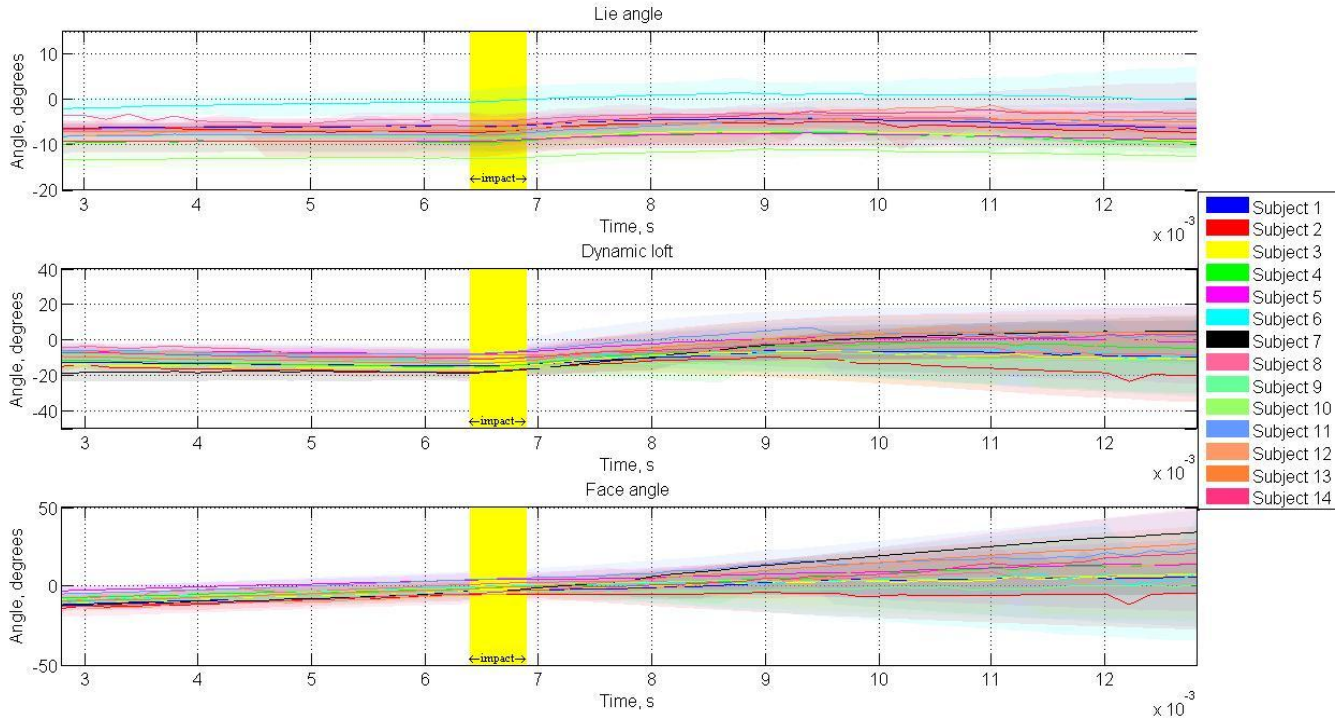

Figure 39 - Average and range of club rotation angles for all subjects

4.5.2.2 Clubhead path and velocity

Figure 40 contains a plot of all the attack angles calculated for subject 3.

The data appears noisy for all subjects; this is due to using the differential of the data to calculate change in position from one stage to the next. Considering the plot in Figure 41, it can be seen that the positional data for the centre of clubface point as plotted here for Subject 14, contains minimal noise. Interestingly, for all subjects, the angle of the clubhead path increases leading up to impact, this could represent the way in which golfers attempt to hit up through the ball with a driver to increase distance. During impact with the ball, the change in attack angle is more dramatic in comparison to the rotations of the clubhead in the roll, pitch and yaw orientations as it depicts the clubhead being pushed down from the oblique impact with the ball.

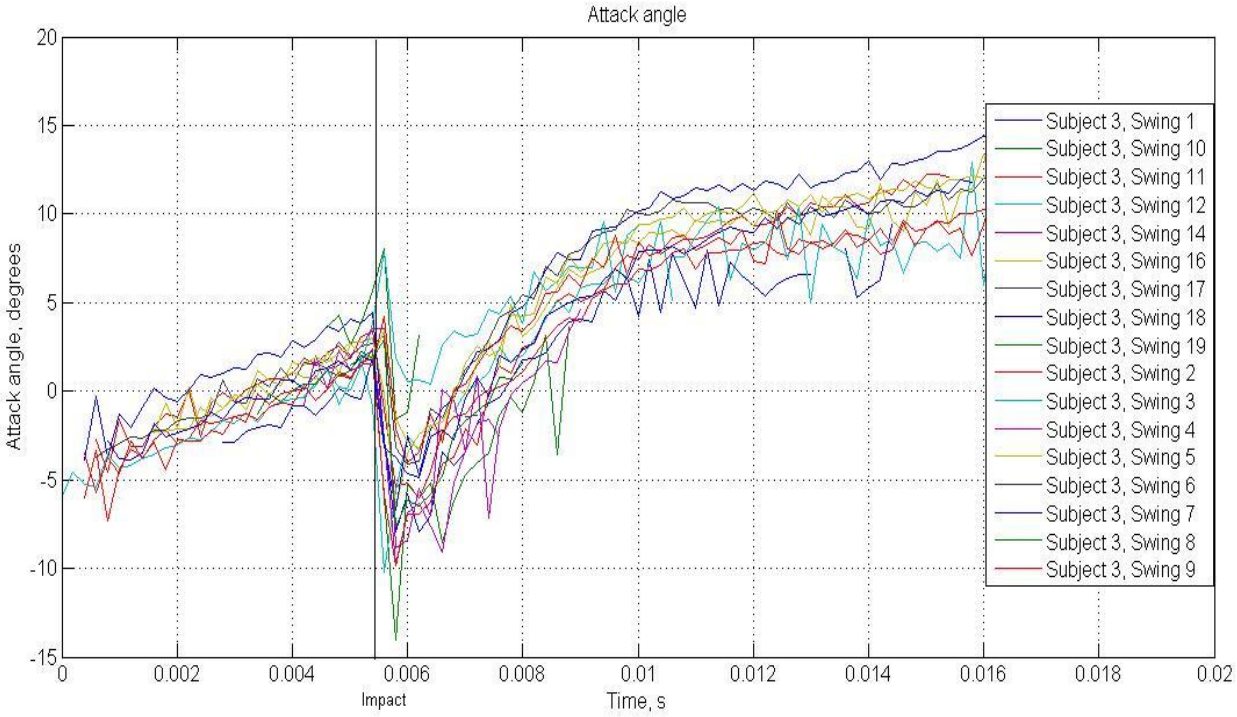

Figure 40 - Subject 3 attack angles

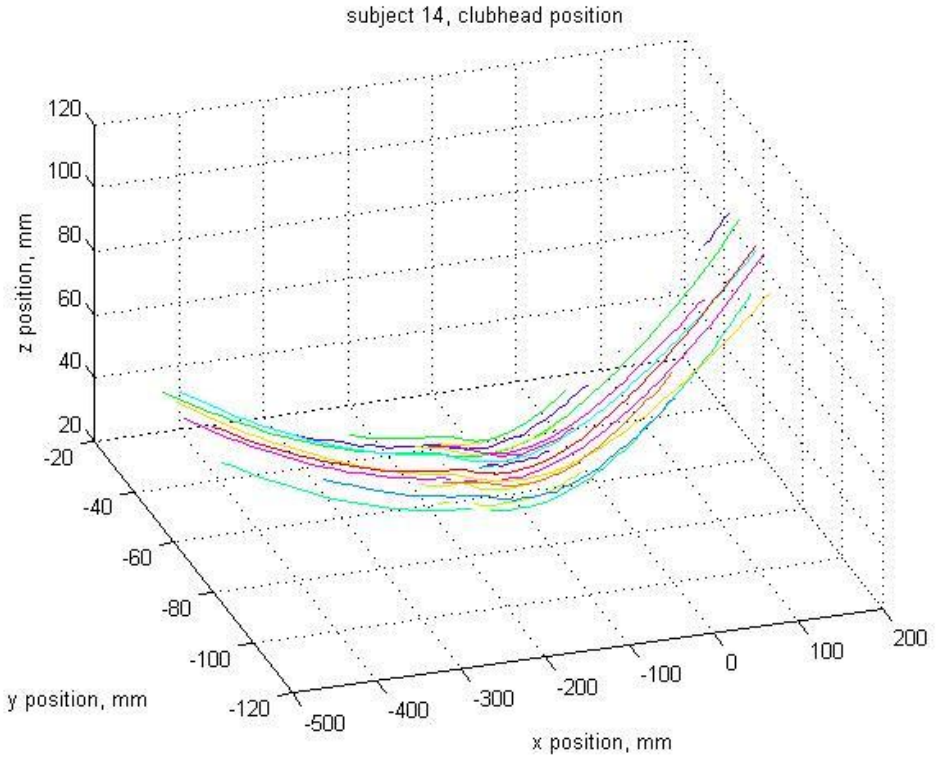

Figure 41 - Subject 14 clubhead position

For each swing, the speed was calculated for the centre of clubface marker as well as a point on both the heel and toe. As expected, the speed of each point dramatically decreased during and after impact. It was found that due to the rotation of the clubhead during the impact phase of the swing, a large variance exists in the speed of each area of the club. A closing clubface would result in a much higher speed at the toe whereas a toe impact would cause the toe speed to decrease relative to the heel.

Figure 42 presents a series of plots showing the speed of the three points on the clubhead during each swing for Subject 4. Figure 42a demonstrates the consistency of the centre of face speed for this subject. In both Figure 42b and Figure 42c it can be observed how a swing which has a high toe speed will have a low heel speed, and this indicates a closing face. This can be observed in swing 1, represented by the navy line, which has the highest toe speed and the lowest heel speed. A review of the impact locations for this subject shows that this swing resulted in a particularly

low-heel impact position. Swing 24, the outlier in both the toe and heel speed plots was the result of a high-toe impact location. For all subjects, the average toe speeds were higher than the centre of clubface speed leading up to impact, demonstrating how the clubface closes in before striking the ball.

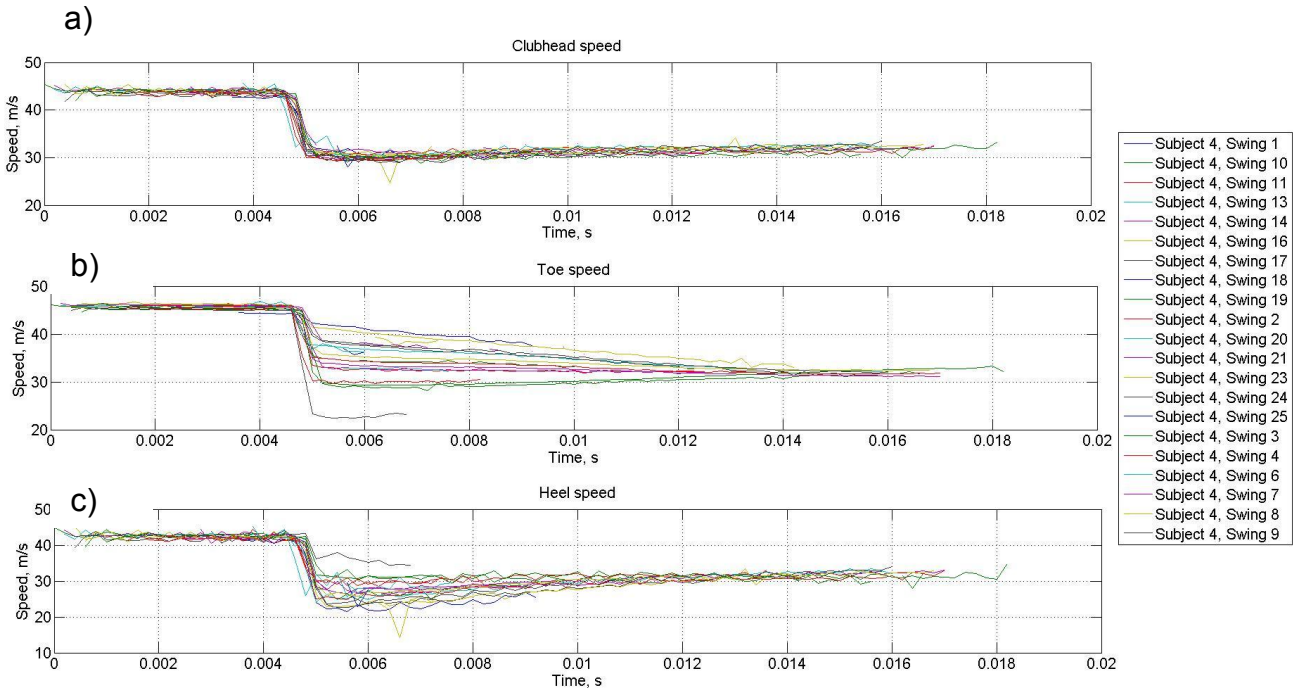

Figure 42 - Clubhead speeds for Subject 4

The speed of any point in the point cloud can be measured, once an adapter has been created for the point of interest. Here the author considered the speed of the 4 points for which positional data had previously been exported for the 6DOF calculations as well as the centre of clubface point. These point positions were imported into Matlab via a script and the speed between each stage was calculated using the 3D Pythagorean Theorem. For swings involving very off-centre impacts, there were large differences between toe and heel speed post impact. The largest difference being in Subject 14's 9th swing as shown in Figure 43 where it was measured to be 25.9 m/s. This demonstrates how considering the clubhead as just one lump mass moving at a single speed unacceptably simplifies the real situation.

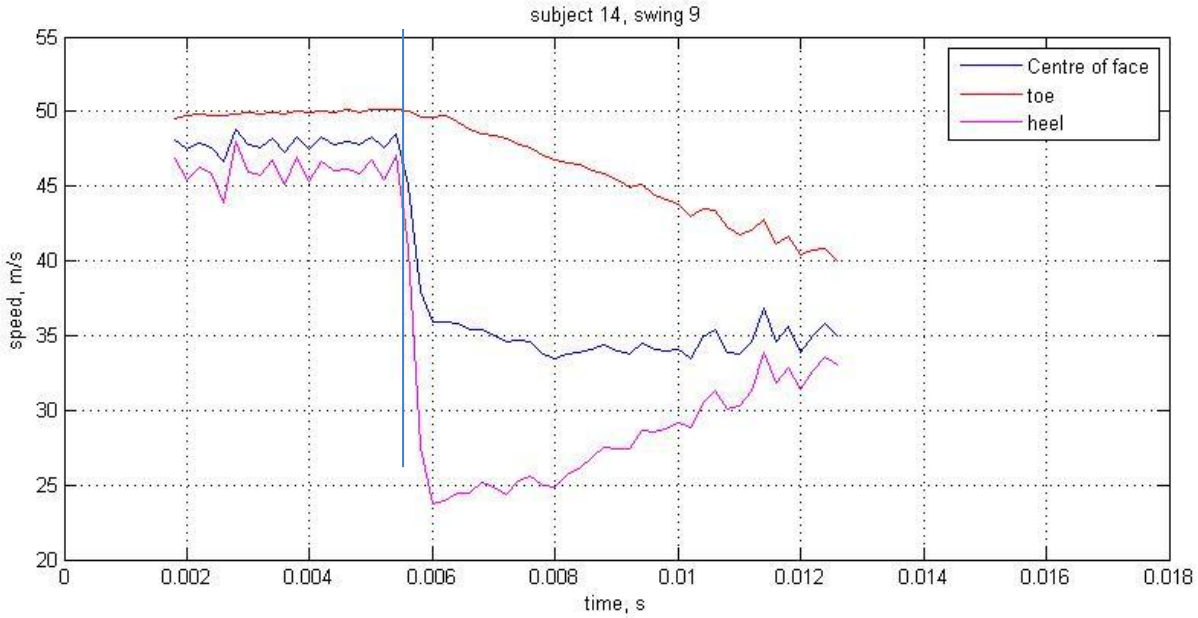

Figure 43 - Clubhead speeds for Subject 14 swing 9, vertical line donates start of impact phase

4.5.3 Comparison of Trackman vs PONTOS, validation

The face angles and dynamic loft at impact were compared with the values measured by the commercially available radar system, Trackman. Trackman provides just a single reading for both values at impact, providing the club has been registered by the hardware. These values are calculated from a model (of which there is no information publicly available) rather than measured so provide an approximation of the clubhead orientation rather than an accurate representation. Regardless of this, the data collected with the Trackman system was used as a method of validation for the rotations calculated with the newly developed PONTOS system, as it is still considered the 'gold standard'.

Both the previously calculated clubhead rotations and the values collected with Trackman were imported into Matlab and the differences between each were found for the initial point of impact. An example of the output is shown in Figure 44, where the yellow vertical line denotes the impact region, the blue data line represents the data measured with the new PONTOS based system and the red line is the single value given by Trackman.

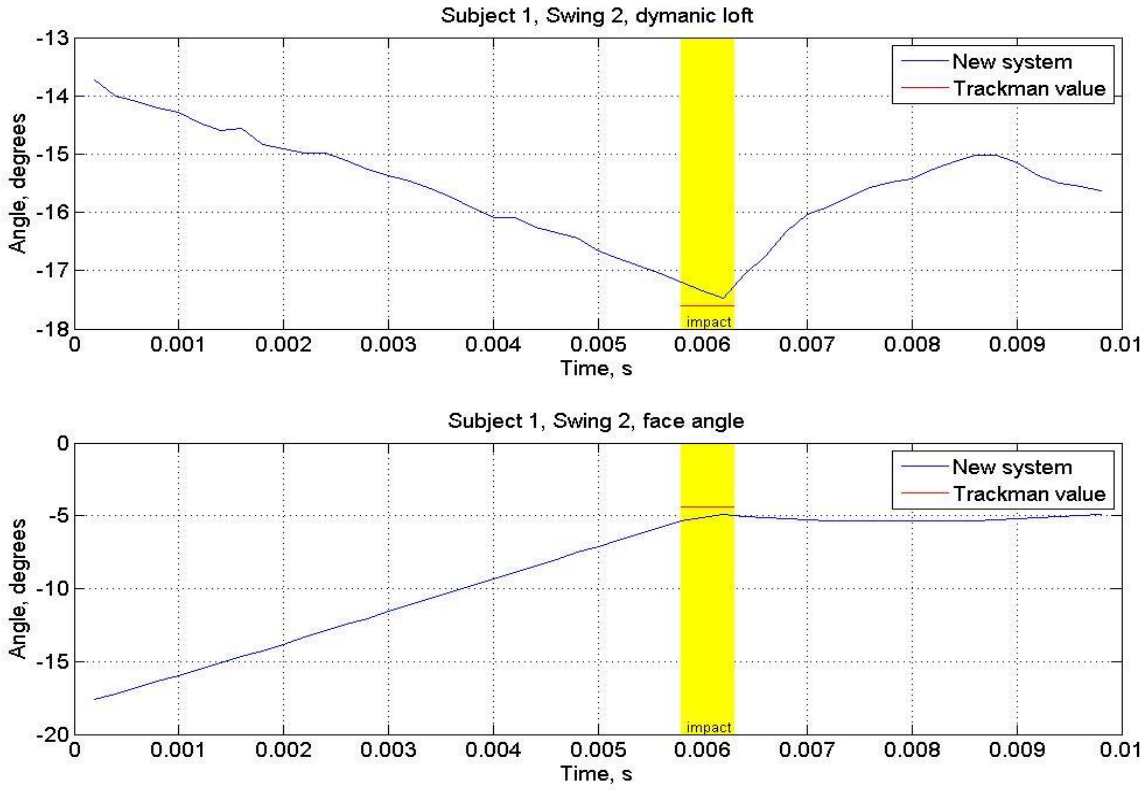

Figure 44 - PONTOS vs Trackman comparison

For the comparison calculation, the value taken as the angle from the PONTOS measured data was the measurement at the start of impact. The averages of the difference between the two values for each subject were calculated and are shown in Table 3. As the values in this table show, there was very good agreement between the two systems, and this could be considered as the worst case scenario for some swings; as seen in Figure 44, the difference between the two angles decrease further into the impact time range. These results have shown that the new system developed in this chapter is producing good results, consistent with commercially available systems but providing an additional level of detail.

Subject	Average Face Angle difference (degrees)	Average Dynamic Loft difference (degrees)
Subject 1	2.1	2.1
Subject 2	1.6	1.3
Subject 3	3.4	2.2
Subject 4	3.1	6.2
Subject 5	2.4	3.0
Subject 6	2.0	3.9
Subject 7	3.9	2.3
Subject 8	2.3	1.8
Subject 9	2.1	1.1
Subject 10	3.2	1.3
Subject 11	2.3	2.9
Subject 12	5.7	3.2
Subject 13	3.7	2.5
Subject 14	5.2	3.8

Table 3 - Average differences between PONTOS and Trackman Face angle and Dynamic loft

4.5.4 Shaft bending

Shaft deflection profiles were captured for all twenty swings for each golfer, however, this is a variable which is very consistent from swing to swing so only one plot demonstrating a typical trace is required per golfer. All of the strain data were converted via an FFT to display the frequencies it contained. A low pass rectangular window filter was applied at 15Hz, as the strains contained a low level of noise. A calibration carried out before data collection enabled a transformation from the measured strain, to metres of deflection at the clubhead, the results were plotted in as inches of deflection to allow a direct comparison to the output from Shaftlab.

An example of a strain gauge output for two golfers is given in Figure 45 and shows the shaft strain data from the takeaway up until just before impact, as it is the strain

in the shaft prior to the point of impact which should be replicated by a simulation of both robot and model. The two plots are split into two distinct sections, the first being the backswing and the second the downswing. The plot in red shows the strain in the toe up/down direction, whereas the blue line shows the lead/lag strain induced by the clubhead. Each golfer's deformation plot fitted one of the four profiles defined by Butler and Winfield (1994), Figure 45a demonstrates a 'double peak' profile whereas Figure 45c is classified as a 'ramp'.

This data will enable comparisons to be made between simulated swings and golfer swings and will enable an assessment to be made on the success of virtual robot adaptations made via changes to the model.

4.5.5 Clubhead vibration

Clubhead acceleration was captured for each swing as an indication of the final goal of this project, to match the same clubhead oscillation during a simulation of a golf swing. As in the case of the shaft deformation, the acceleration profile for each swing is very consistent. The data captured was quite noisy so the same filtering method as implemented in section 4.5.4 was applied. Only the highest frequencies (>30Hz) were removed as filtering too heavily created low frequency oscillations in the data. Regardless of the noise, the plots show a smooth swing with no evidence of vibration of the clubhead. Two example plots are shown in Figure 45 (b) and (d) where the red line represents the accelerometer in the toe up/down orientation and the blue shows the acceleration perpendicular to this in the lead/lag direction. The toe up/down accelerometer is the first to peak as at the takeaway the golfer will usually twist the grip to point the toe in the direction of travel.

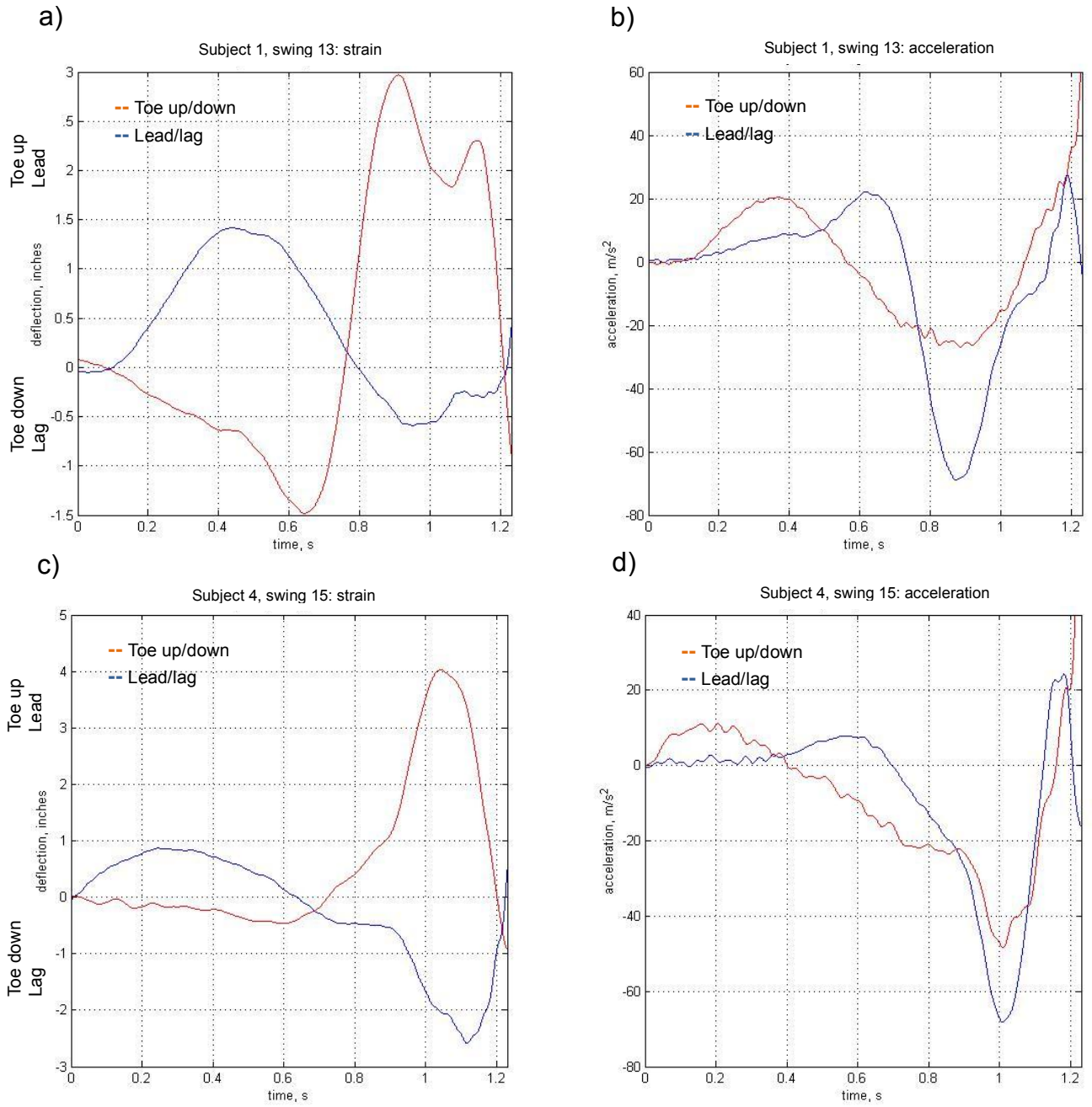

Figure 45 - (a) Subject 1, swing 13 strain and (b) acceleration. (c) Subject 4 swing 15 strain & (d) acceleration

4.6 Conclusion

The goal of this chapter was to measure a wide selection of variables during a golf swing to gain a better understanding of the mechanics of a swing and to provide measured data which could be used in conjunction with a mathematical model. A club was instrumented with two strain gauges and two accelerometers, one of each

pair aligned with the toe up/down direction of motion and the other aligned to measure motion caused by the lead and lag of the clubhead. CODA motion markers were also mounted onto the club and the shoulders of each golfer to determine kinematic data for that subject. These variables were measured alongside the clubhead variables which were measured using the new system developed in the previous chapter. 14 golfers participated in the study, each performing 20 swings in an indoor environment. Swing variables were measured for each and subsequently analysed.

The data collected with the PONTOS system was processed in Matlab following the methodology in section 3.6. The first variable of the swing which was analysed were the impact locations for each swing as it is this variable which determines the direction the golf shot takes after impact. It also provides insight into changes in clubhead orientation during impact. Impact locations had been measured during the study with impact stickers and a comparison was made with calculated impact positions, these results were encouraging, the impact locations calculated with PONTOS captured point position showed good agreement with the positions given by the stickers. A 6DOF analysis was conducted on measured point positions for four markers distributed around the clubhead. The lie angle, dynamic loft and face angle during the swing were defined as the roll, pitch and yaw respectively and were calculated for 0.01s around the impact phase of the swing. For all swings it was found that the clubhead gradually increases in loft (averaging around 5 degrees) while the face angle closes (up to 20 degrees in 0.0055s) leading up to impact. Attack angle and clubhead speed were both calculated via the 3D Pythagorean Theorem with PONTOS measured point positions. The plots of attack angle demonstrated for the majority of swings that during impact the clubhead lifted slightly, this has been surmised to be the result of golfer attempting to hit up into the ball. The flexibility of this newly developed system meant that clubhead speed didn't have to be considered as a single variable, but rather could be measured at multiple positions on the clubhead. For this study, three areas were analysed, speeds of the centre of the clubface, the toe and the heel. The variance of speed across the clubhead was much larger than expected with one particular swing involving a very off-centre impact resulting in a difference from toe to heel of 25.9m/s.

Plots were generated for shaft strain and clubhead acceleration for each subject. These two variables are so consistent for each golfer that only a single plot is required to describe that players swing type.

The clubhead orientation data collected with the new system showed no obvious clubhead oscillation and will not be used against outputs from the mathematical model. This data will, however, allow a final measure of the success of any future adaptions made to the robot as suggested by this research, as a comparison between human and robot swing variables could be made.

This shaft strain and clubhead acceleration data will be essential in validating the mathematical models in the following chapters, along with the CODA kinematic data collected in this study, as it is these three swing variables which are unique to a particular golfer.

Chapter 5

An investigation into passive gripping mechanisms

5.1 Introduction

As discussed in the literature review, it was a previous study by Harper et al, (2005) conducted at the Sports Technology Institute (STI) at Loughborough University, where the rigid collet grip of the Miyamae V golf robot was identified as the most influential factor affecting the level of clubhead oscillation during the simulation of a golf swing. It was these oscillations which prevented the robot from accurately reproducing the same shaft deformation profile as a golfer. A subsequent study by Schmidt et al (2007) considered golfer grip forces during a swing. The results obtained by Schmidt (2007) added further to the hypothesis that the Miyamae V's collet grip was neither flexible enough nor capable of applying the same range of force as a human hand, and a new gripping mechanism would need to be developed.

Before advancing to modelling the robot, the decision was made to implement a physical solution which could be tested in situ on the robot to give an indication of the results that could be achieved. As an initial attempt to dampen clubhead oscillations and monitor the system's response, it was decided that a passive approach should be adopted in the form of a passive gripper as it would be simple to manufacture and implement. Two prototype passive grippers were therefore developed. The first was a pneumatic gripper in the in the form of an aluminium cylinder which could be clamped into the robot's existing grip and contained inflatable rubber tubes which could be inflated to various pressures, this was found to have minimal impact on the level of clubhead vibration. A second clamping mechanism was produced which allows a vibration damping material to be positioned at the interface between the club shaft and the robot's grip. This purpose of this material was to isolate vibration at the robot's existing rigid robot collet from the golf club's shaft.

A silicone was eventually selected as the most suitable material for this purpose

based on its availability, ease of manufacture, similarities to human skin properties and most importantly its damping constants. Several silicone sleeves with differing material properties were produced to be positioned around the top of the golf club shaft and secured in the clamping mechanism. The mechanism was then attached to the existing collet grip allowing each sleeve to be tested. Simple swing motions were then programmed into the robot. Accelerometers were positioned on the clubhead and collet so that acceleration of the clubhead could be monitored, minus whole body acceleration measured at the collet, and the success of the grip could be quantified by its ability to dampen robot induced vibrations.

This chapter discusses the development process of the passive gripper mechanisms and the methods which were tested for their effectiveness at damping out clubhead oscillations. The results from this investigation were used as an indication as to how this research should progress to the next stage of development.

5.2 Current robot grip

The Miyamae V's existing gripping mechanism is in the form of a collet clamp which is situated just below the robot's wrist joint as shown in Figure 46. Six teeth positioned around the circumference of the grip and extending its full length are tapered at either end on their external face. Two bands of metal slide along the length of the grip which are connected by a lever and screw thread, when the bands are pushed apart, they slide up the exterior taper forcing the teeth to clamp inwards onto the club.

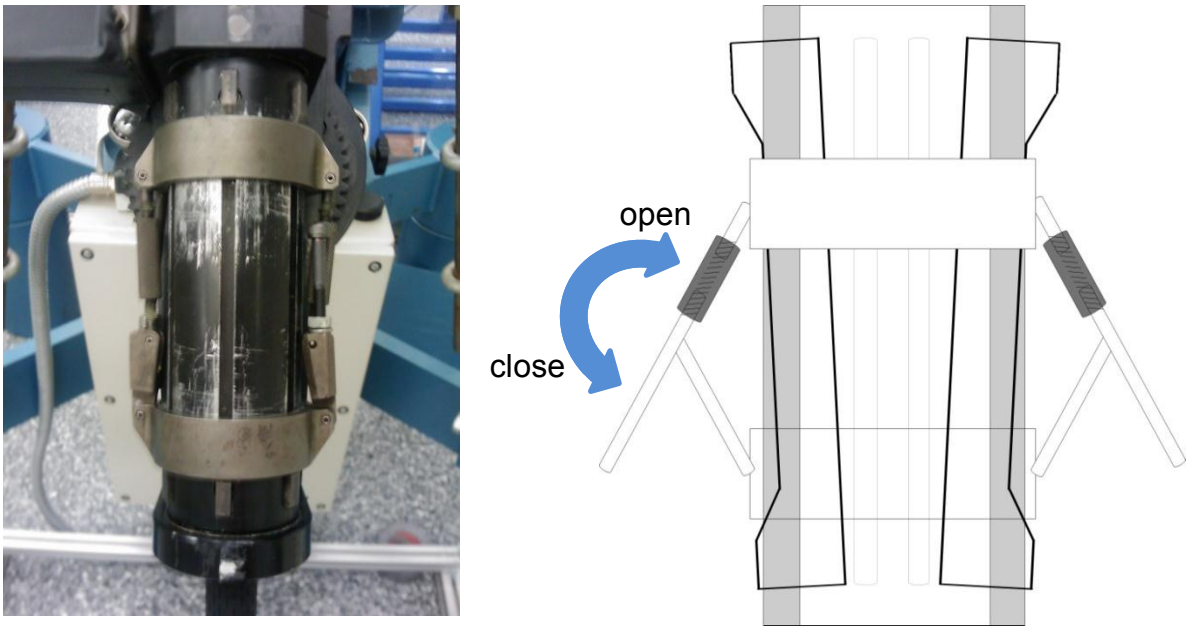

Figure 46 - Miyamae V collet grip

A club is secured in the collet by entering the grip end of the club into the base of the collet whilst the collet is unclamped. This is achieved by rotating the two clamp levers outwards which pulls in the two metal bands and releases the inner gripping teeth. Once the club has been positioned correctly, the arms are then rotated upwards, forcing the two bands apart, which lock into position. All gripping force is provided through the six teeth applying a high pressure at these contact points. Two adjustment screws at the sides of the collet allow different sized club grips to be securely clamped.

5.3 Robot grip force tests

With the hypothesis being that the majority of the vibrations transferred to the club could be isolated at the robot grip level some preliminary tests were carried out to achieve a greater understanding of its operation with regards to the force it applies during a swing and to assess how the method of gripping the club could be detrimental to the robot's ability to simulate a human golf swing.

Following the methodology presented in Schmidt's (2007) work, an experiment was conducted to establish the magnitude and character of the force exerted by the Miyamae V's collet clamp onto a golf club during a full golf swing. Tekscan thin-film

force sensors were used to measure grip force so that comparisons between the robot and several golfers with varying handicaps could be made.

A Tekscan 9811 sensor was attached to the grip of a standard driver with double sided tape, and both secured and protected with Micropore tape as shown in Figure 48. The sensors were connected to a Tekscan cuff which was securely strapped to the subject's arm and provided feedback to the PC via a wired connection. Schmidt had concluded that the weight of the handle was low enough not to interfere with the golfer's swing. Tekscan enables the use of an external trigger through a trigger box which was produced from a wiring diagram provided by Tekscan. The trigger box required a TTL voltage drop of 5V, this was provided by light gates positioned behind the tee, perpendicular to the direction of shot. The light gates were also used to trigger an oscilloscope which recorded data from a sound level meter positioned close to the tee; this was to determine the time of impact for alignment of force traces. A lag was found in the Tekscan trigger in Schmidt's experiments so a test was also completed to determine the lag so that each force trace could be aligned by point of impact. A hammer was used to strike the Tekscan sensor, breaking the light beam to trigger Tekscan, and the sound of the impact was recorded by the sound level meter. The lag in the sound level meter was assumed to be negligible and therefore the lag was deemed to be the time difference between the detection of the sound at the sound level meter and the recording of the impact force by Tekscan. It was found that, after the primary test, where a lag was present, no further lag was found until the trigger box was disconnected and reconnected thus it was decided that in any further tests using the trigger, the first reading would be disregarded.

Testing took place in the STI lab and shots were hit from a golf mat into a net positioned 4m from the tee position. Six subjects, all golfers between the ages of 23-40 with handicaps of between 5 and 20 were tested. They all wore a single golf glove on their left hand and were asked to complete 10 full swings with the instrumented driver, with time between each swing for warming up and practice shots. Before each player test, a pre-load reading was taken with Tekscan to determine loads due to curvature of the sensor. Tekscan was set-up to record for 3s post trigger at a frequency of 264Hz.

Figure 48 - Tekscan thin film force sensor mounted onto a golf grip

Post-processing of the data was carried out in Matlab. A point of impact for each swing was determined from the oscilloscope trace of the sound level meter output and each player's 10 force traces were aligned by this and plotted against time. Two example plots are shown in Figure 47 and Figure 49.

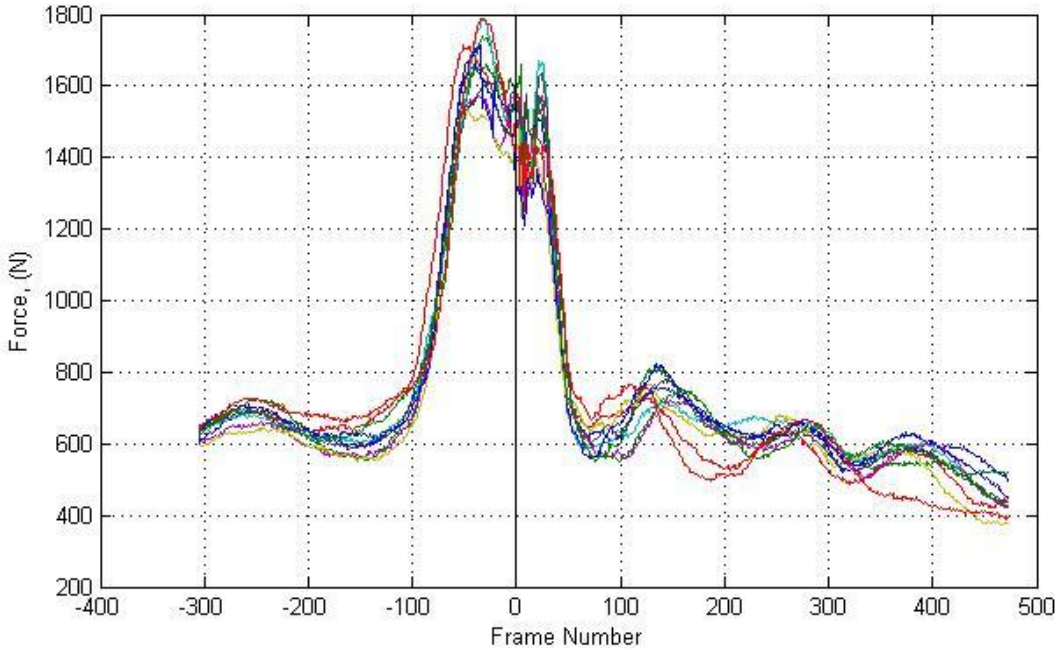

Figure 47 - Golfer grip force trace 1.

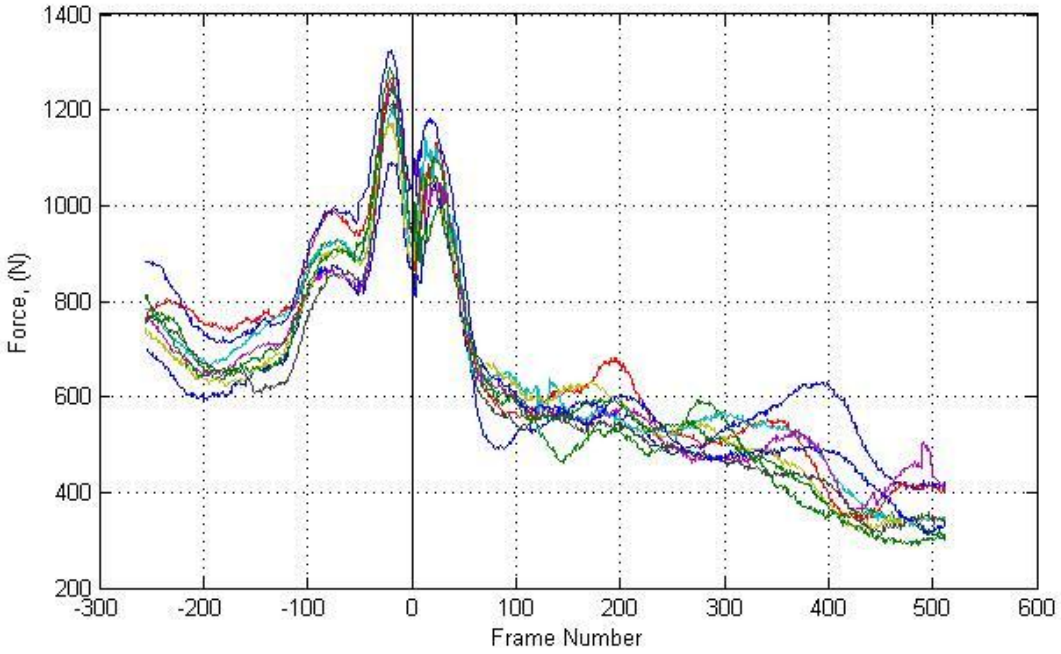

Figure 49 - Golfer grip force trace 2.

The results obtained in this small study are consistent with Schmidt's findings, that every golfer has a unique grip force signature which is consistent throughout each swing; peak forces were also in the same range.

The next phase of this study was to repeat the above methodology to measure the grip force of the robot. The same driver was used but instrumented with a higher pressure rated sensor, 150 psi, as initial tests showed that the robot's grip force was much higher than the range of the 75 psi sensor. Due to space issues inside the robot cage, light gates could not be used to align the force traces, however it was found they were not needed as the robots force trace was so consistent, alignment could be done by eye.

Figure 50 presents the force traces from three swing simulations and it is very apparent that they lack any resemblance to a human golfer's grip force trace. Instead of the golfer's dynamic force, a mainly constant force was applied around ten times the magnitude of the golfer's. The deviation from a constant force is most likely to come from forces due to the oscillation of the club and the three different phases of

force level are likely to be due to the torque profile applied to the robot.

This test has concluded that the initial assumptions about the robot's grip were correct; that its peak forces are much larger than a golfer generates. However, these forces are somewhat required in this scenario to ensure that the club stays firmly grasped by the robot throughout the swing as a matter of safety. A further investigation is required in order to conclude if these potentially excessive forces are required or if there are other means to achieving the same secure attachment of the golf club.

It was first thought that new gripper materials could be tested within the current collet clamp however the maximum diameter of the robot's collet clamp is 30mm which does not allow a sufficient amount of space for additional materials. For this reason, coupled with the uneven pressure distribution it applies with its interior collet teeth, a temporary material clamp would need to be developed which could be clamped into the existing collet clamp and allow more flexibility in the way the club could be gripped.

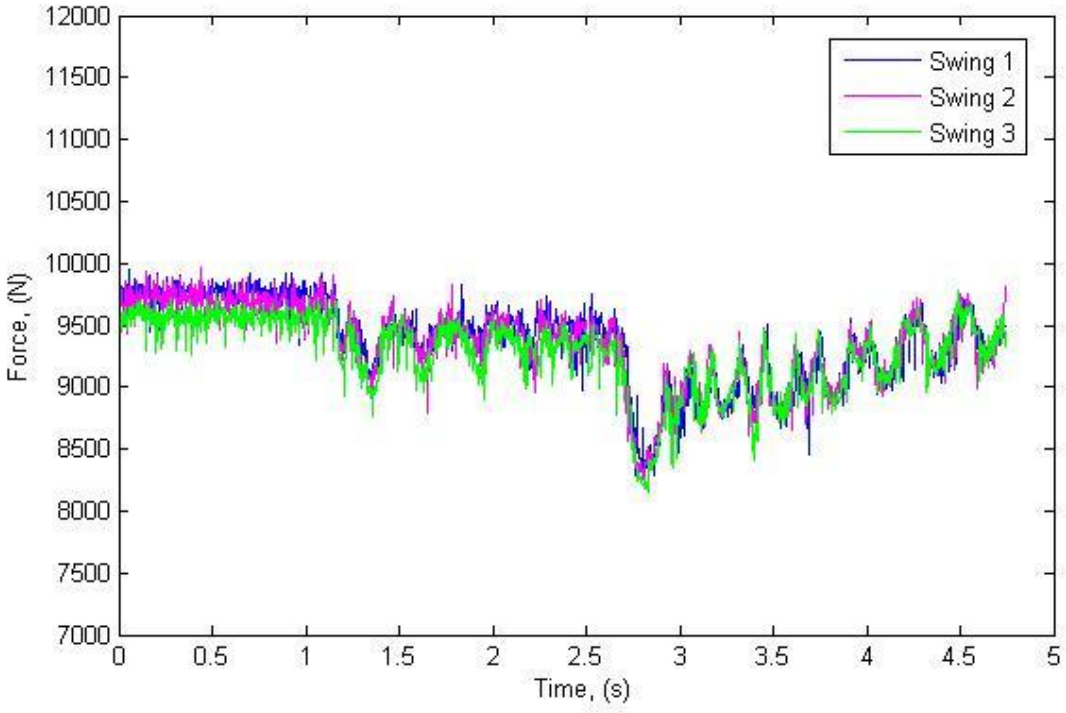

Figure 50 - Robot grip force trace

5.4 Pneumatic grip

To reduce the rigidity in the method of clamping a club, the stiffness or spring constant of a gripper material should be decreased to add compliance into the system, whilst simultaneously increasing the damping constant to reduce oscillations.

A prototype ‘gripper’ was produced in order to easily add different levels of compliance into the system and to test different levels of spring constants to find a useful range for a suitable gripper material. This was achieved through the development of the pneumatic grip shown in Figure 51. The grip consists of three rubber inner tubes (see Figure 51 (b)) extending the length of the outer shell and positioned radially. Each tube has an air flow control tap and all three taps are connected to an inflation point, the tap is attached in series to control the flow to each tube so that their respective pressures can be varied. The outer body of the pneumatic grip is aluminium, with the top tapering in to a smaller cylinder which can be entered into the robot’s collet grip and rigidly clamped into position.

Figure 51 - Pneumatic grip (a) exterior (b) interior

The pneumatic grip could be inflated whilst supporting the golf club and the air pressure in the device measured with a pressure gauge. The air pressure could be varied to allow a different level of stiffness or spring constant of the inner tubes, and the effect on the oscillatory response of the clubhead investigated.

5.4.1 Testing of pneumatic grip

To enable tests to focus on the level of damping provided by the pneumatic grip and subsequent materials, the rubber golf grip was removed from a golf club leaving just the steel shaft. An aluminium flange shown in Figure 52 was then glued into the end of the shaft to provide a safety stopper to prevent centrifugal forces from pulling the club from the robot's grip.

Figure 52 - Grip-less driver with end safety flange

To measure the response of the clubhead during the application of different grip forces, an accelerometer was used. The accelerometer was positioned at the toe of the golf club and attached with beeswax, a small piece of tape was then placed over the top of the accelerometer to prevent it from becoming detached and getting damaged. The accelerometer was connected to a National Instruments data acquisition box and the data was captured using Smart Office software from M+P International. Responses were captured for 8s at a frequency of 2048Hz with a trigger set on the accelerometer's channel from a positive voltage slope of 0.001V which based on the sensitivity of the accelerometer at 0.19pC/ms^2 corresponds to an acceleration of 1.9ms^{-1}.

The three tubes were inflated to a uniform pressure and three trials were conducted

at pressures of 62, 124, and 159 KPa. A test was also conducted on the club when held in the rigid collet to allow a comparison between the rigid collet and the pneumatic grip. Once the pressure had been measured the clubhead was set oscillating by providing an initial displacement from its equilibrium position of around 0.15m towards the ground. It should be mentioned that the intention was to excite the clubhead oscillations parallel to the swing plane of the robot, as they would be during a swing, but due to the robot's drive not being engaged, the robot's joints were free to move, preventing a fixed clamp from being achieved and subsequently making it impossible to initiate any clubhead oscillation.

Acceleration of the clubhead was captured for each grip pressure and plotted in Matlab. The responses for each trial are shown in Figure 53 along with the response from the robot collet clamp. The results show that by decreasing the pressure in the inner tubes, the oscillation frequency is changed due to the change in stiffness. From rigid to 9psi, the frequency of oscillation reduces from 4.167 Hz to 3.25Hz, however, the level of damping provided by the pneumatic grip was low with a damping ratio, (the ratio of damping constant to critical damping value) of 0.019, which was constant throughout the three pressure trials. The damping ratio of the clubhead oscillations in the rigid collet clamp was found to be 0.0049.

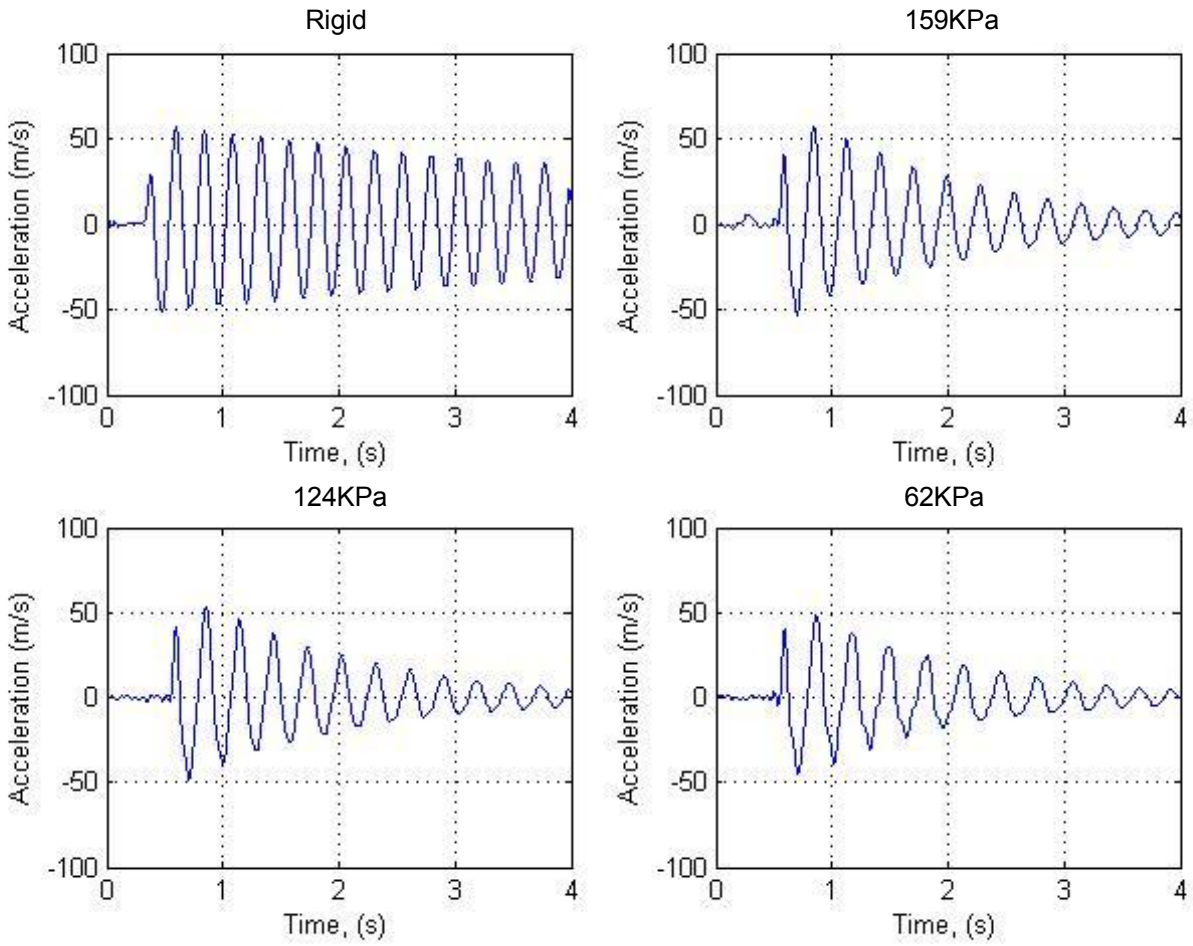

Figure 53 - Clubhead responses (a) Rigid (b) 159KPa (c) 124KPa (d) 62KPa

The results show that introducing compliance into the system has reduced the oscillation of the club but not by enough to deem this gripping mechanism a potential solution. The club continues to vibrate over three seconds after excitation which is equivalent to the duration of a golf swing. It was deduced that this was due to the main source of damping being provided by the thin rubber of the inner tubes, and the damping it provides has been shown to be low. The pneumatic grip was incapable of reducing the clubhead oscillations to an acceptable level and therefore no further tests were carried out with the prototype. A future possibility, however, could lie in the combination of a tube made from a material with a high level of damping which could be inflated to a variety of pressures providing control over the grip force and spring constant.

5.5 Visco elastic gripper

The next phase involved selecting materials with a variety of properties which could be used to encase the golf club grip acting as a passive damping mechanism.

Several factors were considered in the selection of a material for a passive gripper. The two main properties of a material which could affect the clubhead's response are the spring constant and damping co-efficient and these are generally related, i.e. in order to maximise the effect of damping, a material's stiffness is required to be low as motion is required for damping to take place. For instance, considering the material groups shown in Figure 54, which shows Young's modulus versus Tan delta for various classes of materials (Tan delta being a measure of damping), those which provide the highest level of damping, generally have lower Young's modulus values and therefore stiffness. This is shown by the following relationship

$$k = \frac{AE}{l} \tag{5}$$

Where E is the Young's modulus, k is the stiffness, l is the original length of the sample and A is its cross sectional area. As was concluded in the pneumatic grip tests, a material which provides a high level of damping is desirable. Figure 54 shows that the classes with highest level of damping are the polymers, rubbers and particularly the gels, with gels having the lowest spring constant and highest level of damping.

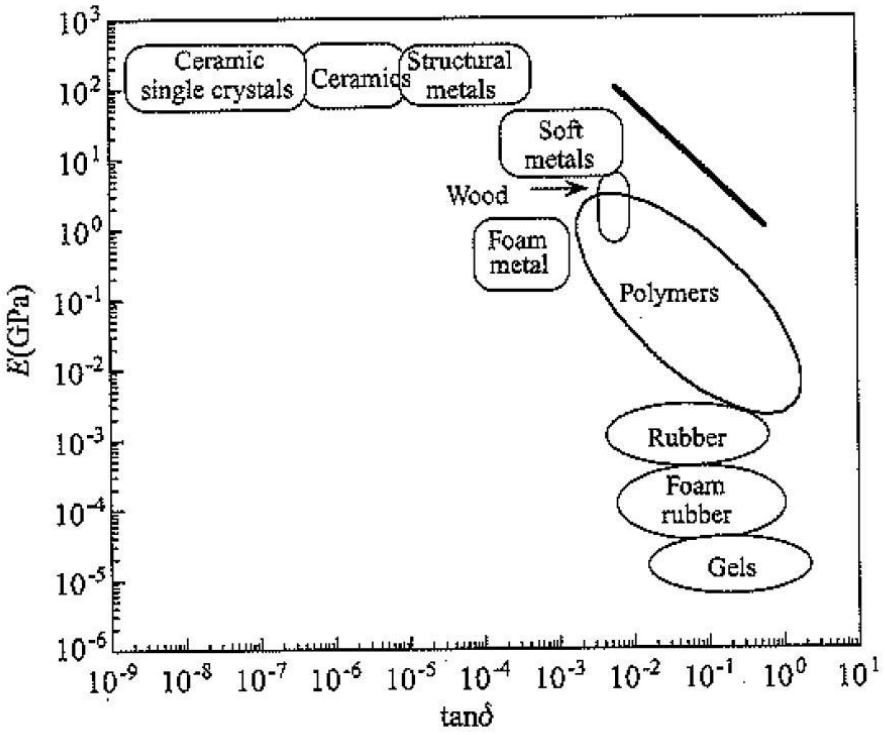

Figure 54 - Young's Modulus versus Tan δ, from Lakes, R. (2009)

Figure 55 from Ashby's materials selection charts (Ashby, M. F. (2005)) lists elastomers such as silicone elastomers and neoprene as materials with the largest loss modulus. The loss modulus represents the energy dissipated as heat during deformation and therefore is a measure of vibration damping abilities. Alongside the desired high level of damping capabilities, other factors considered during the material selection were cost, availability and ease of manufacture. Of the most viable options which included rubber and polyurethane foam, both in sheet form, a silicone gel was selected. Purchasing a liquid silicone system would enable parts to be moulded and cured to various specifications of damping and stiffness depending on the user's requirements. Silicone has been the most popular choice for the outer skin of prosthetics body parts (O'Farrell 1996; Burger 2009). Using a deadener additive available for liquid silicones provides the additional flexibility to produce several gripper prototypes with differing stiffness and damping properties.

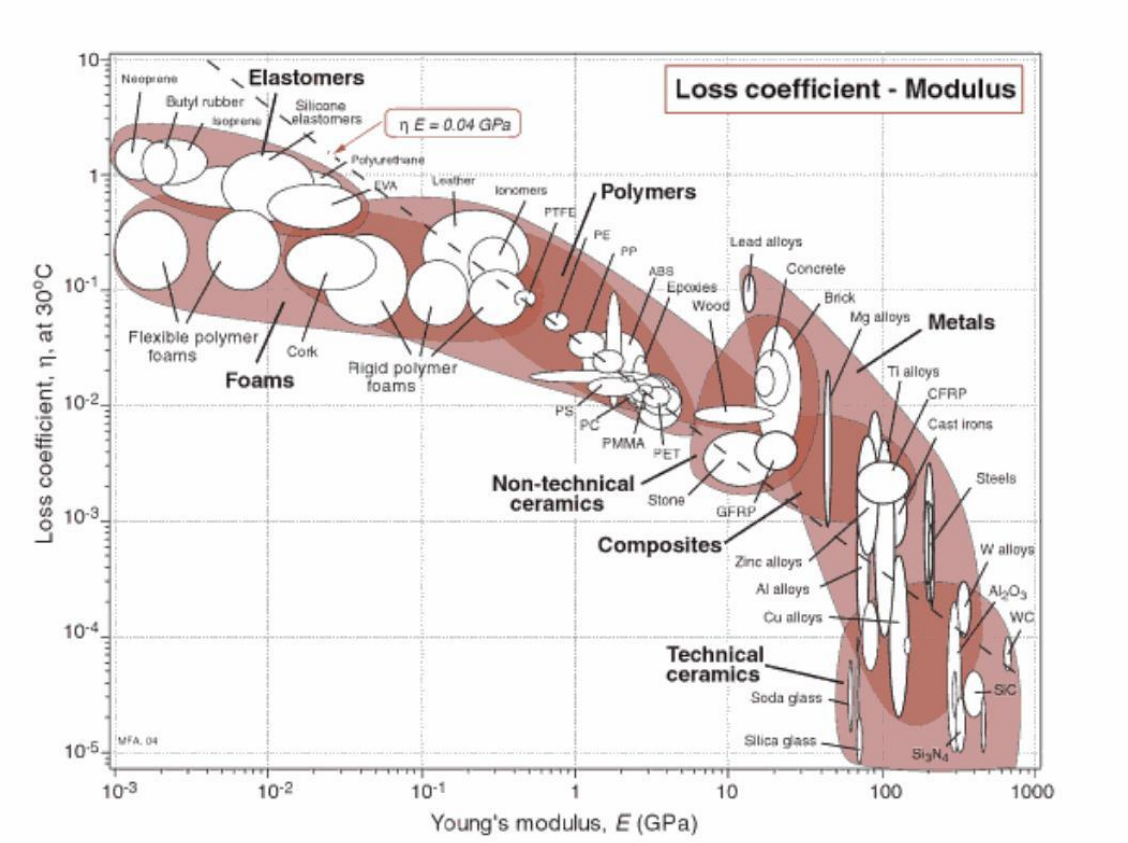

Figure 55 - Loss coefficient versus Young's modulus for different classes of materials from Ashby, M. F. (2005)

5.6 Grip clamp

There was insufficient space within the existing robot collet grip to enable different materials to be incorporated into the gripping mechanism, therefore another clamping mechanism was produced, with the same outer aluminium shell design as used for the pneumatic grip, which would allow more flexibility in the way the club could be held. The three inner tubes were replaced by three steel plates each 165mm long and 15mm wide, with each plate having two threaded bolts attached at either end. The bolts were threaded through the outer shell and could be adjusted with a 3mm Allen key to adjust the plate positions relative to the centre line of the aluminium housing. Two internally threaded cylinders were also attached to each plate and located through the outer shell, bolts screwed into these cylinders provided a stopper to prevent the plates from falling into the centre of the grip. The material clamp is shown in Figure 56. The new material clamp could be rigidly clamped into

the existing robot grip and the club entered into its base; the three plates could then be tightened inwards towards the shaft, clamping onto the prototype grip material. Using a torque wrench to tighten the bolts meant the compressive force on the material could be controlled.

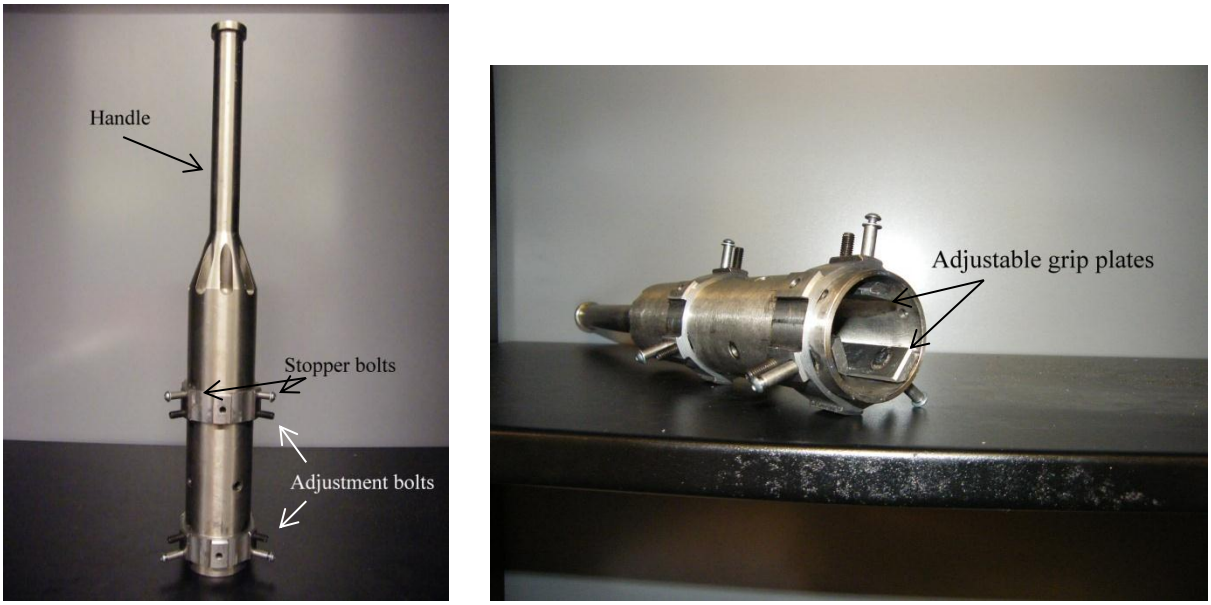

Figure 56 - Grip clamp (a) view 1 (b) view 2

5.7 Silicone sleeve manufacture

A Platsil 10 silicone rubber kit was purchased from Mouldlife, This particular silicone is most frequently chosen for producing prosthetics due to its low hardness (shore 10) and similarity to the touch and appearance of skin. Through the addition of a deadener to this silicone, its properties can be changed, reducing its hardness and causing it to respond more comparably to skin. Silicone deadener can be added as a percentage of the raw silicone's mass of up to 250%, with percentages greater than 30% resulting in a sticky cured gel. The Platsil 10 is supplied as a two part system where equal quantities of parts A and B should be thoroughly mixed before being cured in a mould.

As Silicone cannot be glued, it was decided that the most suitable method of

attaching the cured product to the golf club would be to mould a silicone sleeve which could be pulled down over the top of the shaft. The taper of a golf shaft is only very gradual, across the top 25cm (where the silicone would be positioned) with the diameter only reducing by 0.05cm. This was deemed negligible and so a constant diameter sleeve was manufactured. A mould was designed to produce a silicone sleeve with an internal diameter of 15mm, an external diameter of 35mm and a length of 25cm. The mould, as shown in the technical drawing in Figure 57, consisted of two parts. A 15mm diameter rod mounted onto a rectangular base was used to control the inner diameter of the sleeve. A hollow cylinder with an internal diameter of 35mm was made to form the external surface of the sleeve. The outer piece could be bolted onto the base to ensure the rod was centrally located and to

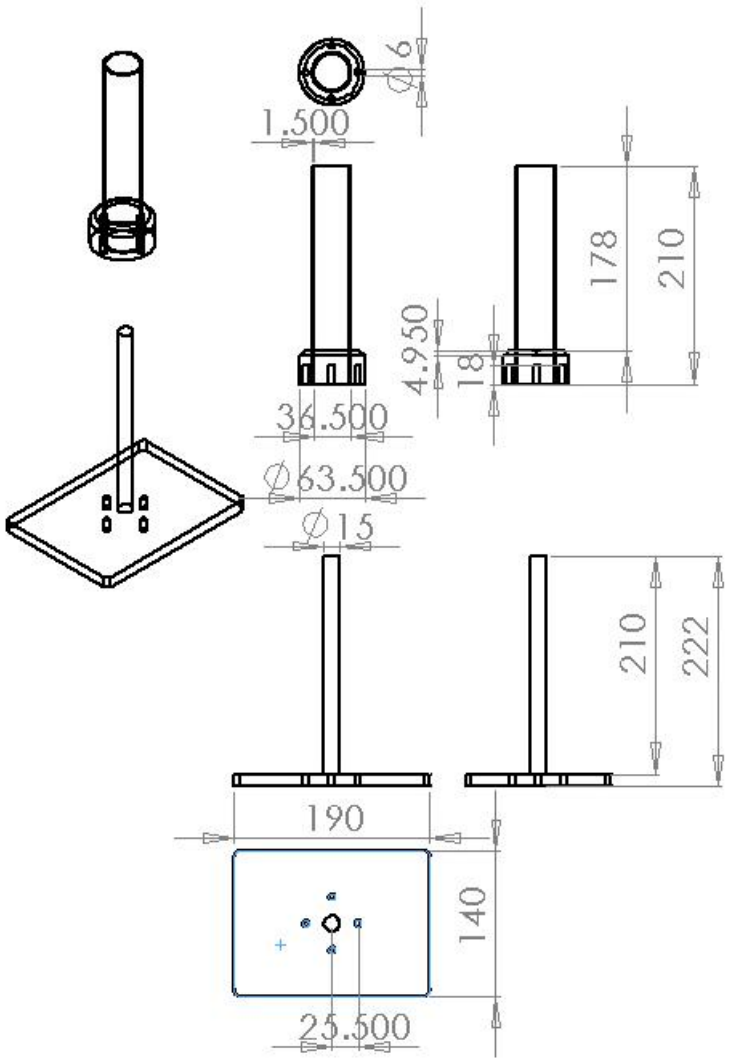

Figure 57 - Silicone sleeve mould

eliminate any seepage of the silicone out of the mould.

A second mould was produced to enable test samples to be created to measure material properties. The mould enabled uniform disks of silicone to be produced simultaneously to the sleeve curing. To enable a greater flexibility when considering the options of which materials testing machine to use, a sample size was selected which could be used by all. Instron do not specify any restrictions on sample size, whereas a guideline is given by Mettler for the ideal dimensions of a sample for the DMA machine. The geometry factor g (used to calculate modulus) should be calculated from the diameter d and thickness l of the sample with the following equation;

$$g = \frac{4l}{\pi d^2} \tag{6}$$

An ideal geometry factor is specified as between 25 and 30. Based on this and the maximum size of the clamp (20mm diameter), a sample size was selected with a diameter of 19mm and a thickness of 8mm. The mould was designed in the style of a press to encapsulate the silicone completely and ensure the top and bottom edges would be parallel. The centre of an aluminium cylinder was bored out to an internal diameter of 20mm. A second bore of 19mm was made but this time only extending ¾ of the length of the cylinder; this created a lip where the base of the silicone disk would sit. A solid cylinder of diameter 19mm was produced as a plunger which would slide down through the external cylinder and then sit against the lip. The top of the silicone disk's reservoir was provided by an end cap which was stepped so that it would sit inside the opposite end of the external cylinder flush with a secondary lip 8mm from the first lip. An overflow hole of 1.5mm was drilled into the side of the cylinder, into the reservoir to allow excess silicone to escape. (See *Figure 58*).

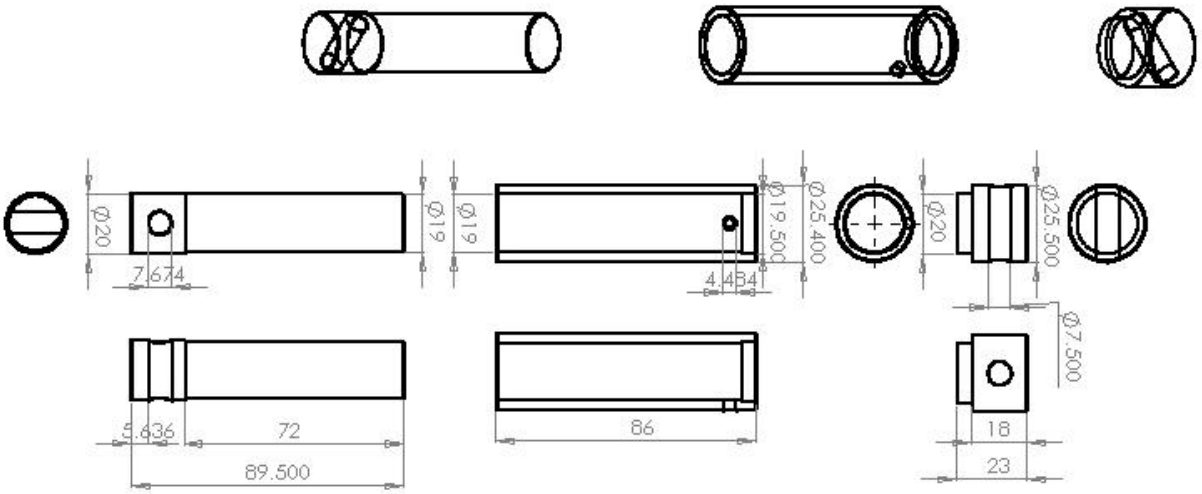

Figure 58 - Test sample mould

Silicones with varying amounts of deadener were produced by combining equal quantities of parts A and B weighed to a precision of 0.01g. The desired percentage of total mass of deadener was then added and the 3 parts mixed. When combining the parts, care was taken to incorporate minimal air, as air bubbles in the cured silicone would affect the material properties. Working time of Platsil 10 is 5 minutes; providing enough time to process the silicone and pour it into the mould. The silicone was poured in through the top opening of the sleeve mould whilst the mould was continuously agitated to encourage air bubbles to the surface. The remaining mixture was then poured into the sample mould with the lower plunger positioned around 5mm below its lip, the cap was then pushed in, seating it against its lip, followed by the plunger being fully inserted. Cure time for this particular silicone was 30 minutes during which it was left at atmospheric pressure and room temperature. A consideration was made to cure the silicone in a pressure pot to remove all air bubbles, however the air present in the cured parts was minimal and evenly distributed so this was deemed unnecessary.

The silicone sleeve was removed from the mould by unbolting the external cylinder and peeling the sleeve from the central section of the mould. The end cap and plunger of the sample mould were removed using a lever through the drilled holes in either end. The silicone disk could then be simply pressed out.

5.8 Gripper testing

Three silicone sleeves and corresponding sample pieces were produced with the following percentage of deadener, 50% (the least stiff), 25% and no deadener (the stiffest) and were selected to provide a range of damping levels. They were then tested for their effectiveness at damping clubhead acceleration in a static test where the clubhead was set oscillating and the rate of decay of oscillation provided a measure of the damping properties of that silicone sleeve.

Each sleeve was pulled over the end flange of the driver and positioned at the top of the shaft. The encased shaft was then secured in the material clamp through equal adjustment of the three allen bolts. The bolts were tightened until the material showed approximately 33% reduction in thickness, a torque wrench was then used to provide a uniform force across the plates. The material clamp was then subsequently clamped in the robot collet.

An accelerometer was mounted with beeswax onto the toe of the clubhead and connected to a National Instruments 9234 data acquisition box driven by Smart Office software. Data was recorded at 2048Hz for 4s with a pre-trigger of 12.5% (0.5s). The clubhead was then displaced around 150mm with a motion perpendicular to the clubface and released. Its acceleration was then captured. The three responses are shown in Figure 59.

The damped frequencies of the oscillations for the 0%, 25%, and 50% deadener silicones were, 3.64Hz, 3.55Hz and 3.08Hz respectively, with corresponding damping ratios of 0.02, 0.08 and 0.11, 0.08 being the same as human skin (Boyer 2009).

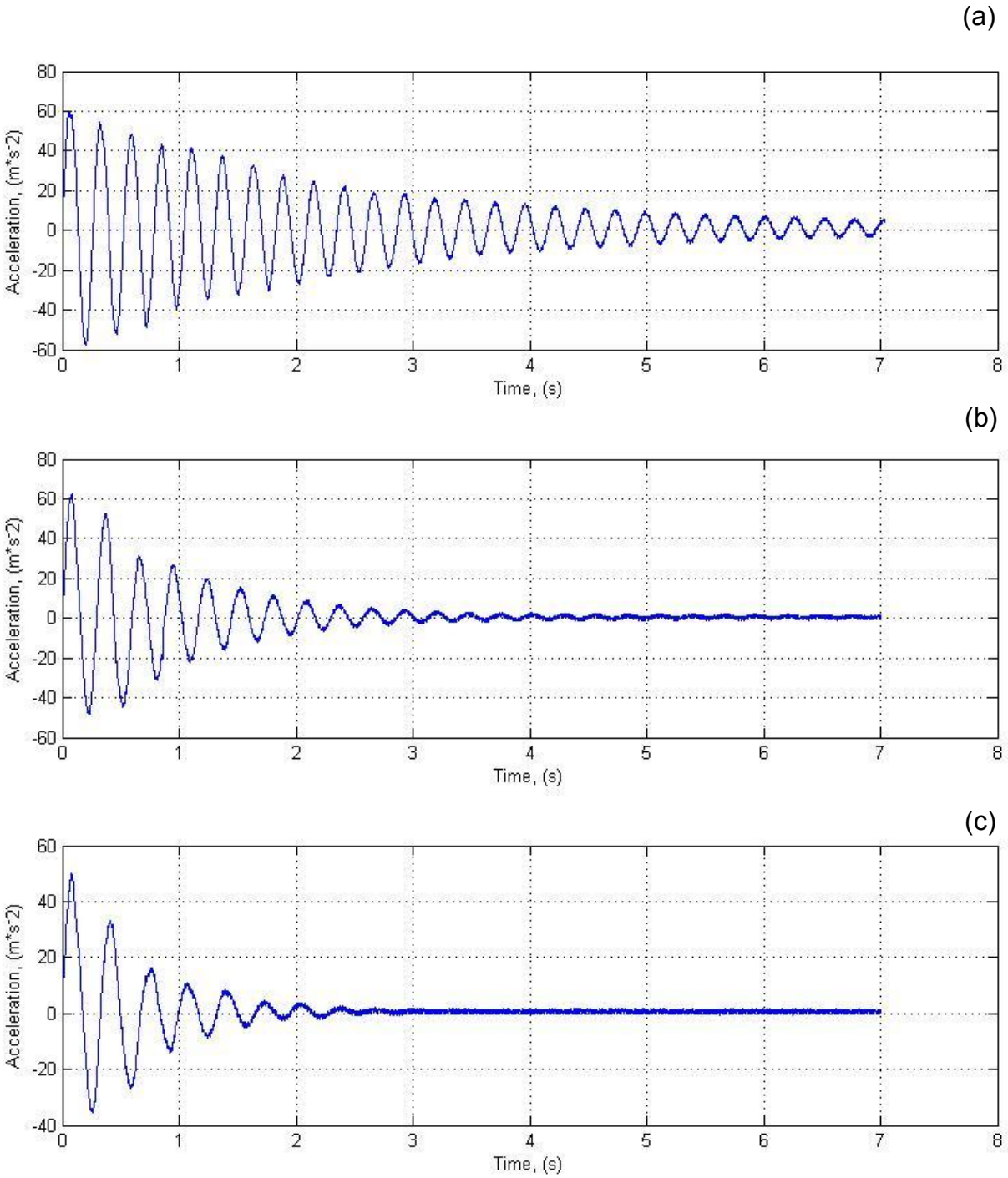

Figure 59 - Clubhead vibration for three silicone materials inserted into the robot grip, (a) 0% deadener, (b) 25% deadener, (c) 50% deadener

The tests showed that by adding a compliant material between the golf club and robot clamp interface, clubhead oscillations could be significantly reduced. This result proved encouraging and led to the progression of this research to the next phase; using a mathematical model of the robot's collet to predict material properties

for a gripper which would provide the same acceleration profile as held by a human hand.

5.9 Summary

A pneumatic gripping mechanism was developed to test the effect of varying the spring constant between the golf club shaft and the robot's rigid grip on clubhead vibration. It was found however, that just reducing the spring constant wasn't enough to reduce clubhead oscillations as the level of damping present in the inner tube rubber was not high enough with a damping ratio of only 0.019. A second prototype gripper was then produced to enable new grip materials to be tested without removing the current robot grip rendering the robot unusable. Preliminary tests of this material clamp proved successful with the level of compression of the grip material being easily adjusted by rotation of the Allen key bolts. The device provided a firm grip on the material and a rigid connection between the robot and its exterior shell.

A silicone system, Platsil 10, was used to produce prototype grips with varying properties and three silicone sleeves were manufactured and tested in the material clamp for their ability to damp clubhead oscillations. Results showed that adding 50% deadener to the silicone mixture resulted in a reasonably high damping ratio of 0.11.

At a first glance, one might consider the ideal material for this application to have similar properties to human skin. However, the many assumptions made when modelling the golfer's different levers and joints (arm, wrist) in terms of lack of flexibility in other areas of the system, result in a slightly altered specification for a grip materials properties. The 50% deadened silicone has a very high damping ratio when compared to skin (around 0.08 (Boyer 2009)), and yet didn't achieve comparable levels of damping of the clubhead. Further material properties should be tested to gain a greater understanding into the damping of the clubhead vibrations which could be achieved. The generation of a mathematical model of the robot in the following chapter will allow a higher number of grip material properties to be tested, without the time consuming process of grip manufacture.

Chapter 6

Mathematically Modelling a Golf Robot

To make an informed prediction of properties that an effective gripper material should possess, a mathematical model of the Miyamae V's collet clamp mechanism was generated. This chapter details several iterations of a mathematical model of the Robot's collet and basic structure, which was created in order to simulate and monitor the effect of adding a compliant material at the boundary between a golf club shaft and the rigid steel collet. An early iteration modelled the collet as a fixed boundary. This was to provide a scenario that allowed an easy method of comparison between the motion of an oscillating clubhead supported in a stationary collet and a simulation. By adopting the silicone sleeves produced in the previous chapter as a compliant interface between the golf club and the robot, their material properties could be used to align simulation to real life and provided a level of validation of the model. A torque was then applied to both the collet in the model and the physical robot collet, to simulate and monitor the effect of the compliant sleeve on the dynamic motion of the clubhead. For each model, equations of motion were derived for the collet, a section of the shaft and the clubhead. These equations were subsequently solved in Matlab. An attempt was made to calculate a damping constant that when applied at the grip interface would critically damp the clubhead's oscillations but this was found to be unachievable. Accelerations of a clubhead when swung in a simple motion by a human were measured to make a stripped back comparison between the damping of the human hand and a simulated compliant material at the robot's grip boundary.

6.1 Fixed collet model

A three degree of freedom (DOF) model was created to represent a golf club held in the robot's collet grip. The collet was initially modelled as fixed in space to allow comparative tests to be conducted on the physical club to validate the model, before moving onto dynamic tests where a torque would be applied to the collet. The club was modelled as two separate masses representing the section of the shaft clamped

in the robot's collet, m_g, and the clubhead m_{cl} as shown in Figure 60. The clubhead was modelled as a point mass at the end of the shaft, able to move only in a linear direction, perpendicular to the axis of the shaft. The two masses were joined by a pair of spring and dashpot elements, with stiffness and damping coefficient values K_{sh} and C_{sh} respectively, to represent the damping and flexibility of the shaft. The shaft was modelled as massless so its physical mass was divided proportionately between the grip and clubhead elements. In reality the shaft's flexibility varies along its length and its stiffness could be modelled as a function of the position along the shaft. This method was considered too complex for the initial model, however it would be considered at a later stage if the initial model was unable to simulate the behaviour of the club and it was deemed necessary. The grip section of the club was supported in the collet by four sets of spring and dashpot elements to model the compliance of the silicone sleeve. These variables could be altered to simulate the effect of different materials at the shaft and collet interface and are illustrated in Figure 60. The values of each spring/dashpot set can be controlled independently to enable combinations of different materials in four different areas; this was reduced to two for the current model for simplicity. The 3DOFs describe the physical situation as follows, two to represent the rotational and translational motion of the grip mass, m_G, and a further DOF to represent the translational motion of the clubhead mass, m_{cl}. It was assumed that the system would rotate about pivot point of unknown position, between the two sets of compliance elements. Free body diagrams (FBD) of the system are shown in Figure 61.

Dashpots, c_1 and c_2, represent the damping coefficient of the grip, k_1 and k_2 represent the stiffness of the grip, x_G and x_{cl}, the displacements of the grip and club respectively. The parameter, d, is the horizontal distance between the two sets of spring and dashpot elements and l is the length of the grip section of the shaft. I_G is the inertia of the grip section and Θ_G, its rotation. $F(t)$ is the driving force applied to the clubhead on impact with the ball.

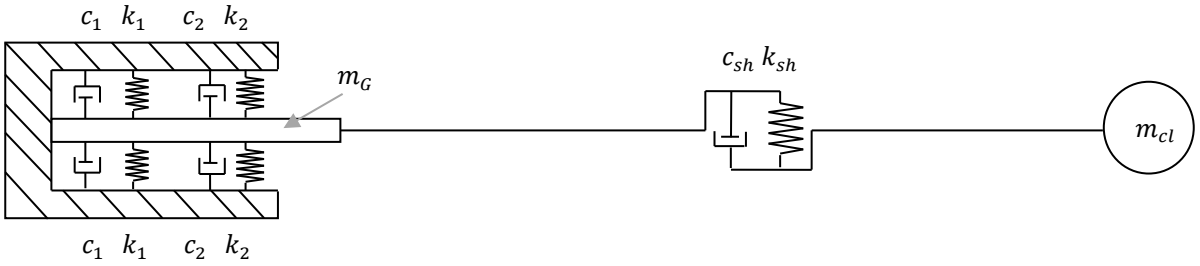

Figure 60 - Fixed collet model

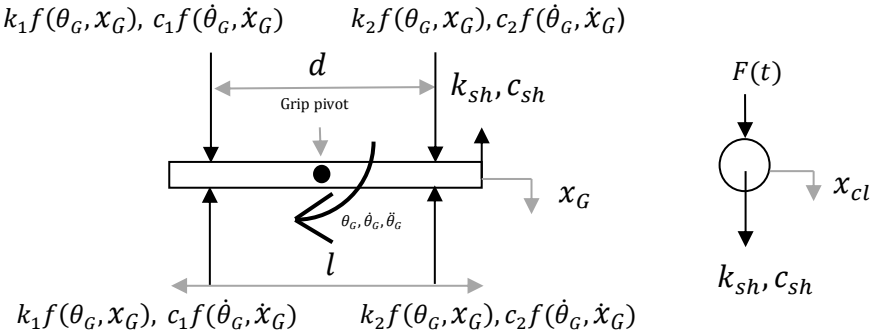

Figure 61 - Free body diagrams of grip and clubhead

6.1.1 Equations of motion

The FBDs of the system were used to derive the equations of motion which were written in the form

$$m\ddot{x} + c\dot{x} + kx = F(t) \tag{7}$$

Equation (8) describes the grip translation, equation (9) the clubhead translation and equation (10) the rotation of the grip.

$$m_G\ddot{x}_G + \dot{x}_G(2c_2 + 2c_1 + c_{sh}) + \dot{x}_{cl}(-c_{sh}) + \dot{\theta}_G\left(c_2 d - c_1 d + c_{sh}(L_{cl} - \frac{l}{2})\right) + x_G(2k_2 + 2k_1 + k_{sh}) + x_{cl}(-k_{sh}) + \theta_G\left(k_2 d - k_1 d + k_{sh}(L_{cl} - \frac{l}{2})\right) = 0 \tag{8}$$

$$m_{cl}\ddot{x}_{cl} - \dot{x}_G c_{sh} + \dot{x}_{cl} c_{sh} - \dot{\theta}_G c_{sh}(L_{cl} - \frac{l}{2}) - x_G k_{sh} + x_{cl} k_{sh} - \theta_G k_{sh}(L_{cl} - \frac{l}{2}) = F(t) \quad (9)$$

$$I_G \ddot{\theta}_G + \dot{x}_G \left(c_2 d - c_1 d + c_{sh}(L_{cl} - \frac{l}{2})\right) + \dot{x}_{cl}\left(-c_{sh}(L_{cl} - \frac{l}{2})\right) + \dot{\theta}_G \left(c_1 \frac{d^2}{2} + c_2 \frac{d^2}{2} + c_{sh}(L_{cl} - \frac{l}{2})^2\right) + x_G \left(k_2 d - k_1 d + k_{sh}(L_{cl} - \frac{l}{2})\right) + x_{cl}\left(-k_{sh}(L_{cl} - \frac{l}{2})\right) + \theta_G \left(k_1 \frac{d^2}{2} + k_2 \frac{d^2}{2} + k_{sh}(L_{cl} - \frac{l}{2})^2\right) = 0 \quad (10)$$

The equations of motion were then rearranged into matrices, the mass matrix *M*, the stiffness matrix *K* and the damping matrix *C*. A driving force was applied at the clubhead, *F(t),* and is described by the right hand side of the equation.

$$\begin{bmatrix} m_G & 0 & 0 \\ 0 & m_{cl} & 0 \\ 0 & 0 & I_G \end{bmatrix} \begin{bmatrix} \ddot{x}_G \\ \ddot{x}_{cl} \\ \ddot{\theta}_G \end{bmatrix} +$$

$$\begin{bmatrix} 2c_1 + 2c_2 + c_{sh} & -c_{sh} & c_2 d - c_1 d + c_{sh}(L_{cl} - \frac{l}{2}) \\ -c_{sh} & c_{sh} & -c_{sh}(L_{cl} - \frac{l}{2}) \\ c_2 d + c_{sh}(L_{cl} - \frac{l}{2}) - c_1 d & -\frac{c_{sh} l}{2} & \frac{c_2 d^2}{2} + c_{sh}(L_{cl} - \frac{l}{2})^2 + \frac{c_1 d^2}{2} \end{bmatrix} \begin{bmatrix} \dot{x}_G \\ \dot{x}_{cl} \\ \dot{\theta}_G \end{bmatrix} +$$

$$\begin{bmatrix} 2k_1 + 2k_2 + k_{sh} & -k_{sh} & -k_1 d + k_2 d + k_{sh}(L_{cl} - \frac{l}{2}) \\ -k_{sh} & k_{sh} & -k_{sh}(L_{cl} - \frac{l}{2}) \\ k_2 d + k_{sh}(L_{cl} - \frac{l}{2}) - k_1 d & -\frac{k_{sh} l}{2} & \frac{k_2 d^2}{2} + k_{sh}(L_{cl} - \frac{l}{2})^2 + \frac{k_1 d^2}{2} \end{bmatrix} \begin{bmatrix} x_G \\ x_{cl} \\ \theta_G \end{bmatrix} = \begin{bmatrix} 0 \\ 0 \\ F(t) \end{bmatrix} \quad (11)$$

6.1.2 Solution - Central difference method

The equations of motion were solved using the Central Difference method (Rao, 1990), one example of finite difference numerical computation. This method of solution employs the Taylor expansion and is ideally used when the differential equations of motion cannot be integrated in closed form, such as when a system is linear, as in this case. Initial displacements and velocities are specified and an initial acceleration is calculated from these values. Displacements are then calculated for a particular time $t=t_{i+1}$ based on the previous displacement at $t=t_{i-1}$ and the

displacement at time $t = t_i$. Corresponding accelerations and velocities can then be calculated. The equations of motion matrices shown above were solved using a bespoke Matlab function. This method allows quick computation of results for a solution which may involve very small time periods and therefore many iterations of the central difference method. The calculation of the critical time step was included in the Matlab function to enable a stable solution to be found.

To calculate the critical time, the natural frequencies of the system were found by calculating its eigenvectors and corresponding eigenvalues. Eigenvalues are related to the natural frequencies of a system by the following relationship (Bower, 2009):

$$\lambda_i = {\omega_i}^2 \tag{12}$$

Where λ_i is the i^{th} eigenvalue and ω_i its corresponding angular frequency. The values of λ_i are the eigenvalues of the mass normalised matrix $\tilde{k}$, given as;

$$\tilde{k} = M^{-\frac{1}{2}} K M^{-\frac{1}{2}} \tag{13}$$

f_{max} is then the maximum value found from the relationship;

$$f_{max} = \frac{1}{2\pi}\sqrt{\lambda_k} \tag{14}$$

It then follows that the critical time step for the given system is;

$$t_{cr} = \frac{1}{\pi}\frac{1}{f_{max}} \tag{15}$$

As long as the time step used in a solution is less than t_{cr}, the solution will be stable.

Variables used in the solution were either directly measured from the system modelled or were calculated from data measured during specific material tests. The magnitude of force applied could be adjusted to match a force applied to the physical system and was applied as an instantaneous force at the first time increment, replicating a sudden impact to the clubhead mass. The force could be applied gradually to the system, a more realistic scenario; however, this would not have any effect on the rate of decay of oscillation as this only dictates the initial peak of acceleration, so as long as this remains constant throughout the simulations, it has

no meaningful effect on the overall comparison.

Desired outputs of the solution were specified in the Matlab code; these were selected as plots of clubhead and grip translation and grip rotation and each of these value's respective velocities and accelerations. This enables a visual comparison to be made between each element of the system, illustrating the change in response due to a change in variables.

6.2 Validation

Before the model could be implemented as a predictive tool for desirable grip material properties, validation was required.

6.2.1 Rigid collet simulation

As a method of checking the validity of the fixed collet model, a simulation was generated to model the club vibrating in the robot's collet clamp and the response was compared to measured data from the physical scenario. Stiffness values for the grip, k_1 and k_2 were set very high at 500kNm^{-1} to simulate a rigid grip. A real club's natural frequency, $f_{n,}$ was measured using a shaft frequency analyser which also provided a method to measure the stiffness of the shaft k_{sh}. This procedure involved clamping the grip of the club rigidly into the device and creating an oscillation of the clubhead. From the oscillations, the shaft frequency analyser was able to calculate the natural frequency of the club. The stiffness was calculated to be 139N/m from a natural frequency f_n, of 4.167Hz, using the following relationship.

$$k_{sh} = (2\pi f_n)^2 m_{cl} \tag{16}$$

Damping coefficient values for the grip were equated to zero as it is assumed that the grip and collet interface is rigid. An impact force was applied to mass m_{cl} and its response was plotted for a period of 8 seconds with data points being generated at intervals of 0.5ms. The response is shown in Figure 62b.

A test was then conducted on the real system using a driver without a rubber grip (this was to eliminate all compliance from the system); the club was then clamped

into the robot's collet grip. An accelerometer was mounted with beeswax onto the toe of the clubhead and connected to a National Instruments data acquisition device. The measured output voltage was displayed by Smart Office software as acceleration. Data was recorded at a frequency of 2048Hz for 8s with a pre-trigger of 12.5%. The clubhead was displaced to an initial displacement of around 0.15m along a line perpendicular to the clubface and released. Its acceleration was then captured. The response of the clubhead is shown in Figure 62a.

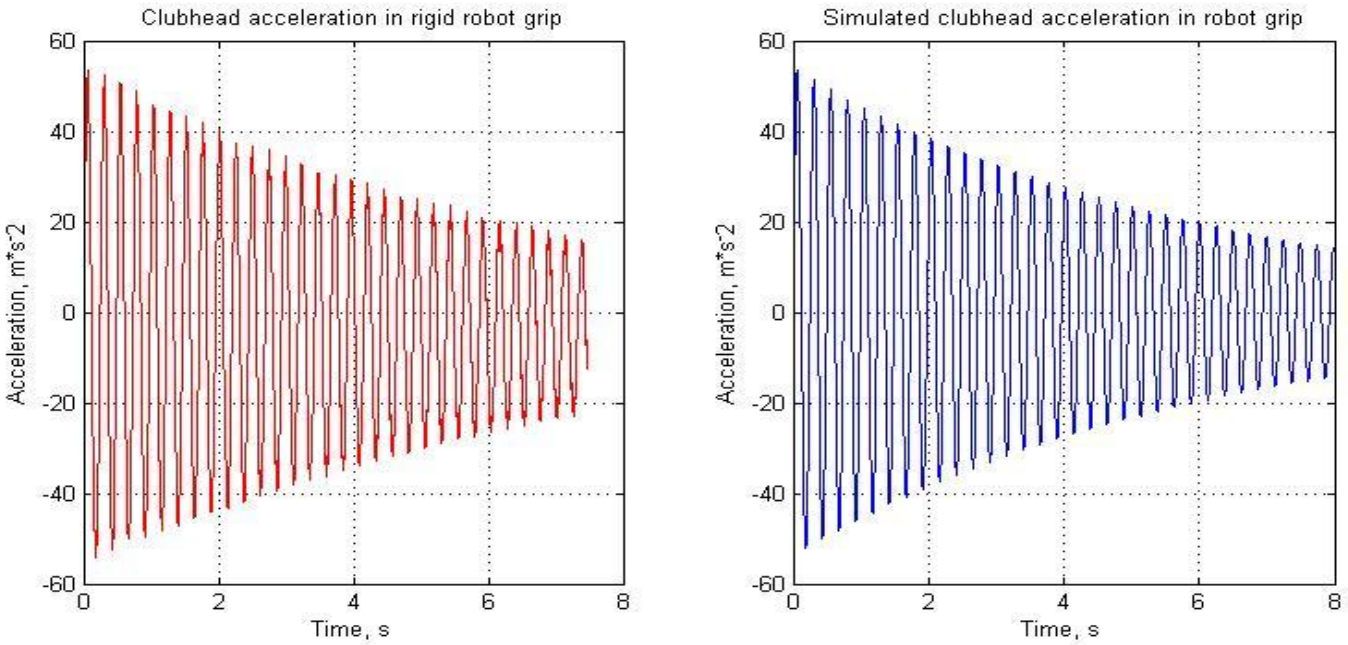

Figure 62 - Comparison of (a) real versus (b) simulated clubhead motion, rigid grip.

The pre-trigger response has been removed which is the reason for the premature cut-off of the actual clubhead response. As the model is driven by a force and not a position, the force applied was scaled to give a comparable initial displacement to the real scenario. A value for the real club shaft's damping ratio was calculated from the graph shown in Figure 62, as the robot's grip was assumed rigid, the damping was assumed to be provided solely by the shaft. The value used for c_{sh} in the simulation was calculated from the measured shaft damping ratio. The graphs show good agreement in terms of frequency of the clubhead's oscillation which has been measured at 4.15Hz for the real scenario and 4.02Hz in the simulation. The

respective damping ratios were calculated to be 0.0076 and 0.0067 for the real and simulated responses respectively. This simulation demonstrates that the fixed collet model is capable of accurately simulating clubhead acceleration in the robot's rigid collet grip.

A best fit computation for the grip values was carried out to fit the model simulation to the measured data, as it is understood that due to the number of approximations present in the model, there will be a difference between real measured values and simulated values. The values which provided the best match were a stiffness value of 400kN/m and a damping value of 5Ns/m.

The next stage of the validation required changing the damping values of the grip section, and for the real situation this meant using the data collected in the previous chapter for the three silicone sleeves, made from 0%, 25% and 50% deadened silicone. Material properties needed to be measured for each of these sleeves to facilitate their use in the simulation.

6.2.2 Material properties

Stiffness and damping values for gripper materials were calculated from materials tests so that they could be entered into the model and used as a method of its validation. Silicone samples produced in a sample mould, the production of which is described in section 4.6, were compressively stressed in an Instron Electropuls and an Instron 5569 machine.

6.2.2.1 Material stiffness

To measure stiffness, the 3 silicone samples were in turn stressed in an Instron 5569 machine as shown in Figure 63. The standard 50kN load cell was replaced with a 1kN load cell to enable a higher resolution of measurement. The specification for the load cells states the accuracy at 1/500 of the cell's capacity, so for the 1kN cell this would be ± 2N. Each sample was lubricated before testing to limit the effect of surface friction on the measured force. A displacement value of 3mm was specified and applied in a cyclic manner for 1 cycle.

The measured force enabled stiffness to be calculated for that particular sample and its specific dimensions, as k can be found from the gradient of the loading section of a load/displacement plot. The reason the loading portion was given preference over the unloading portion was due to its representation of the material's immediate response to loading whereas the unloading portion is affected by the energy dissipated which is an indication of the material's damping properties. The stiffness of springs acting in parallel can be summed; therefore a stiffness value can be easily scaled for any material sample differing in area and thickness from the sample tested. The relationship between displacement and load measured for each sample was quite linear, less so at the maximums of each plot as can be seen by the gradient of the three graphs in Figure 64. The curve present at the start and end of loading was most probably caused by the compression of the lubricant present on the surface of the sample combined with the sample not fully contacting the load cell plate at these times. The measured data was differentiated to find stiffness values throughout the compression of the sample; a value from the middle of the range was selected as it was assumed the most representative of that sample and would be the working range in later tests

The three measured values of k for each of the 0%, 25% and 50% deadened silicone samples were 480N/m, 265N/m, and 190N/m respectively.

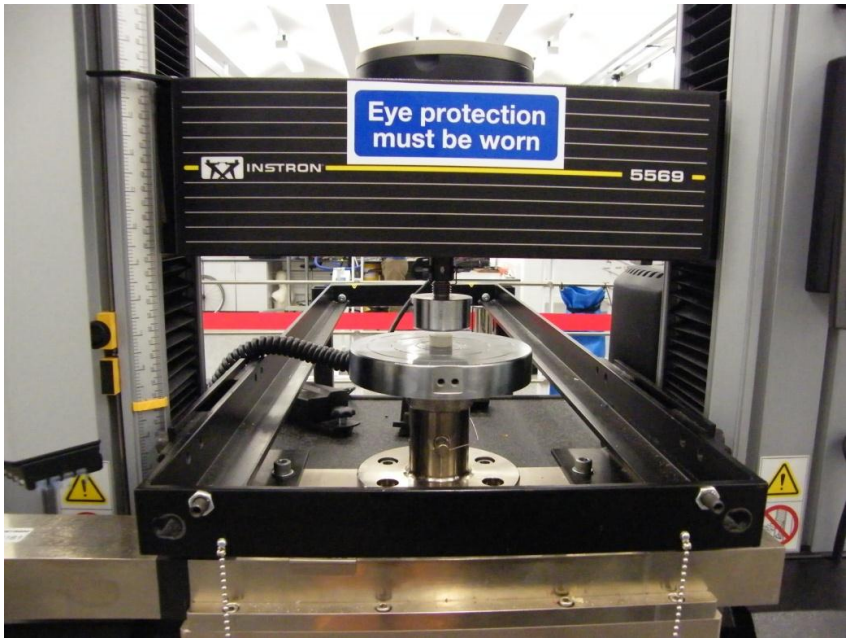

Figure 63 - Instron 5569 with silicone sample positioned for testing

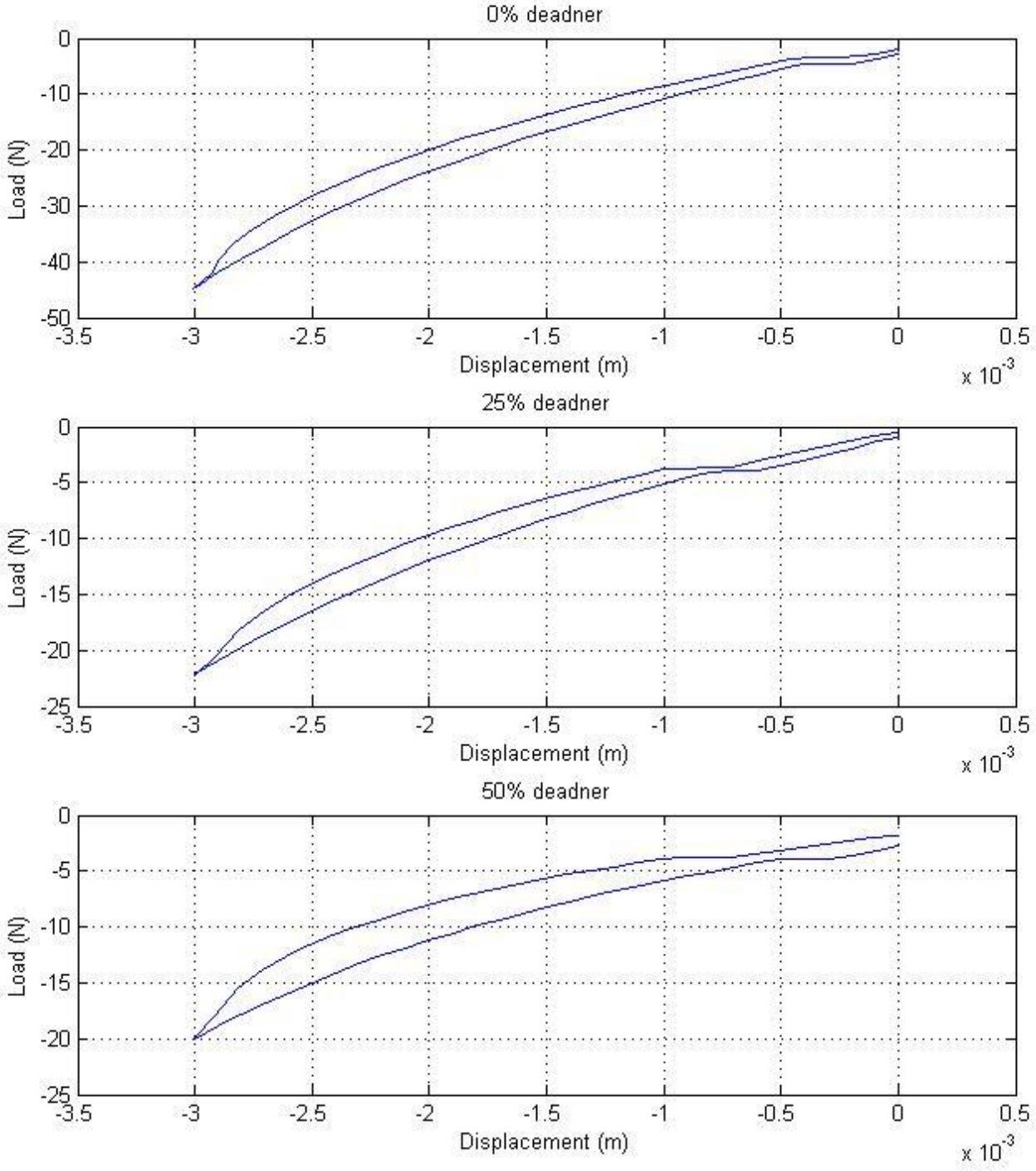

Figure 64 - Instron tests, (a) 0% deadner silicone, (b) 25% deadner silicone, (c) 50% deadner silicone

6.2.2.2 Material damping co-efficient

Finding the damping coefficient of a material requires a more detailed computation. For a given material, its value will vary depending on the system it is applied in. For a particular material, another measure of damping, the damping ratio ζ can be found and is linked to the damping coefficient by the following relationship:

$$\zeta = \frac{c}{c_r} \tag{17}$$

Where c is the damping coefficient and c_r is the critical damping value for a particular system. The force exerted by a dashpot onto a mass is proportional to its velocity, with the damping coefficient being the constant multiplier of the velocity. Therefore, for a particular system, the force provided by the dashpot will change.

One measurable variable which is constant for a material (at a given frequency) is $Tan\ \delta$.

$$Tan\ \delta = \frac{E''}{E'} \tag{18}$$

Where E' is the storage modulus of a material and is the component of the stress/strain ratio in phase with the applied strain and E'' is the loss modulus, the component out of phase (Lakes, R. 2009). $Tan\ \delta$, therefore is a measure of damping which can be related to a damping coefficient for a particular system. From the relationship in equation 18, the following can be derived;

$$E'' = \sin(\delta)\frac{stress}{strain} \qquad E' = \cos(\delta)\frac{stress}{strain} \tag{19a, 19b}$$

δ is defined as the phase angle difference between the load and displacement curves when plotted against the same timescale as illustrated by Figure 65. The Instron Electropuls machine is more suited to applying high frequency oscillatory forces and therefore was implemented in this section of the testing. Load and displacement data could be filtered to remove any high frequency noise present and plotted against time. A Matlab function was created to handle all the post processing. Taking the input as the raw data from the Electropuls, the user is presented with an

FFT plot of the frequency components present in the measurement. A prompt for a cut-off frequency is then made. A low pass filter was applied to remove all frequencies above 20Hz. The time of each maxima is located for both load and displacement and an average of the time difference, Δt is calculated and related to the phase angle δ as follows.

$$\delta = 2\pi\left(\frac{\Delta t}{T}\right) \tag{20}$$

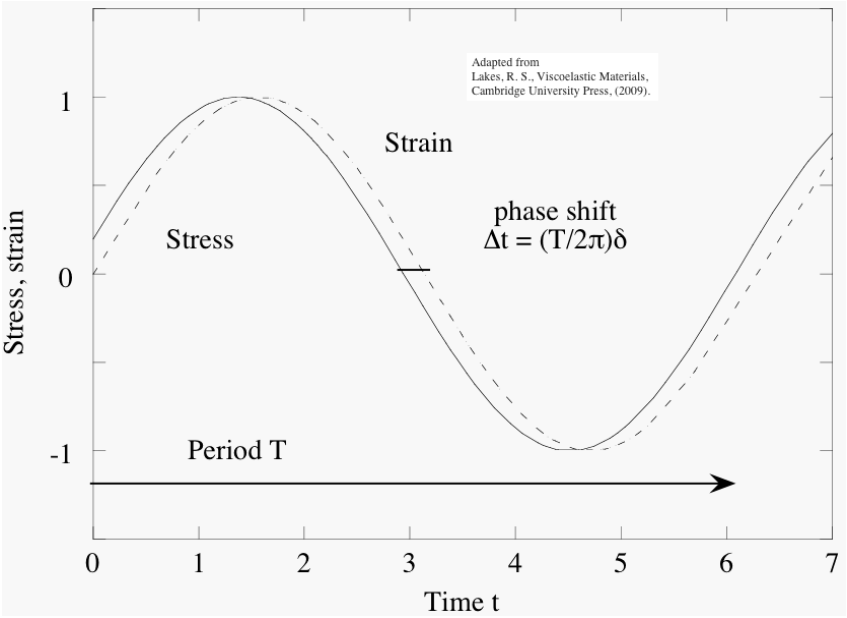

Figure 65 - Calculation of δ (Lakes, 2009)

$Tan(\delta)$ can be used to calculate the damping co-efficient for each material by using the following relationship (Hillberry, 1974);

$$c = \frac{A*E^{"}}{\omega*h} \tag{21}$$

Where $E^{"}$ is calculated from equation 19a and A, ω and h are cross sectional area of sample, angular frequency of applied displacement and height of sample respectively.

As mentioned above, $Tan\,\delta$ is dependent on the frequency of the oscillatory motion applied to it. This means that when testing the samples for their respective damping

values, the force applied to the sample should oscillate at a frequency similar to the major frequency components present in the club during a swing.

Each sample's top and bottom surfaces were covered in PTFE tape. This was to provide a low friction interface between the material sample and the metal plate. Upon contact between the sample and force plate, the displacement reading was zeroed so that the strain could easily be calculated from the displacement readings. A displacement profile was generated with an initial ramp of -2mm followed by a section where the sample was strained in a cyclic manner from -4mm to 0mm. A frequency sweep was made, testing the samples at 1-20Hz with 1Hz increments. The data used in the remaining calculations was captured for the trial involving a cycle frequency of 4.0Hz as this corresponds to the most dominant frequency of the modelled system and the corresponding force was measured.

For the three silicone samples tested, (0%, 25% and 50% deadened silicone), $Tan\,\delta$ values at a frequency of 4.0Hz, were measured to be, 0.13, 0.17 and 0.26 respectively with corresponding c values for the sample size as given in *Table 4*.

When considering the dimensions of the silicone sleeves used in the robot's gripper and how the material values found in this testing should be scaled, it becomes clear that at any given time, the full circumference of the sleeve will not be acting as a spring in the direction of the clubhead's motion. As illustrated in Figure 66, during an oscillation of the club within the sleeve, the resultant force from the spring provided by the silicone sleeve can be approximated to a function of θ, the angle between the direction of oscillation and the direction in which the springs act. To account for this, an extra 'effective spring constant' section of code was added to the Matlab function. The sleeve is split radially into n equal segments and a loop will calculate the effective spring stiffness and damping for each segment. The stiffness values are then summed, as both springs and dashpots in parallel result in the sum of their individual values, (Lobontiu, 2010). This calculation resulted in stiffness and damping values for each of the sleeves as shown in the summary table below.

	Stiffness k of sample (Nm^{-1})	Effective stiffness k of sleeve (Nm^{-1})	Damping coefficient c of sample (Nsm^{-1})	Effective damping coefficient c of sleeve (Nsm^{-1})
0% deadened silicone	14500	290000	300	6000
25% deadened silicone	9000	180000	400	8000
50% deadened silicone	6500	130000	600	12000

Table 4 - Sample and sleeve material properties

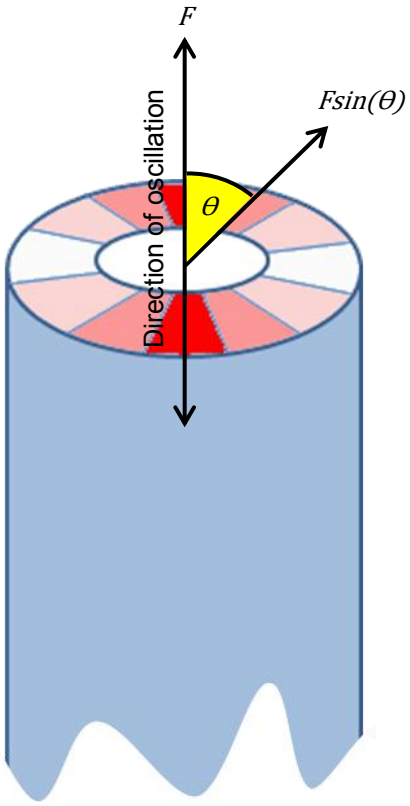

Figure 66 - Calculating effective area of sleeve

6.2.2.3 Simulation of fixed collet

The simulation was run as before with damping coefficients for the grip calculated from the method mentioned in the previous section. Stiffness values measured previously for each sample were entered along with the damping coefficients into the fixed collet model. Figure 67 shows the three responses with comparisons between simulation and actual response. All three simulations show good agreement. In all cases the frequency of oscillation between real and simulated responses have slight differences particularly in the responses for 0% and 50% deadened silicone where the measured values are 3.87Hz and 2.89Hz compared to the simulation with values of 3.76Hz and 3.12Hz respectively. The simulations generally seem to over-damp the clubhead oscillations with quite a noticeable difference in rate of decay in the 0% deadener silicone sample, however they follow the right trend and have predicted the clubhead response well.

At this stage, confidence in the fixed collet model, in terms of modelling a semi-static response of different grip materials, was achieved and the decision was taken to advance the model to the next more dynamic stage, where the collet was no longer fixed but could have a torque profile applied to it to simulate actual robot motions of the wrist joint.

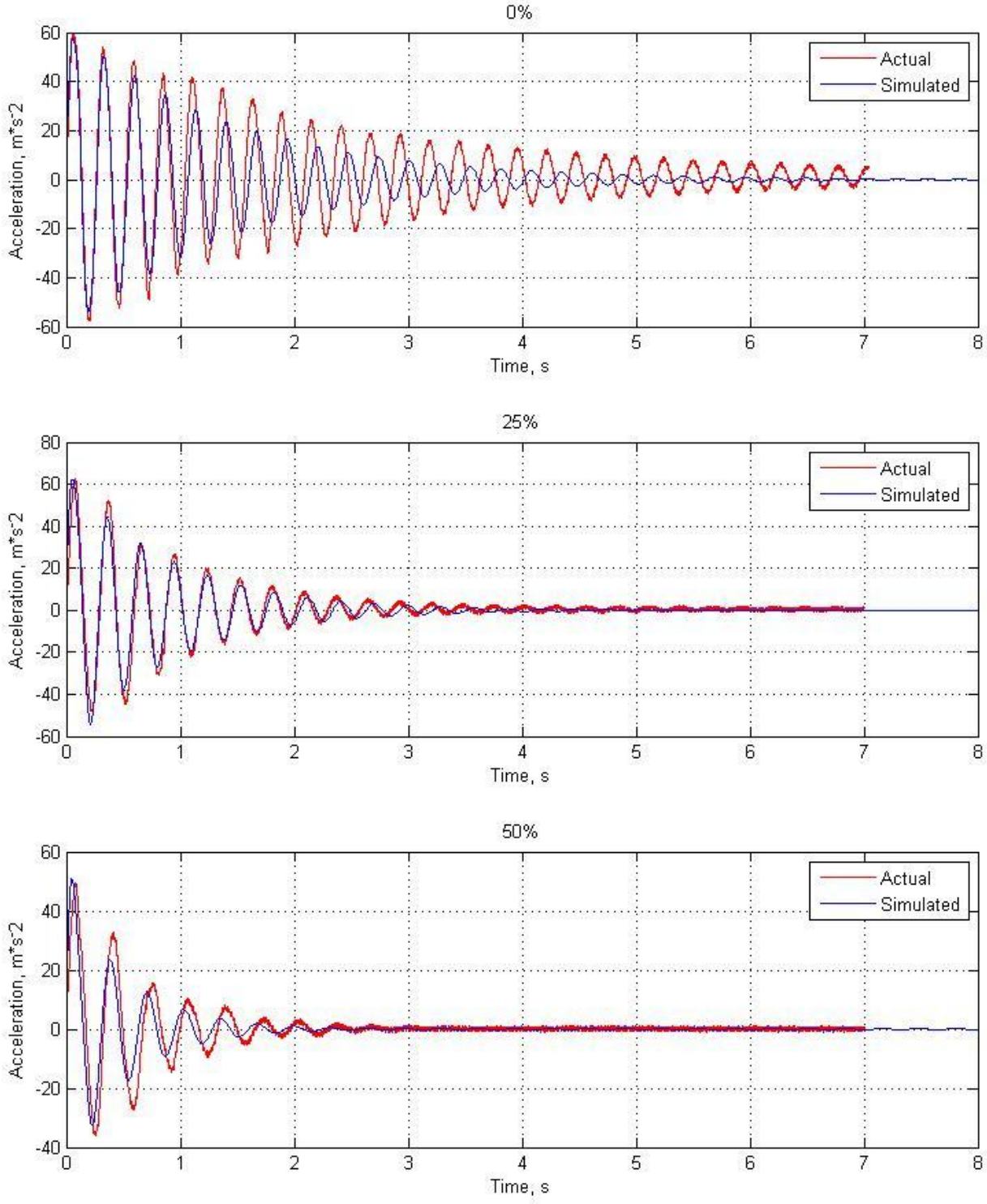

Figure 67 - Static collet clubhead acceleration, real versus simulation, (a) 0% deadened silicone, (b) 25% deadened silicone, (c) 50% deadened silicone

6.3 Advanced Model

The level of complexity of the model was increased by the inclusion of an additional degree of freedom; a rotation at the top of the collet to simulate the wrist rotation on the Miyamae V. This was to enable more dynamic tests on the chosen grip materials, a situation more similar to the condition they would undergo as a gripping mechanism. An additional FBD for the collet was drawn and is shown in Figure 68; four new equations of motion were derived using the same methods as before. The equations of motion shown below are for collet rotation (22), grip rotation (23), grip translation (24) and club rotation (25).

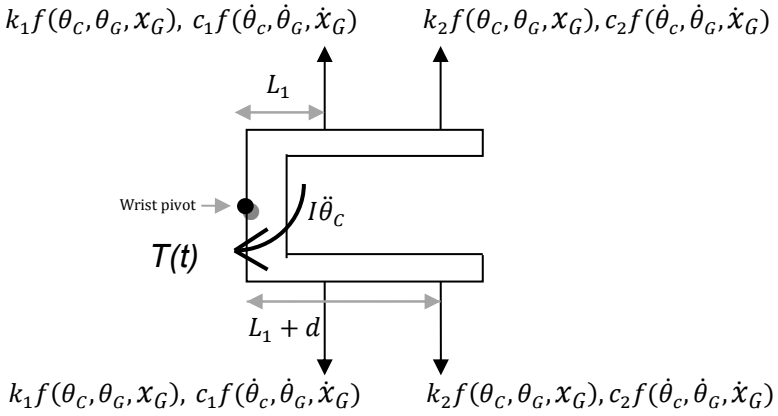

Figure 68 - Collet FBD

$$I_C\ddot{\theta_C} + \dot{x}_G(-2c_2 l_2 - 2c_1 l_1) + \dot{\theta}_G(c_1 d l_1 - c_2 d l_2) + x_G(-2k_1 l_1 - 2k_2 l_2) + \theta_G(k_1 d l_1 - k_2 d l_2) = T(t) \quad (22)$$

$$I_G\left(\ddot{\theta}_C + \ddot{\theta_G}\right) + \dot{x}_G\left(c_2 d - c_1 d + c_{sh}(L_{cl} - \frac{l}{2})\right) + \dot{x}_{cl}\left(-c_{sh}(L_{cl} - \frac{l}{2})\right) + \dot{\theta}_G\left(c_1\frac{d^2}{2} + c_2\frac{d^2}{2} + c_{sh}(L_{cl-}\frac{l}{2})^2\right) + x_G\left(k_2 d - k_1 d + k_{sh}(L_{cl} - \frac{l}{2})\right) + x_{cl}\left(-k_{sh}(L_{cl} - \frac{l}{2})\right) + \theta_G\left(k_1\frac{d^2}{2} + k_2\frac{d^2}{2} + k_{sh}(L_{cl-}\frac{l}{2})^2\right) = 0 \quad (23)$$

$$m_G(\ddot{\theta}_C\left(l_1 + \frac{d}{2}\right) + \ddot{x}_G) + \dot{x}_G(2c_2 + 2c_1 + c_{sh}) + \dot{x}_{cl}(-c_{sh}) + \dot{\theta}_G\left(c_2 d - c_1 d + c_{sh}(L_{cl-}\frac{l}{2})\right) + x_G(2k_2 + 2k_1 + k_{sh}) + x_{cl}(-k_{sh}) + \theta_G\left(k_1 d + k_2 d + k_{sh}(L_{cl-}\frac{l}{2})\right) = 0 \quad (24)$$

$$m_{cl}\left(L_{cl}\ddot{\theta}_C + \ddot{x}_{cl}\right) - \dot{x}_G c_{sh} + \dot{x}_{cl} c_{sh} - \dot{\theta}_G c_{sh}\left(L_{cl} - \frac{l}{2}\right) - x_G k_{sh} + x_{cl} k_{sh} - \theta_G k_{sh}\left(L_{cl} - \frac{l}{2}\right) = 0 \quad (25)$$

The variable names are the same as the previous model in section 5.1 with the addition of the collet rotation component Θ_c and length l_1 which describes the distance from the pivot on the collet to the position of the end of the top spring at the collet end.

The equations of motion were again solved using the central difference method using a function written in Matlab. In this simulation a torque profile could now be specified and applied to the collet to simulate swing motions of the robot. A square torque wave was generated (see Figure 69a) starting with a positive torque for the first third of the simulation to gradually accelerate the collet, this was followed by a negative torque with the same magnitude for the second third to decrease the acceleration and bring the collet to a halt. For the final third of the profile the torque was set to zero to allow the collet to come to a rest to enable the clubhead oscillation post swing to be monitored. An instantaneous torque will result in an instantaneous acceleration which is difficult to achieve in reality and would result in a large acceleration of the robot at the start of the profile. As it is the aim of this project to minimise clubhead oscillation through a gripping mechanism, it seems sensible to consider worst case scenarios with very rapid accelerations in a robot profile. The magnitude of the torque was selected through a trial and error basis until a profile was found which simulated a motion of the robot wrist from -90˚ through to 90˚. The value of torque which was found to provide this profile was 0.637Nm. The total time for the simulation to be completed was set to 1.5s, deemed quick enough to provide a high enough acceleration to excite high clubhead displacement from the line of the shaft but slower than typical clubhead speeds that you would expect during a golfer's swing as a safety precaution. Three simulations were run to simulate a grip made from the same three silicones as in the previous section, with 0%, 20% and 50% deadener compositions, using the same damping coefficients and stiffness values as

used in the fixed collet simulation. Each simulation was completed with an output of plots of the system response.

An output was taken of the collet position throughout the swing and used to generate a swing profile for the robot in terms of wrist position. The swing profile data is shown in Figure 69b. The silicone grips' damping properties in a dynamic motion were then tested using a similar set-up as the previous simulation in section 5.2.1 but because the robot was now powered the accelerometer cable had to be routed out of the robot cage without crossing the robot's swing path. An accelerometer was positioned onto the clubface aligned in the direction of swing with a positive acceleration being in the direction of the backswing and a negative collet angle (see Figure 70). The robot's wrist was moved into the profile start position and a trigger set off of a positive slope on the accelerometer's channel. A robot swing was performed and feedback data from the robots servo was downloaded. The accelerometer data captured contained both the clubhead acceleration relative to the shaft as well as its whole body acceleration from the collet position. For a like-for-like comparison, the global acceleration had to be removed from the accelerometer data, this was done by taking feedback acceleration data from the robot wrist servos and converting this into a linear acceleration at the clubhead's position from the wrist pivot. This data was then filtered and subtracted from the accelerometer acceleration.

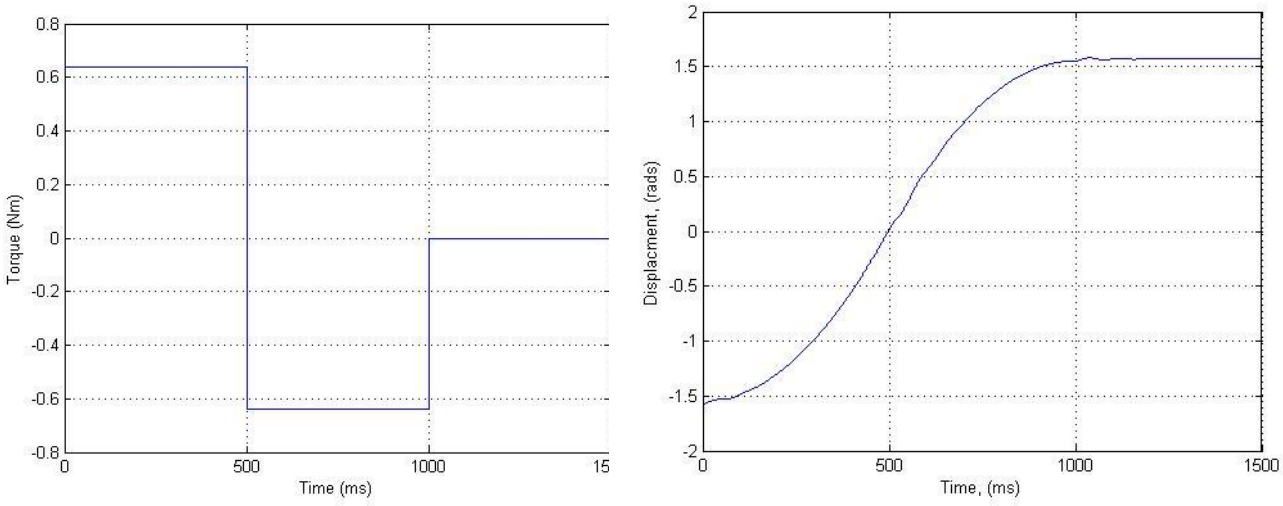

Figure 69(a) - Square Torque wave applied to model, (b)- Simulated position of collet

Figure 70 - Accelerometer orientation

The three simulations with each of the grip material properties applied are shown in Figure 71 and are compared against the measured clubhead oscillation. The three phases of the graph are representative of the three different torques applied. The accelerations start at zero but due to the instant torque and therefore almost instant accelerations, the initial values aren't visible in the plots. Figure 72 shows the high positional accuracy that was achieved by the robot whilst performing the swing profile.

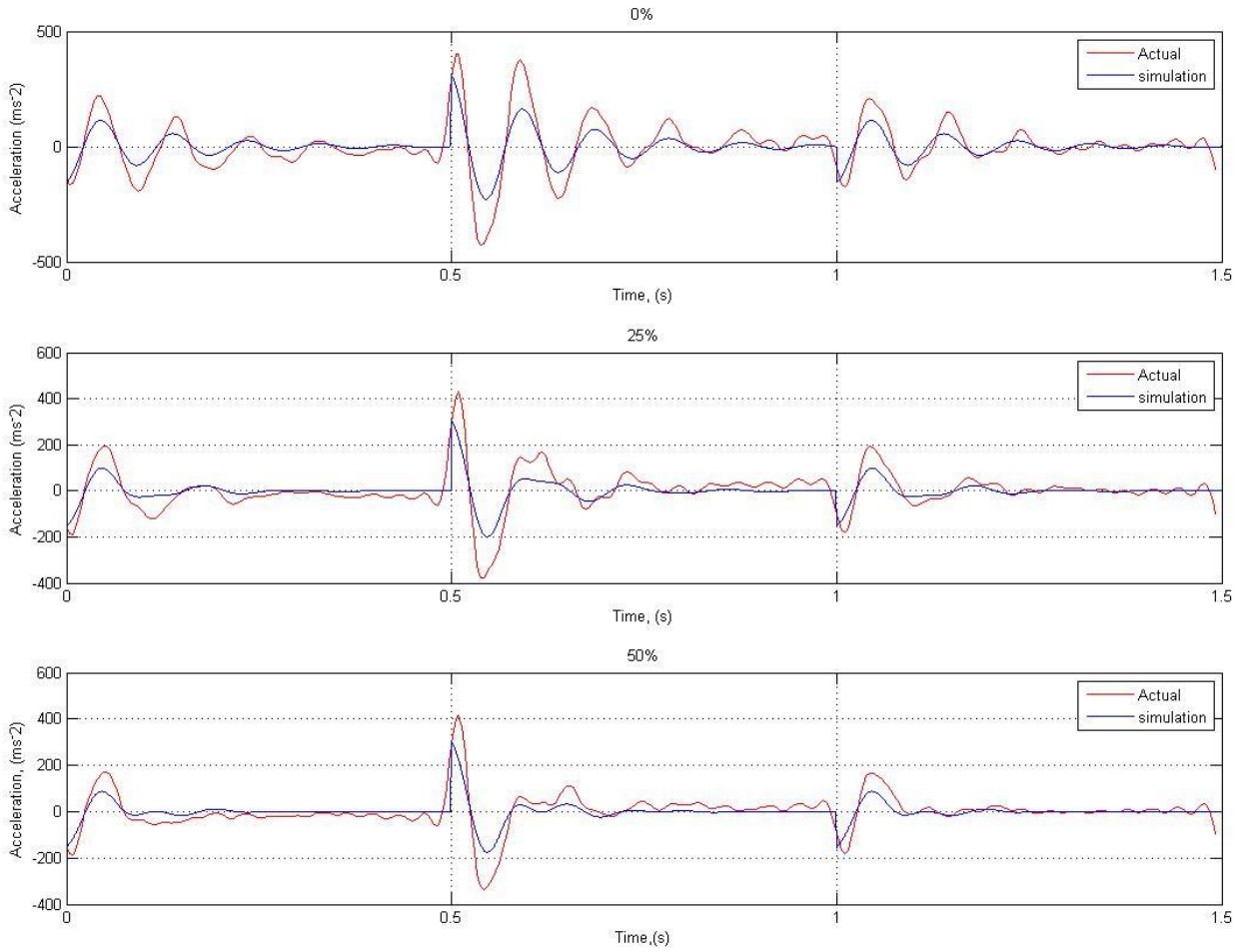

Figure 71 - Dynamic silicone tests, real versus simulated for (a) 0% deadened silicone, (b) 25% deadened silicone, (c) 50% deadened silicone

The responses are compared in the acceleration domain as it is not appropriate to integrate accelerometer data as measured data is sensitive to small DC offsets and any error in the measurement will be amplified by integrating twice giving misleading results. The agreement between the graphs is good where a decrease in acceleration amplitude can be seen from the most highly damped silicone to the least for both measured and simulated.

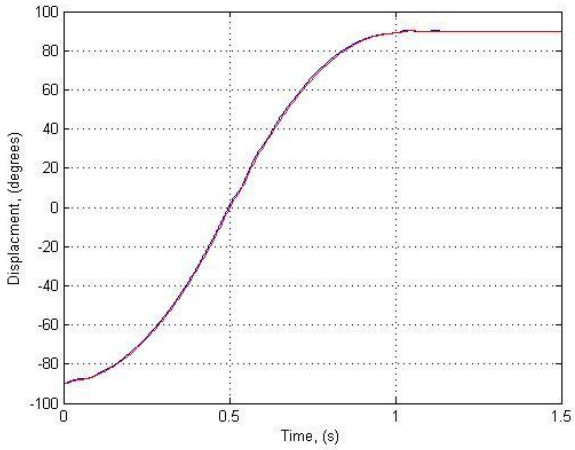

Figure 72 - Simulation wrist displacement v's robot performed wrist displacement

The results from the simulations give confidence that the model is working well and allow experimentation with material properties to predict a material which may give the desired results. However, through further simulations it was found that the success of damping clubhead oscillations to the same level as encountered with a human swing was limited. Another factor to be aware of is that when a material with low stiffness is inserted into the grip, the level of control over the club position is reduced to a level which could affect clubhead orientation during impact. This is supported by the model simulation which shows high levels of rotation in the grip section of the golf club. Of course some motion will be required in order for damping to take place.

To enable a visualisation to be made of this large shaft motion inside the silicone gripper, a simple test was carried out. An accelerometer was glued to the driver's shaft, just below the silicone sleeve and acceleration was measured during a simple swing motion. The material clamp used to constrain the club when using the silicone sleeve grips was removed and the golf club was rigidly clamped in the original robot collet, a second swing was then performed and shaft acceleration was measured at the same position. The acceleration of the collet was subtracted from the responses to distinguish between acceleration due to vibration and acceleration due to motion of the robot. The outcomes were used to generate the plots in Figure 73. It is clear that the acceleration of grip portion of the shaft is undergoing much higher levels of vibration due to the increased compliance introduced by the silicone sleeve.

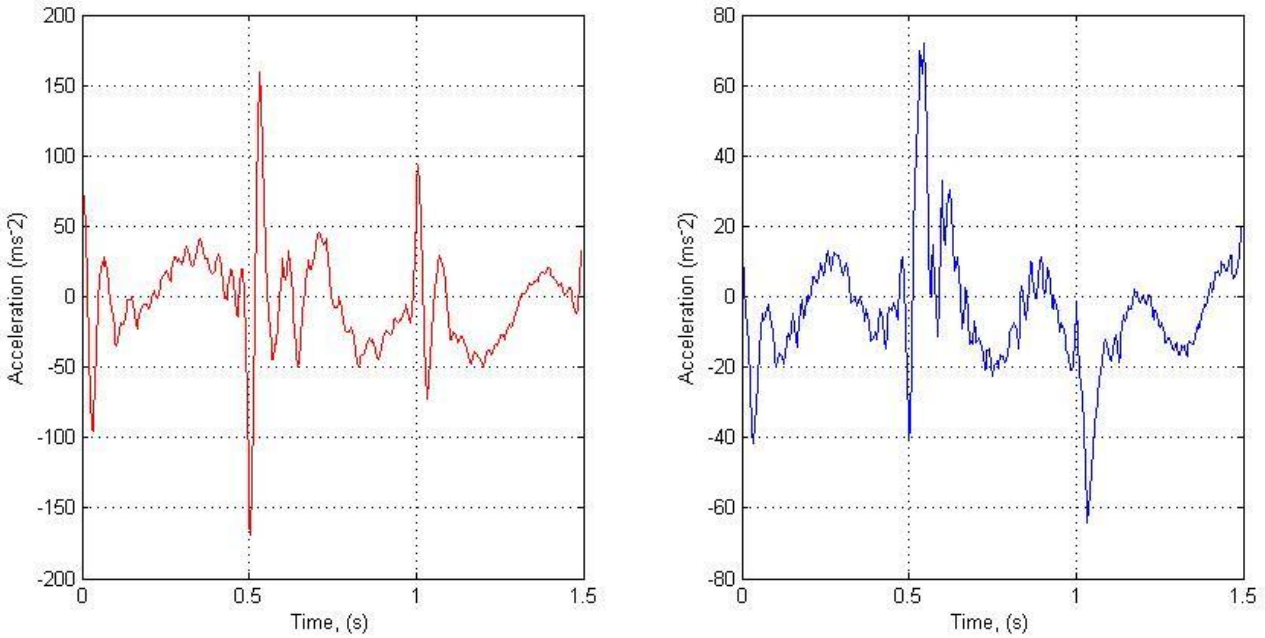

Figure 73 - Comparison of acceleration at grip, (a) With 50% deadener silicone grip, (b) With rigid grip

6.4 Critical damping calculation

In an attempt to find the most effective value of damping for the modelled system, a method was followed in order to find a critical damping coefficient for a gripper material, to determine whether the system could be critically damped as it is assumed the human hand boundary condition approaches a critically damped situation. The method used was developed by Bulatovic (2001) and can be used to find a critical damping value for a multi-degree of freedom system. The example given in the paper describes the solution for a 2 DOF system and this was adapted to solve the 3DOF problem for the fixed collet model. The method finds the minimum value of damping coefficient for a particular system at which the eigenvalues become negative numbers. For the model presented in this paper, a critical damping value was required for the grip, so considering a single material present in the gripping interface, c_1 and c_2 were set equal and will be referred to hereon as c_g, likewise, k_1 and k_2 will be referred to as k_G.

In the method, the eigenvalue problem is considered, and takes the form

$$(\lambda^2 M + \lambda C + K)U = 0 \tag{26}$$

Using the mass, damping and stiffness matrices calculated from the equations of motion, M, C and K respectively, the value of k_G was set to a low value of 100Nm to allow for maximum effect of the damping coefficient. Equation 26 was expanded and the discriminant of the resulting polynomial, Δ , was expressed as the power sum in equation 28, where the determinant of P_k is equal to Δ

$$\Delta = \sum_{i>j} \lambda_i - \lambda_j \tag{27}$$

$$P_k = \sum_{j=1}^{2n} \lambda^k{}_j \tag{28}$$

The resulting values of which are used to form the eigenvector matrix

$$P = \begin{bmatrix} 2n & p_1 & P_{2n-1} \\ p_1 & p_2 & .. \\ p_{2n-1} & .. & p_{4n-2} \end{bmatrix} \tag{29}$$

If Δ_k,is equal to the leading principal minors of the matrix P, then $\Delta_{2n}=\Delta$, the determinant of P_k.

Each element of the matrix *P* depends on the unknown roots of the system, however the roots of the expansion of equation 26, are Eigenvalues of the state matrix A.

$$A = \begin{bmatrix} -M^{-1}C & -M^{-1}K \\ I & 0 \end{bmatrix} \tag{30}$$

Each element of P can be found from powers of the state matrix and a trace, the sum of all of the diagonal elements of the matrix, being taken from the resulting matrix.

$$p_k = Tr(A^k), \;\; k = 1,2 \ldots\ldots, \tag{31}$$

The leading principal minors of P are then found and Δ_6 (Δ_{2n}) is solved to find values of c_G. A legitimate solution has to be a positive and real value of c_G which then needs to be substituted into the other four principal minor equations with all results required to be positive and real. If a value of c_G is found (one which satisfies the above requirements) it can be entered into the damping matrix C and used to solve the Eigenvalue problem where all solutions for λ should be real and negative due to the positive definiteness of the matrices M, C and K.

The outcome of this method showed that a critical damping value cannot be found for this system, i.e. there were no solutions for Δ_6 which gave real positive values when substituted into the remaining principal minor equations. The explanation for this outcome could be due to the damping value of the shaft being fixed. If the damping of the shaft could be adjusted, the system could be not just damped more effectively but critically damped. It strongly suggests from this outcome that due to the flexibility of the shaft and the relatively large mass of the clubhead that any change at the grip end of the shaft, is not significant enough to damp out the motion of the club at the end of the flexible shaft.

When comparing this scenario with that of the human system, it is unsurprising that the effect of grip damping is minimal. Human hands may be flexible and compliant but they are not attached to a rigid system; every joint of the human hand, wrist elbow and shoulder is flexible and offers its own contribution to the effect of damping of the entire system. For a robot grip to provide the same level of damping, the damping properties would need to greatly exceed the damping effect provided by the human hand but as demonstrated in section 6.3, large levels of compliance can result in an uncontrollable motion of the golf club.

In order to better mimic the human hand arm system, the model will be further adapted in the latter sections of this thesis. To model the flexibility of the wrist a spring and damper could be added between the drive of the model and the collet so that the collet can move independently from the drive gear allowing it to flex and dissipate more energy from the oscillating club.

6.5 Human held clubhead acceleration

The silicone sleeves have been shown to be successful at reducing the level of clubhead oscillation during a robot swing, but oscillations are still present and at this stage it is unclear as to the level of reduction that is required in order to replicate the same response of the clubhead when a similar boundary condition is applied to the golf club as when swung by a golfer. The next tests carried out, aimed to provide an answer to this question, to find out how much a club vibrates when being held by a golfer.

In order to test this, two accelerometers were used, one positioned on the club's face in the direction of the swing, with a motion through the impact stage representing a positive acceleration. A second accelerometer was taped onto a golfer's right hand, the direction of positive acceleration opposite to the clubhead accelerometer. The knowledge of the acceleration at the golfer's hand would enable its subtraction from the response measured at the clubhead to allow only clubhead oscillation to be calculated. The club used was a Shaftlab driver so that the shaft deformation could also be measured. This system uses two strain gauges mounted in the toe up/down and lead/lag directions and is calibrated to find deflection in the two directions.

The two accelerometers were connected to a National Instruments data acquisition box, as before, and Smart Office software used to capture their responses. A trigger was set on the hand accelerometer, for a negative peak of 0.001V, and data captured for 3s at a sample frequency of 2048Hz.

Rotation of the golfer's arms about his body were found using a CODA motion system, with a marker positioned on each shoulder to define a virtual marker at the base of the neck, for the fixed arm pivot of the robot, and two markers in the club to define its angle about this pivot. A marker drive box was attached to the golfer's chest to drive the two shoulder markers and one taped to his wrist to drive the club markers. Marker positions were captured at a rate of 400Hz for 3s with the system being triggered manually. The positions found could be used to create a swing profile for the robot so that if indeed a grip was found to be successful in eliminating clubhead oscillation, it could be compared to the clubhead oscillation when swung by the golfer.

The subject was asked to hold a club out in front of their body with their arms locked straight and in line with their shoulders. They were then requested to move the club in three separate motions, -90 to 90 degree rotation around their body, 0 to -90 to 90 to 0 and -90 to 90 to -90, as illustrated in Figure 74. These basic motions were selected over a full golf swing so that grip and wrist rotation could be removed to simplify both the swing profile generated and the processing of the clubhead acceleration. Figure 75 shows the data captured for the -90,90 swing with (a) showing the arm positions (green line) and wrist positions (blue line) captured by CODA. The shaft strain is presented in Figure 75(b) and confirms that the majority of

the strain is in the lead/ lag direction, as would be expected as long as the subject kept the motion planar.

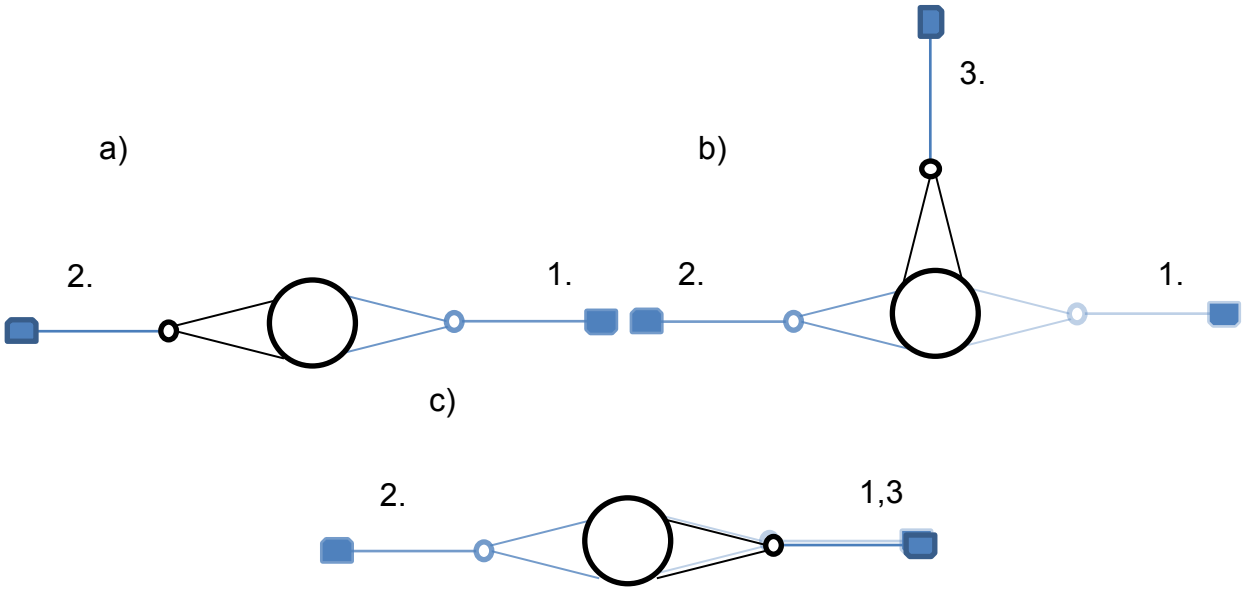

Figure 74 - Swing motions

It can be seen when comparing the acceleration of the hand to the clubhead in Figure 75c, that for all cases, the data follows the same shape of motion but on a different scale, therefore illustrating there is no oscillation of the clubhead due to unwanted vibrations, the only acceleration of the club is caused by the motion of the club as it is moved by the golfer's hand. This indicates that the requirements for the new gripping mechanism are to approach a critically damping situation if possible so that any vibration imparted onto the clubhead is quashed with a minimal number of oscillations. This is required in order to simulate the response when held by a human hand, as it is assumed that the method of driving the robot will always induce a higher level of clubhead vibration than a golfer, resulting in a need for a greater level of damping. This will need further investigation as the accelerations and motion in this experiment differ from a full golf swing.

An interesting observation made in this simple test was that when the subject was asked to swing the club with locked wrists, it was found nearly impossible to achieve

as is shown in Figure 75a. The momentum of the swinging clubhead provided too much force on the subject's wrists causing them to 'give' allowing the clubhead further travel than the target angle of 90 degrees. This highlights another possibly crucial difference between a golfer and the robot in that the golfer's body is a completely flexible system allowing damping not just by the skin but through its joints. If a solution cannot be found through a high damping grip material, an adaption may need to be made to add a flexible element at the robot's wrist joint.

6.6 Summary

A mathematical model of the robot's collet clamp has been derived and found to successfully simulate clubhead acceleration responses both during quasi-static oscillations and during a dynamic simulated swing when compared to experimental data. However, a value of grip damping could not be found which reduced the clubhead oscillation to an acceptable level.

As seen in Figure 67(c), the response using a 50% deadened silicone grip, the clubhead still vibrates for several periods of oscillation, whereas a desirable response, would be closer to critical damping as the robot excites more vibration in the clubhead than a golfer, so these additional vibrations are required to be quashed with the least number of cycles. This also suggests that some flexibility may need to be added somewhere further up the chain in the robot's links.

Clubhead oscillation for a club swung by a human was measured and found to contain negligible clubhead vibration setting the benchmark for future grip prototypes. It was during this experiment that the flexibility and compliance in a golfer's wrist was highlighted as a further means of vibration damping and has directed future developments towards considering adding a flexible joint at the robot's wrist.

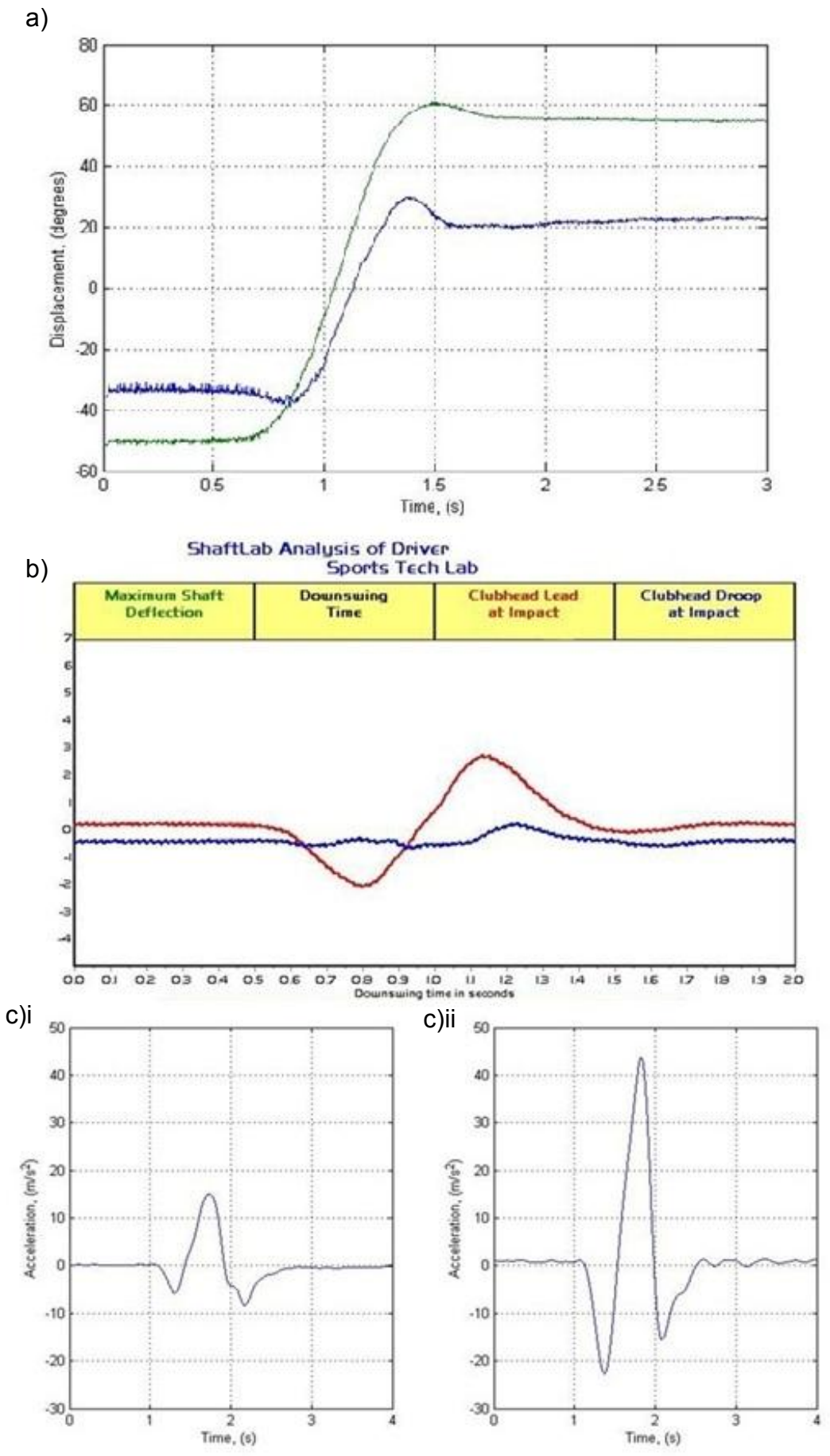

Figure 75 - (a) CODA arm and wrist positions, (b) Shaft deformation, (c)i Acceleration at hand, (c)ii Acceleration at clubhead

Chapter 7

Modelling a Flexible Wrist

The work conducted in Chapter 6 involving the development of a mathematical model of the robot has demonstrated that the result of implementing a compliant robot grip to reduce clubhead vibration to an acceptable level is limited. The very rigid structure of the robot requires a higher level of damping between the origins of the swing drive; the motor, and the end effector; the golf club. The human arm, as does the rest of the body, possesses multiple degrees of freedom each controlled by muscle pairs (Raikova, 1992) which in turn act as dampers (Hill, 1970). Each of these components contributes to minimise the excitation of vibration and quickly quash vibrations excited in an object in contact with aforementioned body. It is not this author's goal to produce a model, and subsequently a robot, which is anatomically correct, but rather to develop a model which will provide recommendations for possible adaptions to the existing robot adding compliance where possible while maintaining the same underlying architecture. As indicated by tests in section 6.5, a golfer's wrist is a flexible joint with its stiffness controlled by muscles (Bruno, J. 1995). Damping is a function of velocity; therefore, for a damping force to be provided, motion is required, making a joint, an ideal location for vibration to be damped. The wrist of the robot was recognised as an additional area where compliance could be added. To explore the effect of adding compliance here, a flexible wrist joint was added to the model, composed of a spring and damper element.

This chapter documents several iterations of adaptions of the previous model developed in chapter 6 to include a flexible wrist joint. In the initial model developed in this chapter, the system is pinned in space with a rotational spring and dashpot element between this pin and the collet. The collet is able to rotate about the pin while its motion is restricted and controlled by these two variable wrist elements. The wrist elements were set to emulate a rigid wrist scenario to mimic the model before the addition of the wrist compliance and a simulation was produced to validate that the output was the same as previously modelled in chapter 6. Simulations were then produced with arbitrary wrist stiffness and damping values to demonstrate how the

effect of the flexible grip found previously in chapter 6 can be enhanced with the addition of a flexible wrist. Calculations were then carried out to find the values of wrist stiffness and damping which provided the lowest levels of clubhead oscillations in a simulation where the system was excited by an instantaneous impact force on the clubhead. A drive was then added at the wrist to match the driven model in chapter 6 to allow further comparisons with the simulations and measured data presented in section 6.3 and to add validity to the new model.

To increase the likeness between the model and robot, a second drive was added to the model to represent the arm position during the robot swings. The arm positions were derived from kinematic data collected from a human swing motion as discussed in section 6.5 and the flexible wrist was left passive with its motion dictated by the wrist element variables. The wrist stiffness and damping elements in this model were adjusted to provide a fit between human measured wrist angles from the data captured in section 6.5 and the simulated wrist angle produced by the model. As a final refinement of the model it was deemed necessary to add a drive to the wrist which could also be programmed with kinematic data, increasing its similarity to the robot and allowing a greater level of control over the wrist position. A simulation was completed to trial the new model and validated its ability to simulate a full robot golf swing in preparation for the comparisons in chapter 8 between measured and simulated golf swing variables. For this simulation the aim was to demonstrate the model's ability to simulate a full golf swing as swung by the robot without any adaptions. Accelerometer data collected from a robot swing was compared against a simulated clubhead acceleration response to validate the model. This comparison allowed an insight into the current performance of the robot in order to compare the level of success the fully realised model has on minimising clubhead vibrations, before any further simulations of the model with the added compliance.

The aim of this chapter is to develop the model further through the addition of a flexible wrist and demonstrate the comparability between simulated clubhead accelerations to measured accelerations from a human and finally the robot.

7.1 Adaptation of mathematical model to include wrist joint

The first stage of advancing the previously developed model from chapter 6 to include a flexible wrist involves regressing slightly. The drive applied to the model was removed to return the model to a simpler pinned collet model. This was to allow a level of validation to be carried out during the development of the model to gain confidence in its ability to simulate a club swung by a human. The first model to include a flexible wrist joint is illustrated in Figure 76. As shown in this figure the majority of the architecture of the model remains the same, whereas now a new joint is added which is in this instance, pinned in space. Between the joint and existing model there are two new elements, a rotational spring and dashpot to represent the additional compliance which are named k_w and c_w respectively. These new elements provide a rotational force to the collet when driven and act against and dampen its motion. The point at which the force acts is at the same pivot point used previously, at the base of the collet, but is shown remote from this point in the figure for transparency. This is illustrated more clearly in the free body diagram shown in Figure 77.

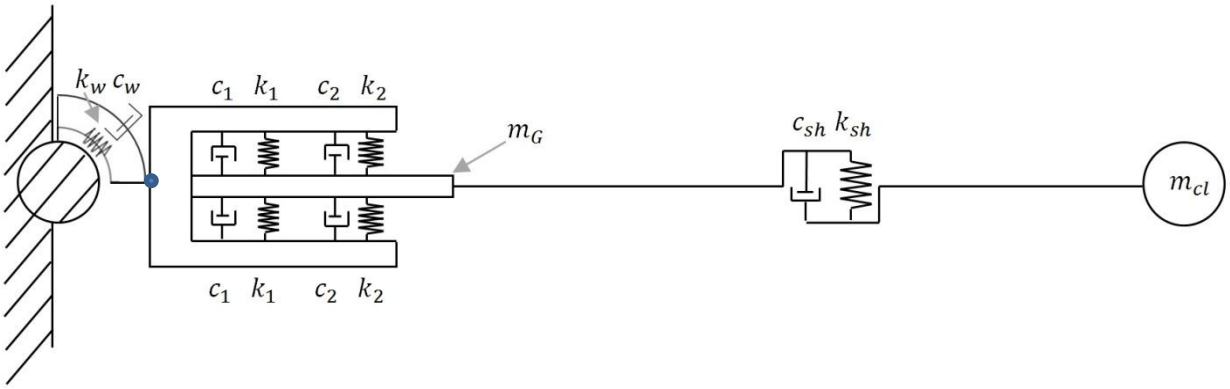

Figure 76 - Fixed wrist joint model

7.2 Deriving the equations of motion

7.2.1 Free body diagram (FBD)

A free body diagram (FBD) was derived for the altered system and is presented in Figure 77. The collet is the only mass in the system for which the applied forces

have changed as the clubhead motion grip mass's motion are relative to the collet. Therefore only one new FBD is required. The labels each denote the following. k_1, k_2, c_1 & c_2 are the two pairs of springs and dashpots which represent the grip compliance. θ_c, θ_G and θ_w are the collet, club grip and wrist rotations respectively. L_1 is the distance between the pivot and the first set of spring/dashpot elements and d is the distance from the first set of elements to the second. $L_1 + d$ is referred to as L_2. The two new elements as mentioned above, the spring and dashpot at the wrist, are labelled as k_w and c_w respectively. A positive rotation of the collet is given as a rotation in the clockwise direction illustrated by the small arrow.

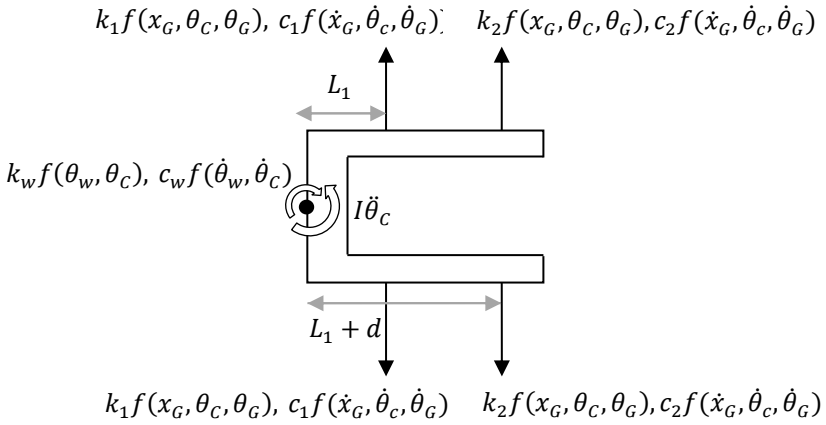

Figure 77 - FBD of collet

Equations of motion were derived from the FBDs in Figure 77 and the previous chapter. Four equations were required, one to describe each of the collet rotation, the grip translation and rotation and the clubhead translation, presented in equations 32-35 below. New variables which have yet to be defined here are L_{cl} and l, the total length of the club and the section contained by the collet, respectively.

$$I_{col}\ddot{\theta}_{col} + c_w\dot{\theta}_{col} - \dot{x}_G(2c_1l_1 - 2c_2l_2) + \dot{\theta}_G(c_1dl_1 - c_2dl_2) + k_w\theta_{col} - x_G(2k_1l_1 - 2kl_2 + \theta_G(k_1dl_1 - k_2dl_2) = 0 \quad (32)$$

$$m_G\left(l_1+\frac{d}{2}\right)\ddot{\theta}_{col}+m_G\ddot{x}_G+\dot{x}_G(2c_2+2c_1+c_{sh})+\dot{x}_{cl}(-c_{sh})+\dot{\theta}_G\left(c_2d-c_1d+c_{sh}(L_{cl}-\frac{l}{2})\right)+x_G(2k_2+2k_1+k_{sh})+x_{cl}(-k_{sh})+\theta_G\left(k_2d-k_1d+k_{sh}(L_{cl}-\frac{l}{2})\right)=0 \quad (33)$$

$$I_G\ddot{\theta}_{col}+I_G\ddot{\theta_G}+\dot{x}_G\left(c_2d-c_1d+c_{\ sh}\left(L_{cl}-\frac{l}{2}\right)\right)+\dot{x}_{cl}\left(-c_{sh}\left(L_{cl}-\frac{l}{2}\right)\right)+\dot{\theta}_G\left(c_1\frac{d^2}{2}+c_2\frac{d^2}{2}+c_{sh}\left(L_{cl}-\frac{l}{2}\right)^2\right)+x_G\left(k_2d-k_1d+k_{sh}\left(L_{cl}-\frac{l}{2}\right)\right)+x_{cl}\left(-k_{sh}\left(L_{cl}-\frac{l}{2}\right)\right)+\theta_G\left(k_1\frac{d^2}{2}+k_2\frac{d^2}{2}+k_{sh}\left(L_{cl}-\frac{l}{2}\right)^2\right)=0 \quad (34)$$

$$m_{cl}l_{cl}\ddot{\theta}_{col}+m_{cl}\ddot{x}_{cl}-\dot{x}_Gc_{sh}+\dot{x}_{cl}c_{sh}-\dot{\theta}_Gc_{sh}\left(L_{cl}-\frac{l}{2}\right)-x_Gk_{sh}+x_{cl}k_{sh}-\theta_Gk_{sh}\left(L_{cl}-\frac{l}{2}\right)=F(t) \quad (35)$$

The equations of motion were rearranged into matrices and set to equal a force matrix where a force as a function of time is applied to the clubhead, simulating an excitation impact on the clubhead, as shown in equation 36. The equations of motion were solved as before with the central difference method. The calculations were computed with a Matlab script which allowed the user to specify variable values, to monitor their effect on the output.

$$\begin{bmatrix} I_{col} & 0 & 0 & 0 \\ I_G & 0 & I_G & 0 \\ m_G\left(l_1+\frac{d}{2}\right) & m_G & 0 & 0 \\ m_{cl}L_{cl} & 0 & 0 & m_{cl} \end{bmatrix}\begin{bmatrix} \ddot{\theta}_{col} \\ \ddot{x}_G \\ \ddot{\theta}_G \\ \ddot{x}_{cl} \end{bmatrix}+$$

$$\begin{bmatrix} c_w & -2c_1l_1-2c_2l_2 & c_1dl_1-c_2dl_2 & 0 \\ 0 & c_2d-c_1d+\left(c_{sh}\left(L_{cl}-\frac{l}{2}\right)\right) & 0.5d^2(c_1+c_2)+c_{sh}\left(L_{cl}-\frac{l}{2}\right)\left(L_{cl}-\frac{l}{2}\right) & -c_{sh}\left(L_{cl}-\frac{l}{2}\right) \\ 0 & 2c_1+2c_2+c_{sh} & c_2d-c_1d+c_{sh}\left(L_{cl}-\frac{l}{2}\right) & -c_{sh} \\ 0 & -c_{sh} & -c_{sh}\left(L_{cl}-\frac{l}{2}\right) & c_{sh} \end{bmatrix}*$$

$$\begin{bmatrix} \dot{\theta}_{col} \\ \dot{x}_G \\ \dot{\theta}_G \\ \dot{x}_{cl} \end{bmatrix}+$$

$$\begin{bmatrix} k_w & -2k_1l_1-2kl_2 & k_1dl_1-k_2dl_1 & 0 \\ 0 & k_2d-k_1d+\left(k_{sh}\left(L_{cl}-\frac{l}{2}\right)\right) & 0.5d^2(k_1+k_2)+k_{sh}\left(L_{cl}-\frac{l}{2}\right)\left(L_{cl}-\frac{l}{2}\right) & -k_{sh}\left(L_{cl}-\frac{l}{2}\right) \\ 0 & 2k_1+2k_2+k_{sh} & k_2d-k_1d+k_{sh}\left(L_{cl}-\frac{l}{2}\right) & -k_{sh} \\ 0 & -k_{sh} & -k_{sh}\left(L_{cl}-\frac{l}{2}\right) & k_{sh} \end{bmatrix}*$$

$$\begin{bmatrix} \theta_{col} \\ x_G \\ \theta_G \\ x_{cl} \end{bmatrix}=\begin{bmatrix} 0 \\ 0 \\ 0 \\ F(t) \end{bmatrix} \quad (36)$$

For each solution plots would be provided to the user, of responses of the four degrees of freedom, in the acceleration, velocity and displacement forms.

7.3 Simulations of new model

The drive behind developing the model further came from the limited benefits apparent from adding a compliant material at the interface between club and robot. However, even though the vibration wasn't reduced to the required level, some supression of clubhead vibration was provided. Therefore the work presented in this chapter seeks to combine the limited success of adding a damped grip, with a flexible wrist joint to minimise clubhead vibrations.

It was decided appropriate to use the grip stiffness and damping values for the 50%

deadened silicone sleeve in all further simulations as it was the outcome of implementing this grip that demonstrated the largest reduction of clubhead vibration, without permitting excessive motion inside the collet.

Initially, the value of the wrist stiffness was set high to mimic the model without the compliant wrist. This was done as a sanity check to confirm that the model provided the same outcome as the previous rigid model, the clubhead acceleration from this simulation is presented in Figure 79a, with the simulation from the previous comparison in chapter 6 in Figure 78. Further simulations were produced with this model with arbitrary values for the wrist stiffness and damping input to gain an understanding of the model's sensitivity to change in values and to find a suitable range for the level of damping and stiffness that would be required. After completing several iterations of model simulations, it was found that the inclusion of a flexible wrist in this basic simulation was able to quash clubhead vibrations very effectively, approaching the point of critical damping. If the value of stiffness was set too high, the motion of the wrist joint would be inhibited to the point that the dashpot element added minimal effect, so this had to be considered when selecting the values.

The first of the following four plots, Figure 78, shows the response of the model from the previous chapter where the model simulated a club suspended in the fixed robot collet and excited with an impact on the clubhead, this was then plotted against measured accelerometer data. Figure 79a as mentioned was produced with the new model with the wrist set rigid to aid a comparison between the outputs from the new pinned collet model to the previous model in chapter 6. Here the grip conditions were set to that of the 'rigid grip' and the wrist stiffness was set high at a value of 100kNmrad^{-1} and the damping set low to a value of 2Nmsrad^{-1}. The two succeeding plots Figure 79b and Figure 79c demonstrated the response of the model to alternative wrist stiffness and damping combined with the grip boundary conditions of the 50% deadened silicone. The values of damping and stiffness used to generate these plots were 30Nmsrad^{-1} and 1000Nmrad^{-1} and 50Nmsrad^{-1} and 500 Nmrad^{-1} respectively. In all plots an impact of -1600N was applied to the clubhead for 5ms. The figures show the acceleration response of the clubhead for a duration of 2s after impact.

The similarity between Figure 78 and Figure 79(a) is high with a comparible magnitude of acceleration and frequency of oscillation. The slight vibration present at the start of Figure 79(a) could be due to a slight vibration feedback from the collet. The two further figures, Figure 79(b) and Figure 79(c) give an insight into the level of clubhead vibration reduction that could be achieved with the implementation of a flexible wrist. The level of vibration has been reduced along with a lower peak acceleration., with the third simulation showing the clubhead oscillation being reduced to approximately 2 full cycles. To achieve the best scenario through combination of wrist variables, an investigation was made into computing the wrist variables required to produce the lowest level of clubhead vibration.

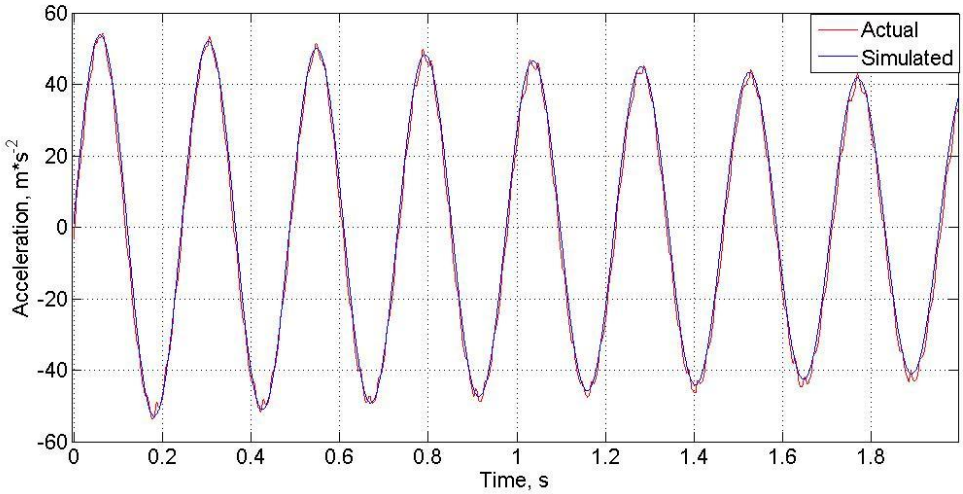

Figure 78 - Clubhead acceleration comparison from chapter 5 experiment. Measured clubhead acceleration versus the simulated acceleration when clamped in a rigid grip

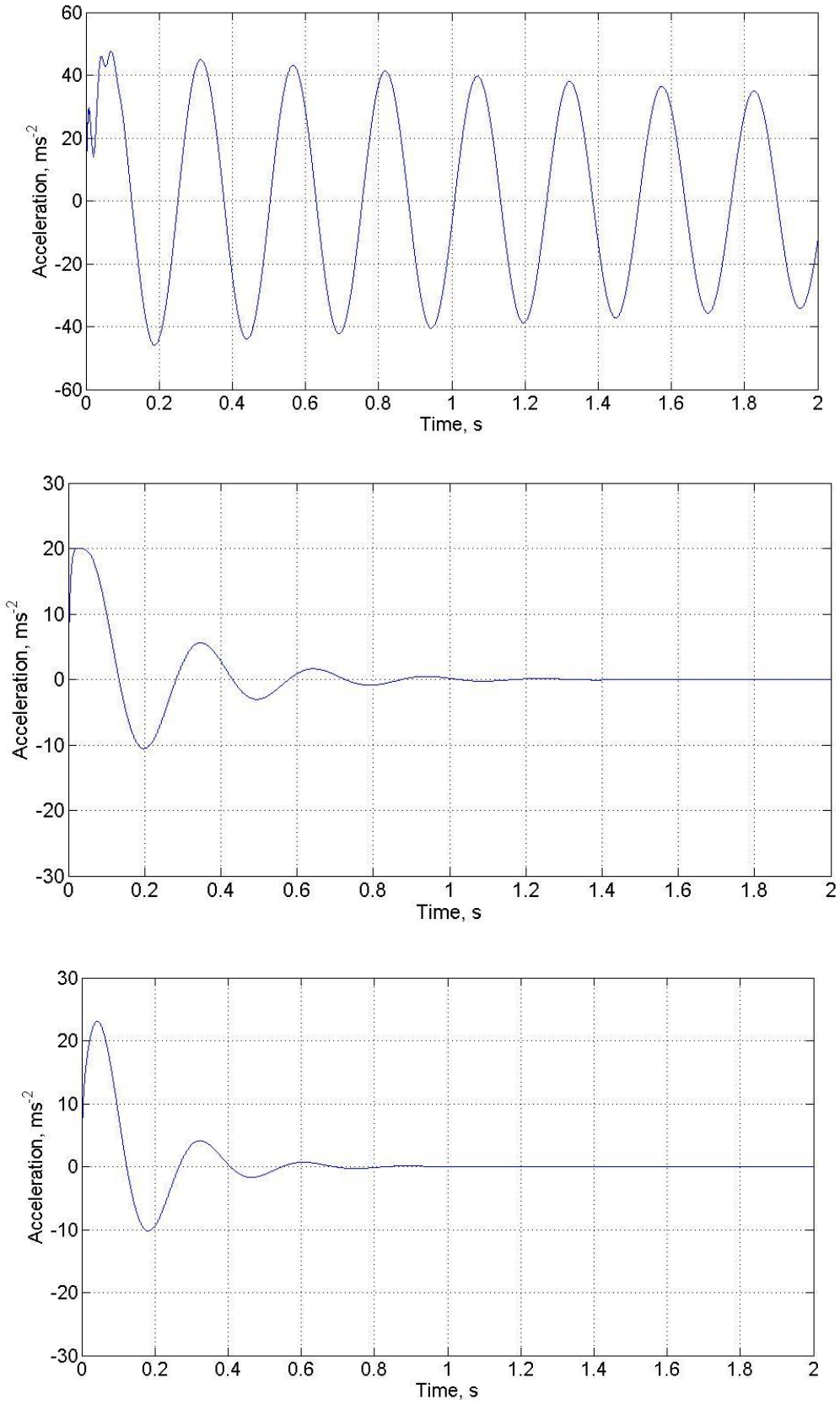

Figure 79 - Response of clubhead to varied wrist element variables (a) Rigid grip, Wrist: C:2 Nmsrad^{-1} K:100kNmrad^{-1} (b) 50% deadened silicone grip, Wrist: C:30Nmsrad^{-1} K:1000Nmrad^{-1} (c) 50% deadened silicone grip, Wrist C:50Nmsrad^{-1} K:500Nmrad^{-1}

7.3.1 Sensitivity analysis and minimum vibration calculation

A Matlab script was written to provide the user with a selection of computations which could be executed based on parameters entered into the model. One calculation option included in the script can find the combination of wrist stiffness and damping co-efficient which provided the least clubhead vibration in the basic pinned model. Three calculations are made to determine this; the root mean square is found, as well as the logarithmic decrement and the maximum peak value. The root mean square value gives an indication to the average level of vibration throughout the simulation whereas the logarithmic decrement best describes the rate at which a vibration is damped. A maximum peak value simply provides the quickest form of feedback as a large peak value could be indicitive of a large vibration as well as being the result of a system which is too flexible, providing too much clubhead motion. The logarithmic decrement and maximum peak calculations involved processing the data through an FFT. Once the dominant oscillation frequency in the data had been retrieved from this transformation, the comparisons could be made on a peak by peak basis. When provided with these three calculations, the user can then best assess which combination of variables gives the desired output.

During preliminary simulations it was found that through altering the value of mass and subsequently the inertia of the collet, a noticeable change in clubhead acceleration could be achieved. For the flexible wrist to have an effect on the response of the collet's motion and subsequently the clubhead vibration, an oscillation of the collet is required, providing a velocity which generates the damping force. If the collet is too heavy and has a high inertia, it will have less motion which acts against the wrist compliance and therefore the damping effect on the clubhead vibration would be minimal. This was an interesting find and led to the realisation that the collet inertia values should be altered as part of the minimum vibration calculations. At this point, initial simulations had involved the selection of arbitrary values for the wrist stiffness and damping, with no reason behind their selection. To aid future variable selections and to gain a sense of the range of values and combinations that could provide the best outcome, a sensitivity analysis of the model was conducted in conjunction with the minimum vibration calculations.

7.3.1.1 Calculations and results

The script was altered to allow the response of the clubhead to alterations in wrist stiffness and damping alongside collet inertia to be found. An initial value can be set for each of the three variables and an increment specified along with a number of desired iterations. A loop provides computations for all possible combinations of the three variables and the parameters defining the level of vibration are calculated.

The first feedback that was sought from this script was to enter a range of wrist stiffness and damping values, along with the real collet inertia values to provide an adequate indication as to it's sensitivity to changes in wrist variables and the resulting level of vibration. A simulation was generated with the collet inertia set to the real value for the robot collet, 0.02809kgm^2. Initial wrist variable values were set low at 2Nmsrad^{-1} and 50Nmrad^{-1} for the damping and stiffness respectively 75 iterations of the code were made to generate a broad spectrum of clubhead acceleration responses with increments of 2Nmsrad^{-1} and 75Nmrad^{-1} for the damping and stiffness respectively. It was confirmed that the stiffness and damping values were realistic in terms of the potential to buy a spring and dashpot with the same variables if they were required for a real test. A manufacturer was found which stocked rotational dashpots will values ranging from 0 to 18,000Nmsrad^{-1}, springs can also be purchased with a very large range in which the values selected for these tests fit into. The desired outcome of this test was not in any way to achieve a specific clubhead motion, but to simply gain an insight into how sensitive the model is to changes in wrist variables and how precise the future selection of variables should be, along with levels of clubhead damping that could be achieved.

The results were presented in a series of 3D surface plots as this provided the best visual feedback. Figure 80 and Figure 81 show the calculated logarithmic decrement and RMS values for each combination of the wrist damping and stiffness values. As can be seen in the plots, the highest logarithmic decrement and lowest RMS values were typically found with a combination of a low stiffness and damping value. The maximum value of logarithmic decrement was 3.078 with stiffness and damping values of 50Nrad^{-1} and 9Nmsrad^{-1} respectively, with the majority of the damping of the clubhead seen at a stiffness below 2000Nmrad^{-1} and 40Nsrad^{-1} which is

consistent with the low levels of vibration seen in the responses in Figure 79. The lowest RMS value of 4.116 was found with a combination of wrist stiffness and damping at 200Nmrad^{-1} and 4Nmsrad^{-1}.

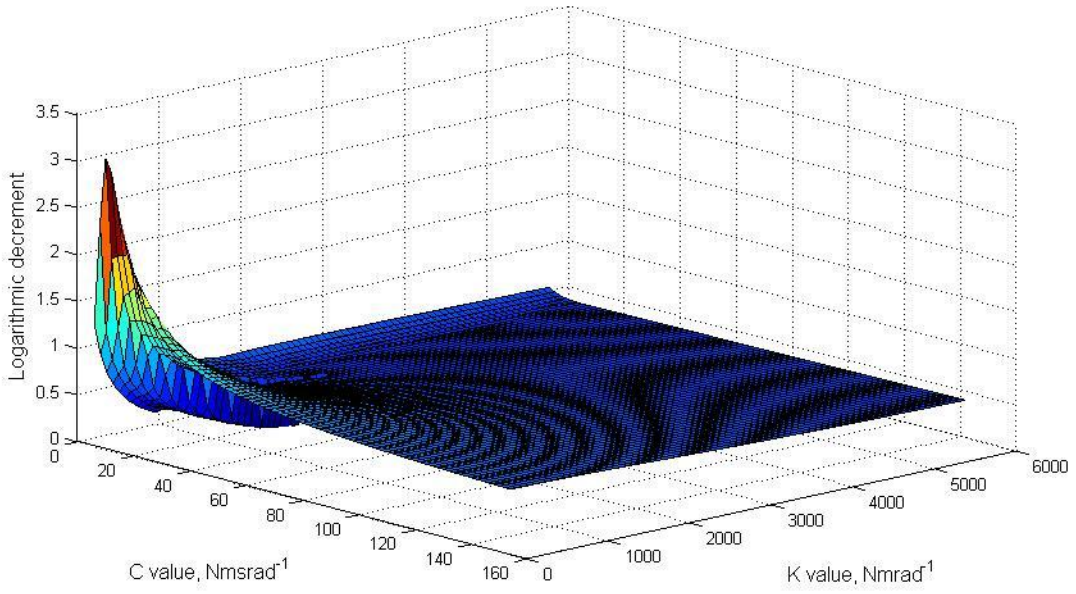

Figure 80 - Logarithmic decrement of clubhead vibration with actual collet inertia and varying values of wrist stiffness and damping.

The level of sensitivity to change in wrist element variables was much higher than it had been found when altering the grip element variables, this was very encouraging. However, changing the inertia of the collet also provides a level of control over the response of the clubhead, and this could be a possible alteration made to the robot in the future, so was worth investigating.

The second analysis considered how logarithmic decrement, RMS and peak acceleration were affected by a change in collet inertia. It was decided to keep the wrist compliant, as the collet was required to move in order to assess the effect of the change in its inertia. A mid range of stiffness and damping values was selected for the wrist of 1000Nmrad^{-1} and 30Nmsrad^{-1}. These values were hard coded into the script with the only variable varying per each cycle of the loop being the collet inertia. An initial value was selected as 0.002kgm^2, with increments of 0.001 being applied during each iteration for 75 iterations, this placed the real inertia of

0.028kgm^2 central to the range. An output was generated for each of the changes in logarithmic decrement and root mean square as a function of the change in collet inertia. The highest logarithmic decrement and lowest RMS value were both caused by a collet inertia of 0.0102 kgm^2. To assess the levels of clubhead acceleration that could be achieved with this collet inertia, the first simulation loop was repeated with the same variability in the wrist elements and the collet inertia set at 0.0102 kgm^2. Surface plots were produced as before for the logarithmic decrement and the RMS.

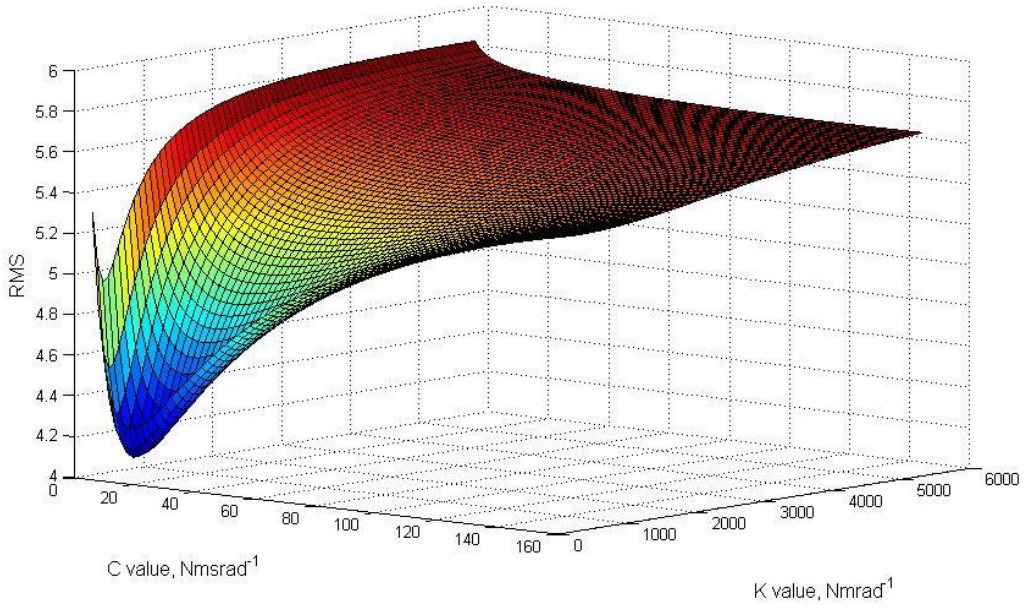

Figure 81 - RMS of clubhead vibration with real collet inertia and varying values of wrist stiffness and damping

It was found that through making this change to the collet inertia, the average logarithmic decrement was higher at 0.6171 as opposed to 0.6105 in the previous analysis.Additionally the lowest RMS value was lower at 3.9720 indicating a lower level of vibration, this was seen with a combination of wrist stiffness and damping of 200Nmrad^{-1} and 15Nmsrad^{-1}. The lowesr 'maximum peak' value was also lower at 18.7ms^2 as opposed to 19.3ms^2. Figure 82 illustrates the RMS values that were achieved with this value of collet inertia. For this plot the same initial values and increments were used as before.

For the simulations of golfer full swings to be completed later in this research, the original collet inertia will be used but in the event that a good simulation cannot be achieved, the collet inertia can be reduced. Based on the results seen in this analysis. A good level of vibration reduction at the clubhead should be seen with a wrist stiffness range of 200 - 600Nmrad^{-1} and a damping coefficient value of between 5 - 40Nmsrad^{-1}.

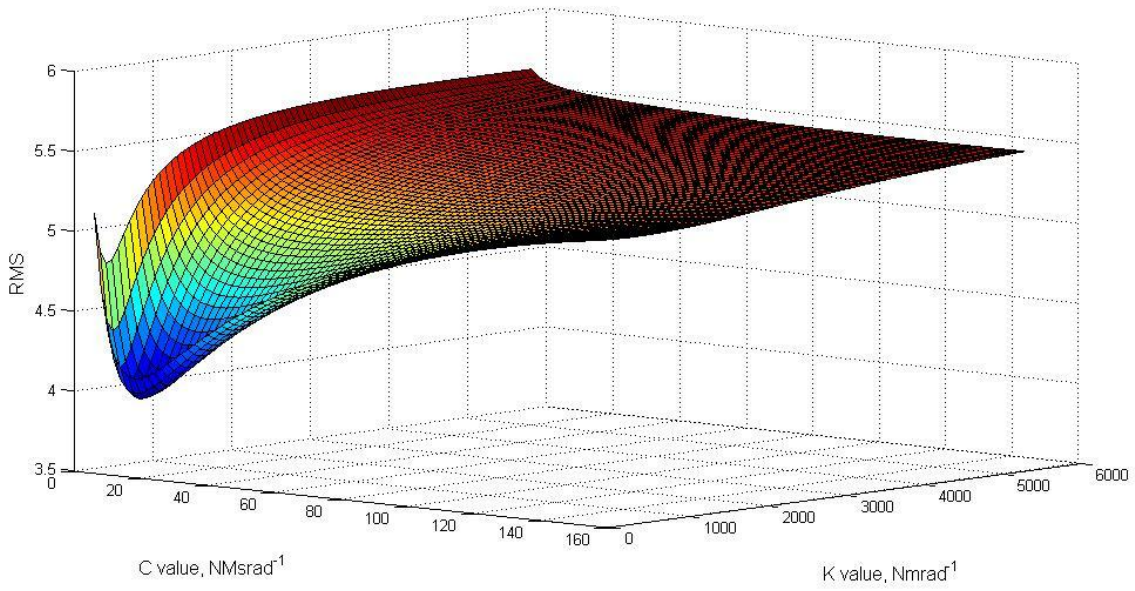

Figure 82 - RMS for model iterations with new lower collet inertia values.

7.4 Driven wrist

Once the initial simulations had been completed, confidence was gained in the concept of an addition of a wrist joint to the model and the scope of the results which could be acheived. To analyse the model's response to a defined wrist rotation, a drive was now applied at the wrist, replacing the vibration exciting impact force previously applied to the clubhead. The drive was specified as a rotation of the wrist, θ_w, and was applied to the collet through the wrist dashpot and spring elements. The wrist drive was added to the equations of motion resulting in the following matrices.

$$\begin{bmatrix} I_{col} & 0 & 0 & 0 \\ I_G & 0 & I_G & 0 \\ m_G\left(l_1+\frac{d}{2}\right) & m_G & 0 & 0 \\ m_{cl}L_{cl} & 0 & 0 & m_{cl} \end{bmatrix}\begin{bmatrix} \ddot{\theta}_{col} \\ \ddot{x}_G \\ \ddot{\theta}_G \\ \ddot{x}_{cl} \end{bmatrix}+$$

$$\begin{bmatrix} c_w & -2c_1l_1-2c_2l_2 & c_1dl_1-c_2dl_2 & 0 \\ 0 & c_2d-c_1d+\left(c_{sh}\left(L_{cl}-\frac{l}{2}\right)\right) & 0.5d^2(c_1+c_2)+c_{sh}\left(L_{cl}-\frac{l}{2}\right)\left(L_{cl}-\frac{l}{2}\right) & -c_{sh}\left(L_{cl}-\frac{l}{2}\right) \\ 0 & 2c_1+2c_2+c_{sh} & c_2d-c_1d+c_{sh}\left(L_{cl}-\frac{l}{2}\right) & -c_{sh} \\ 0 & -c_{sh} & -c_{sh}\left(L_{cl}-\frac{l}{2}\right) & c_{sh} \end{bmatrix}*$$

$$\begin{bmatrix} \dot{\theta}_{col} \\ \dot{x}_G \\ \dot{\theta}_G \\ \dot{x}_{cl} \end{bmatrix}+$$

$$\begin{bmatrix} k_w & -2k_1l_1-2kl_2 & k_1dl_1-k_2dl_1 & 0 \\ 0 & k_2d-k_1d+\left(k_{sh}\left(L_{cl}-\frac{l}{2}\right)\right) & 0.5d^2(k_1+k_2)+k_{sh}\left(L_{cl}-\frac{l}{2}\right)\left(L_{cl}-\frac{l}{2}\right) & -k_{sh}\left(L_{cl}-\frac{l}{2}\right) \\ 0 & 2k_1+2k_2+k_{sh} & k_2d-k_1d+k_{sh}\left(L_{cl}-\frac{l}{2}\right) & -k_{sh} \\ 0 & -k_{sh} & -k_{sh}\left(L_{cl}-\frac{l}{2}\right) & k_{sh} \end{bmatrix}*$$

$$\begin{bmatrix} \theta_{col} \\ x_G \\ \theta_G \\ x_{cl} \end{bmatrix}=\begin{bmatrix} c_w & k_w \\ 0 & 0 \\ 0 & 0 \\ 0 & 0 \end{bmatrix}\begin{bmatrix} \dot{\theta}_w \\ \theta_w \end{bmatrix} \quad (37)$$

There were no real golf swing scenarios from which kinematic data could be measured and implemented as the drive for this model, but this model could simulate the basic rotation and resulting acccelerations of the robot swing reported in section 6.3. This model would also provide an opportunity to test the minimum vibration wrist value ranges specified in the previous sectionwhen applied in a dynamic swing.

The square torque swing profile generated in section 6.3 was used to drive this model and the robot. The 50% deadened silicone grip values were applied to the model and the wrist spring set rigid to mimic the robot. A comparison was made between the measured and simulated clubhead acceleration and a good agreement was found as shown in Figure 83.

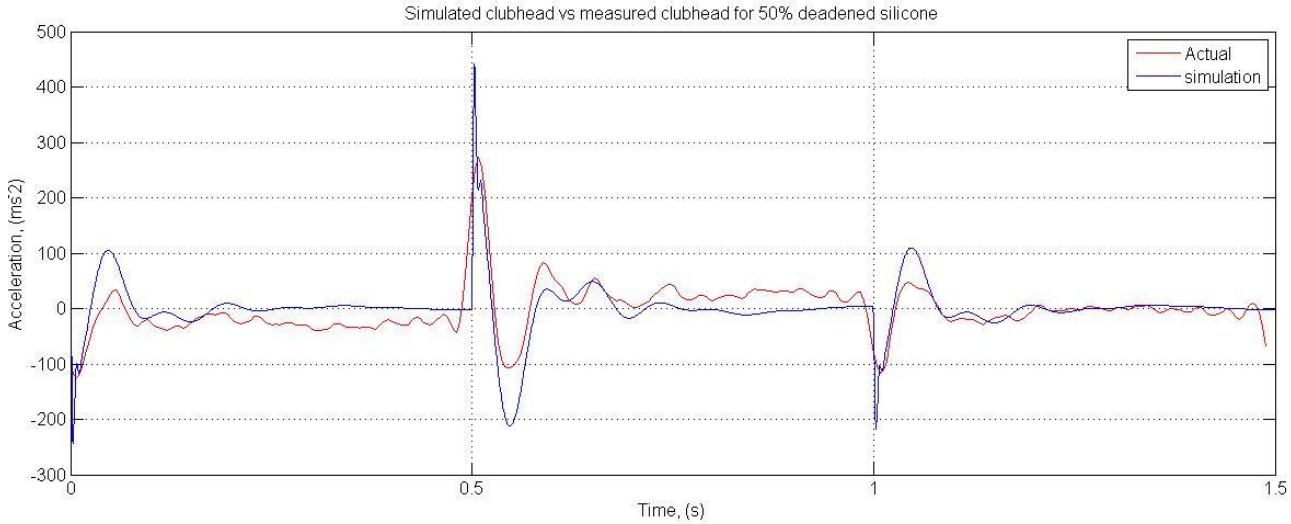

Figure 83 - Wrist spring set rigid to match an incompliant wrist simulation as simulated in chapter 6.

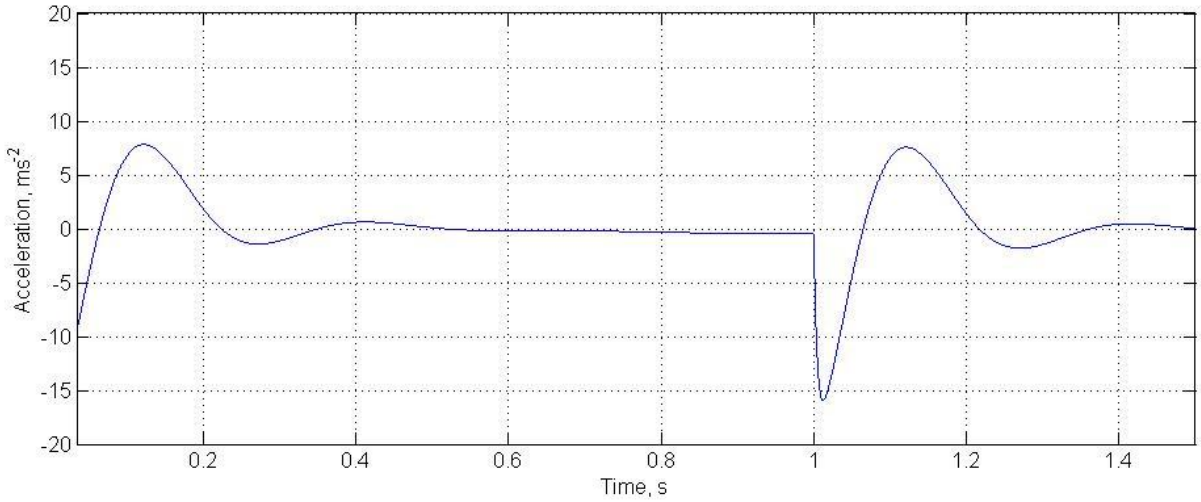

Figure 84 - Clubhead acceleration for driven wrist model with flexible wrist

The values of wrist stiffness and damping calculated from the minimum vibration analysis as providing the lowest levels of clubhead vibration were then coded into the script, it was expected that the result from section 7.3.1 should somewhat follow through and provide a good outcome in this now driven wrist simulation. The differences between the previous simulations and these being that the magnitude of wrist motion in this driven wrist model is higher than in the simulation where just an excitation impact at the clubhead is applied and the change in direction half way through the drive would add an additional area of interest. The source of motion in

this model is also different, no longer at the clubhead, it is at the opposite end of the model, at the wrist. With a wrist stiffness and damping co-efficient of 200Nmrad^{-1} 30Nmsrad^{-1} the clubhead acceleration response shown in Figure 84 was achieved. The magnitude of acceleration is now much smaller with the maximum peak being 15ms^{2} and the change in torque at the 0.5s stage is no longer visible in the clubhead response. This plot shows a huge improvement in the reduction of clubhead vibration when a flexible wrist is applied compared to the limited results achieved with the compliant grip.

7.5 Mathematical model with added arm link

To increase the realism of the model in terms of similarity of structure to the golf robot, the decision was made to add a virtual arm link to the model. This addition would increase the functionality of the model as it would provide the option to drive the model with golfer kinematic data for a direct comparison between golfer and model, and if required, model to robot. The new link was given the same length as the robot arm link with a pivot point at the top and the wrist joint at the bottom. The arm link was not modelled as a mass, for simplicity the pinned wrist point was now rotated around the arm pivot at a distance of the arm link and at the arm link's

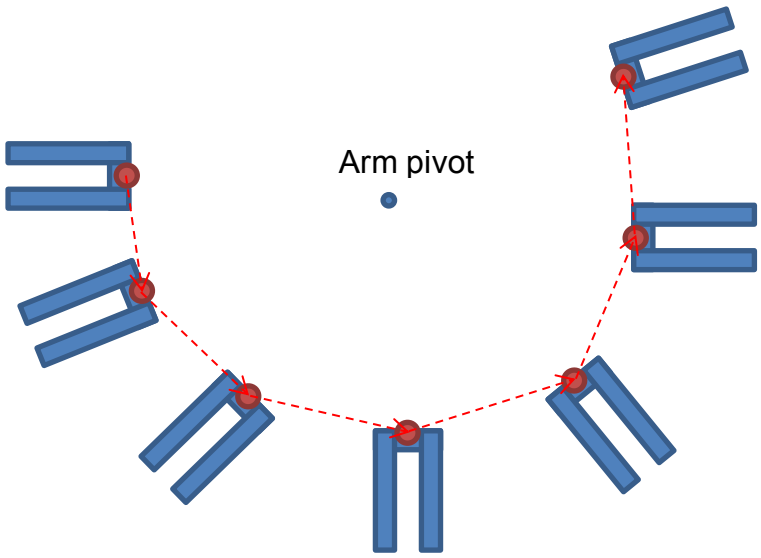

Figure 85 - Mapping of collet relative to arm pivot

acceleration. The arm link is included in the diagram in Figure 86 and Figure 87 as a visual aid in mapping the model to the robot's structure. In practice, it could be visualised as the wrist joint moving in space at positions dictated by the arm position and acceleration as shown in the figure below.

This method of adding the arm link doesn't require any additional degrees of freedom to be considered.

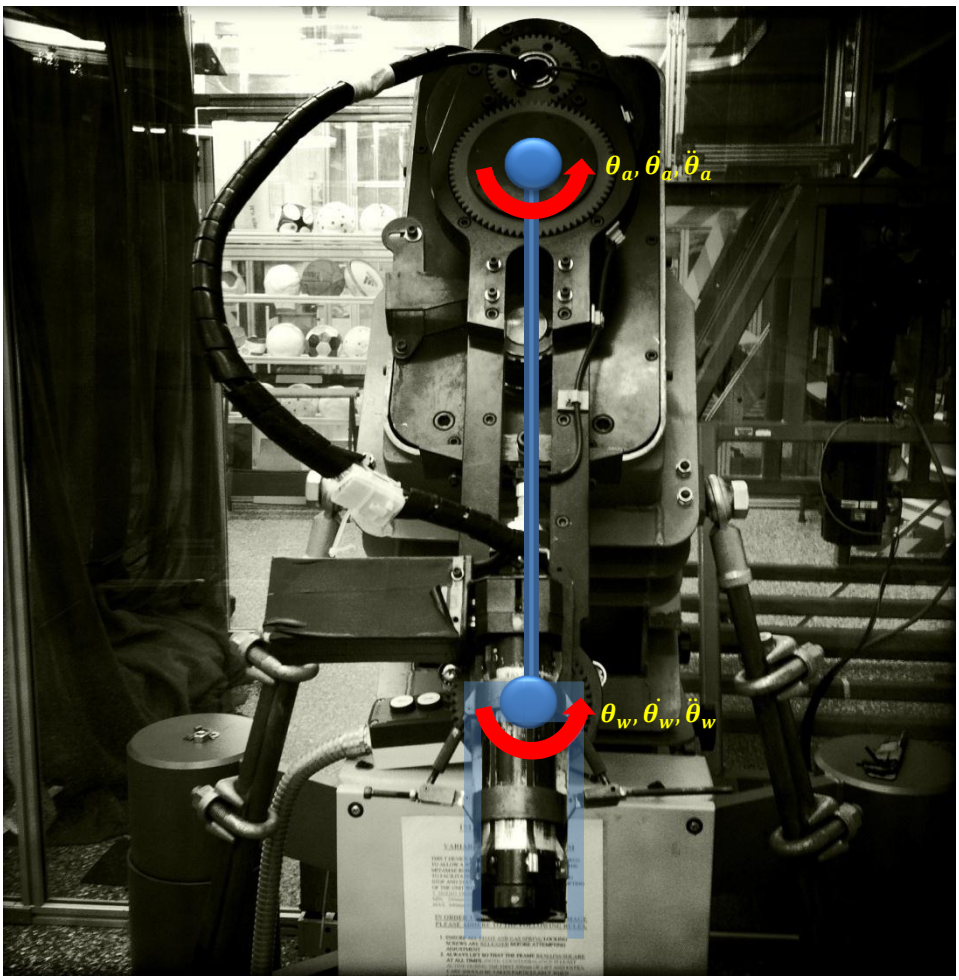

Figure 86 - Mapping model to robot structure

The model drive is provided by the arm's motion. This is applied to the collet mass via the spring and dashpot elements as before with an additional component. A new component was added to the equations of motion to account for the fact that the collet and wrist are now considered as acting as two interconnecting bodies as illustrated by Figure 88. The accompanying equation to this figure is as follows:

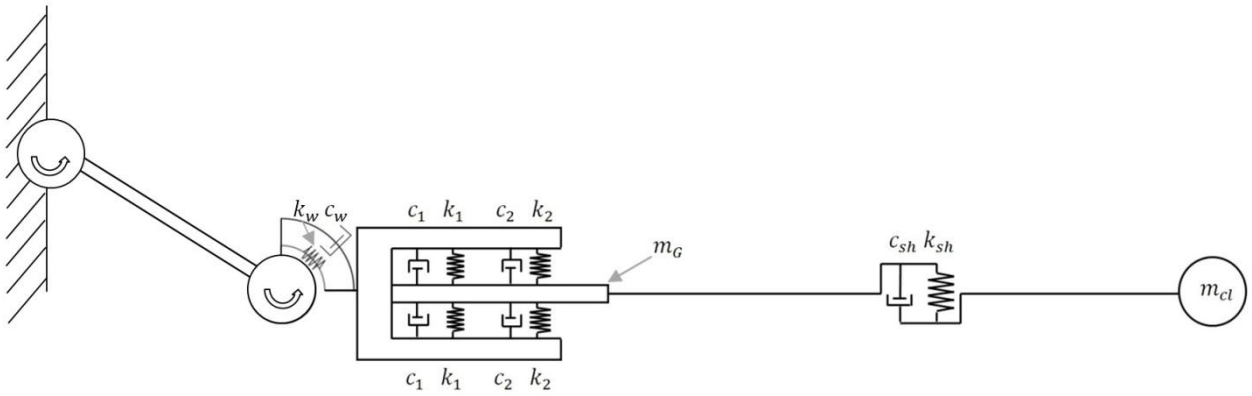

Figure 87 - Model with arm link

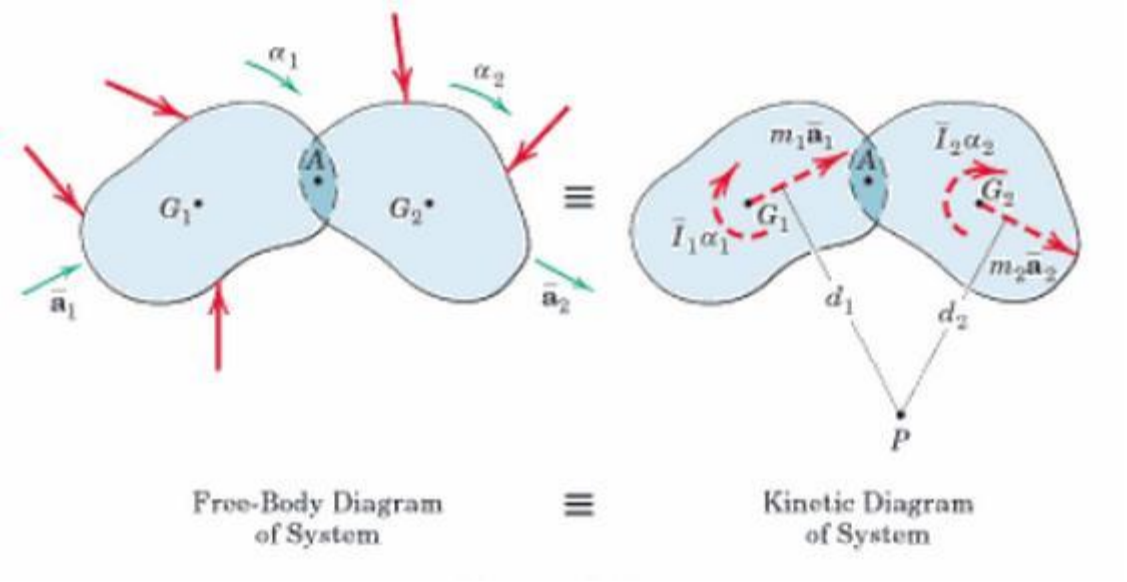

Figure 88 - Acceleration of interconnecting bodies, Meriam(2012)

$$\sum M_p = \bar{I}\alpha + m\bar{a}d \tag{38}$$

When considering the acceleration of two bodies joined by a pivot, A, The sum of moments about point P is equal to the sum of $I\alpha_1$, $I\alpha_2$, m_1a_1d *and* m_2a_2d. In the model of the golf robot this point would represent the pivot at which the collet rotated and P would be the point about which moments are taken. Therefore the moments about

the collet pivot are equal to the sum of the translation accelerations with one being the length of the arm link multiplied by the rotational acceleration of the arm joint and the second being the global acceleration of the collet multiplied by the distance between the centre of rotation of the collet and the point about which the moments are taken, l_{col}, this constitutes $\bar{a}$ in equation 37 with the two accelerations combining to produce $\ddot{x}_{col}$. These variables are illustrated in Figure 89. This is then multiplied by the mass of the collet and the distance between the point at which this acceleration acts and the points about which the moments are taken, the resulting equation is given in equation 39. $\bar{I}$ in this equation is the centroid moment of inertia.

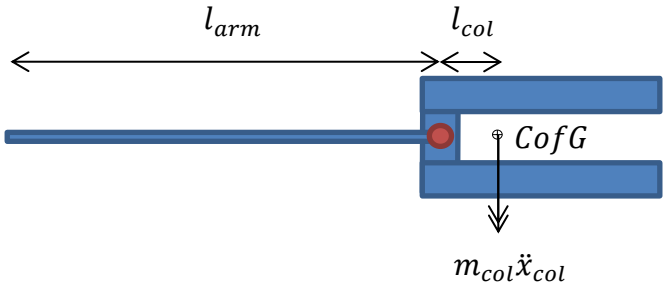

Figure 89 - Definitions of collet parameters

$$\sum M_p = \bar{I}\ddot{\theta}_{col} + m_{col}l_{col}(l_{arm}\ddot{\theta}_{arm} + l_{col}\ddot{\theta}_{col}) \tag{39}$$

It follows that from substituting equation 40 into equation 39 and rearranging to collate all variables involving the driven arm, the right hand side matrices of the equations of motion look as follows:

$$= \begin{bmatrix} -l_{arm}l_{col}m_{col} & c_w & k_w \\ 0 & 0 & 0 \\ 0 & 0 & 0 \\ 0 & 0 & 0 \end{bmatrix} \begin{bmatrix} \ddot{\theta}_a \\ \dot{\theta}_a \\ \theta_a \end{bmatrix} \tag{40}$$

The rotation of the collet is now controlled by the wrist spring and dashpot elements.

The decision was made to leave the wrist passive at this stage to aid the clarity of the accelerations of each element; with an acceleration applied about the arm pivot, does the collet behave in a manner which we would expect?

The basic golf swings as described in section 6.5 demonstrated how a golfer is unable to keep their wrists fixed even during a relatively slow motion. These arm rotations from these swings were used to drive the model with the wrist left passive. The aim of these simulations would be to recreate the additional rotation due to the flex in the wrist and to select values for wrist stiffness and damping which allowed these rotations while providing comparable clubhead accelerations. Two of the basic swing types are illustrated in Figure 90 and Figure 91, where basic human swings are compared against model simulations of those swings, neither swing contained a ball impact. The acceleration of the clubhead in the measured plots is measured relative to the golfer's hand and in the simulations, the acceleration is relative to the collet.

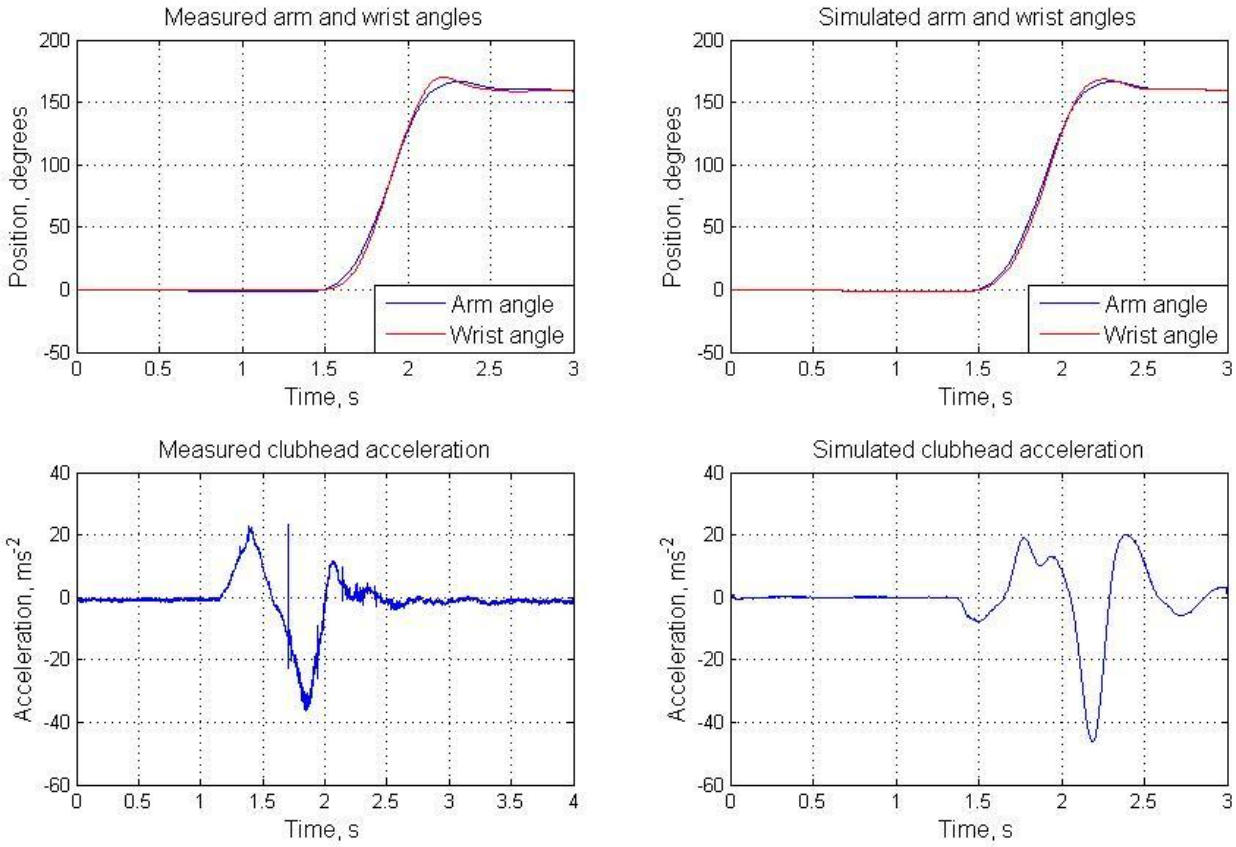

Figure 90 - Basic swing, arm rotation 0 to 180

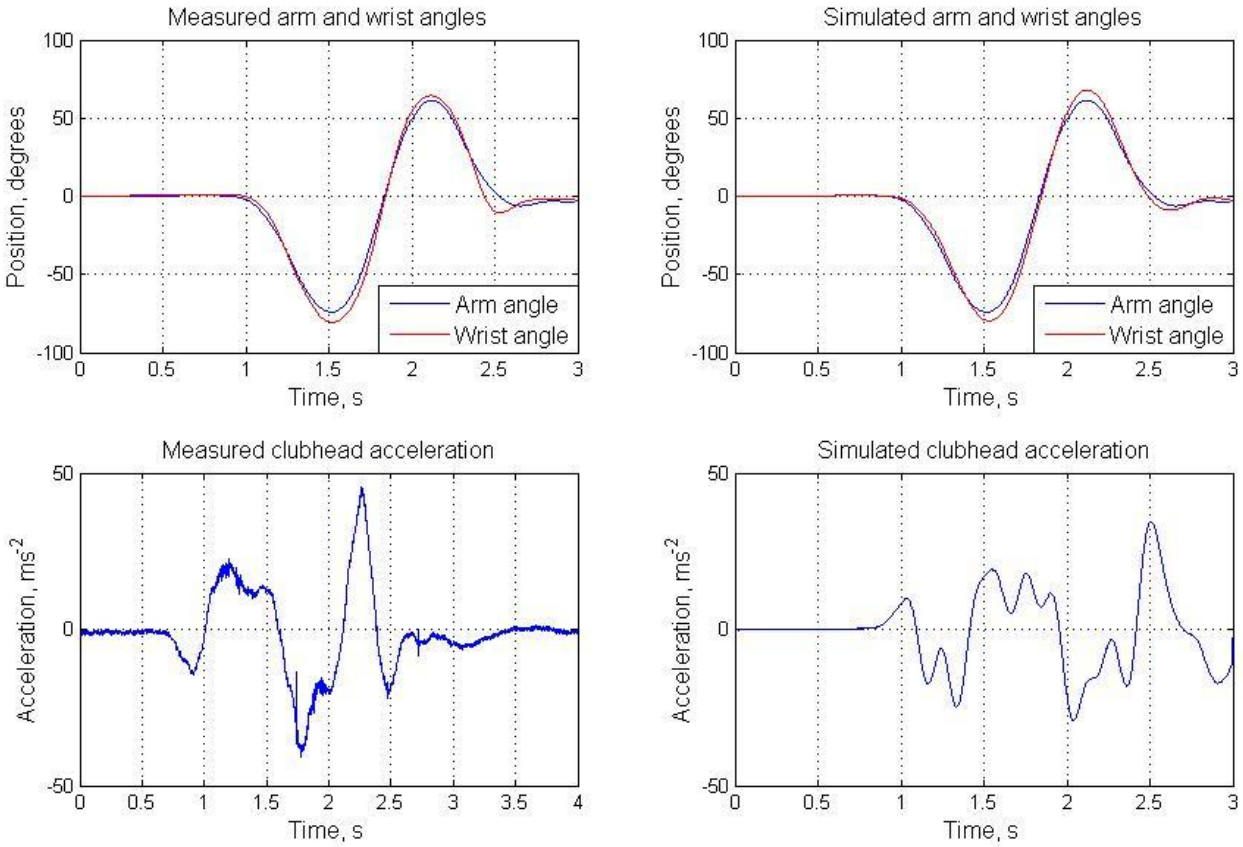

Figure 91 - Basic swing, arm rotation 0 to -90 to 90 to 0

In both simulations the measured data is presented to the left and the simulations are on the right. Clubhead acceleration is presented below the plot of the swing profile arm angles and the resulting collet position. The values of stiffness and damping which provided the best fit to the swing presented in Figure 90 were 500Nmrad^{-1} and 5Nmsrad^{-1} respectively. For the swing in Figure 91 these values were 350Nmrad^{-1} and 3Nmsrad^{-1}. These differences in wrist values could be explained by the human wrist acting as a variable spring and damper which can be controlled by the golfer through activating the muscles controlling the wrist to differing levels. The damping values required to match the data are low with the stiffness of the wrist providing most control over the position of the collet. Both simulations provided good agreement between both position and clubhead acceleration. The measured clubhead acceleration is not aligned as there was no defining point by which to align from. Aligning the two acceleration plots visually is possible, bearing in mind that the time base isn't consistent, and for both swings the maximum accelerations were similar. The simulated acceleration plot in Figure 90 is

larger than the measured peak with values of -45 and -35ms^{-1} respectively; which could be attributed to approximations in the model. In Figure 91, there is more clubhead oscillation; however the overall graph shape is similar with the defining peaks of the measured acceleration still present, generally in the simulation the main peaks in the clubhead acceleration is lower.

The results from these simulations are positive with the model able to simulate basic swings of a golf club well in terms of wrist position and clubhead acceleration.

7.6 Development of flexible wrist link

The final stage of this model was realised by allowing the wrist to be driven for a greater level of control over the resulting collet rotation. This would provide complete comparability between robot swings and the model as this meant swing profiles derived from golfer data could be used to drive both model and robot. It would also allow comparisons to be drawn between a golfer's full swing and the model, to assess the model's ability to simulate a human swing. The one variable which is not included in this model is the grip rotation. The flexibility of the wrist, however, would result in a different clubhead position compared to the rigid robot model. To allow the implementation of swing profiles as a method to drive the model, a feed-forward methodology would need to be employed by examining the 'overshoot' caused by the flexibility in the wrist and counteracting this by reducing the angular position of the wrist input in the swing profile. Currently the model is driven by a rotation at the arm joint and the wrist joint is free to rotate. It is the force provided by the wrist dashpot and spring that return the wrist to its 'zero' position.

An additional element was added to the drive of the model, the wrist position, θ_w, as governed by the data contained in a swing profile. If the wrist elements were set to provide a rigid wrist as currently on the robot, the resulting angular position of the collet would be its global position dictated by the arm and wrist positions. However, if compliance was added at the wrist, the collet's motion would include an additional rotation due to the flexibility of the wrist. At the point of the wrist being in this passive zone of motion, the spring and dashpot at the wrist should act to reduce the magnitude of vibration in the club and more specifically the clubhead. The equation

of motion for the collet was updated to include the wrist rotation with the drive matrices adapted from equation 40 to equation 41.

$$= \begin{bmatrix} -l_a l_w m_{col} & c_w & k_w \\ 0 & 0 & 0 \\ 0 & 0 & 0 \\ 0 & 0 & 0 \end{bmatrix} \begin{bmatrix} \ddot{\theta}_a \\ \dot{\theta}_a + \dot{\theta}_w \\ \theta_a + \theta_w \end{bmatrix} \tag{41}$$

Before progressing to simulations of full swings and attempting to match the clubhead acceleration as seen in a golfer's swing, the model's response was verified against a robot swing. All compliance was removed from the model by increasing the spring values at the grip and wrist and a swing profile with no grip rotation was implemented as the drive for the robot and model. Swing time for the profile was set to 3s, a 1s longer duration than for a full speed swing as without the ball impact, this was deemed unsafe for the robot to perform. Clubhead acceleration was captured from the robot swing with an accelerometer mounted on the clubface of the robot with beeswax and the feedback was captured via a National Instruments USB data acquisition device. Conversion and processing of the response was partially completed in Smart Office and then filtered and cropped in Matlab. A Swing profile was generated from the servo motor feedback from the robot and used to drive the model. The swing profile and accompanying clubhead accelerations for robot and model are presented in Figure 92 and Figure 93. The resulting accelerations have not been aligned but a comparison is possible as the time base is the same.

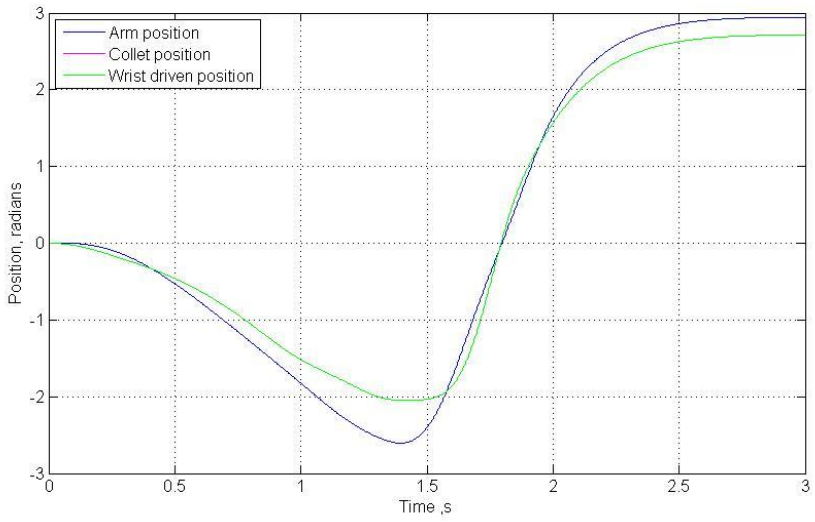

Figure 92 - Swing profile, driven arm and wrist positions along with the resulting collet position.

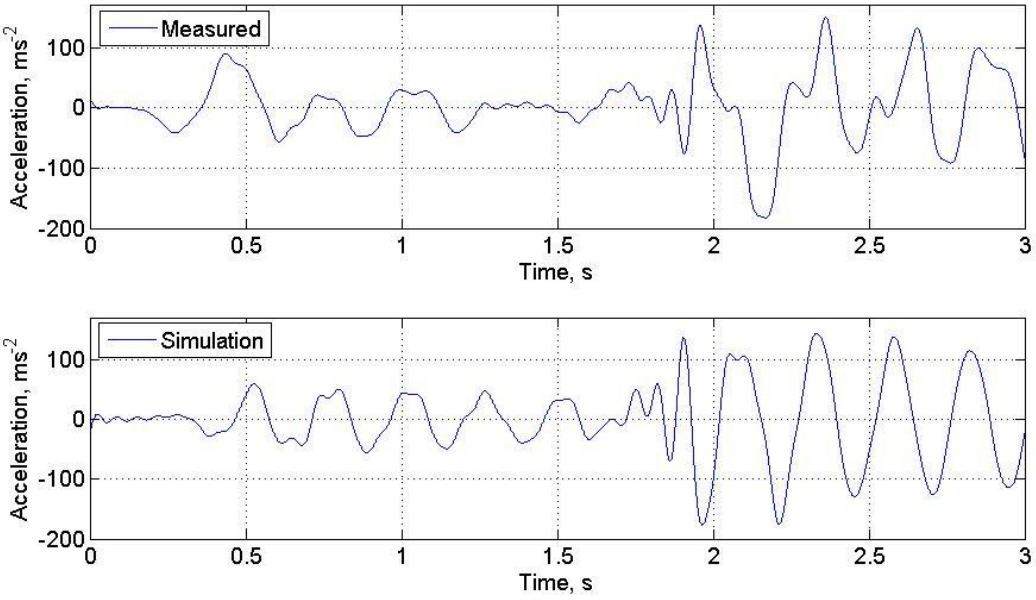

Figure 93 - Clubhead acceleration, measured (top) and simulated (bottom).

Figure 92 illustrates that the position of the collet, due to the rigid wrist, precisely matched the driven position. The clubhead acceleration plots in for both measured robot and simulated robot in Figure 93 are similar, with comparable acceleration magnitudes and oscillation frequency, the measured data having a slightly lower frequency than the 4Hz frequency in the simulation which is the natural frequency at which the clubhead oscillates. This frequency shift could be due to the way in which the mass of the club is modelled. In the model the club mass is distributed between the grip element and the clubhead. The acceleration of the clubhead in the simulation is larger than in the measured data but still within an acceptable range. This is accepted by the author as a good simulation of the robot swing.

7.7 Evaluation

This chapter involved the further development of the model presented in chapter 6, where a flexible wrist was added between the collet and the pivot point about which the collet rotates. Limited success had been achieved through the implementation of a compliant damping gripper however the results were encouraging. It was the investigative work considering clubhead vibration when swung by a human in a basic motion at the end of chapter 6, which revealed the flexibility of a human wrist during

a swinging motion and inspired the investigation into what could be achieved through adding additional compliance at the wrist.

The initial adaptations made to the model included considering an un-driven, pinned model where the rotational flexible wrist spring and dashpot were added between the collet and the pin. Equations of motion were adapted to include this change and preliminary simulations were run. It was found that by exciting the model through an impact at the clubhead and varying the values of stiffness and damping at the wrist, vibrations were damped very effectively, but this wasn't related to any measured golf swing data. Several iterations of the model were run via a bespoke script to find the best combination of wrist element variables to provide the minimum clubhead vibration and to analyse the sensitivity of the model to changes in wrist variables. It was during these simulations that the effect of collet inertia on the subsequent clubhead vibration was realised and an additional simulation loop was run to find a value of collet inertia which provided the minimum level of clubhead vibration. The collet could be adapted on the physical robot if it were required to provide the desired output, the value of collet inertia which provided the most improvement was $0.01 kgm^2$. A final minimum vibration analysis was then run with the alternative collet value hard coded into the script. A general reduction in vibration was seen and final wrist variable values which should provide a good reduction in clubhead vibration were suggested. These values were a stiffness range of 200 - $600 Nmrad^{-1}$ and a damping coefficient value range of between 5 – $40 Nmsrad^{-1}$. A drive was then added at the wrist and it was found when implementing the minimum vibration values, a huge decrease in clubhead acceleration was achieved when compared to the measured clubhead acceleration when swung by the robot with just the compliant grip.

To improve the practicality of the model and similarity to the robot, an arm link was added to the model. This provided the ability of direct comparison with a basic human swing. The wrist was left passive and the arm driven with positional data captured from a golfer in chapter 6. Comparisons between the golfer swing and simulated swing angular positions showed good agreement with comparable clubhead accelerations.

The final stage involved adding a drive at the wrist link as both a human golfer and

the robot provide a drive at the wrist, and this would provide more control over the motion of the collet as well as enabling direct comparison from golfer, robot and model swings. This final model is able to simulate the driven wrist and arm positions well. To demonstrate the reduction in clubhead acceleration that can be achieved with this model when compared to a model which simulates a swing from the robot in its current state with no compliant grip or wrist, a simulation was made with all spring values set high to simulate the current robot's ability. This could then be compared with simulations in the next chapter which will involve simulating a full swing by a golfer with compliance at the grip and wrist, to allow an insight into the effect implementing a flexible grip and wrist on the robot could have.

Chapter 8

Simulating a Golf Swing

8.1 Introduction

Chapter 7 documented the completion of the mathematical model of the robot. It has successfully been used to simulate a full golf swing as swung by the robot without any compliance and also simulate slow speed simplified swing motions performed by a human. However, further validation is required before the model can be implemented as a functional tool for simulating a full human golf swing to determine how the robot could be adapted to achieve the same output. At the inception of this research, two swing variables were selected as the most indicative of the outcome of a swing. These variables were the orientation of the clubhead at impact and the shaft deflection profile throughout the swing. These variables will be used throughout this chapter to compare simulated results with human data, where clubhead acceleration will be used as the means to assess the clubhead orientation as it is assumed that vibration in the clubhead is the most dominant factor which could result in incorrect clubhead orientation in swing simulations. The work in this chapter now progresses to the next stage of simulating a full golf swing, takeaway to follow through as swung by a golfer. The aim of this chapter is to programme the fully realised model with golfer swing profiles so that a comparison can be made between measured and simulated clubhead acceleration and shaft deflection. The similarities between measured and simulated will assist in the assessment of the success of the model in simulating human golf swings. Programming the model with a single swing profile and adjusting the stiffness and damping from the current ‘rigid’ robot scenario to a system which contains compliance will provide an insight into the results that could be achieved through implementing a compliant grip and wrist on the robot. The final simulations included in this chapter are driven with robot feedback data as for every robot swing the actual angular rotations differ from the input swing profile due to the method by which the robot is controlled, the feedback data also lacks the ‘smoothness’ of the swing profiles and therefore increases the level of vibration in the whole robot system. These simulations aimed to demonstrate the effect the

compliant model has on clubhead vibrations excited by the spiky robot feedback data.

Thus far, the solutions proposed in this thesis to remove unwanted clubhead oscillations in a robotic golf swing have considered suppressing existing fully realised vibrations. An alternative method and one that can be used in conjunction with this form of solution is to minimise the production of these vibrations at the source through the method in which the robot is programmed. From this scope a project at Loughborough University was completed where a new tool was produced to generate swing profiles which would minimise the initiation of vibrations in the clubhead, as it had been found that the current methodology for creating swing profiles could be optimised to produce a smoother take away. The following chapter contains an introduction to the method in which a swing is programmed into the robot as a foundation of understanding the process behind generating swing profiles. The methodology behind the generation of swing profiles is presented including the implementation the new swing profile generation tool developed by Cockram (2010) which sought to produce profiles which minimise the level of acceleration induced vibration in the clubhead. This was seen as an additional approach for further reducing clubhead vibration which could work alongside the implementation of additional compliance in the system and is presented before the completion of any further simulations so that the combined result from adjusting the input to the model as well as adding compliance to the model could be assessed.

Kinematic data from the golfer testing reported in chapter 4 was processed via this new tool and applied as an input to the model. Resulting clubhead acceleration was then compared to the measured responses from the golfer testing. Shaft deflection profiles for the swings captured in the study in chapter 4 are created through the mapping of strain gauge output to metres of deflection of the clubhead. These profiles are then compared to clubhead displacement simulated by the model. The measured clubhead acceleration from a golfer's swing is also compared against clubhead acceleration output from the model.

Data from six of the participants from the study reported in chapter 4 were converted into six swing profiles and used to drive the model. These six golfers were selected as a group that showed most diversity in swing type. Comparisons are made

between clubhead vibration and the shaft deflection profiles and the outcomes are discussed. Wrist stiffness and damping values are tuned to best fit the human data and the overall success of the model is evaluated.

8.2 Swing profile generation

The robot modelled in this thesis, the Miyamae Robo V, requires a command file which contains ‘swing profile’ information as the method of input for the simulation of a golf swing. For easy of comparability, this was also made the method by which the model is driven. The main objective when creating swing profiles is to create a smooth swing (i.e. keep the acceleration profile smooth) to limit the visible oscillations. The methodology followed was based on that given in Harper's (2006) research and involved the same equipment. In the interest of understanding the process in which swing profiles are created for the model, as they are primarily produced based on the robot’s requirements, a brief overview of the process by which profiles are produced and programmed into the robot will be given in the following section.

8.2.1 Robot programming methodology

The Miyamae Robo V robot has three servo motors which each provide the drive for a single degree of freedom, the arm joint, wrist joint and the grip rotation. Throughout the swing, the motor controller is continuously monitoring the difference between each motor’s current position and the target position based on this adjusts the electrical current to each drive to try to reduce this difference. Its motion control system is controlled by a software package called Robot Manager which is installed on a dedicated PC for the robot. A generic swing profile is available as a quick option of performing a swing but isn’t representative of a real golf swing. To program the robot with actual swing data, a swing profile can be generated from either user generated data or from kinematic data collected from a swing as demonstrated in chapter 4. On the completion of a swing simulation, the feedback from the motors is automatically downloaded and presented at a frequency of 250Hz as the actual displacement, velocity and acceleration for each of the three axes. There is often a

small discrepancy between the target data and the performed swing feedback data. It has been found that the robot can sometimes lag behind the target positions particularly for golfers with particularly large grip and wrist angular velocities. This lag can be reduced by employing a feed forward loop where the feedback from one swing can be combined with the preliminary swing profile to provide a false target with the result being a closer fit to the golfer's swing than the primary swing simulation, this method is illustrated in Figure 94. This method was also employed by Harper (2006).

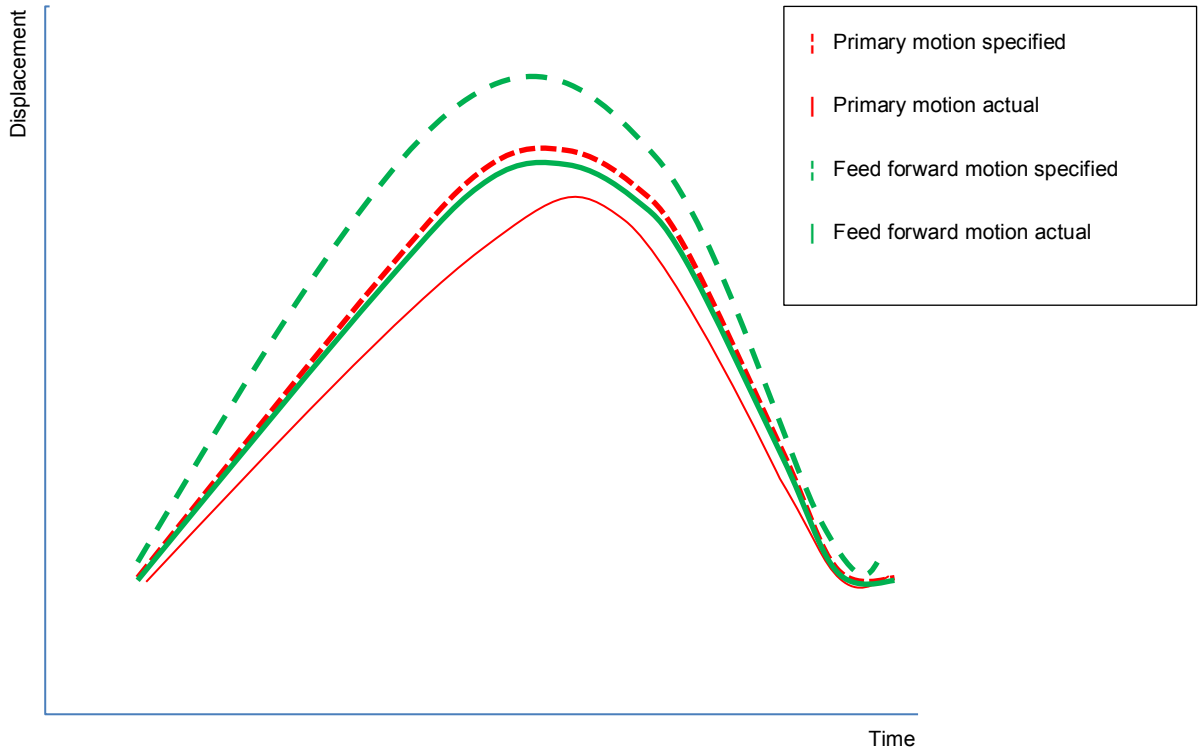

Figure 94 - Illustration of feed forward method

8.2.2 Processing kinematic data

A swing profile is defined by 1000 points per axis of rotation and these points should be planar, i.e. the arm and wrist angular positions should exist on a single plane, the 'swing plane'. The rotations calculated in the CODA software as discussed in section 4.3.3, are relative to the planes defined by the axis markers and are calculated relative to the ground. To be used as a swing profile, these angles need to be transformed to the swing plane. The method employed by Harper (2006) to calculate

the orientation of the swing plane was to take the calculated angle of the golf club relative to the floor at impact and make a transformation of the co-ordinate system about the x axis (the axis running parallel to the direction of the shot) at the same magnitude as this angle. With the existing number of approximations already present in this method of simulating a swing, it was realised that the accuracy of this segment of the process could be improved. The CODA measured positional data was exported to an excel file and cropped to a smaller section focusing on the impact phase of the swing as this is the most important phase of the swing with regards to producing a shot with a similar outcome. Previously, the method employed by Harper (2006) to derive the position of impact during the swing, was to assume it occurred at the point where the clubhead was at bottom dead centre as shown in Figure 95.

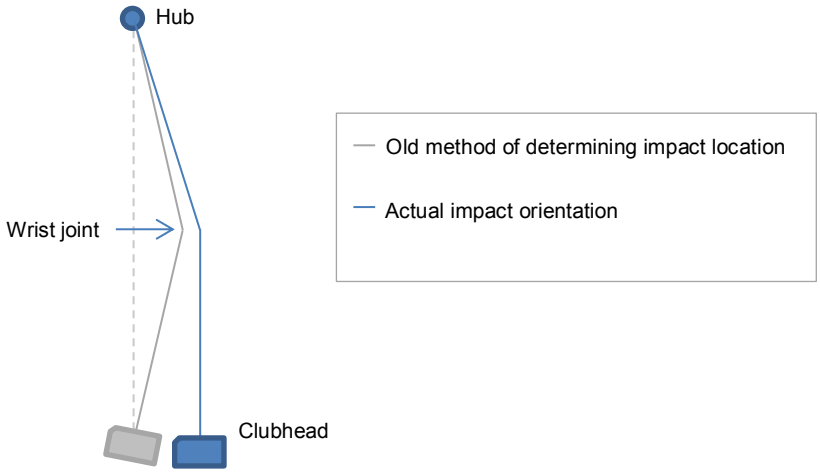

Figure 95 - Determining point of impact

When trying to simulate a motion where even a couple of degrees of clubhead rotation can result in a completely different outcome of a shot (Cochran 1986), and with the knowledge that a golfer rotates the clubhead into the impact phase, miscalculating the point of impact would provide an incomparable shot to the swing that is being simulated. The method of determining impact used in this study was, as outlined in chapter 4, to place an additional CODA marker onto the tee prior to each date collection, the co-ordinates of this position were then compared with the

position of the clubhead from the top of the backswing to the follow through and the clubhead position with the minimum distance to the tee was taken as the point of impact. The radius of the ball (21mm) was subtracted from the x co-ordinate of the tee position to place this point at contact with the ball rather than the centre of the ball. This point of course would not have actually marked impact as CODA assumes that the shaft is rigid. At the time of impact, the shaft bends in the 'lead' direction, this is typically around two inches. Part of this bend can be attributed to the clubhead's centre of gravity, typically one inch behind the clubface, attempting to align itself with the line at which the centrifugal force acts (Wesson, 2008). The distance between the centre of the shaft and the clubface is assumed negligible placing the clubface also two inches further forward than where it would be had the shaft been rigid. However, aligning the robot's tee position would take place while the club is static and the shaft un-flexed, so as long as the clubhead position at impact is consistently considered as the point of a straight shaft meeting the ball, this is a satisfactory approximation. With respect to the model, this would apply as the grip section of the club being aligned with the ball. Figure 96 shows the typical bend of the shaft from end to end leading to and during impact.

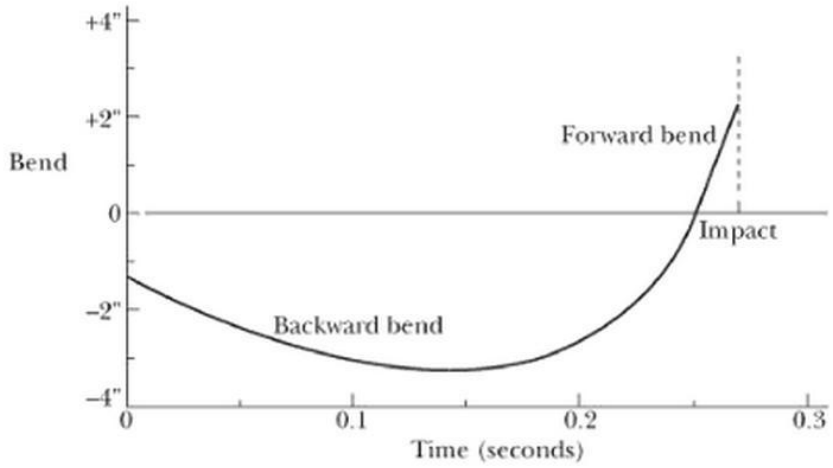

Figure 96 - Bend of the shaft in inches during a typical swing. (Wesson (2008).

Once the impact location had been found, the data was cropped to approximately forty five degrees prior to and post impact was plotted in Matlab. A plane of best fit to the cropped clubhead positional data was calculated as shown in Figure 97. The arc on the plane indicates the position of the clubhead for the impact section of the

swing. The angle of this plane to the ground (the XY plane) was calculated and deemed the ‘swing plane angle’, however the line of intersection of these two planes was not parallel to the x axis and therefore not parallel to the direction of shot. Therefore a second rotation was also calculated, the rotation of this plane about the z axis. These two rotations were used for the CODA transformation, an option provided by the CODA motion software.

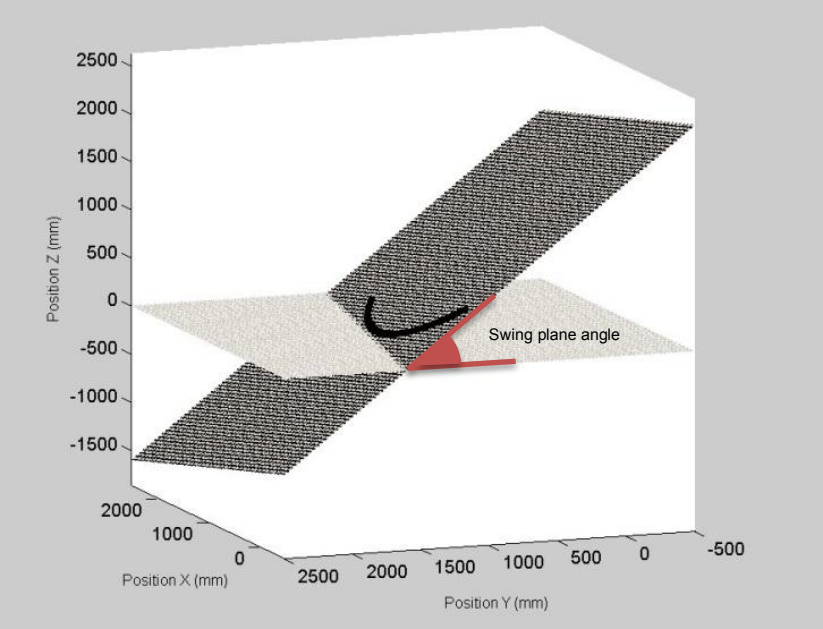

Figure 97 - Determining the swing plane

Figure 98 shows a screen shot of the CODA markers once a transformation had been performed. The golf club as represented by the red line now moves approximately horizontal to the XY plane which now represents the swing plane. Once the transformation has been made, an excel file can be exported from the CODA software containing the positions of the markers relative to the newly defined coordinate system projected onto the XY plane and rotations of the defined club and arm elements.

A tool is available for the generation of swing profiles, Profile Designer and is installed on the robot PC, but as Harper (2006) found, the fit that it generated to the data, resulted in a highly turbulent acceleration profile. This tool was bypassed and a Matlab function was written in order to process this data and generate one thousand positional data points required to drive each axis. As a means of achieving the smoothest swing possible, the first 45˚ and the last 90˚ of the swing were removed

(as they are viewed as not crucial) and replaced with a new start and end created with a linear acceleration and deceleration respectively. As a further smoothing method, only one point out of every eight of the data produced in CODA was selected and a cubic spline was then fitted to the remaining points. The thousand points per axis were then exported from the function and used to create a robot command file which also includes a header containing key phases of the swing, the most important being the impact phase, this provides the functionality of positioning the robot at its impact orientation so that the tee can be aligned ready for an impact. The command file takes the form of a Profile Output Data (POD) file which could be uploaded to the controller.

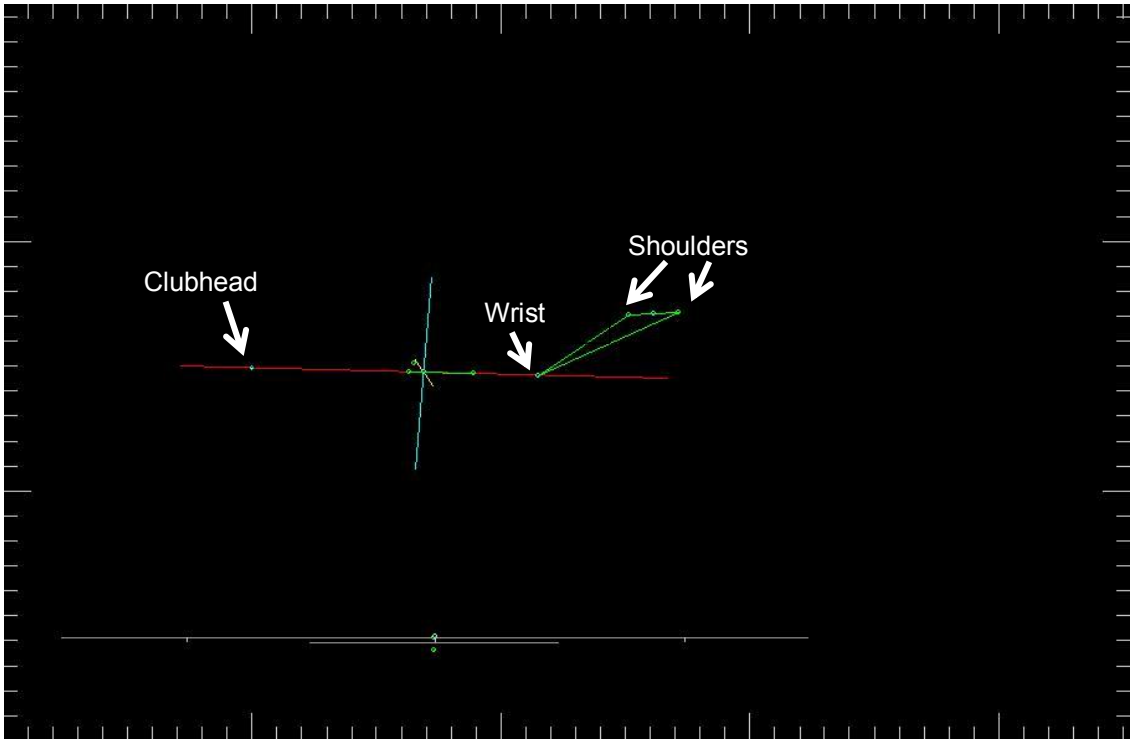

Figure 98 - CODA transformed marker view

Preliminary tests of swing profiles generated via the method described above indicated that a 'smooth' swing profile (one with low levels of acceleration peaks) can reduce the vibration levels present in the feedback from the robot motors. However, the method was still in an unrefined state and difficulties were found when trying to incorporate the generated linear acceleration start and finish of the swing. A project based in the Sports Technology Institute at Loughborough University was completed where a new tool was produced to generate swings profiles which would minimise

the initiation of vibrations in the clubhead through the application of smooth start and finish sections to the profile as well as by the filtering of the raw data.

8.2.3 New swing profile generation tool

To simulate individual golfer's swings, as mentioned previously the Miyamae V robot is programmed with kinematic data collected from actual golf swings with the goal being to match this positional data as accurately as possible. However, forcing a profile to match these exact coordinates can result in unnatural, swing profiles containing large acceleration spikes which are required to match the 'un-smooth' positional data. The method in which the robot is driven, i.e. the swing profile shape can have a large effect on the resulting clubhead acceleration. This was demonstrated by driving the model with four different swing profiles, all of which rotate the robot's arm from 0 to π radians, however the swing profile shapes differ slightly. The four different torques were applied to the arm of the model with the resulting arm angular positions shown in Figure 99.

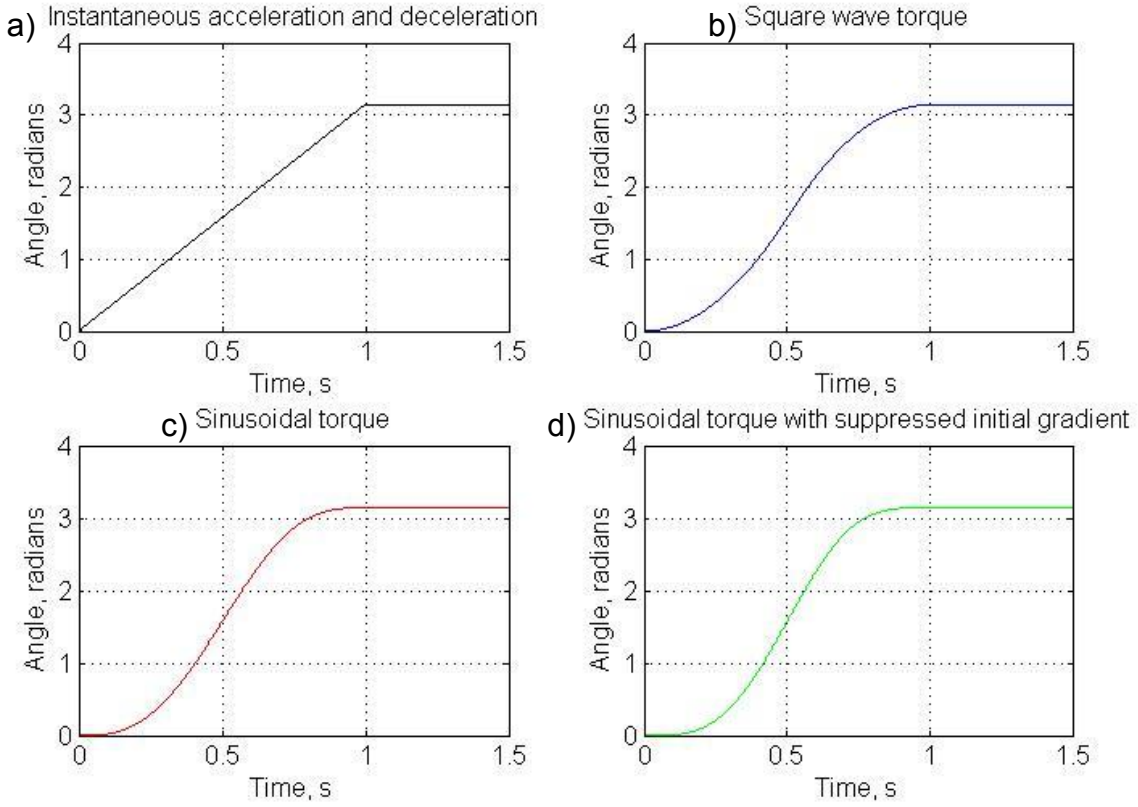

Figure 99 - Torque profiles applied to model to analyse the effect of swing profile on clubhead displacement

The four profiles were generated from the following, a torque applied as an instantaneous acceleration at the beginning of the profile and an instantaneous deceleration 2/3rds through the profile, a square wave torque, a sinusoidal torque of half a sine wave and a sinusoidal torque with a suppressed initial gradient. For the final third of each profile the driven arm position was kept at π radians to allow the clubhead vibration to be monitored at the close of the swing. The resulting clubhead displacements from the four torque profiles are shown in Figure 100. As is shown in the figure, the small difference in the torque that is applied to the model in order to produce the same rotation of the arm over the same time period can have a big impact on the oscillations in the clubhead displacement. The most violent clubhead vibration is seen in the simulation where an instantaneous acceleration is applied, with the maximum clubhead displacement being over two times greater than any of the other simulations. Applying the sinusoidal torque resulted in the least clubhead displacement.

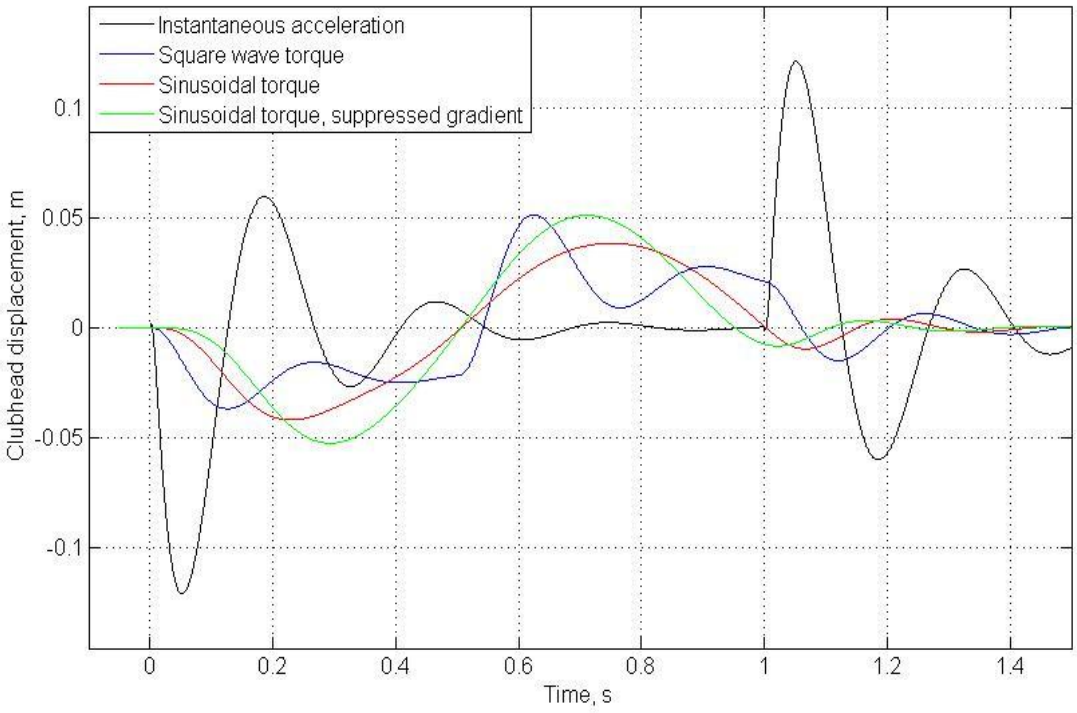

Figure 100 - Clubhead displacement response from four differing torque profiles

This study demonstrates how important the method of driving the model and subsequently the robot can be, where small changes in the swing profile can result in

large clubhead oscillations.

The work conducted by Cockram (2010) discussed how a compromise could be found between correlating the swing profile with the kinematic data whilst producing a smooth swing profile. Cockram (2010) produced a Matlab driven tool presented via a graphical user interface allowing the user to import kinematic data for the three axes of rotation for a swing. The user is able to crop the data to a limit based on the user entered time of impact and fits a more gradual and natural build up and follow through to the swing. The new sections are generated as an exponential curve and matched to the cropped velocity data. More data points are retained around the time of impact to increase the comparability of clubhead position at this crucial phase. The whole swing is then processed through an elliptic filter, selected for its ability to provide the best fit to the golfer data. This new tool provides the user with the option to view the resulting velocity and acceleration based on the point to which the data is cropped. The export from the tool is in the POD format required for the robot, with the swing time being specified by the user. An additional level of functionality is also provided in the option to import feedback from a robot simulated swing as a feed forward approach to indicate areas where the robot has failed to achieve the target positions.

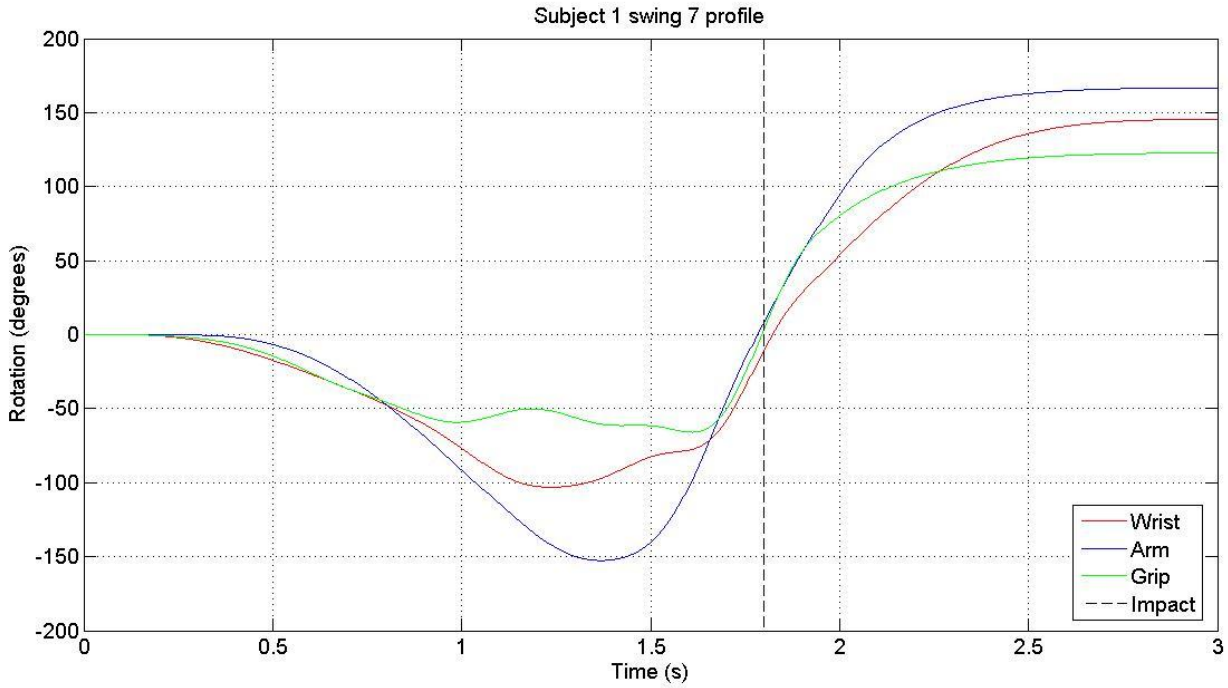

Figure 101 - Example swing profile generated by the new swing profile generating tool

A secondary profile can then be exported to account for this discrepancy. An example of a swing profile produced via this method is shown in Figure 101.

Some compromises are made between realism and ‘smoothness’ during the creation of a swing profile and these compromises are kept to a minimum during the critical phase of a swing, the impact phase. The outcome demonstrates a real swing whilst keeping the acceleration profile of the robot to a minimum, which should provide lower levels of clubhead vibration.

8.2.3.1 Comparison between two profile generating methods

To compliment this research, this author collaborated with Cockram (2010) to measure the success of controlling the robot’s level of vibration through the implementation of swing profiles generated with the new swing profile generating tool. Feedback data of the acceleration of the robot’s three axes of rotation was downloaded from the robot’s controller to enable comparisons between swings generated with and without the new tool. As presented in Cockram’s research, an FFT was taken of the feedback acceleration and it was found that the new method of producing swing profiles resulted in a decrease in high frequency accelerations in all axes of rotation.

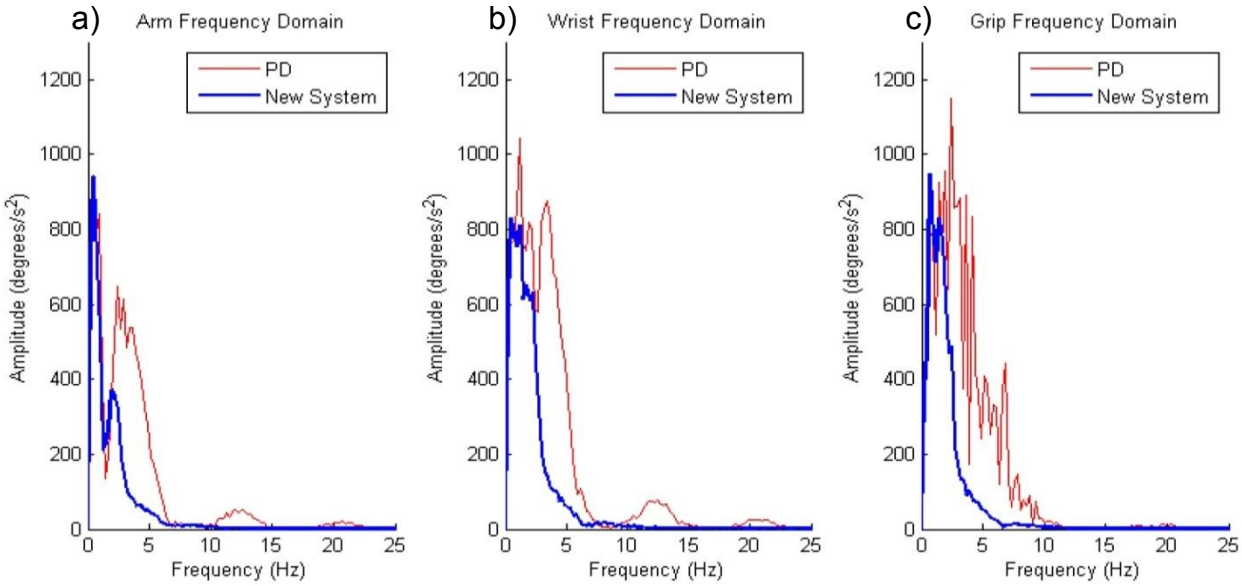

Figure 102 - Frequency spectra of feedback acceleration data from robot swing. (Cockram 2010)

This is demonstrated for one subject in Figure 102 where the blue line, PD (profile designer) refers to the old method of generating profiles and the red line represents the new swing profile generation tool. The lower the frequencies of acceleration present in the motion of the robot would imply a decrease in difficulty for the robot to match the programmed positions. Secondly, this should result in a reduction of clubhead vibration, and this was confirmed from accelerometer measured accelerations of the clubhead during these swings, an example of this is given in Figure 103. This figure shows the measured clubhead acceleration for two robot simulations of the same golf swing. The plot in pink is the clubhead response for a swing where the swing profile was generated using the previous method of swing profile generation. The blue plot shows the clubhead acceleration for the same swing when the swing profile was generated with the new swing profile generating tool. This swing was performed without at impact but the time at which impact would have occurred would be at just after 2s. The acceleration of the clubhead is similar during the backswing section of the swing, however, the clubhead acceleration is much lower around the time of impact which is the most crucial phase of the swing. Clubhead acceleration during the impact phase and after is seen to be much lower for the swing generated with the new tool.

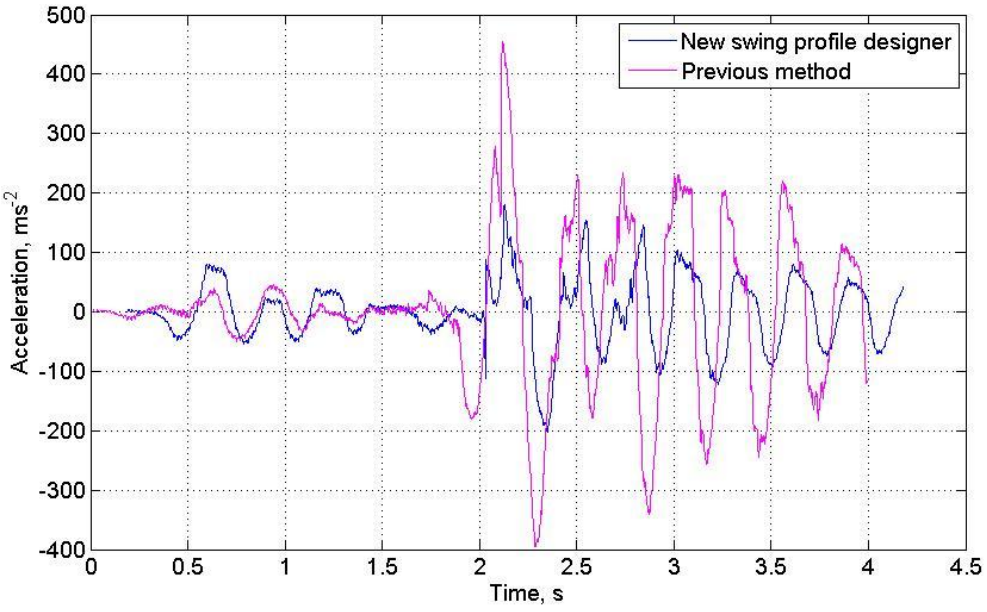

Figure 103 - Comparison of measured clubhead acceleration from two robot swings, one generated via the old method of swing profile generation and one using the new tool

The new swing generating tool was used to produce all further swing profiles for this study to work in conjunction with the results obtained by the method of damping the vibrations excited in the clubhead via a flexible grip and wrist for the best possible results.

8.3 Mathematical model swing profiles

To produce the human versus model swing comparisons outlined in the introduction to this chapter, swing profiles would need to be produced. Taking into consideration the compliant wrist in the model, an adapted method of swing profile generation was required as it currently doesn't allow for the flexibility present in this system. For each of the six golfers whose swings were to be studied, CODA exported and transformed data was imported into the swing profile generation tool (SPGT) along with time of impact and cropped to provide a smooth swing whilst maintaining a close fit to the initial swing. The SPGT generated profile output data (POD) files were then processed by a custom Matlab function which prepped the data ready to be used as the drive for the model. Arm and wrist positions were differentiated to provide the velocity and acceleration information and a swing time base was created.

A Matlab script developed in the previous chapter which enables a selection of options to the user included the option to drive the model with swing profile data. On selection of this sub function of the code, the script to prep the swing profile data is called and the resulting variables are provided to the model for the simulation. The values of wrist stiffness and damping calculated in chapter 6 as the best fit to the simple swing data were implemented initially and adjusted accordingly to provide the best fit to the clubhead acceleration data. These wrist values were combined with the grip stiffness and damping values for the 50% deadened silicone. The decision to use these wrist values and not the values calculated as the most 'vibration minimising' in section 6.3.1.1, was due to the issues seen in section 5.3.1 where a large increase of flexibility at the grip resulted in an excessive amount of motion of the grip section of the club within the collet. It was also factored that the damping effect of the dashpot would vary based on the high velocity of the travelling wrist joint in the full swings.

As seen in in the basic swing motion in the previous chapter, the flexibility of the golfer's wrist was only visible at the point of extreme changes in velocity. The desired outcome of adding the flexibility in the wrist joint is to witness during the full swings, an overshoot of the wrist position as the spring threshold is reached and for the disparity between driven position and actual collet position to have recovered by the point of impact. It would then be desired for the passive motion of the wrist joint not to be visible again until the top of the follow through. The damping provided by the wrist joint at the top of the back swing is anticipated to suppress the majority of clubhead vibrations excited by the initial takeaway whilst being close enough to the time of impact to limit the possibility for new vibrations to be introduced.

A simulation of each of the 6 swings was generated. As expected the minima and maxima of the wrist position plot saw an overshoot as shown in the figure below.

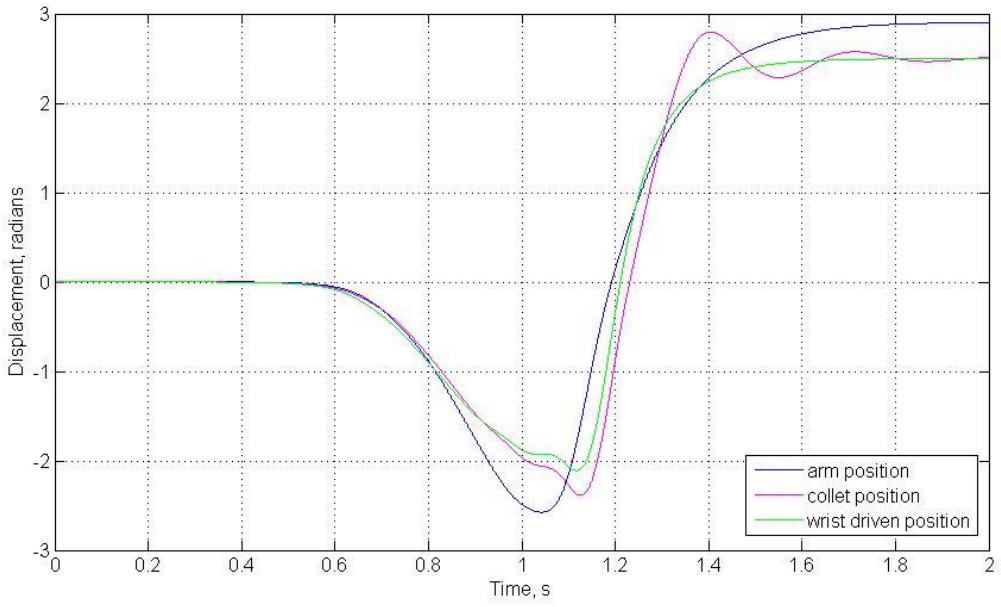

Figure 104 - Subject 8 swing, example of collet overshoot due to flexible wrist.

It was found that for all swings a good fit between the resulting clubhead acceleration and shaft strain and the golfer measured data was achieved with a wrist stiffness of 300Nrad^{-1} and a wrist damping coefficient of 15Nsrad^{-1} and the collet inertia was kept at the measured value of 0.028kgm^2. It was found that the response of the clubhead

was not very sensitive to changes of the wrist element variables and this could be attributed to the small region of wrist motion that is now accounted for by the flexible wrist, compared to a wrist that in the previous simulations was fully flexible with no drive. A feed forward approach was then trialled to take the difference between the desired position of the wrist and the simulated position as an attempt to cancel out the overshoot caused by the flexible wrist. The difference was then removed from the model swing profile and the simulation repeated. This method did not produce the desired outcome as any low frequency oscillations present in the collet position as demonstrated in Figure 104 were emphasised by this method and the 'smoothness' of the swing profile as a whole was compromised. Therefore it was viewed that a more complex method of model swing profile generation would be required, where the flexibility is accounted for at the time of impact and cancelled out by a counter motion whereas at the top of the backswing and follow through the wrist drive positions could remain the same as in the initial swing profile. This is beyond the scope of this research, so the comparisons made here forth between shaft strain and clubhead acceleration will attempt to factor this in to the analysis made.

8.3.1 Clubhead acceleration

8.3.1.1 Resolving the direction of acceleration

During the study of human golf swing parameters in chapter 4, clubhead acceleration was measured with two accelerometers mounted to the hosel of the club to measure the acceleration parallel and perpendicular to the plane of the clubface. The goal is to match the clubhead acceleration measured during the human swing with a model simulation. Unlike the golfer and the robot, the model neglects to model one of the degrees of freedom usually included in a swing profile, the grip rotation. The rotation of the grip in the human swing results in the direction of the acceleration measured by the accelerometers continuously changing relative to the direction of swing. To enable a comparison to be made between the measured data and a simulation, the two accelerometer traces were combined and resolved in the direction of the swing, this would align the acceleration with the swing plane. This was computed by cropping and resampling the accelerometer data to contain the 1000 points, the

same number per axis as the swing profile. The time of impact in the accelerometer traces was calculated by taking the differential of the lead/lag acceleration and finding the initial point where the differential reached a threshold of $30 ms^{-2}$. The accelerometer traces were aligned with the swing profile grip rotation data by the time of impact and the overlap of data padded with NaN values to ease the process of comparison. The resultant acceleration was calculated with the following equation:

$$resultant = a\,sin\theta + b\,cos\theta \tag{42}$$

Where a is the acceleration acting in the plane of the clubface and b is the acceleration acting perpendicular to the clubface. θ is the rotation of the grip. Figure 105 gives a schematic of the top of the clubhead to illustrate the resolving of acceleration direction. The arrows indicate a positive acceleration.

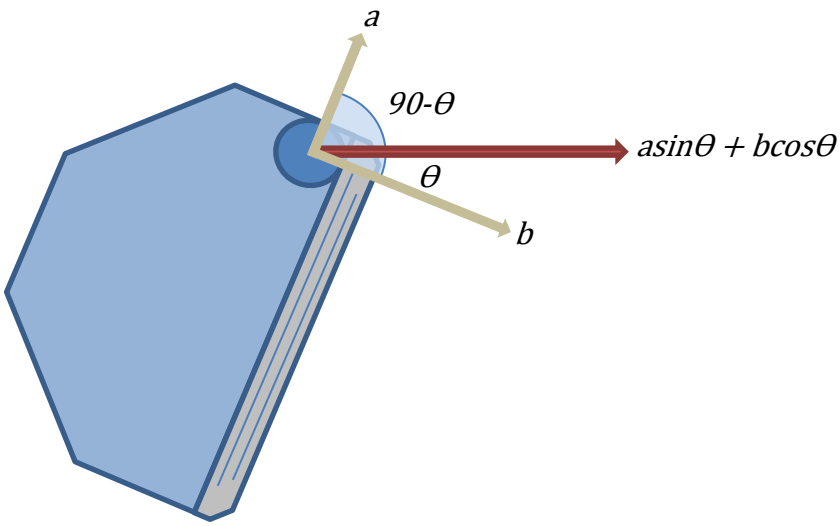

Figure 105 - Calculation of resultant acceleration parallel to swing plane based on measured accelerations a and b and grip rotation angle θ

This computation was completed in a Matlab script where a loop took each grip position and calculated the relative resultant acceleration. The resulting acceleration was then not filtered as changing the sampling frequency from 5120Hz to 333Hz reduced the noise in the measurement and it was felt no further smoothing of the data was required. This would also preserve the similarity between the measured and processed data. Figure 106(a) illustrates how the two accelerations were combined to produce one resultant acceleration; this is presented alongside the

swing profile grip rotation in Figure 106(b). The grip angles were inverted to convert a clockwise rotation (when viewed form above) to a positive rotation. A sanity check was made of the direction of the acceleration and is consistent with the expected motion of a clubhead. After the initial takeaway the resultant acceleration is dominated by the lead/lag acceleration as would be expected. The grip rotation causes the toe up/down acceleration to gradually dominate the resultant value. During the downswing, the clubhead accelerates towards the tee creating a positive acceleration in the lead up to impact and following impact the acceleration is positive until the completion of the swing.

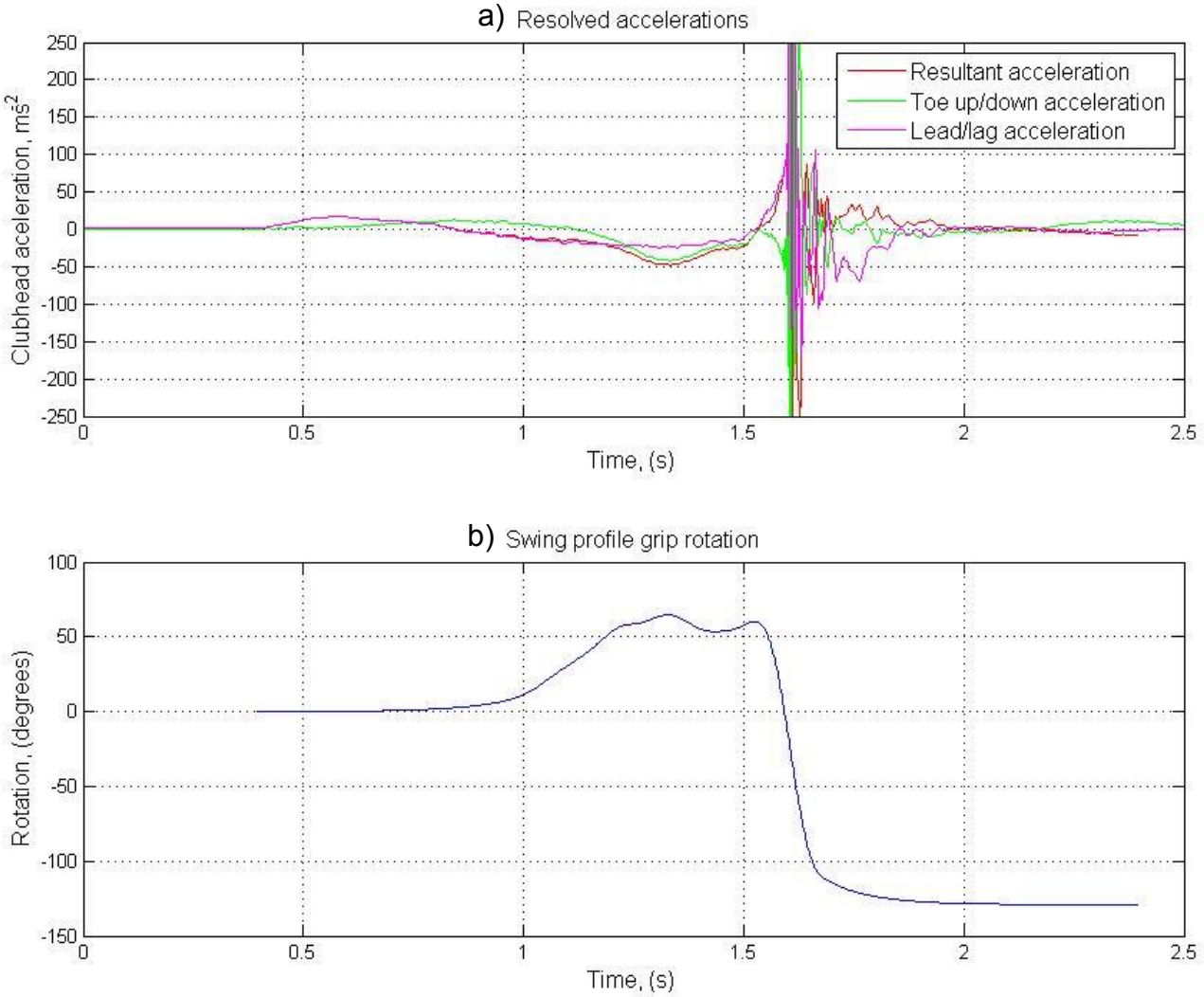

Figure 106 - Resolved clubhead accelerations

8.3.2 Shaft deflection profiles

Another swing variable measured during the testing in chapter 4 was the shaft deflection. Two strain gauges were bonded to the shaft of the golf club in the same orientation as the accelerometers. One strain gauge measured the strain in the lead/lag direction and the other in the toe up/down direction, as defined in Figure 107. The strain gauge instrumented shaft used to collect the shaft bending profiles provides an output of strain whereas the model provides an output in terms of deflection in metres. To provide a more meaningful output, the measured strain was linked to the metres of deflection of the clubhead during a calibration where the top of the club was fixed in a mounting hole and the shaft was flexed at the clubhead a known distance in both of the orientations in which strain was measured. A reading of output strain was then taken relative to this shaft deflection. The calibration values for the strain gauges in this study were 1m of deflection is equivalent to 0.024 strain. All of the measured strain data for the six swing profiles being analysed was converted to metres of deflection.

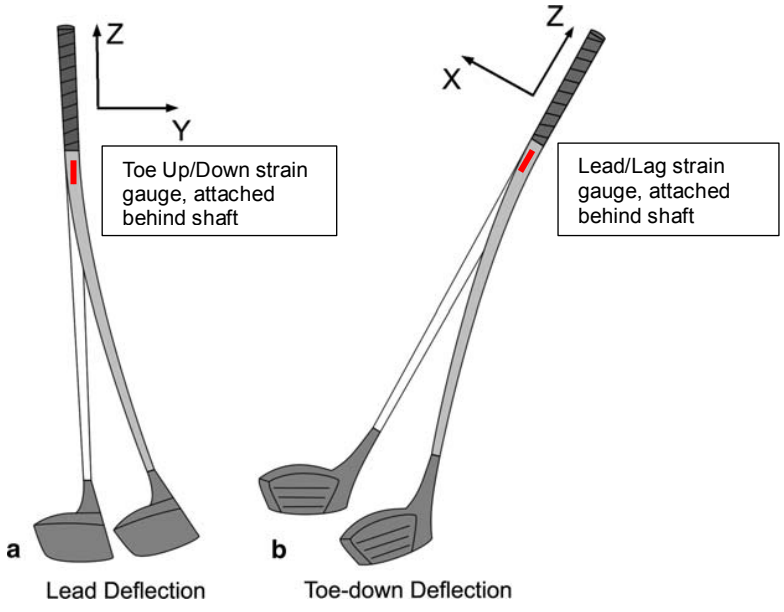

Figure 107 - Shaft flex definitions, Adapted from MacKenzie & Sprigings (2010)

The issue caused by the lack of grip rotation in the model also affected the comparison between the measured and simulated strains as the orientation of the

strain gauges was continuously changing relative to the plane of the swing. Traditionally when the strain is being measured during a swing, it is reported back to the golfer as the two separate measurements, however the resultant strain acting in the direction of the swing was required to allow a comparison with the model. The methodology from section 8.3.1.1 was applied here however, the orientation of the positive strain acting in the plane of the clubface was in the opposite direction resulting in an adapted equation to calculate the resulting strain as given in equation 43:

$$resultant\ strain = b\ cos\theta - a\ sin\theta \tag{43}$$

The strain data was processed alongside the acceleration data as it was captured in the same Smart Office session and exported to the same file. This meant no further computations were required to find the point of impact. The data was then filtered to remove the noise where all frequencies above 30Hz were removed through an FFT analysis. A plot demonstrating the outcome of resolving the strains for a swing is shown in Figure 108, this is presented alongside the grip rotation.

The polarities of the measured strains were checked to confirm they were correct. After the initial takeaway where the rotation of the wrist is a negative value, the resulting position of the clubhead relative to the line of the shaft is in a leading orientation with a positive strain, dominated by the lead/lag strain. During the downswing, the clubhead lags behind the positive rotation of the wrist creating a positive strain with regards to the toe up/down strain gauge but resolved in the swing plane, this is a negative strain up until the point of impact where the ‘kicking’ forward of the clubhead results in a positive resultant strain.

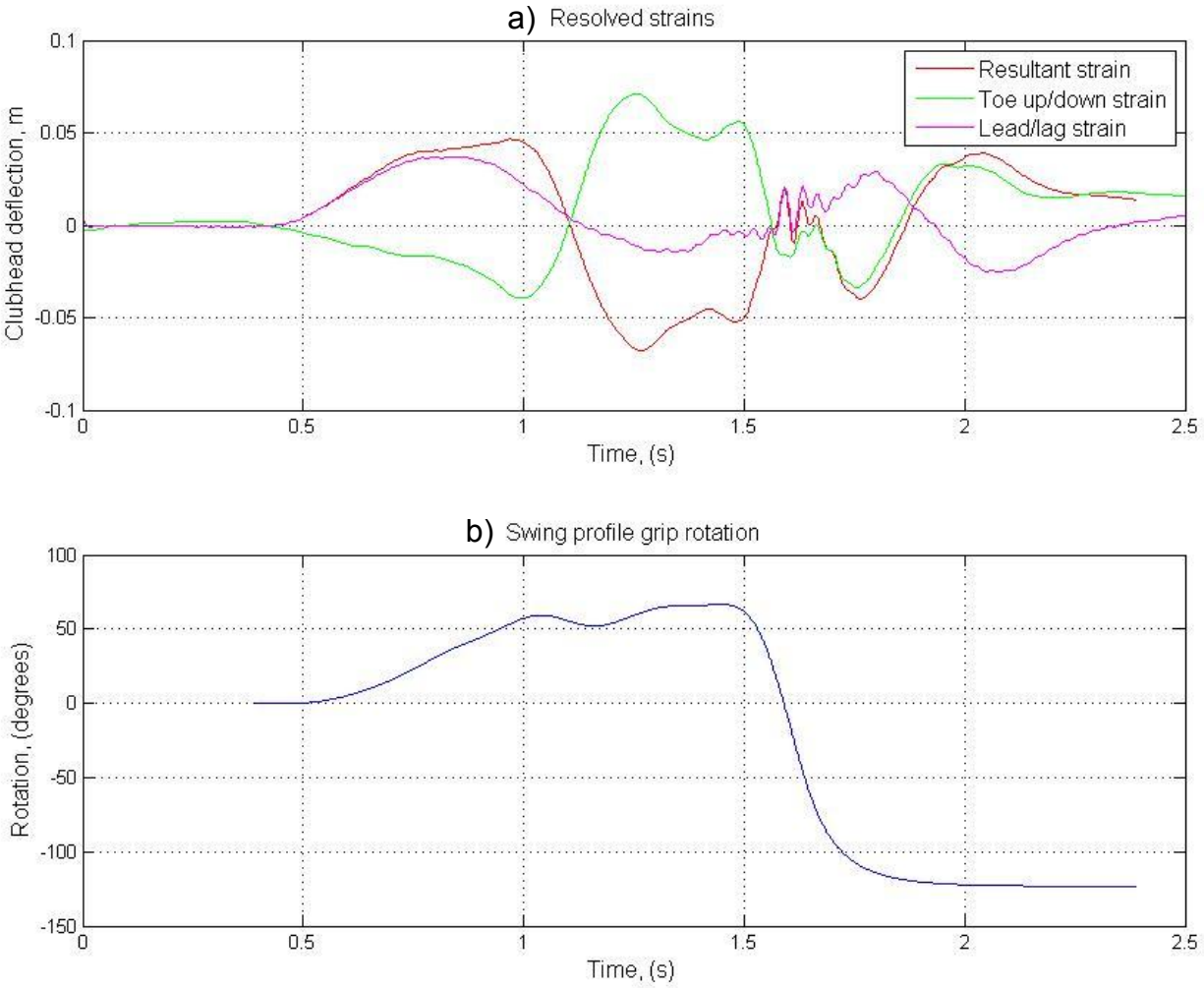

Figure 108 - a) Resolved strains and b) grip rotation

8.4 Model simulations

The swing profiles as produced in section 8.3 were used as the input for the simulations, and a force was applied to the clubhead at the time of impact. The value of the impact force applied in the model was 1kN, this was not based on measured data but an arbitrary value was selected and varied until the simulated clubhead response caused by the impact was of the same magnitude as the acceleration in the resolved accelerometer plot. The impact force was applied for a duration of 0.5ms, approximately the duration of clubhead impact with a ball. The appendix includes the measured and simulated resultant strain for the six swings which were analysed. Two of the swings for Subject 1 and 9 are presented here. The outputs from the model for these two swings are given in Figure 109 and Figure 110 respectively. For each swing output the four degrees of freedom are plotted in the displacement, velocity and acceleration domains.

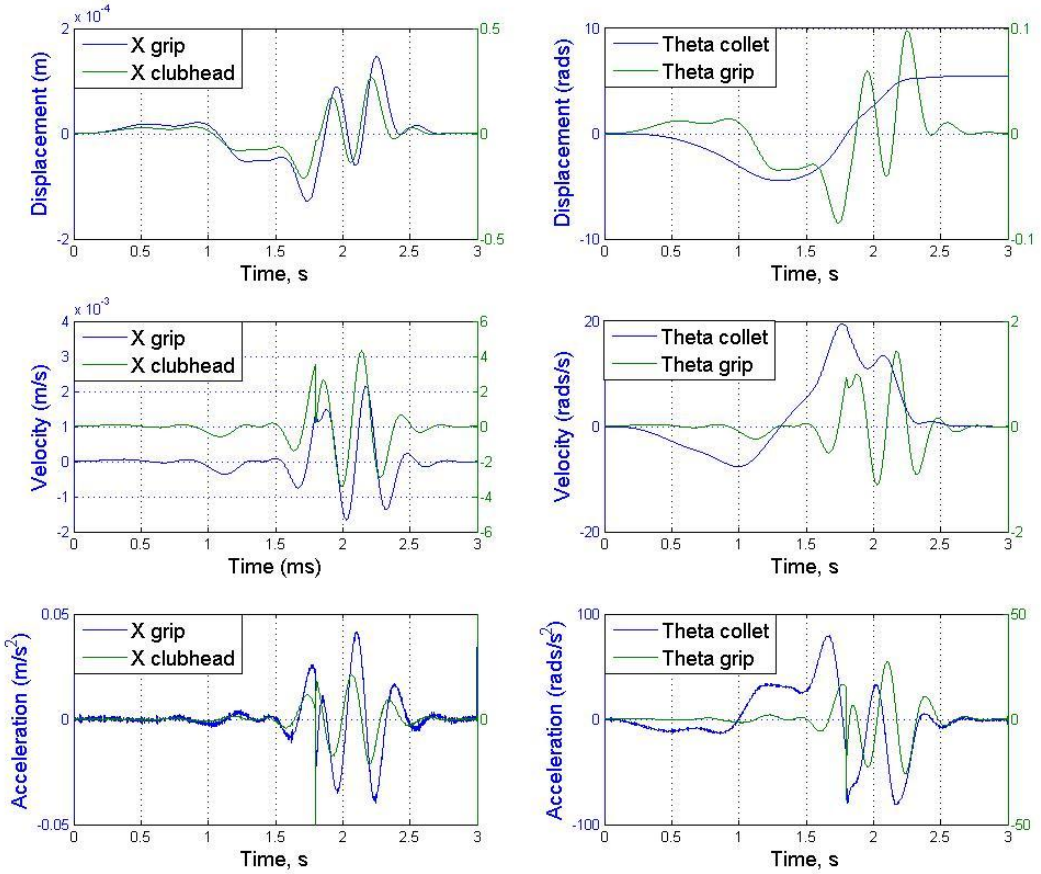

Figure 109 - Simulation output for Subject 1 swing profile

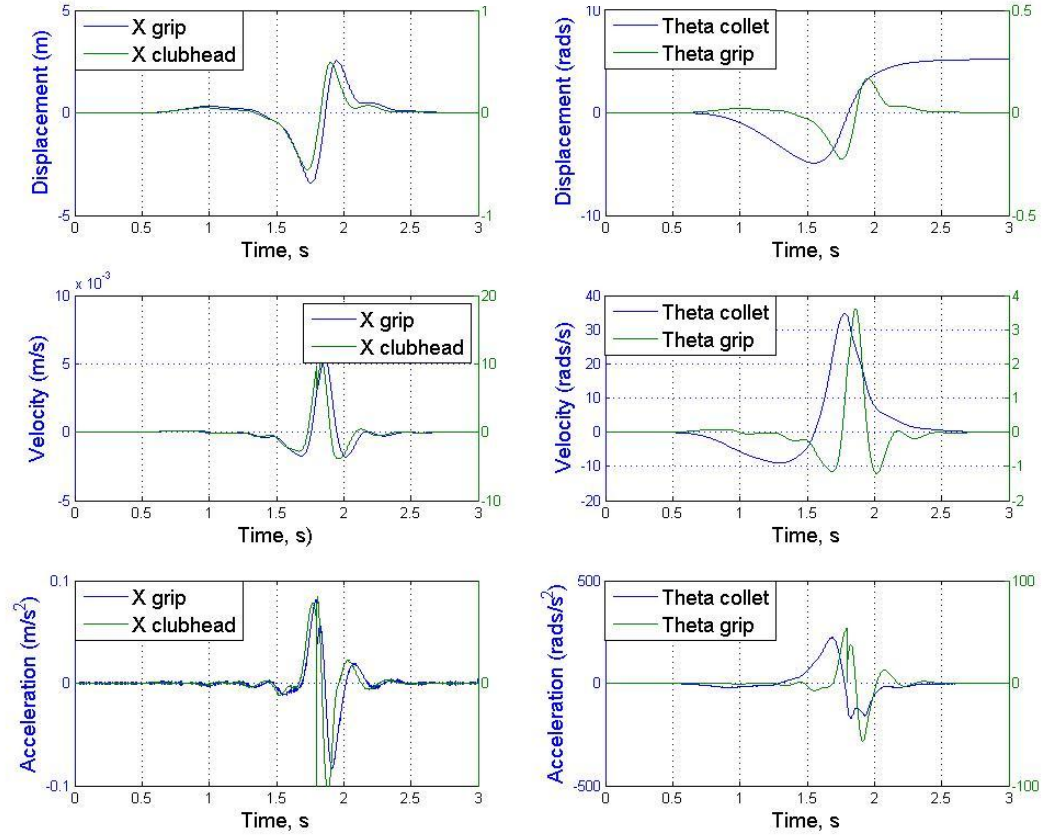

Figure 110 - Simulation output for Subject 9 swing profile

8.4.1 Clubhead vibration comparisons

The resolved acceleration contained the acceleration of the clubhead due to the motion of the golfer as well as acceleration components due to the bending vibration of the flexible club, whereas the output from the model provides the acceleration of the clubhead relative to the collet. To enable a comparison, the simulated acceleration of the collet was converted from an angular acceleration to a linear acceleration at the clubhead and then added to the clubhead acceleration which is calculated relative to the collet, this was preferable over removing the measured wrist acceleration from CODA as the data contained noise.

Two examples of the comparisons between measured and simulated clubhead accelerations are given in Figure 111 and Figure 112. Impact can be seen in the measured responses as the point of high frequency oscillations and a single high frequency oscillation in the simulations show impact. The impact position given in the simulations was adjusted as the flex of the wrist meant that it lagged behind causing a later time at which it reached impact position, this lag is illustrated in Figure 104.

It was found that the simulations for all golfers had consistently higher clubhead accelerations and can be seen in the two example plots, this can be seen particularly for Subject 9 in Figure 112. The amplitude of the major peak before impact would have been increased by the additional flex of the wrist, the additional discrepancy could be due to the many approximations in the model. The acceleration of the clubhead also includes the acceleration component of the grip which would also cause it to seem greater than for the measured accelerations.

The shapes of the plots encouragingly show some similarity with the biggest success of the simulation being the minimal signs of clubhead vibration when compared to the previous robot simulation in Figure 93. If a new method of creating swing profiles were generated to account for the additional motion at the wrist and grip, it would be expected for the simulations to show a greater level of agreement with the measured clubhead accelerations.

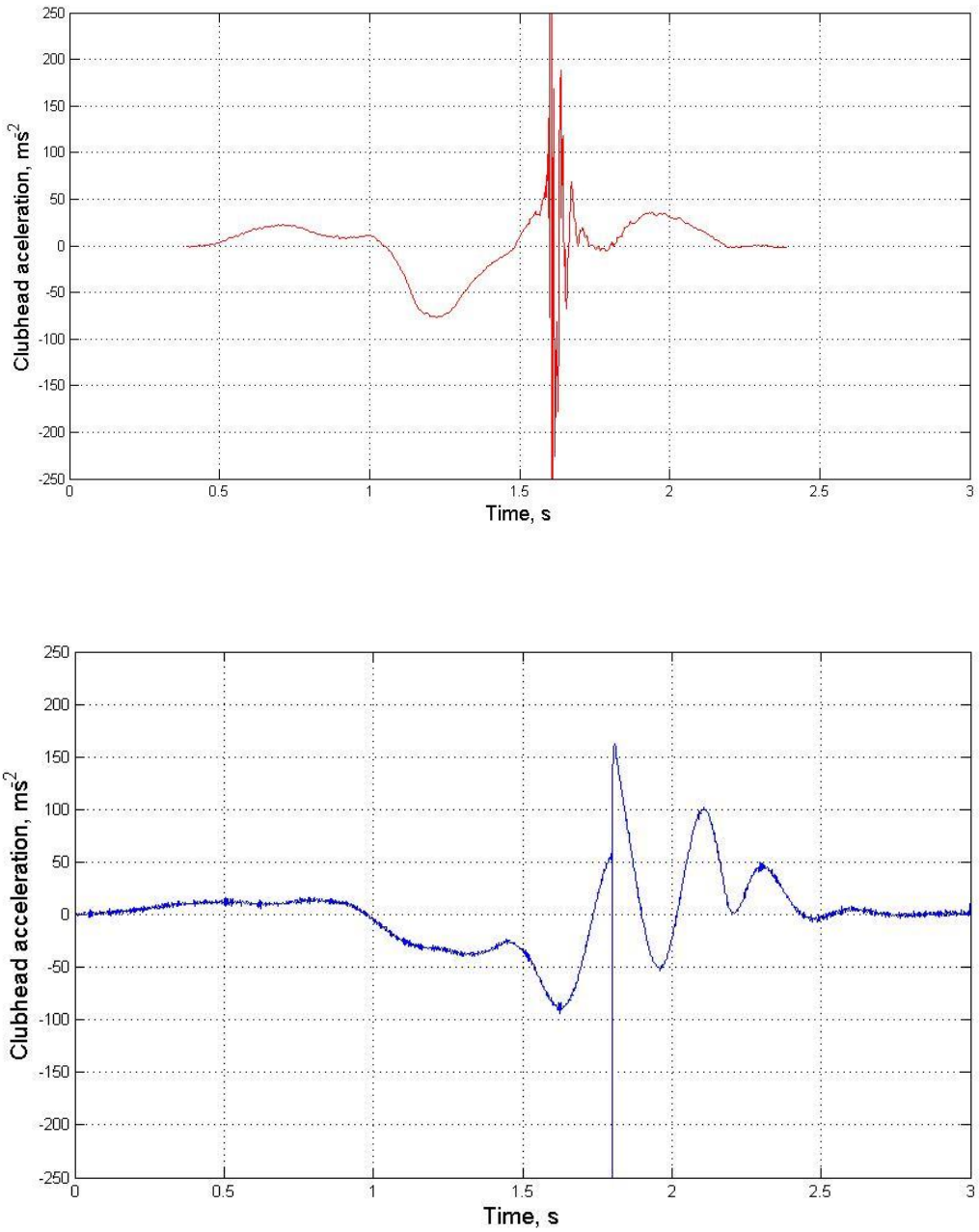

Figure 111 - Subject 1 clubhead acceleration, (a) measured and (b) simulated

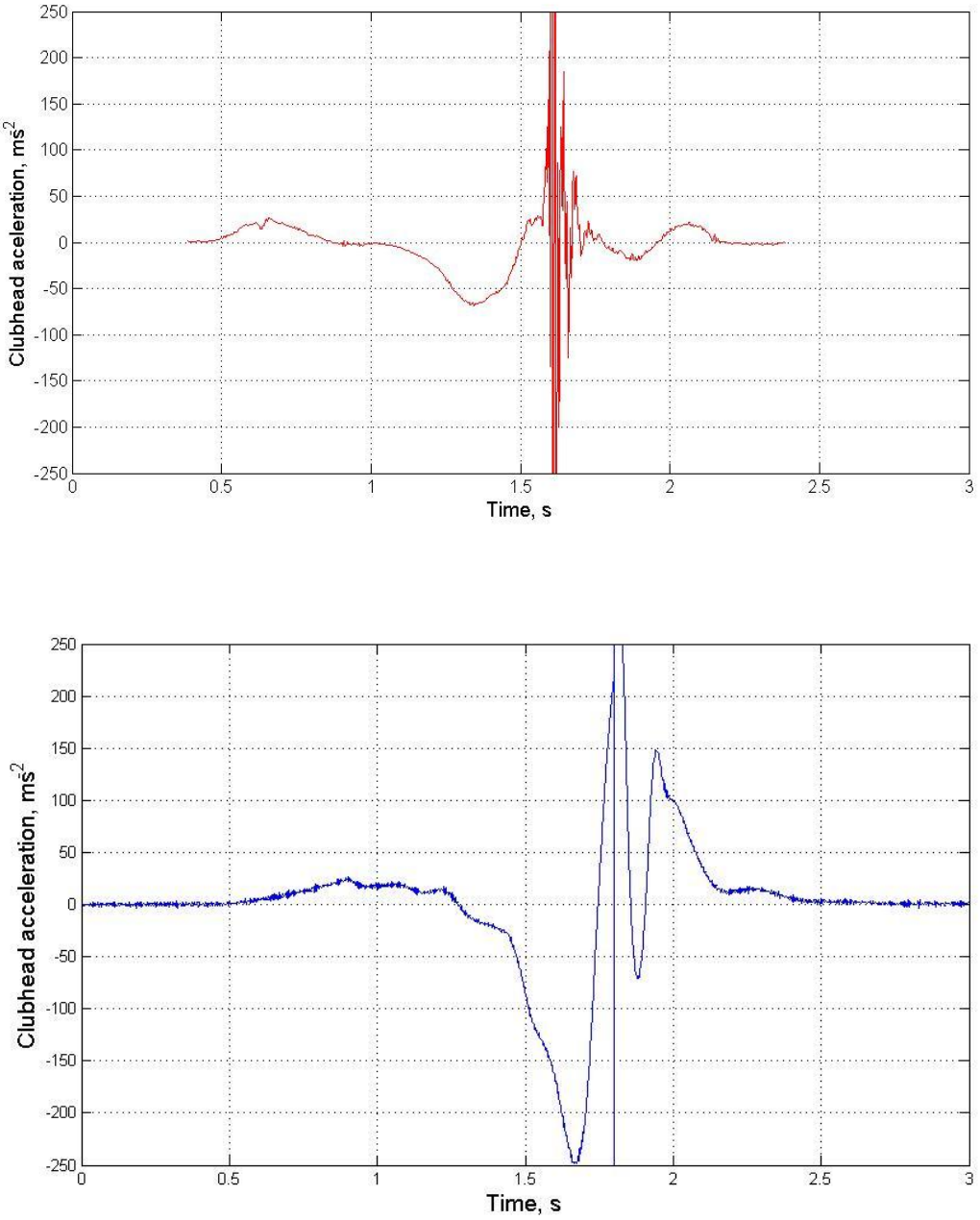

Figure 112 - Subject 9 clubhead acceleration, (a) measured and (b) simulated

8.4.2 Deflection profile comparisons

A comparison was made between the measured shaft deformation and the corresponding simulated response. Figure 113 and Figure 114 illustrate the results which were achieved in this comparison for Subjects 1 and 9. The time of impact is

indicated by the vertical line in the simulation plots and for the measured data is at the start of the high frequency oscillations around 1.6s. As seen in the clubhead acceleration comparisons, similarly with the clubhead deflections, the values are higher for the simulations than for the measured values. The position of the clubhead in the simulations is taken relative to the collet so will contain an additional displacement due to the rotation of the grip, this will not be present in the measured strain so will also account for some of the disparity. Referring back to Figure 109 and Figure 110 it can be seen that the grip rotation accounts for approximately 0.07 and 0.2m of the clubhead displacement respectively.

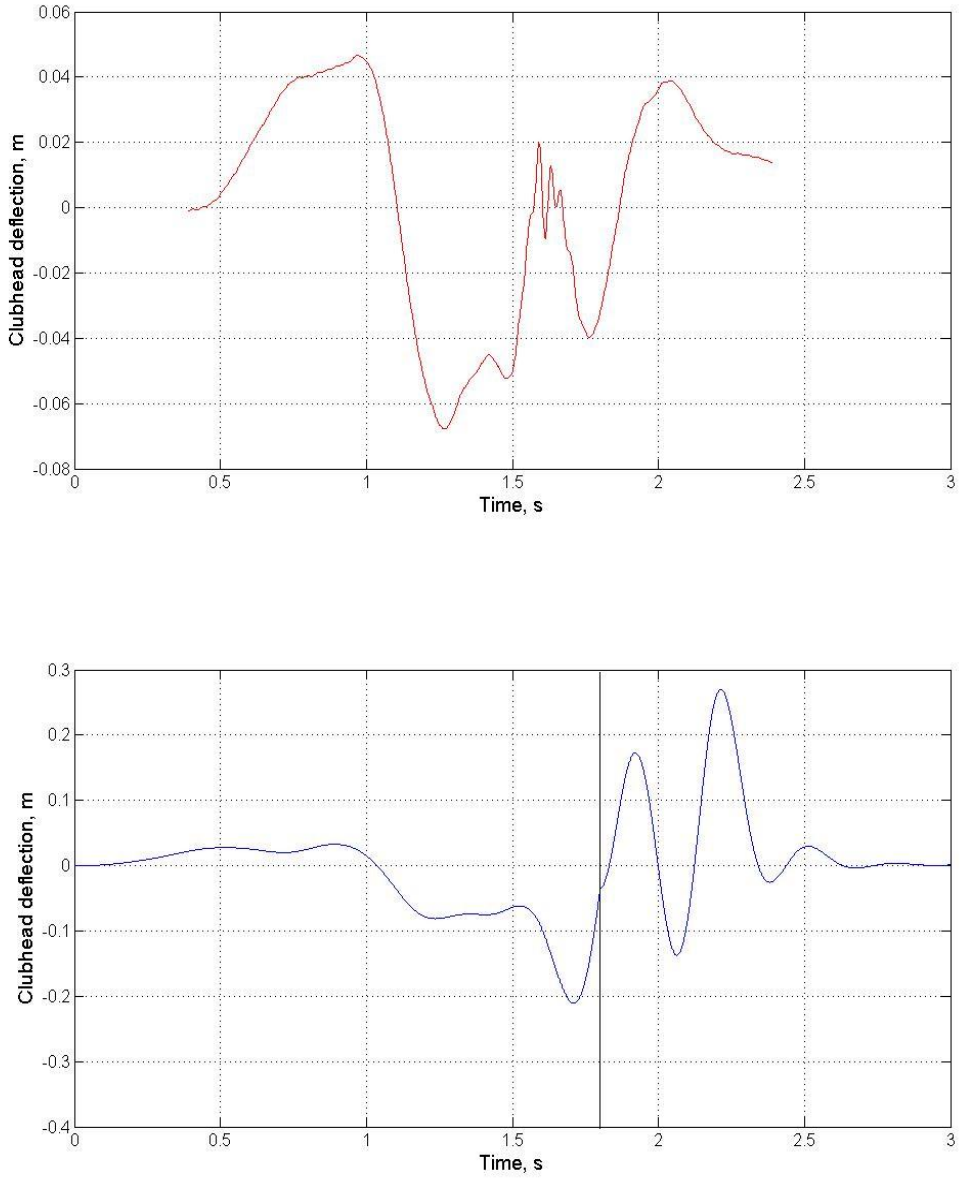

Figure 113 - Subject 1 clubhead deflection, (a) measured and (b) simulated

The plot for Subject 9 shows very good agreement in terms of the shape of the response. The plot for Subject 1, again shows some large oscillation after the point of impact, which somewhat mirrors the larger oscillations measured after impact for that subject. This clubhead oscillation isn't a major concern as the main concern is to match the swing variables leading up to impact. The low level of clubhead oscillation seen in both plots is also encouraging.

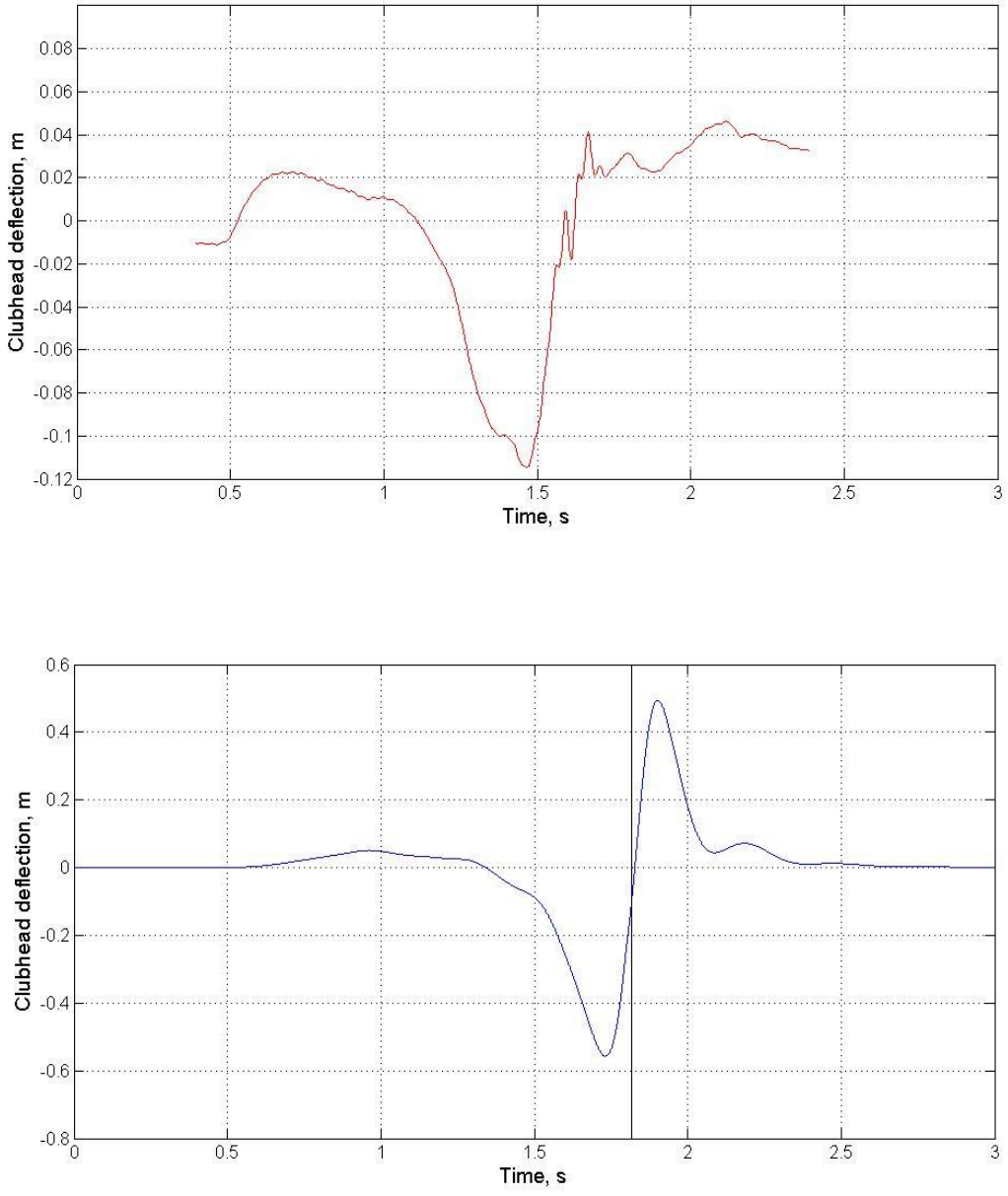

Figure 114 - Subject 9 clubhead deflection, (a) measured and (b) simulated

8.5 Simulation of rigid system compared to flexible system

To demonstrate the difference that can be achieved through the addition of a flexible grip and wrist in the model of the robot, compared to a model which contains no compliance and therefore models the current robot, the grip and wrist were made rigid and the six simulations generated in the previous section were repeated. Comparisons between the clubhead displacements for two swings are shown in Figure 115 and Figure 116.

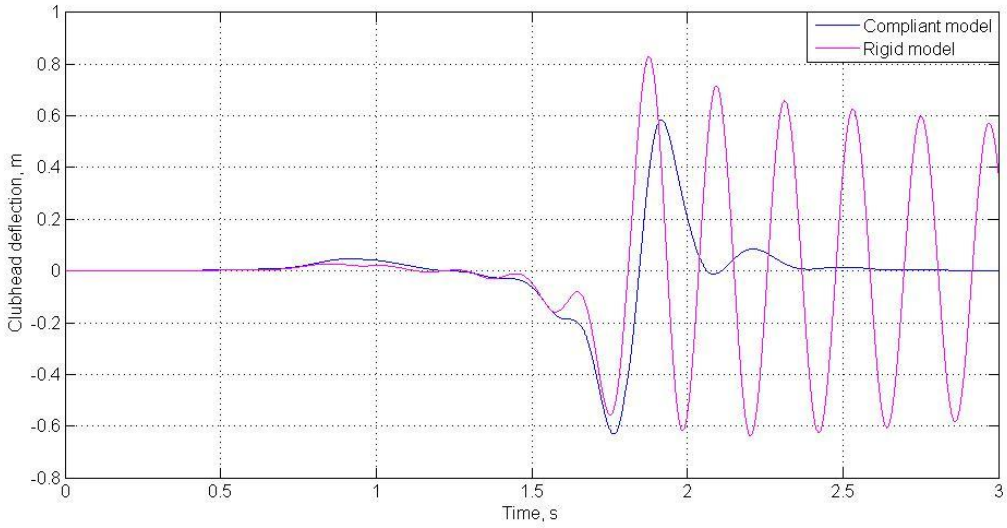

Figure 115 - Rigid vs compliant model simulation, clubhead displacement for Subject 6, swing 6

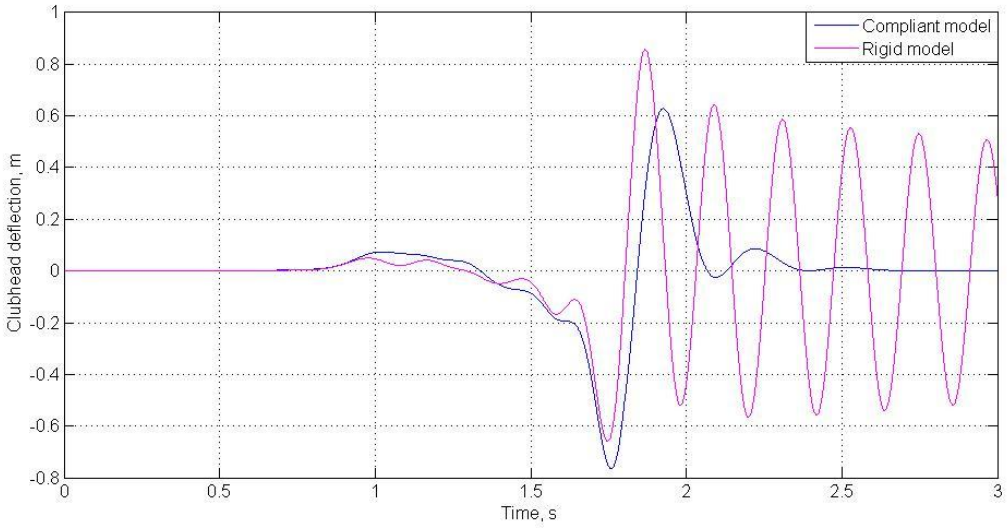

Figure 116 - Rigid vs compliant model simulation, clubhead displacement for Subject 8, swing 2

As shown in the figures, the introduction of a compliant wrist and grip into the model has reduced the clubhead vibrations present in the displacement plots throughout the swing. The most noticeable reduction is seen after the point of impact at 1.8s for both simulations, in the compliant model the clubhead vibration is damped out within 0.5s whereas in the rigid simulation large clubhead oscillations continue to the end of the simulation. There is also a noticeable reduction of vibration before the time of impact. The minimum point for both compliant displacement plots is lower than for the rigid simulations this is most likely due to the overshoot of the wrist caused by its flexibility and the compliance at the grip.

8.6 Simulations driven with robot feedback

It is recognised that so far, all simulations presented in this chapter have been driven by swing profiles generated from human kinematic data which are also used to drive the robot, however, in every swing performed by the robot, the feedback data shows a disparity between the input positions and the actual angular displacements achieved by the robot. Not only are these differences seen at times where the robot has overshot or lagged behind its target position, there are also higher frequency vibrations visible in the data. Therefore, to complete the investigation into the success of the final model, it should be driven with feedback data downloaded from the robot controller. Two swing profiles created previously by this author in a subsidiary experiment were used to drive the robot. At the completion of the swings, the feedback data was downloaded from the robot controller and used to generate swing profiles to use as an input for the model. It was shown previously in chapter 7 section 7.6 how the model, when set to mimic the rigid structure of the robot is capable of replicating the same clubhead accelerations. The two following figures demonstrate the clubhead displacement of the two swings when driven with the robot feedback. Two simulations were made, one replicating the rigid robot and one with a compliant wrist and grip. Neither of the swings performed involved any grip rotation or an impact with a ball. The swing times of the two simulations are 2.5 and 3 seconds respectively.

As seen in both plots, the difference between the model which mimics the robot and the model with compliant grip and wrist is very large. For both swing profiles the

majority of the clubhead vibration is quashed resulting in a clubhead displacement which is far more similar to a clubhead displacement profile of a golfer. Even initial clubhead oscillations seen at the start of both swings is damped out before the impact phase of the swing. This result demonstrates the large effect on clubhead vibration that can be achieved through adding compliance into the model system and theoretically the robot system.

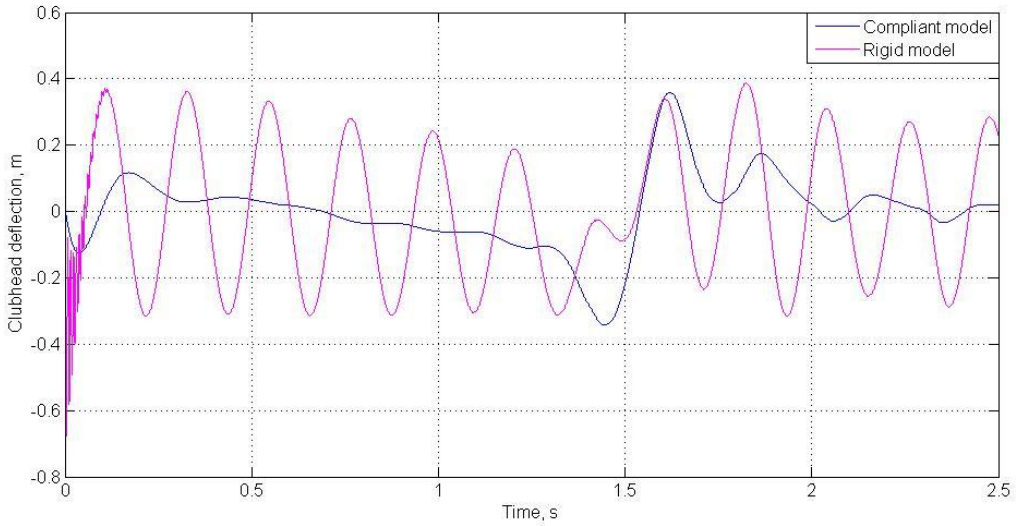

Figure 117 - Simulation of golfer A driven with robot feedback, rigid model compared against flexible model

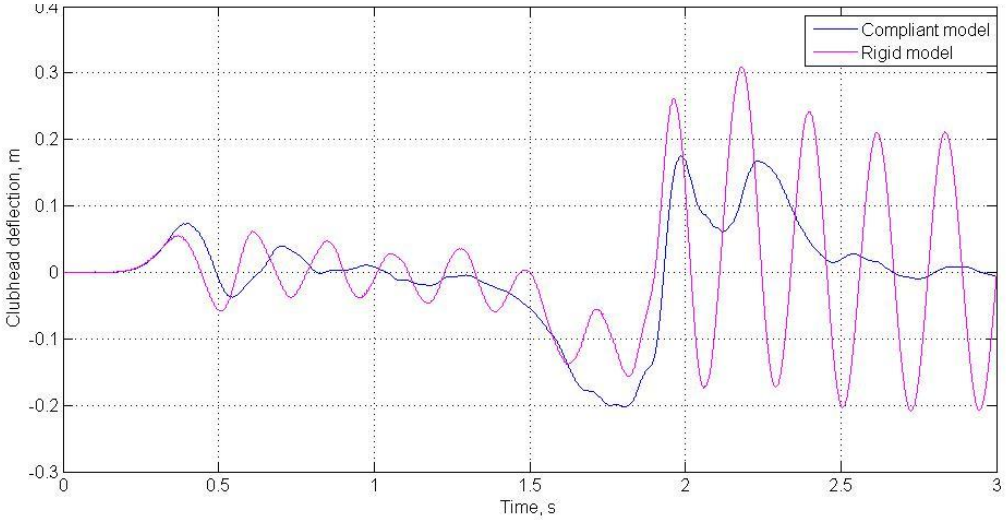

Figure 118 - Simulation of golfer B driven with robot feedback, rigid model compared against flexible model

8.7 Discussion

The aim set out at the introduction to this chapter was to demonstrate the results that could be achieved through implementing the adapted model from one which mimicked the robot's current swing to one where vibration suppressing elements had been added. This would return this research back to the fundamental goal of being able to simulate a human golf swing in a way that produced comparable accelerations of the clubhead and deflections of the clubhead.

The methodology required to generate swing profiles for the robot was described and the importance of the 'smoothness' of the swing profile and the method with which the robot and model are driven was underlined. A new swing profile generating tool which was produced in a parallel project designed to complement this research was described and has been used to generate all swing model and robot swing profiles.

An attempt was made to use a feed forward method to adjust the swing profiles to allow for the flexibility that now exists at the model wrist, however this was found to require an adaption to be made to the swing profile generating tool in order to account for the flexibility at the wrist while still providing a smooth swing profile. This is outside the scope of this research. The clubhead deflections and accelerations measured during the study in chapter 4 were not aligned with the swing plane as a real golf swing involves a rotation of the grip, a rotation which is not included in the model. Both of these variables were resolved in the direction of the swing and compared against the simulations. It was found that the wrist variables in the final model had low sensitivity to change so across all subjects the wrist stiffness and damping could be set to 300Nrad^{-1} and 15Nsrad^{-1} achieving good results for all subjects. It was found that although the simulations tended to have higher clubhead accelerations and subsequently deflections, the shapes of the responses were comparable with the greatest success being the minimal levels of clubhead vibration present in all of the six swings which were analysed. The discrepancies found between the magnitudes of the measured and simulated data show that the model is not representing the real robot to a satisfactory level of accuracy. While it has been mentioned that part of the additional clubhead motion is due to the flexibility of the

grip and wrist, this increase in magnitude also indicated that some of the parameters measured for slower speed swings are now not applicable to the full speed complete swings modelled in this chapter. Studies of the role that the shaft plays in a golf swing have reported a phenomenon where the shaft of the club stiffens due to the centrifugal force acting on it during a swing, particularly in the quickest part of the swing; the downswing (Butler & Winfield (1994)). This is consistent with the larger magnitude of clubhead motion seen in the simulations compared to the measured data. Butler and Winfield (1994) reported that during the downswing phase of a swing, the shaft was seen to stiffen with an increase in frequency of the first mode of vibration from 4.26Hz to 10.01Hz; over double. The shaft of the club used in the study in chapter 4 and from which the shaft frequency for the simulations was measured had a first mode frequency of 4.167Hz. If this were to increase to 10 during the downswing, this would have a large effect on the resultant clubhead position. Considering this and the effect of a change in the shaft damping, the model will need further developing to produce outputs which are more relevant to quick full swings.

8.8 Future work

The adaptions made to the mathematical model of the robot were made with the premise that if successfully implemented on the model, they could be applied to the physical robot with similar success. If this were the case, as mentioned in chapter 8, a new method of swing profiles is required if a flexible wrist is to be implemented, one which will take into account the flexibility at the wrist and the grip. Through adding the compliance to the system, less control is now possible over the resulting clubhead positions during the swing. It may be more applicable during future simulations of both model and robot, to attempt to match the position of the golf club grip section from real swings, this can or cannot be relative to human angular positions throughout the swing as there is no gain in replicating the golfer's arm and wrist angles. An accurate simulation is only required to map the correct position of the club in space during the swing. Once the grip variable is accurately simulated, this should provide the correct clubhead positions.

The model requires further refining. The stiffness of the shaft could vary throughout

the swing to incorporate the phenomenon of centrifugal stiffening in the downswing into the model with the aim to reduce the magnitude of clubhead motion.

If the suggested adaptions were made to the robot, new compliant wrist and grip components would be required. The silicone sleeves and material clamp developed in chapter 5 could be refined and implemented as long as each golf club used for robot simulations had a flange at the end of the shaft which would act as a safety feature preventing the club from slipping free from the grip. Rotational springs and variable rotational dashpots are readily available for purchasing and could be combined into a new wrist where the level of damping provided by the dashpot could be adjusted on a per golfer basis.

Once adaptions have been made to the robot, the swing variables measured in chapter 3 and presented in chapter 4 provide a comprehensive study of 14 golfers' swings which would allow a comparison of swing variables to be made with robot simulations of those swings.

Chapter 9

Conclusions

9.1 Conclusions

The work presented in this thesis documents and discusses the research carried out by this author which sought a solution to the clubhead vibrations present in all golf swings simulated by the Miyamae golf shot Robo V in the Sport Technology Institute at Loughborough University. At present, the robot is unable to simulate golf swings as performed by golfers with comparable clubhead deflection profiles or clubhead acceleration, with clubhead vibrations being present in both.

A literature review was carried out, discussing previous work carried out in this field where similar issues have been reported and which could provide a direction in which a possible solution could be found. It was decided based on this review, that a passive solution for damping clubhead vibrations should be applied. To test the results that could be achieved with a passive damping solution, the method which was selected as the most viable in this scenario was to produce a mathematical model of the robot in order to apply virtual adaptions to the robot in the model to assess their effectiveness at damping clubhead vibration before implementing any changes to the physical robot. Before the modelling commenced, a study was made of the various variables which define a golf swing and these were measured for a selection of swings from 14 golfers. The aim of this study aim being to understand the motion of the clubhead and shaft during a swing so that this author might be able to replicate them with simulations of the mathematical model.

A new system for monitoring clubhead orientation and path through the impact phase of a swing was developed as the commercially available systems provided a system neither accurate nor flexible enough with regards to the options of variables available to the user. The new system captured clubhead data at 5000Hz via the PONTOS motion analysis system coupled with HSV cameras and the point positions provided were imported into Matlab and analysed to provide clubhead dynamic loft, face angle, lie angle attack angle, speed and impact location. It was found that the new

system is capable of accurately measuring the impact location of the ball on the clubface during a swing providing a good level of marker visibility is achieved. This location can be analysed alongside the resulting clubhead rotations and path, demonstrating the large rotations that can result from off centre impacts. It was also observed that the velocity of points on the toe can differ greatly from those on the heel with a difference of 25.9m/s measured in one swing.

This system was used alongside accelerometers and shaft mounted strain gauges to measure clubhead vibration and deflection respectively, to provide variables which could be directly compared with simulated values from the mathematical model. The measurement of golfer kinematic data during this study provided the data required to generate swing profiles which were used as an input to the model.

Shaft strain data and clubhead acceleration data was captured for robot swing simulations providing an example of the levels of vibration that exist during robot swings. The study of human swing parameters demonstrated that the human swing differs greatly to the robot simulations of human swings and that a successful simulation of a swing should contain very minimal clubhead vibration.

To gain an idea of the results that could be achieved through adding compliance to the robot. A passive grip solution was implemented with preliminary trials being carried out to test out the effect of adding a compliant material at the interface between the robot's collet and the golf club. Silicone sleeves were produced and clamped onto the golf club shaft with a gripper which could be attached inside the robot's current grip to minimise impact on the use of the robot. A clubhead mounted accelerometer provided feedback of the level of vibration present in the clubhead during basic swings during the testing of each of the three silicone sleeves. The results were encouraging showing a large reduction in the level of clubhead vibration, with the most damping silicone sleeve reducing the time taken for all oscillation to cease from 7s to 2s. This however was not an acceptable level of vibration for a swing simulation but it was noted that the sleeve which provided the greatest level of damping also allowed motion of the club due to the sleeve's low stiffness. It was decided to test the theory of adding compliance into the robot further by generating a mathematical model of the robot and virtually adding the compliance. This would allow a large number of variations to be made in quick

succession and the outcome could be analysed with respect to the displacement, velocity and acceleration of the robot's collet, and the club grip and clubhead.

The first model provided the ability to test the implementation of a compliant grip and it was found that the results were somewhat limited. Stiffness and damping values were calculated for the silicone sleeves through material tests and applied to the mathematical model to provide some validation. Comparisons between measured clubhead acceleration and measured acceleration showed a good level of agreement. Recognising the level of flexibility and damping at the human wrist and how this could be applied to the robot, a second model was produced which modelled the robot's wrist as a compliant joint. To maximise the similarity between model and robot, an arm link was added to the model and both the arm and wrist of the model could be driven by a swing profile. As a method of validating the final model, the wrist joint and grip were set rigid and clubhead acceleration was compared to measured acceleration captured during a real robot swing. The outcome of this test was satisfactory, with good agreement shown between the two plots.

Simulations were made using swing profiles generated from kinematic data measured during the study of golfer swing parameters as the driving method and the resulting clubhead deflection and acceleration were compared with those measured during the golfer's swing. Wrist stiffness and damping values were varied to find values that provided a good fit between shaft deflection and clubhead acceleration in human golf swings to the same variables in robot simulations. It was found that compared to early simulations where the model modelled the robot in its existing state, the clubhead vibrations present in the deflection and acceleration profiles were reduced dramatically and there existed a reasonable agreement between the profiles of the measured and simulated responses, with the flexibility of the grip and wrist identified as adding to the disparity between the measured and simulated clubhead variables. Final simulations which were driven with robot feedback data demonstrated that even without a smooth profile as the input for the model, the compliance at the grip and wrist were capable of damping clubhead vibration dramatically.

Overall the outcome of adding a compliant wrist and grip to the model was found to be successful and that through the implementation of a flexible grip and wrist on the robot, it is predicted that there should be a large reduction in the level of clubhead oscillation that is seen during a robot swing.

Appendix

Measured

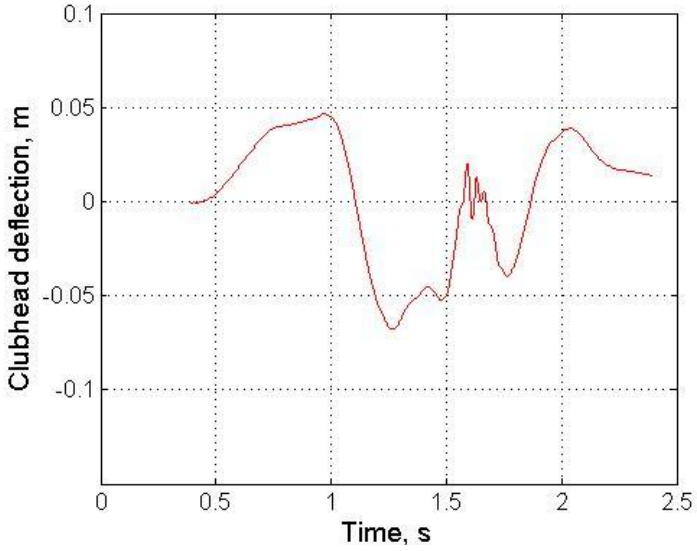

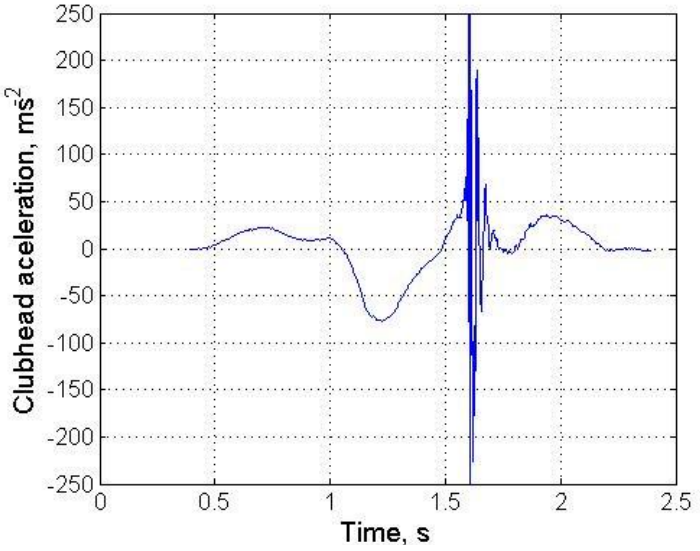

Simulated

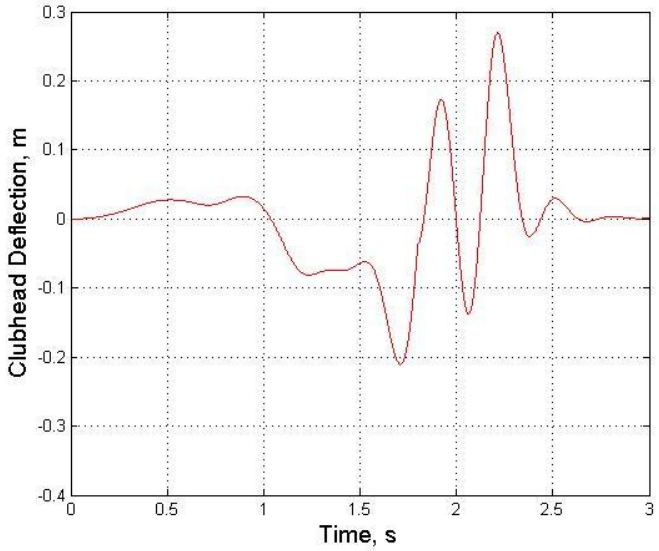

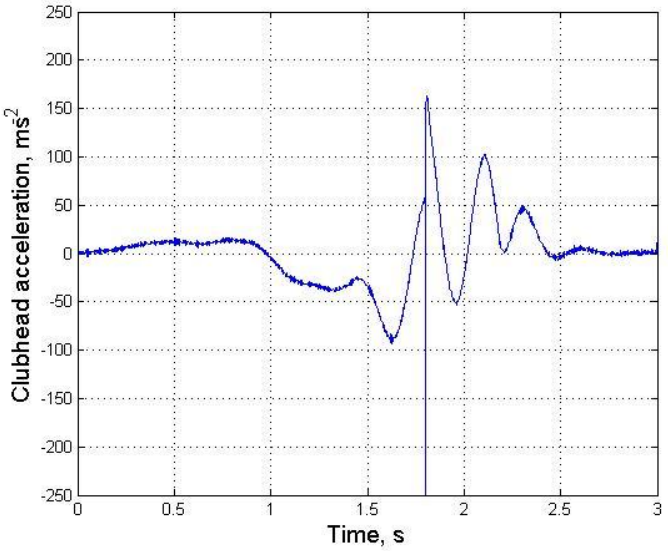

Appendix Figure 1 - Subject 1, swing 16: Measured and simulated clubhead deflections and accelerations

Measured

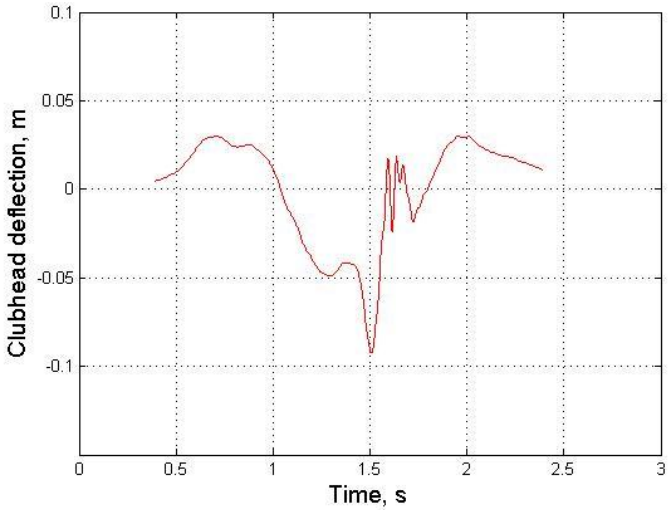

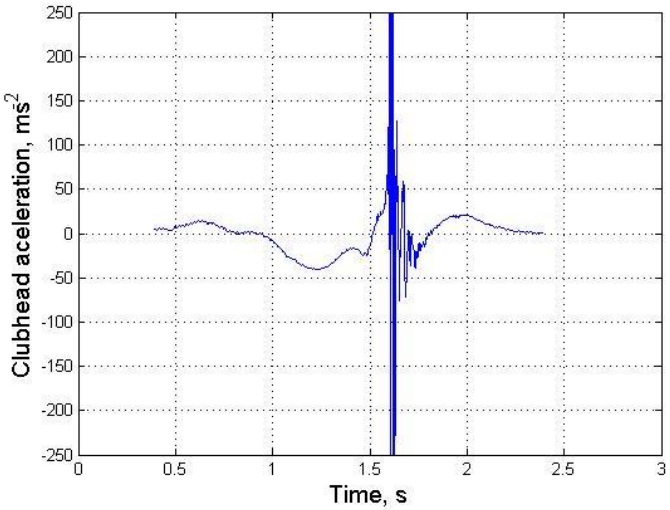

Simulated

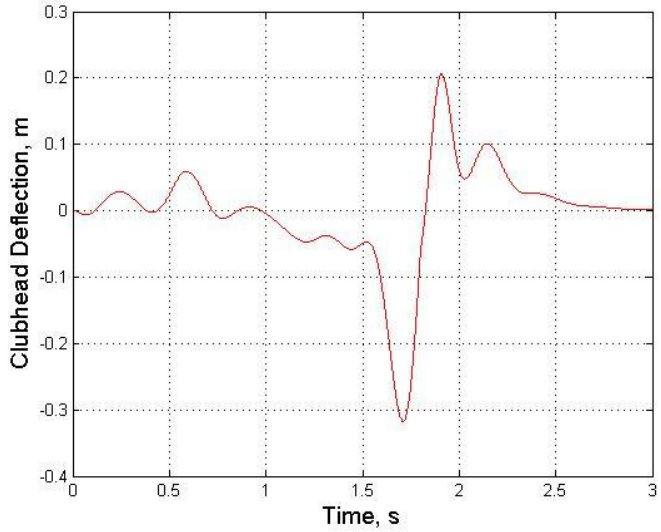

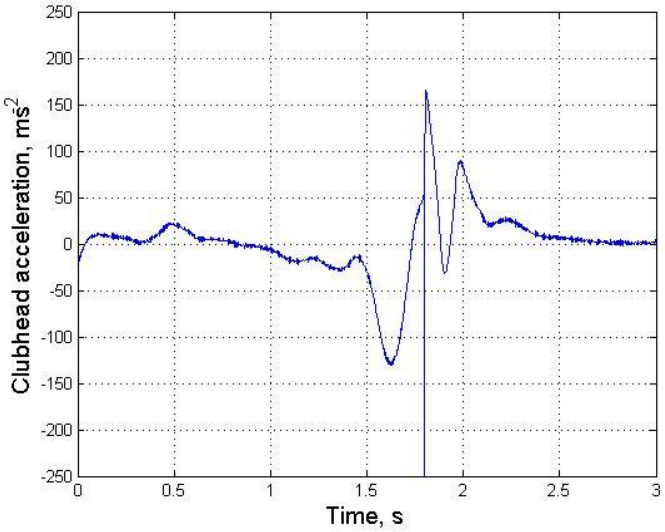

Appendix Figure 2 - Subject 2, swing 12: Measured and simulated clubhead deflections and accelerations

Measured

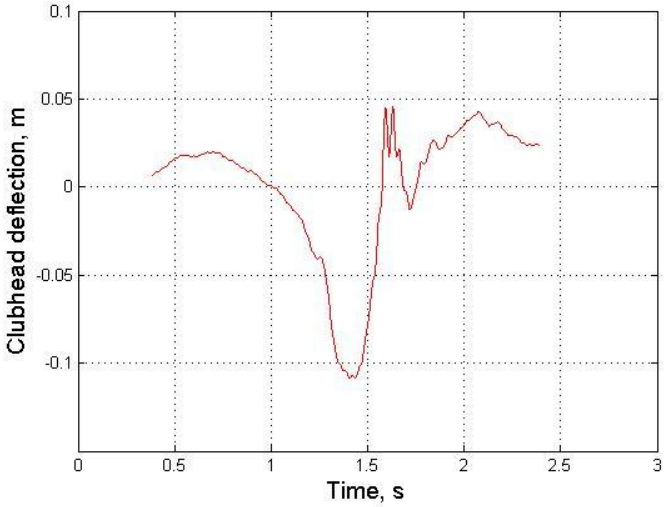

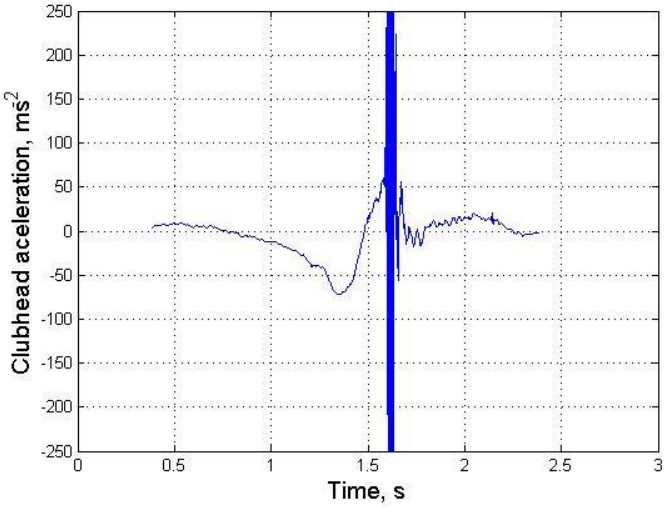

Simulated

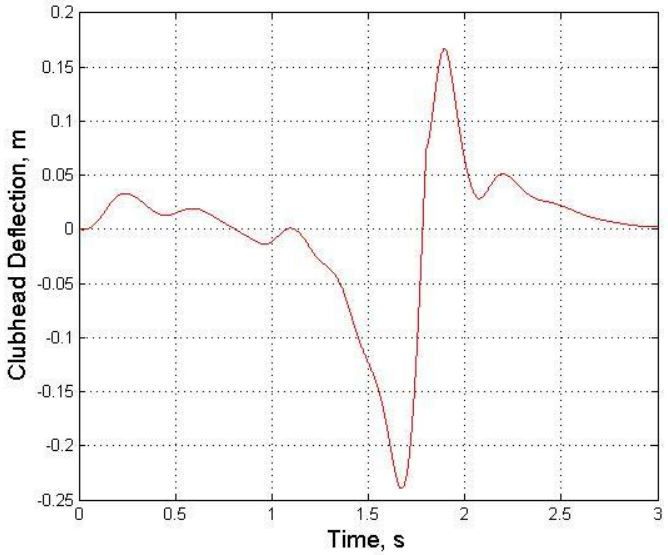

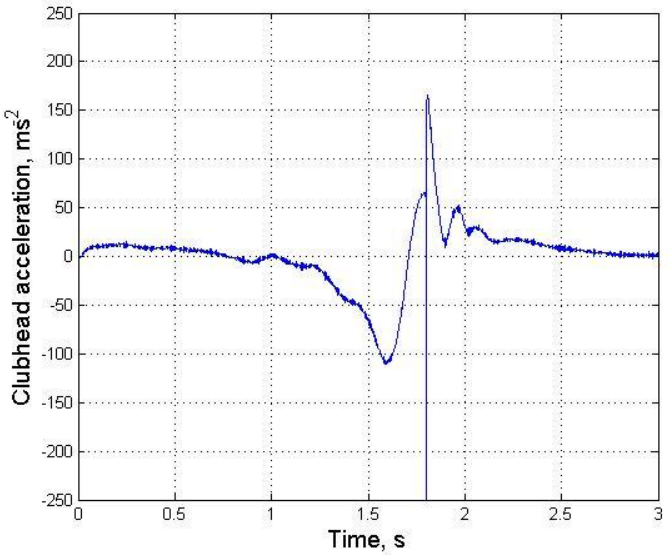

Appendix Figure 3 - Subject 4, swing 2: Measured and simulated clubhead deflections and accelerations

Measured

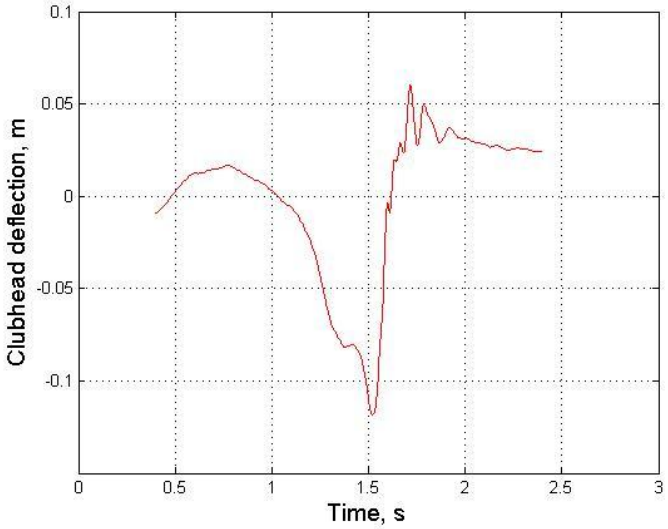

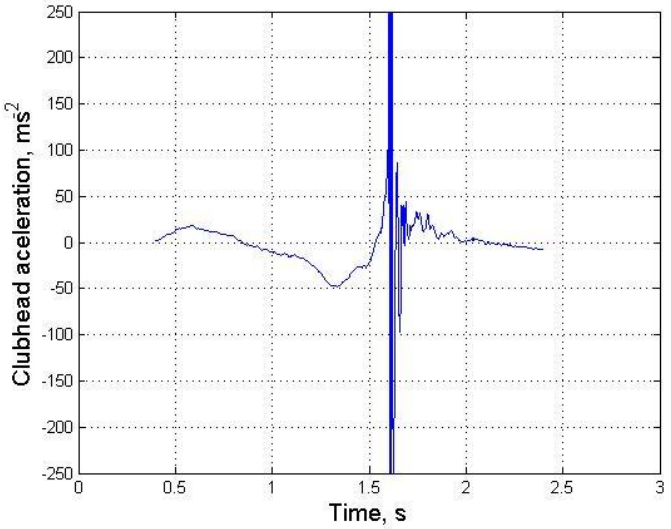

Simulated

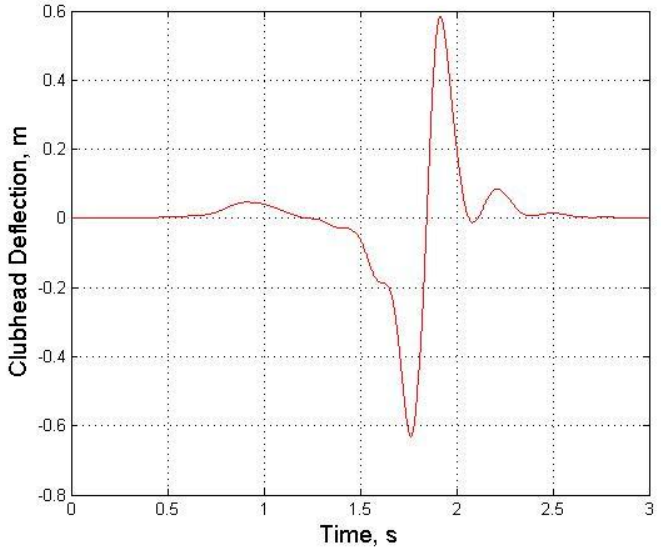

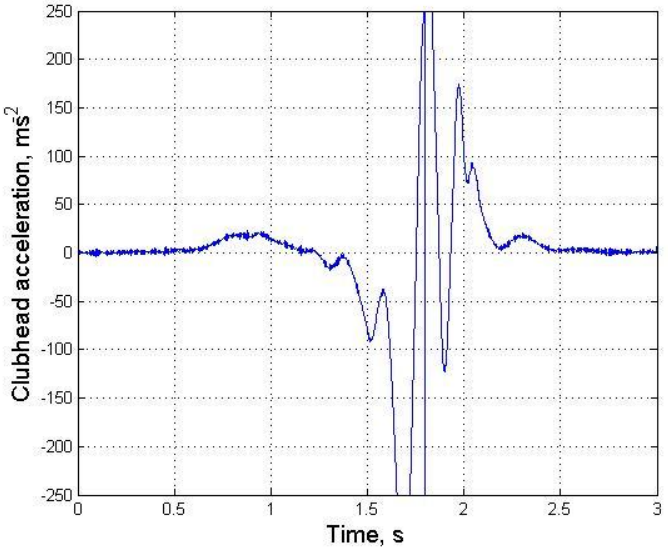

Appendix Figure 4 - Subject 6, swing 6: Measured and simulated clubhead deflections and accelerations

Measured

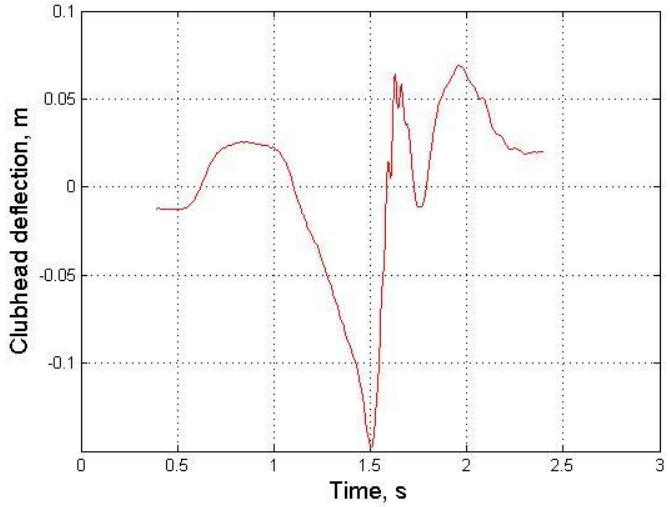

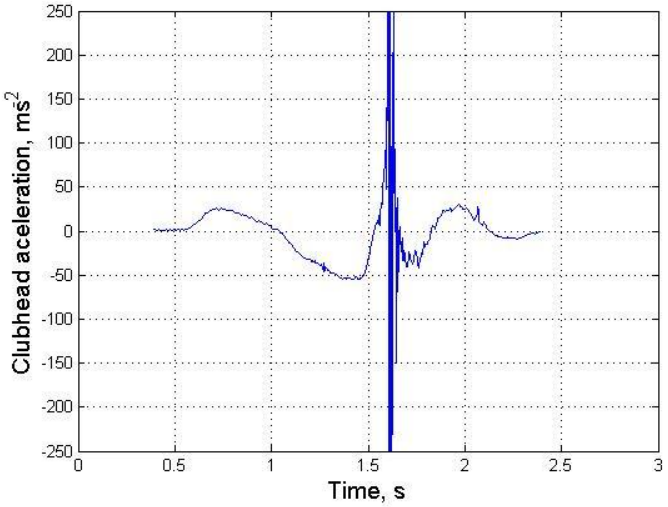

Simulated

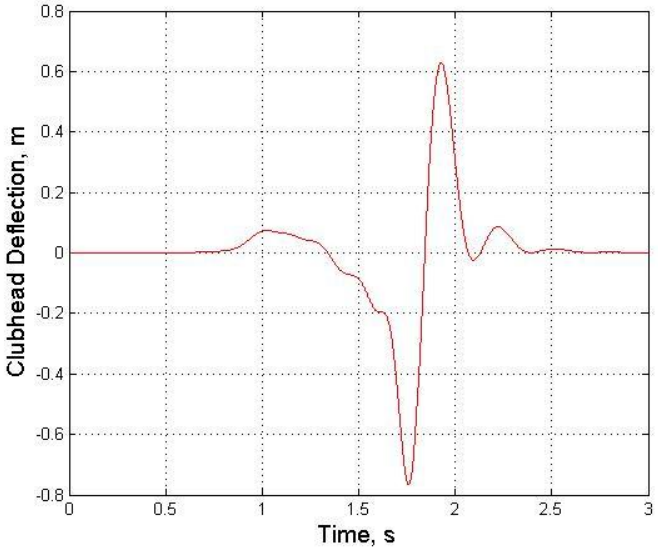

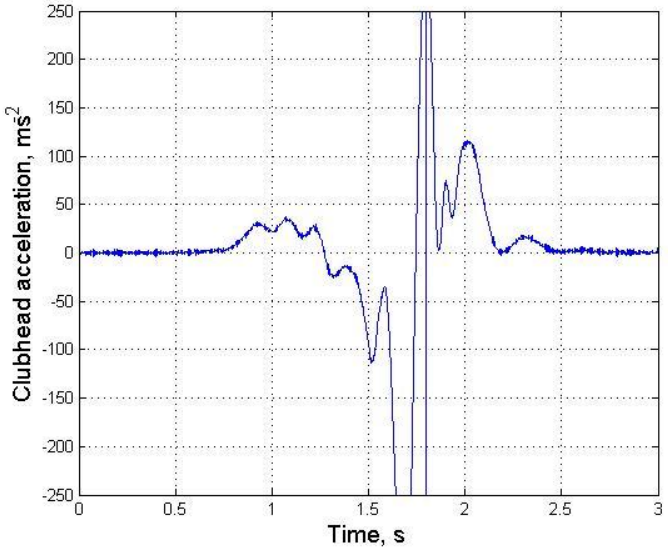

Appendix Figure 5 - Subject 8, swing 2: Measured and simulated clubhead deflections and accelerations

Measured

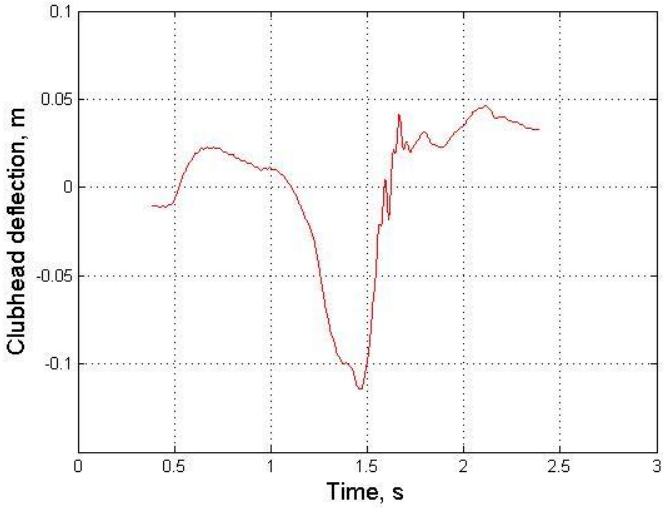

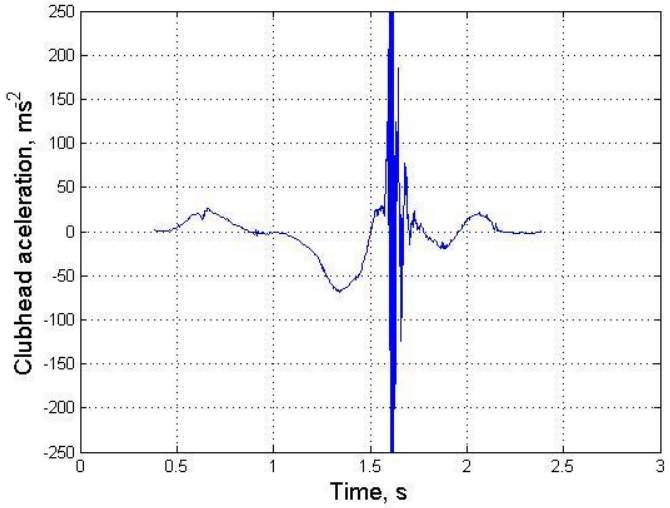

Simulated

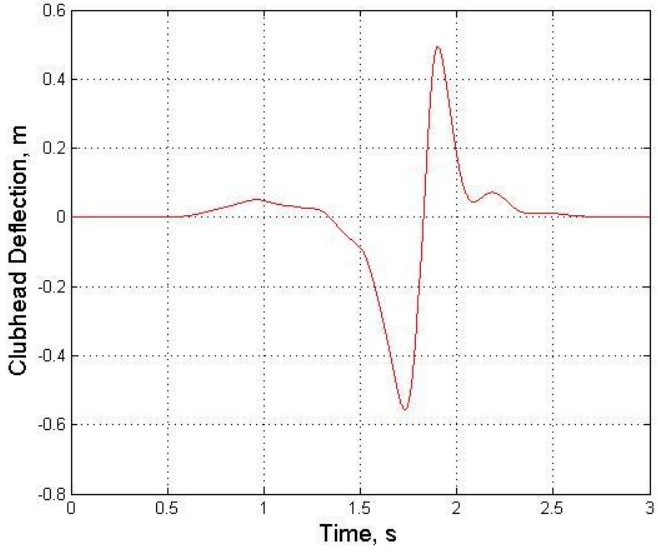

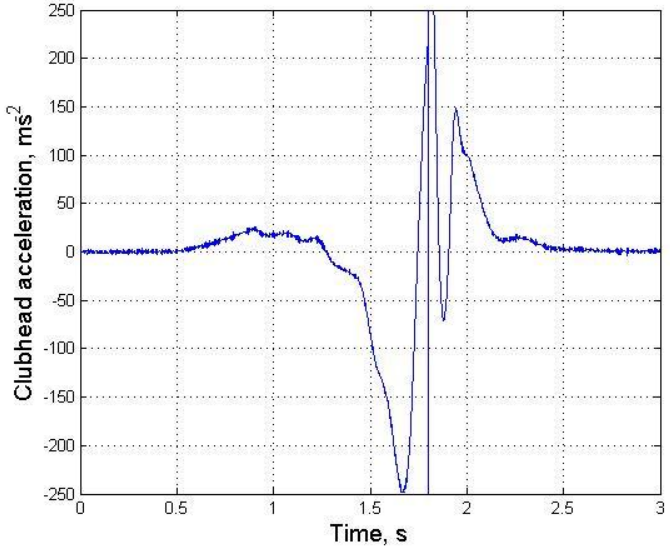

Appendix Figure 6 - Subject 9, swing 9: Measured and simulated clubhead deflections and accelerations

References

Alexander, R.M., 1988 *Elastic Mechanisms in Animal Movement*. Great Britain: Cambridge University Press.

Anderson, E.H., Glaese, RM., Neill, D., 2008. A comparison of vibration damping methods for ground based telescopes. *Proceedings of the SPIE - The International Society for Optical Engineering*, 7012, doi:10.1117/12.790195.

Andersson, R.L., 1989. Aggressive trajectory generator for a robot ping-pong player. *IEEE Control Syst.Mag*. 9(2), 15-21.

Ascari, L., 2009. Bio-inspired grasp control in a robotic hand with massive sensorial input. *Biological cybernetics*. 100(2), 109.

Bandopadhya, D., Bhogadi, DK., Bhattacharya, B., Dutta, A., 2006. Active Vibration Suppression of a Flexible Link Using Ionic Polymer Metal Composite. *Robotics, Automation and Mechatronics*, 2006 IEEE Conference on, 1(6), 1-3.

Behrens, S., 2000. *Passive and Semi-active Vibration Control of Piezoelectric Laminates*. Thesis (PhD). University of Newcastle, Australia.

Bhattacharya, B., 2000. Active and passive vibration control of flexible structures using a combination of magnetostrictive and ferro-magnetic alloys. Proc SPIE, 4073, 204-214.

Biddiss, E., Chau, T., 2008. Dielectric elastomers as actuators for upper limb prosthetics: challenges and opportunities. *Medical Engineering and Physics*, 30(4), 403-18.

Biddiss, E., Chaua, T., 2006. Electroactive polymeric sensors in hand prostheses: Bending response of an ionic polymer metal composite. *Medical Engineering & Physics*, 28, 568-578.

Blakemore, M., 2013. PGA Professional, Golf instruction tips and lessons. Available from: www.pgaprofessional.com [Accessed Dec 2013].

Bower, A.F., 2009. *Applied Mechanics of Solids*. Florida: CRC Press.

Briggs, L.J., 1959. Effect of Spin and Speed on the Lateral Deflection (Curve) of a Baseball; and the Magnus Effect for Smoothing Spheres. American Journal of Physics, 27(8), 589-596.

Brody, H., 1989. Vibration damping of tennis rackets (Amortissement des vibrations dans les raquettes de tennis). *International Journal of Sport Biomechanics*, 5(4), 451-456.

Budney, D.R., 1979. Measuring Grip Pressure During the Golf Swing. *Research Quarterly*, 50(2), 272-277.

Butler, J.H., 1994. Winfield DC. The dynamic performance of the golf shaft during the downswing. *In:* A.J. Cochran, M. Farrally, ed. *Science And Golf II: Proceedings of the world scientific congress of golf*. London: Taylor & Francis, 259-264.

Caldwell, D.G., 1990. Chemically stimulated pseudo-muscular actuation. *International journal of engineering science*, 28(8), 797.

Campbell, K.R., 1983. A triple pendulum model of the golf swing. *Journal of Biomechanics*, 16(4), 298-298.

Chen, M.Z., 1995. Zheng YF. Vibration-Free Handling of Deformable Beams by Robot End-Effectors. *Journal of Robotic Systems*, 12(5), 331-347.

Churchill, S., Peters, D.M., Bevins, J., 2007. The Validity of Marker Reconstruction Modelling for Biomechanical Analysis in Sport. *6th International Symposium on Computer Science in Sport*, 3rd - 6th June, 2007, Calgary, Canada. (Unpublished).

Cochran, A., Stobbs, J., 1986. *Search For The Perfect Swing, The Proven Scientific Approach to Fundamentally Improving Your Game*. Chicago: Triumph Books.

Cockram, R., Roberts, J.R., 2010. Control System for a Golf Robot. Loughborough UK, Loughborough University.

Connolly, C., 2007. A golf swing analysis tool from Callaway Golf. *Sensor Review*, 27(1), 14-16.

Crowe, A., Atteveldt, H., Groothedde, H., 1980. Simulation Studies of Contracting Skeletal Muscles During Mechanical Stretch. *Journal of Biomechanics*,13, 333-340.

Cura, V., 2003. Study of the different types of actuators and mechanisms for upper limb prostheses. Artificial Organs, 27(6), 507-516.

Doll, T.J., Schneebeli, H.J., 1988. The Karlsruhe dexterous hand. *Proc. Symp. on Robotic Control*, Karlsruhe.

DW-World. Available from: http://www.dw.de/europes-first-bionic-hand-still-going-strong-a-year-on/a-15213846 [Accessed March 2011].

Ehara, Y., Fujimoto, H., Miyazaki, S., Tanaka, S., Yamamoto, S., 1995. Comparison of the performance of 3D camera systems. *Gait Posture*, 3(3), 166-169.

Fassler, H., Beyer, H.A., Wen, J., 1990. A robot ping pong player: Optimized mechanics, high performance 3D vision, and intelligent sensor control. *Robotersysteme*, 6(3), 161-170.

Fischer, T., 1998. Sensor system for controlling a multifingered gripper on a robot arm. *Proceedings of the 1998 IEEE/RSJ Intl. Conference on Intelligent Robots and Systems*, 1509-1514.

Fuhrer, R., 2009. Crosslinking Metal Nanoparticles into the Polymer Backbone of Hydrogels Enables Preparation of Soft, Magnetic Field-Driven Actuators with Muscle-Like Flexibility. *SMALL*, 5(3), 383-388.

GOM mbH, 2012. *PONTOS datasheet*. Available from: www.GOM.com [Accessed

Jan 2014].

Harper, T.E., Jones, R., Roberts, J.R., 2006. *Robotic Simulation of Golfers' Swings*. Thesis (PhD). Loughborough University.

Hatze, H., 1976. Forces and duration of inpact, and grip tightness during the tennis stroke. *Medicine and Science In Sports*, 8(2), 88-95.

Hatze, H., 1992. Objective biomechanical determination of tennis racket properties. *International Journal of Sport Biomechanics*, 8(4), 275-287.

Hatze, H., 1992. The effectiveness of grip bands in reducing racquet vibration transfer and slipping. *Medicine and Science In Sports and Exercise*, 24(2), 226-230.

Head technology. Head intelligence. Available from: www.head.com/tennis/technology.

Hennig, E.M., Rosenbaum, D., Milani, T.L., 1992. Transfer of tennis racket vibrations onto the human forearm. *Medicine and Science In Sports and Exercise*, 24(10), 1134-1140.

Henrich, D., Worn, H., 2000. *Robot Manipulation Of Deformable Objects*. London: Springer-Verlag London Limited.

Hillbury, B.M., 1974. A Review of Recent Developments in Forced Vibration Dynamic Testing of Elastomers. Rubber and Related Products: New Methods for testing and Analyzing, *ASTM STP 553*, American Society for Testing and Materials, 142-161

Hocknell, A., Mitchell, S.R., Jones, R., Rothberg, S.J., 1998. Hollow golf club head modal characteristics: Determination and impact applications. *Experimental Mechanics*, 38(2), 140-146.

Hogan, B., 1979. *Five lessons: The Modern Fundamentals of Golf*. New York: Pocket Books.

Huang, G.T., 2006. Get a Grip. New Scientist, (2537), 46-49.

Huber, J.E., Fleck, N.A., Ashby, M.F., 1997. The selection of mechanical actuators based on performance indices. *Proceedings of the Royal Society of London, Series A (Mathematical, Physical and Engineering Sciences)*, 453(1965), 2185-205.

Huxley, A.F., Simmons, R.M., 1971. Mechanical properties of the cross bridges of frog striated muscle. *Journal of Physiology*, 218, 59-60.

Irwin, H., 1980. *Play better golf.* New York: Gallery Books.

Jones, L.A., Lederman, S.J., 2006. *Human Hand Function*. Oxford: Oxford University Press.

Jones, R., 2009. Face of the future. *Post Magazine*, May 3, 30.

Lakes, R.S., 2009. *Viscoelastic Materials*. Cambridge: Cambridge University Press.

Lin, J., Furusho, J., Sakaguchi, M., Zhang, G.G., Sato, F., 1999. Narou T, et al.

Development and Simulation of a Tennis Robot. *Proceedings of the IEEE International Conference on Systems, Man and Cybernetics*, 4, 836-841.

Lobontiu, N., 2010. *System Dynamics for Engineering Students: Concepts and Applications*. Massachusetts: Academic Press.

Luxton, T., 1985. The real truth about the golf swing. Maidstone: Kingswood Publishing.

MacKenzie, S.J., Sprigings, E.J., 2009. Understanding the mechanisms of shaft deflection in the golf swing. *Sports Engineering*, 12(2), 69-75.

Maltby, R., 1990. *Golf Club Design, Fitting, Alteration and Repair*. Ohio: Ralph Maltby Enterprises.

Meriam, J.L., Kraige, L.G., 2001. *Engineering Mechanics: Dynamics*, 5th ed. New Jersey: Wiley.

Modi, K.P., Sahin, F., Saber, E., 2006. An Application of Human Robot Interaction: Development of a Ping-Pong Playing Robotic arm. *Systems, Man and Cybernetics, 2005 IEEE International Conference*, 2, 1831-1836.

Moore, P., 2007. What driver loft will provide an acceptable launch angle the highest percentage of time? *In:* P. Moore, ed. *The mad science of golf: On moving past golf industry hype and learning to play better golf*. Illinois: AuthorHouse, 41-42.

Nishino, S., Tsujiuchi, N., Koizumi, T., Komatsubara, H., Kudawara, T., Shimizu, M., 2007. Development of Robot Hand with Pneumatic Actuator and Construct of Master-Slave System. *Proceedings of the 29th Annual International Conference of the IEEE EMBS*, 3027-3030.

Price, A., Jnifene, A., Naguib, H.E., 2006. Biologically inspired anthropomorphic arm and dextrous robot hand actuated by smart-material-based artificial muscles. *Proceedings of the SPIE - The International Society for Optical Engineering*, 6173, 1-12.

Price, A.D., Jnifene, A., Naguib, H.E., 2007. Design and control of a shape memory alloy based dexterous robot hand. *Smart Materials and Structures*, 16(4), 1401-14.

Ragunathan, S., 2008. Modular Reconfigurable Robotic Gripper for Limp Material Handling in Garment Industries. *International journal of robotics & automation*, 23(4), 213.

Raikova, R., 1992. A general approach for modelling and mathematical investigation of the human upper limb. *Journal of Biomechanics*, 25(8), 857-867.

Rao, S., 2004. *Mechanical Vibrations*. 4th ed. New Jersey: Prentice Hall.

Riley, P.O., Paolini, G., Della Croce, U., Paylo, K.W., Kerrigan, D.C., 2007. A kinematic and kinetic comparison of overground and treadmill walking in healthy subjects. *Gait Posture*, 26(1), 17-24.

Saliba, M.A., Axiak, M., 2007. Design of a compact, dexterous robot hand with

remotely located actuators and sensors. *Control & Automation*, 2007, 1-6.

Schlechter, A., Henrich, D., 2002. Manipulating Deformable Linear Objects: Manipulating Skill for Active Damping of Oscillations. *Intelligent Robots and System, IEEE/RSJ International Conference*, 2, 1541-1546.

Schmidt, E., Roberts, J., Rothberg, S., 2006. Time-Resolved Measurements of Grip Force During a Golf Shot. *Engineering Of Sport*, 2006(2), 57-62.

Schmidt, E.R., Rothberg, S.J., Roberts, J.R., 2007. *Measurement of Grip Force and Evaluation of its Role in a Golf Shot*. Thesis (PhD). Loughborough University.

Schulz, S., Pylatiuk, C., Bretthauer, G., 2001. A New Ultralight Anthropomorphic Hand. *Robotics and Automation, 2001. Proceedings 2001 ICRA. IEEE International Conference*, 3, 2437-2441.

Schutter, J.D., Torfs, D., Bruyninckx, H., 1996. Robot force control with an actively damped flexible end effector. *Robotics and Autonomous Systems*, 19, 205-214.

Shadow Dexterous Hand C5, 2012. Technical Specification. Shadow Robot Company. Available from: www.shadowrobot.com/wp-content/uploads/shadow_dexterous_hand_technical_specification_E1_20130101.pdf [Accessed April 2014].

Smith, C.A., 1995. Passive damping by smart materials: analysis and practical limitations. *Proc SPIE Int Soc Opt Eng*, 2445, 136-148.

Snead, S., 1961. Sam Snead on Golf. Sheffield: Nicholas Kaye.

Sutherland, D.H., 2002. The evolution of clinical gait analysis: Part II Kinematics. *Gait Posture*, 16(2), 159-179.

Thomas, G.R., Deiters, T.A., Best, C., 1995. Simulating Golf Club Performance Using Modal Analysis. Proceedings of the International Modal Analysis Conference, 2460, 989.

Thomson, W.T., 1996. Theory of Vibration with Applications. Florida: CRC Press.

Varoto, P.S., McConnell, K.G., 1995. Using Modal Analysis to Evaluate Golf Club Performance. Sound and Vibration, 29(3), 20-23.

Wilhelm, J., 2009. Methods for Multimodal Vibration Suppression and Energy Harvesting Using Piezoelectric Actuators. *Journal of Vibration and Acoustics*, 131(1), doi: 1115/1.2980378.

Wilkinson, D.D., Weghe, V.W., Matsuoka, Y., 2003. An Extensor Mechanism for an Anatomical Robotic Hand. *Proceedings of the 2003 IEEE International Conference on Robotics & Automation*, 238-243.

Winfield, D., Tan, T., 1994. Optimization of a clubhead loft and swing elevation angles for maximum distance of a golf drive. *Computers & Structures*, 53(1), 19-25.

Wishon, T., 1992. The modern Guide To Shaft Fitting. Worthing: Dynacraft Golf Products.

Wu, S., 1998. Method for multiple mode shunt damping of structural vibration using a single PZT transducer. *Proc SPIE Smart Structures and Materials*, 3327, 159-168.

Yue, S., Henrich, D., 2005. Manipulating Deformable Linear Objects: Sensor-Based Skills of Adjustment Motions for Vibration Reduction. *Journal of Robotic Systems*, 22(2), 67-85.